Spin-glass models and interdisciplinary applications

Elia Zarinelli

THÈSE DE DOCTORAT

DE L'UNIVERSITÉ PARIS-SUD XI

Spécialité: Physique Théorique

Ecole Doctorale de Physique de la Région Parisienne

présentée par

Elia Zarinelli

pour obtenir le grade de

Docteur de l'Université Paris-Sud XI

Sujet :

Spin-glass models and interdisciplinary applications

Soutenue le 13 janvier 2012, devant le jury composé de :

M.	Sergio Caracciolo	Examinateur
M.	Silvio Franz	Directeur de thèse
M.	Alexander K. Hartmann	Rapporteur
Mme	Giulia Iori	Rapporteur
M.	Olivier Martin	Examinateur
M.	Gregory Schehr	Examinateur

Abstract

The main subject of this thesis is the physics of spin glasses. Spin-glass models have been introduced in the 70s in order to describe the behavior of dilute magnetic alloys. Afterwards it has been discovered that some spin-glass models could be considered prototype models to understand the behavior of supercooled liquids. More recently, a close analogy between combinatorial optimization problems and the physics of spin glasses allowed to establish fruitful links between the two domains.

In the first part of this thesis we present the results of the study of Kac-glass models in sandwich geometry. One of the main debated problems in the physics of supercooled liquids is the existence of static correlation functions which present a peculiar behavior near the glass transition. Recently, the so called *point-to-set* correlation functions have been introduced. These correlation functions are be able to detect the amorphous order near the glass transition, which standard *point-to-point* correlations functions are completely blind. Quite interestingly, in the framework of Kac-glass models, it is possible to analytically calculate these functions, introduced in spherical geometry. Motivated by some recent numerical experiments which measured the energy of "amorphous domain walls" between metastable states, we considered Kac-glass models in "sandwich" geometry. This allowed us to test if point-to-set correlation functions are sensitive to the geometry of the system and to characterize the energy needed to put different metastable states in contact with each other.

In the second part of this thesis we study the problem of fluctuations of the pseudo-critical temperature due to the disorder in some spin-glass models. The distribution of the pseudo-critical point and its scaling properties in finite-size disordered systems are highly debated issues which have attracted the attention of physicists since the very first works by Harris. In a first work, we have investigated the finite-size behavior of the Sherrington–Kirkpatrick (SK) model via a full analysis of the Plefka expansion. We have introduced a definition of finite-size pseudo-critical temperature and showed that its fluctuations are described by the Tracy–Widom (TW) distribution. The TW distribution, which describes the fluctuations of the largest eigenvalue of a Gaussian random matrix, describes also the fluctuations of observables of a broad number of physical and mathematical models, like directed polymers in disordered media and growth problems. To our knowledge, this is the first time that this ubiquitous distribution is found in connection with the fluctuations of a physical observable in spin-glass models. In order to have a better understanding of this subject, in a subsequent work, we have investigated the SK model and the Edward–Anderson (EA) model via numerical simulations. We have introduced a suitably defined pseudo-critical temperature, which can be measured via numerical simulations, and studied its fluctuations due to disorder. We have found that for the SK model the fluctuations are described by the TW distribution and for the EA model by the Gumbel distribution. This result shows a strong link between the field of Extreme Value Statistics and the physics of spin glasses.

In the third part of this thesis, we show how typical tools of physics of disordered systems and combinatorial optimization can be used to investigate problems in other domains, like financial problems. In finance, the estimation of the robustness of a financial network to shocks and crashes is a topic of paramount importance in assessing the stability of an economic system. The banking system is thought to be a fundamental channel in the propagation of shocks to the entire economy: the economic distress of an insolvent bank can be transmitted to its creditors by interbank linkages, thus a shock can easily propagate to the whole network. Unfortunately, detailed data on banks bilateral exposures are not always available and the reconstruction of bilateral exposures from incomplete data sets becomes a central issue for the estimation of risk. A commonly used tool for this task is the so-called entropy maximization method, which does not assume any heterogeneity in the structure of the network. This assumption leads to an underestimation of the extent of contagion. We introduce a message-passing algorithm to overcome this limitation and to sample the space of possible structures for the network. We test our algorithm on ensembles of synthetic data encoding some features of real financial networks (sparsity and heterogeneity), finding that more accurate estimations of risk can be achieved. Finally we find that this algorithm can be used to control the amount of information regulators need to require from banks in order to efficiently constrain the reconstruction of the network.

Contents

Introduction

Incipit

> Tous les problèmes de géométrie se peuvent facilement réduire à tels termes, qu'il n'est besoin par après que de connoître la longueur de quelques lignes droites pour les construire.
>
> *René Descartes*
> *La géométrie, 1637*

The incipit of this manuscript is also the incipit of "La géométrie" by René Descartes, one of the most important oeuvres in the history of mathematical literature. A long historical tradition identifies with the oeuvres of Descartes (and Fermat) the beginning of "analytical geometry" [1]. The adjective "analytical" refers to the classical subject of mathematical analysis done in algebraic terms. In the second book of "La géométrie", Descartes lays the groundwork of the analytical approach to Euclidean geometry.

"La méthode" by Descartes sheds some light on how the human knowledge evolves and grows. The capability of overcoming barriers between different and apparently unconnected scientific domains allows to transfer languages and methods from one discipline to another. These different languages and methods can then merge and proliferate, with a general benefit for various disciplines.

Evidently, statistical mechanics itself, the main subject of the present manuscript, is a product of this process of evolution of human knowledge, that, in some sense, can be considered a paraphrase of the *contaminatio* of Latin poetry.

If in the last centuries *contaminatio* typically took place between disciplines in the same scientific domain, in the last years we have witnessed a spill over of physics to other scientific fields. In recent times, physicists, and in particular statistical physicists, have focused their attention on problems coming from biology, engineering, computer science and finance.

Statistical mechanics of disordered systems in general, and spin-glass theory in particular, were very precocious scientific disciplines in this sense. In 1988, Philip Anderson wrote in the columns of Physics Today [2]:

> The history of spin glass may be the best example I know of the dictum that a real scientific mystery is worth pursuing to the ends of the Earth for it's own sake, independently of any obvious practical importance or intellectual glamour. (...)

> The pursuit of the spin glass mystery led, *inter alia* and aside from all the good solid-state physics that resulted, to new algorithms for computer optimization, a new statistical mechanics, a new view of protein structure, a new view of evolution and new ideas in neurosciences.

The approach to the works presented in this manuscript wants to be in the lines of Descartes and Anderson method, drawing from a pool of ideas and methods coming from physics and beyond. Ideas from Spin-Glass Theory are used to study the supercooled liquid phase of glass-forming liquids. The ubiquitous results of Random Matrix Theory in connection with Extreme Value Statistics Theory allow to investigate some features of Spin-Glass models. Finally, from the fruitful interaction of Spin-Glass Theory and Computer Science, we put forward a new algorithm of immediate application in Financial problems. In figure 1 we show how the process of *contaminatio* between the cited topics was strictly interconnected in past literature.

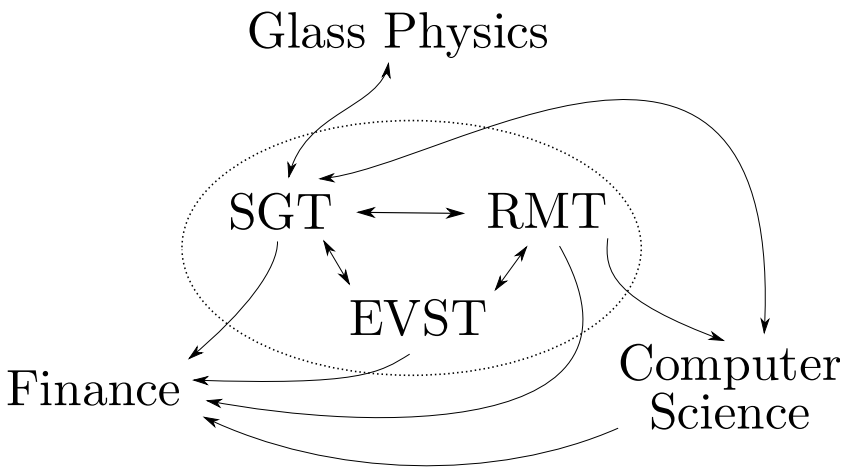

Figure 1: A pictorial representation of the subjects touched in this manuscript. SGT stand for Spin-Glass Theory, RMT for Random Matrix Theory and EVST for Extreme Value Statistics Theory. The direction of the arrows identifies the direction of a *contaminatio* between two topics in literature.

Let us give a short overview of the history and the theory of spin-glass models, the common background of the present work.

Brief historical overview

Spin-Glass models have been systematically studied since the pioneering work of Samuel Edward and Philip Anderson published in 1975 [3]. The purpose was to introduce a model for the description of a class of dilute magnetic alloys, which, some years before, acquired the name of spin glasses. In the same year, David Sherrington and Scott Kirkpatrick [4] applied the ideas introduced by Edward and Anderson to a model, which allowed an exact mean-field approach. They concluded that this approach was ill-defined as it led to a solution with negative entropy. In a suite of inspired papers [5, 6], Giorgio Parisi introduced the so-called full Replica Symmetry Breaking (fRSB) scheme for mean-field spin-glass models, which allowed to solve the negative-entropy conundrum and to understand physical properties of the spin-glass phase. The classical reference which gives a unified view on the first period of spin-glass

history is the book of Mezard, Parisi and Virasoro [7].

Since in the eighties the solution of the Sherrington and Kirkpatrick (SK) model was still an open and debated question, some physicists tried to introduce simpler spin-glass models which shared the same features of the SK model. In 1981, Bernard Derrida introduced the Random Energy Model [8] and in 1984 the p-spin model, a generalization of the SK model, was studied in detail by David Gross and Marc Mezard [9]. For these models, a 1-step Replica Symmetric Breaking (1RSB) scheme was shown to be correct. This allowed to classify spin-glass models in two main categories, depending on the correct Replica Symmetric Breaking scheme to solve the model: 1RSB or fRSB. In 1987 Theodore Kirkpatrick and Peter Wolynes noticed a close analogy between the phenomenology of 1RSB models and the one of glass-forming liquids and structural glasses [10]. In the following years, in a remarkable series of papers [11, 12, 13, 14], Kirkpatrick, Thirumalai and Wolynes reached a deep understanding of this class of spin-glass models and its connections with structural glasses, and proposed the spin-glass inspired "Random First Order Transition" theory of the glass transition.

After the initial successful application of spin-glass models to the study of magnetic alloys and glass forming liquids, in recent years many physical systems have been described using methods and ideas borrowed from spin-glass physics. Let us just mention some of them:

- Colloidal dispersions [15]
- Quantum glasses [16]
- Random lasers [17]
- Granular materials [18]
- Biological systems [19]

Among the systems that can be described and analyzed using the language of disordered systems, there are problems of combinatorial optimization [20]. It has been observed that some algorithms used to solve problems of combinatorial optimization display an easy-hard transition. The presence of such a transition suggested that they should be studied with the typical tools of phase transitions in statistical mechanics. There has been an upsurge of interest in studying combinatorial optimization problems from a statistical physics point of view, both for theoretical analysis [21] and for algorithmic developments [22, 23]. Conversely, some very clever optimization algorithms are adopted by physicists in their studies of ground states of disordered systems [24].

Overview on Spin-Glass Theory

The mathematical model introduced by Edward and Anderson (EA) in [3] in order to describe spin-glasses behaviour can be considered the simplest generalization of the widely studied Ising model describing ferromagnets. The basic degrees of freedom are Ising spins $S_i \in \{-1, +1\}$ sitting on the vertices of a cubic regular graph in d dimensions. The Hamiltonian reads:

$$H[S,J] = -\sum_{(ij)} J_{ij} S_i S_j + B \sum_i S_i \ , \tag{1}$$

where $\sum_{(ij)}$ means the sum over each edge of the graph. The coupling constants J_{ij} can be both ferromagnetic and anti-ferromagnetic, i.e. they can be gaussian random variables. Main features of this model, shared also by other spin-glass models, are:

- *disorder*: the disorder is incorporated in the Hamiltonian of the model by means of random couplings J, which are considered quenched. The value of a generic observable $\mathcal{O}(J)$ depends on the realization of the disorder J. One can show that observables which are intensive quantities are self-averaging. This means that in the thermodynamic limit – the system size which goes to infinity – the distribution of the observable $\mathcal{O}(J)$ is a delta function centered in $\overline{\mathcal{O}(J)}$, where $\overline{\cdots}$ means the average over the distribution of the disorder J.

- *frustration*: frustration in spin-glass models was firstly pointed out by Gerard Toulouse in [25]. The geometrical frustration is due to the fact that bonds between interacting spins can be negative. When trying to minimize the energy of a configuration, not all the spins can be "satisfied", then some of them are "frustrated".

The EA model is, nowadays, poorly understood: an analytical solution is still missing and the existence of a finite-temperature phase transition relies entirely on numerical simulations [26, 27, 28, 29, 30, 31, 32, 33, 34, 35, 36, 37, 38, 39]. On the other hand, much more insight has been reached for the SK model. The Hamiltonian of the SK model is the same of the EA model, but the underlying graph is a complete graph: no notion of space is present. For this model a mean-field approach is expected to be correct. Already in the original work [4], it has been shown that the SK model exhibits a finite-temperature phase transition from an high-temperature paramagnetic phase to a low-temperature spin-glass phase. In simple terms, with "spin-glass phase" we mean a phase in which a magnetic order is present, but the order is not ferromagnetic. In the following, will try to be more precise and understand how it is possible to characterize a spin-glass phase transition.

Before considering disordered models, let us briefly analyze the ferromagnetic Ising model, the simplest mathematical model to describe magnetic materials. The definition of the Ising model is the same as the EA model. The only difference is that the couplings are positive uniform numbers: $J_{ij} = J > 0$. For $B = 0$, in the thermodynamic limit, for $d \geq 2$, the Ising model undergoes a paramagnetic-ferromagnetic phase transition at a finite critical temperature T_c. The order parameter of the phase transition is the magnetization:

$$m_{i,\pm}(T) = \lim_{B \to 0_\pm} \lim_{N \to \infty} \langle S_i \rangle \tag{2}$$

where $\langle \cdots \rangle$ means the average over the Boltzmann measure at temperature T. For $T > T_c$, $m_\pm(T) = 0$: the system is in the paramagnetic phase. For $T < T_c$, $m_{i,\pm}(T) = \pm M(T)$: the system is the ferromagnetic phase. A phase transition can also be characterized by dynamical properties. Suppose that at time $t = 0$ the system is at equilibrium: we choose a reference configuration $S(0)$ drawn with Boltzmann weight. We average $S_i(t)$ over a dynamics which respects the detailed balance starting from the reference configuration $S(0)$:

$$m_{i,S(0)} = \lim_{t \to \infty} \lim_{N \to \infty} \langle S_i(t) \rangle_{S(0)} \ . \tag{3}$$

In the low-temperature phase, $T < T_c$, we obtain that $m_{i,S(0)} = \pm M(T)$, depending on the initial configuration $S(0)$: ergodicity is broken. A phase transition can also be identified via the peculiar behaviour of some physical observables: a discontinuity or a divergence. The ferromagnetic susceptibility – which measures the rate of change of the average magnetization with respect to an infinitesimal uniform change of the external field – is divergent in all the ferromagnetic phase.

We can conclude that in the ferromagnetic phase the system can be found in two quasi-states that can be identified by the external magnetic field, at the level of thermodynamics,

or by the initial condition, at the level of dynamics. We see that the two quasi-states are invariant under translation and connected by the $\mathbb{Z}_2$ symmetry. Turning to the case under consideration, if a model presents a phase where the quasi-states are neither invariant under translation nor connected by any simple symmetry, we say that the system is in the *spin-glass* phase.

We have already pointed out that the SK model exhibits a low-temperature spin-glass phase. In contrast to the ferromagnetic case, the spin-glass phase is much more difficult to characterize. Thouless, Anderson and Palmer [40] firstly discovered that the number of quasi-states in the low-temperature phase is exponential. Given the presence of the disorder it is also impossible to detect quasi-states via a uniform magnetic field. A long debate on what is the correct order parameter of the spin-glass transition took place within the spin-glass community. To cut a long story short, Parisi discovered that the order parameter of the spin-glass transition is the overlap distribution [7]. Given a realization of the disorder, one can sample two independent spin configurations S^1 and S^2 with the associated Boltzmann weight and measure the overlap between the two configurations: $q_{12} = 1/N \sum_i S_i^1 S_i^2$. For a given realization of the disorder J, we denote the overlap distribution with $P_J(q)$. The order parameter of the spin-glass transition is the overlap distribution $P(q)$: the infinite-size limit of $P_J(q)$ averaged over the disorder distribution . The second moment of the overlap distribution is related to the spin-glass susceptibility χ_{SG}:

$$\int P(q) q^2 \mathrm{d}q - \left[\int P(q) q \mathrm{d}q \right]^2 = \frac{1}{N} \chi_{SG} \tag{4}$$

In the paramagnetic phase, $P(q)$ is a delta function centered in 0, while in the spin-glass phase it acquires a non-trivial structure. Spin-glass models can be classified in two categories depending on the behaviour of $P(q)$ in the low-temperature phase:

- *continuous*: spin-glass models for which a fRSB scheme is correct belong to this class, e.g. the SK model. Below T_c, $P(q)$ has support in $[q_{min}(T), q_{max}(T)]$. $P(q)$ is a positive function in the support and displays two deltas at the extremes. The support shrinks continuously to a point for $T \to T_c^-$. The spin-glass susceptibility diverges in the spin-glass phase.
- *discontinuous*: spin-glass models for which a 1RSB scheme is correct belong to this class, e.g. the p-spin model with $p > 2$. Below T_c, $P(q)$ is composed of two delta picks at $q_0(T)$ and $q_1(T)$.

Outline of the thesis

The purpose of the present work is to present new analytical and numerical results regarding the following three topics:

Kac spin-glass models in *sandwich* geometry

Fully-connected spin-glass models in the 1RSB class have been the starting point for the construction of RFOT theory for glass-forming liquids. Fully-connected models are plagued by the unphysical infinite-range nature of the interactions. Finite dimensional spin-glass models in the Kac limit have been introduced in order to take into account in a tractable way the finite range of interactions of glass-forming liquids. On the other hand, the recently-introduced *point-to-set* correlation functions are a correct framework to identify the static amorphous order developing in glass-formers near the glass transition.

In chapter 2, we extend the approach of Franz and Montanari, originally introduced to calculate point-to-set correlation functions in spherical geometry in Kac-glass models, to a different geometry, the so-called *sandwich*-geometry. This will allow us to measure the energy cost and the surface tension to put different metastable states in contact, one of the main ingredients of RFOT theory. Our results have been published in [41].

Fluctuations of the pseudo-critical temperature in spin-glass models

The non-analytic behaviour of thermodynamic functions characterizes a phase transition in infinite-size systems. In finite-size systems the divergences of physical observables, that would result from such a non-analytical behaviour, are suppressed and replaced by smooth maxima, which allows one to identify a pseudo-critical point. In disordered systems, the pseudo-critical point is a random variable depending on the realization of the disorder. In chapter 4 and 5, we present our approaches to characterize the probability distribution of the pseudo-critical point in some spin-glass models: the SK model and the EA model. We will show the important role played by Extreme Value Statistics theory in this characterization. Our results have been published in [42, 43].

Interdisciplinary applications

The correct evaluation of risk is a central topic in finance. Different kinds of risk can be identified. Recent financial crisis points out the importance of systemic risk in financial systems. We say that a financial system is affected by systemic risk, if the failure of a single institution can easily provoke a chain of bad economic consequences – sometimes referred to as a domino effect. The banking system is considered a fundamental framework in which financial contagion can take place. Institutions are often left with the problem of assessing the stability of financial systems by incomplete information sets, e.g. incomplete informations of interbank liabilities. In chapter 7 we introduce a message-passing algorithm for the reconstruction of financial networks from incomplete informations in order to obtain a correct evaluation of systemic risk. Our results have been presented in [44].

Part I

Spin-glass models and the glass transition

Chapter 1

The glass transition

It is customary, when one is about to write about glasses, to cite what Philip Anderson wrote in the columns of Science in 1995 [45] :

> The deepest and most interesting unsolved problem in solid state theory is probably the theory of the nature of glass and the glass transition.

And in fact, nowadays, a satisfying "theory of the nature of glass" is still missing.

In this chapter we will provide an introduction to what is the "nature of glass" and to the "glass transition" [46]. Different approaches have been proposed in the last years in order to formulate a "theory of the nature of glass", see [47, 48] for recent reviews. In our introduction we will focus on the so-called Random First Order Transition (RFOT) Theory [49]. We present some recent developments, namely the introduction of *point-to-set* correlation functions, which allow to introduce a protocol to measure the elusive amorphous static order in glasses.

Statistical physics of disordered system gave a large contribution to the comprehension of the nature of glasses, providing paradigmatic models that exhibited surprising common features with the phenomenology of glasses. We will introduce Kac-glass models, i.e. finite-range spin-glass models that can be solved in the Kac limit. Within this framework it has been possible to define and calculate point-to-set correlation functions, showing that a point-to-set correlation length diverges at a finite critical temperature [50].

1.1 Phenomenology of the glass transition

1.1.1 What is a glass?

Before trying to answer this question, let us answer a simpler question: what is a crystal? If a liquid is frozen below its melting temperature T_m, it can nucleate and undergo a first order phase transition towards a symmetry-broken state characterized by a periodic arrangement of the particles: it becomes a crystal. A crystal is a solid: it does not flow when subject to an infinitesimal stress and, more formally, its static shear modulus is non zero (see [51] for an interesting discussion).

Let us now come back to the previous question. If we cool a liquid below its melting temperature in such a way that it cannot nucleate to the crystalline phase, we obtain a supercooled liquid. The supercooled liquid just below the the melting temperature is in a metastable state – the true ground state is crystalline – but it can be considered in a sort of

"local" equilibrium, since equilibrium theorems still hold. If we continue cooling the supercooled liquid, we would observe an impressive increase of the viscosity of the liquid until we reach a certain temperature T_g, called the glass-transition temperature, at which the system falls out of equilibrium. At this temperature the liquid does not flow any more since equilibration times are longer than experimental times: the liquid has become a glass. A glass is a solid: like a crystal, it does not flow when subject to infinitesimal stress. Contrary to the crystal, a glass has the same symmetries of a liquid. We can say that a glass is an amorphous solid.

Let us remark that the definition of glass-transition temperature is only conventional and anthropocentric. T_g is defined as the temperature at which the viscosity of the liquid is equal to 10^{13} Poise: it becomes too viscous to reach equilibrium in "human experimentally accessible" time scales. It is clear that the glass transition has a dynamical characterization. On the other hand, typical thermodynamic observables does not present any peculiarity approaching T_g – except the entropy, as we will see in few lines. This begs the question: from the point of view of statistical mechanics, shall we be interested to a "transition" which is clearly not a thermodynamic transition? The answer is yes, since – as we will see in the following – the glass transition can be the precursor of an ideal glass transition, characterized by thermodynamical signatures that the usual thermodynamic phase transition are not able to describe.

1.1.2 The ideal glass transition

Even tough it is not possible to perform equilibrium measures in the glass phase, $T < T_g$, also called in the literature deep supercooled phase, it could be interesting to perform extrapolations. Let us give two examples.

Entropy crisis: In 1948 [52], Kauzmann performed some extrapolations of the excess entropy – the difference between the entropy of the supercooled liquid and the entropy of the crystal – in the deep supercooled phase. A plot is shown in figure 1.1 (left). We remark that, for some systems, the extrapolated excess entropy seems to vanish at a finite temperature T_K, named Kauzmann temperature.

Relaxation time: The impressive increase of the relaxation time – or of the viscosity – of liquids in the supercooled phase is vividly shown in the so-called "Angell plot" [53], figure 1.1 (right). Approaching T_g, the relaxation time increases up to 14 decades in a narrow range of temperatures. A qualitative classification in "Strong" and "Fragile" glass-forming can be made on the how the viscosity changes as a function of the temperature – see figure 1.1 (right). A good fit of the relaxation time is given by the Vogel-Fulcher-Tamman law [54, 55, 56]:

$$\tau_R(T) = \tau_0 \exp\left(\frac{DT_0}{T - T_0}\right) . \tag{1.1}$$

This functional form, which dates from the twenties, allows to interpolate between strong – $T_0 \sim 0$ – and fragile – $T_0 > 0$ – behaviour. Let us stress that, once again, the temperature T_0 must be extrapolated from data.

It is quite interesting that in most systems the quantitative relation $T_K \sim T_0$ is valid. If this equality holds, some kind of phase transition should take place at $T_0 \sim T_K$. This phase transition should be characterized by a dynamic – a diverging relaxation time – and by a thermodynamic signature – the vanishing of the excess entropy causes a downward jump of the specific heat. This thermodynamic phase transition at $T_K = T_0$, usually called in the

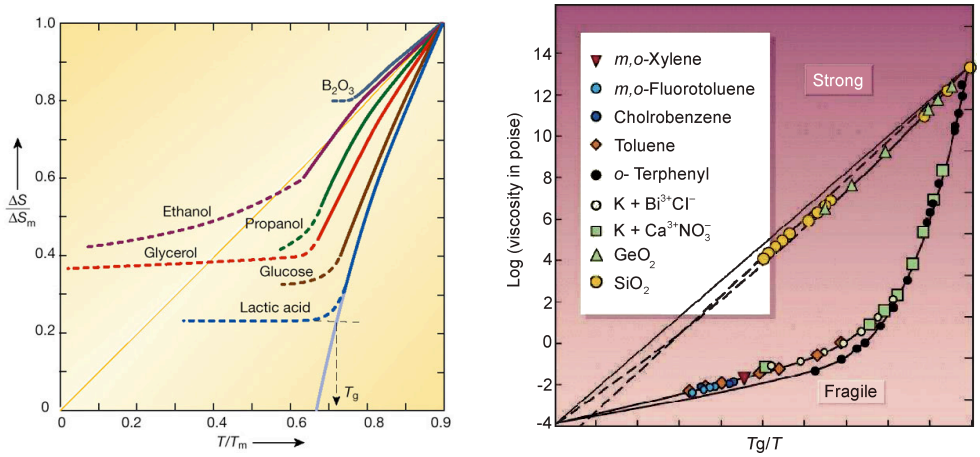

Figure 1.1: Left: temperature dependence of the entropy difference between several supercooled liquids and their stable crystals at atmospheric pressure. ΔS_m is the melting entropy and T_m is the melting temperature. The figure is taken from [46] and adapted from [52]. Right: representation of liquid viscosities showing Angell's strong-fragile pattern. The figure is taken from [46] and adapted from [57, 58].

literature ideal glass transition, can then be responsible of the phenomenology that we see at the accessible temperatures. As said before, the glass "transition" at T_g becomes only a precursor of the real ideal glass transition at T_K.

1.1.3 The Goldstein scenario

One of the most appealing theoretical frameworks which tries to describe the behaviour of supercooled liquids was introduced by Goldstein [59] forty years ago. The paradigm of Goldstein scenario is that the slow dynamics of supercooled liquids can be understood in terms of the topology of the energy landscape of the system. This should be characterized by a global minimum – corresponding to the crystal – and by local amorphous minima. Below T_g, the system evolves in the phase space through activated jumps between different amorphous minima, separated by potential energy barriers. In the real space, the potential energy barriers correspond to the *local* rearrangements of particles. Let us stress that the idea of describing the slowing dynamics of a system in terms of a corrugated energy – or free-energy – landscape provides a quite general framework to describe observed behaviours in liquids and glasses but also in other scientific domains. Some years later, it was found that this feature is also shared by some mean-field spin-glass models.

The entropy crisis phenomenon presented above has a clear description in the Goldstein scenario. We can hypothesize that the entropy of an equilibrium liquid S_L can be split in two parts: a vibrational contribution corresponding to the intra-minimum short-time vibrational dynamics S_{vib}, and a configurational contribution given by the large number $\mathcal{N}$ of different amorphous minima $S_{conf} = 1/N \log \mathcal{N}$. On the other hand the entropy of the crystal can have only a vibrational contribution. If we assume that the vibrational contribution to the entropy of the liquid and of the crystal are the same, we obtain that the excess entropy measured in Kautzmann experiment is the configurational entropy of the supercooled liquid. According to this scenario, lowering the temperature, the number of amorphous minima decreases. We can think that the slow dynamics of supercooled liquids is due to the difficulty of the system to jump between the decreasing number of amorphous minima. If at T_K the excess entropy vanishes, at the ideal-glass-transition temperature the number of thermodynamic amorphous

minima becomes sub-exponential. The system remains trapped within one of these minima and the ergodicity is broken.

Let us now consider the behaviour of the viscosity of fragile glass formers. The viscosity change as a function of the temperature follows a super-Arrenius law: the energy barriers between amorphous minima grow as temperature is decreased. As stressed before, the energy barriers correspond to local rearrangement of particles. Therefore, it is natural to think that when barriers increase, it is because the number of particles involved in the rearrangement increases: an amorphous order propagates into the glass former when the temperature is lowered.

1.1.4 What is missing?

We ended the last paragraph saying that an amorphous order should propagate into the supercooled liquid when the temperature is lowered. This is quite natural, since an increasing relaxation time is in general accompanied by an extension of the cooperative regions. The finding of a static correlation function displaying an increasing correlation length approaching the glass transition should be a strong hint that the ideal glass transition is a correct picture of the behaviour of glass forming liquids. Despite several years of researches in the field, the existence of a diverging static correlation length is still an open question. Simple static correlation functions are featureless in the supercooled regime, notwithstanding the dramatic changes in the dynamics. The static structure of the particles in a supercooled liquid close to T_g, and even in a out-of equilibrium glass former below T_g, is indistinguishable from that of a liquid at temperatures well above T_g. In order to detect increasing lengthscales two possibilities have been pursued.

Firstly, it has been observed that the dynamics of glass-froming liquids is very heterogeneous [60]. The heterogeneity in the dynamic can be quantified by multi-point correlation functions allowed to detect growing *dynamic* correlation lengths [61, 62, 63, 64]. On the other hand, a possibility is to look for a *static* growing lengthscale using nonstandard thermodynamic methods. Recent analytical [65] and numerical [66] results suggest that *point-to-set*, instead of usual *point-to-point*, correlation functions must be considered in order to detect the amorphous order in supercooled liquids.

1.2 Some theoretical framework

We concluded the last section with the claim that *point-to-set* correlation functions can be a correct thermodynamic tool to detect the amorphous order propagating in supercooled liquids approaching the glass transition. In order to justify this statement, in this section we present some theoretical frameworks to the glass transition that have been introduced in the past. We firstly present the p-spin model [9], a spin-glass model in the 1RSB class, presenting some interesting analogies with the phenomenology of the glass transition presented in previous sections. Inspired by the phenomenology of 1RSB models [11, 12, 13], Kirkpatrick, Thirumalai and Wolynes [67, 14] proposed the Random First Order Transition (RFOT) theory of the glass transition. Recently RFOT has been rephrased in a thermodynamical framework by Biroli and Bouchaud [68], allowing to introduce a protocol to detect amorphous order in supercooled liquids, and than to the introduction of *point-to-set* correlation functions.

1.2.1 1RSB spin-glass models

The Random Energy Model [8], the p-spin model [9] and the q-states Potts glass model [69] belong to the universality class of 1RSB spin-glass models. In the following we will consider the spherical p-spin model, see [70] for a pedagogical introduction. The simplicity of this model allows to study analytically its features. The Hamiltonian reads:

$$\mathcal{H}[J,S] = -\sum_{i_1<i_2<\cdots<i_p} J_{i_1 i_2 \ldots i_p} S_{i_1} S_{i_2} \cdots S_{i_p} \quad p \geq 3 \tag{1.2}$$

where the spins are real continuous variables. In order to keep the energy finite, we have to impose a constraint on the spins $\sum_i^N S_i = N$. The couplings are Gaussian independent random variables with variance $p!/(2N^{p-1})$. The study of the thermodynamics of the p-spin model allows to identify a critical temperature T_s. In order to correctly calculate the free energy of the model for $T \leq T_s$, a one-step replica-symmetric ansatz must be used. On the other hand, the study of the dynamics allows to identify a second critical temperature $T_d > T_s$ where ergodicity breaking takes place. Quite remarkably, the thermodynamic is completely blind to this purely dynamic transition.

The physical features of this model become particularly transparent in terms of the Thouless-Anderson-Palmer (TAP) approach [40]. This approach can be considered as a generalization of the Curie-Weiss approach to study ordered magnets. In both approaches a free-energy function is constructed as a function of an order parameter. The minima of the free energy are identified with the states of the system. In the case of ordered ferromagnets, we consider a global order parameter: the magnetization. Two regimes can be identified in function of the temperature: an high temperature regime, where the only minimum of the free energy is the paramagnetic minimum, and low temperature regime, where two ferromagnetic minima appear. In the case of disordered system, a local order parameter must be considered, i.e. the local magnetization. We will not enter here in the details of the derivation of the TAP free energy since more attention will be devoted in chapter 3 for the SK model.

Once the TAP free energy function is calculated, we can investigate its shape as a function of the temperature. Like for ferromagnetic systems, the high temperature phase is characterized by the only paramagnetic minimum. At low enough temperature, the free energy presents a corrugated landscape characterized by the presence of many amorphous minima. We introduce the complexity, i.e. the equivalent of the configurational entropy in the case of glass-forming liquids, $s_c(T,f) = \frac{1}{N}\log \mathcal{N}(T,f)$ which counts the number $\mathcal{N}$ of minima of the free energy function of temperature T at given free energy f. This allows to write the partition function of the system as:

$$Z(T) = \int \mathrm{d}f \exp\left[-\frac{Nf}{T} + N s_c(T,f)\right] \quad . \tag{1.3}$$

For large N we can evaluate the integral using the saddle-point approximation:

$$Z(T) = \exp\left[-N\beta(f^*(T) - T s_c(f^*(T),T))\right] \equiv \exp[-N\beta \hat{f}(T)] \tag{1.4}$$

The value $f^*(T)$ which dominates the integral must verify the equation

$$\left.\frac{\partial s_c(T,f)}{\partial f}\right|_{f^*} = \frac{1}{T} \tag{1.5}$$

and f^* is a function of the temperature T. Let us consider the behaviour of the complexity – the number of metastable states – as a function of the temperature. In this range $T \in [T_s, T_d]$

the complexity is an increasing function, which vanishes at T_s and jumps discontinuously to zero at T_d. For temperatures $T > T_d$ the only minimum of the TAP free energy is the paramagnetic minimum, while for $T < T_s$ the number of minima is sub-exponential. If we consider the behaviour of the free energy, we notice that in the region $T \in [T_s, T_d]$ the free energy of the system $\hat{f}(T)$ is lower than the free energy $f^*(T)$ of the metastable maxima which dominates the integral (1.3). For $T > T_d$ the free energy of the system must be evaluated in the paramagnetic minimum: let's say $f_p(T)$. What happens at T_d? Quite remarkably, at T_d, $\hat{f}(T)$ and $f_p(T)$ perfectly match: the free energy is not singular at the dynamical transition. On the other hand, at T_s a true thermodynamic transition takes place: since the complexity vanishes, the specific heat makes a jump downward.

The phenomenology of the p-spin model, and in general of 1RSB models, presents some interesting analogy with the phenomenology of structural glasses. The presence of metastable states slowing the dynamics – remarkably, the dynamical equation for the p-spin model and the ones for the Mode Coupling Theory [71], the analytical theory of liquids, are formally the same – and the entropy crisis at low temperature are common features of these two so different classes of systems. Some artificial features plague mean-field 1RSB models, that one can try to fix in order to have models closer to reality:

- The long range nature of interactions: in real systems only nearest-neighbors interact.
- The presence of quenched disorder: glass formers are liquids, the frozen disorder is an artifact of spin glasses.
- The absence of crystalline phase: which is always present in glass formers.

1.2.2 Random First Order Transition Theory

In this section we will present how it is possible to construct a theory for finite-dimensional glassy systems inspired by the physics of 1RSB spin-glass models [11, 12, 13]. The original works date back to the eighties, when Kirkpatrick, Thirumalai and Wolynes formulated the Random First Order Transition (RFOT) Theory. In [14], a real space thermodynamic description of metastable states in supercooled liquids was introduced, partly inspired by the p-spin results. The main assumption of RFOT is that different physical portions of a finite-dimensional glass former can be found in different states. Let us suppose that metastable states present a phenomenology close to the 1RSB presented in the previous section. The system is at equilibrium, which implies that every state has the same free energy f^*. In order to keep different metastable states in contact, the system must present interfaces separating different states and thus pay a free-energy cost. One of the main points of RFOT is to characterize the typical length scale ξ of metastable states. Let us suppose that the system is found in a metastable state α and that a different metastable state, γ, tries to nucleate in a region of size R. In that case, the system should pay a free-energy cost due to the new surface created:

$$\Delta F_{\text{cost}} = Y(T) R^{\theta} \tag{1.6}$$

where $\theta \leq d-1$ and $Y(T)$ is a surface tension. On the other hand, being the system at equilibrium, the new metastable state γ has the same free energy than α. The thermodynamic drive to rearrange a region of radius R is provided by the fact that such a region has an exponentially large number of available states. The system has a free-energy entropic gain:

$$\Delta F_{\text{gain}} = -T s_c(T) R^d \quad . \tag{1.7}$$

The balance of entropic gain and surface cost balance at a length scale

$$\xi = \left(\frac{Y(T)}{T s_c(T)} \right)^{\frac{1}{\theta - d}} \tag{1.8}$$

which can be considered as the typical size of a metastable state. The picture deriving from the RFOT theory is thus the following. Suppose that a region of a glass former is pulled by a thermal fluctuation in a new metastable state. If its size is smaller than ξ, the new metastable state is unstable: the surface tension pushes it back to the old state. On the other hand, if the size of the region is larger than ξ, this can nucleate in one of the exponentially-numerous accessible metastable states. In the Goldstein scenario, larger metastable regions would correspond to larger energy barriers to cross dynamically to reach the new state. Metastable regions larger than ξ are thermodynamically stable, but need exponential time to rearrange. We can conclude that the typical size of metastable states is ξ. According to the so-called mosaic picture, we can then imagine a glass former as an ensemble of continuously rearranging metastable states, excited by thermal fluctuations, each one of a typical size ξ, called the mosaic length scale.

Recently a reformulation of the RFOT theory has been proposed [68]. The supercooled and spin-glass communities devoted a lot of interest to this new reformulation as it allowed to set up a protocol to detect the amorphous order in supercooled liquid. Maybe that the old question "What is missing?" of section 1.1.4 has finally found an answer.

1.2.3 RFOT theory revisited

In the first part of this section we will present the gedankenexperiment proposed in [68] in order to reformulate RFOT. Let us suppose that a glass former is trapped in a metastable state α. We identify a sphere of radius R and freeze the system outside the sphere in the state α. We concentrate on the thermodynamics of the system inside the sphere: the frozen system outside the sphere acts as a pinning field, an amorphous boundary condition, on the inside one. The partition function Z_{sphere} is the sum of two parts: a contribution from the metastable states α:

$$Z_{\text{in}} = \exp(-\beta f_\alpha R^d) \tag{1.9}$$

and a contribution from the metastable states different from α:

$$Z_{\text{out}} = \sum_{\gamma \neq \alpha} \exp(-\beta f_\gamma R^d - \beta Y(T) R^\theta) \tag{1.10}$$

If we consider R large enough in order to apply the saddle point method, we obtain:

$$\begin{aligned} Z_{\text{sphere}} &= Z_{\text{in}} + Z_{\text{out}} \\ &= \exp(-\beta f_\alpha R^d) + \sum_{\gamma \neq \alpha} \exp(-\beta f_\gamma R^d - \beta Y(T) R^\theta) \\ &\simeq \exp(-\beta f_\alpha R^d) + \int \mathrm{d}f \exp[s_c(T,f) R^d - \beta f R^d - \beta Y(T) R^\theta] \\ &\simeq \exp(-\beta f^* R^d) + \exp[s_c(T) R^d - \beta f^* R^d - \beta Y(T) R^\theta] \end{aligned}$$

Since the state α is an equilibrium state at a temperature T, its free energy is the same than the other states dominating the integral: $f^*(T)$. As in the 1RSB spin-glass models, the configurational entropy $s_c(T) \equiv s_c(T, f^*(T))$. The partition function allows us to evaluate

the probability p_{in} for the system sphere to remain in the state α or p_{out} to move to another of the exponentially numerous equilibrium states.

$$p_{\text{in}}(R) = \frac{Z_{\text{in}}}{Z_{\text{sphere}}} = \frac{\exp\left[\beta Y R^{\theta}\right]}{\exp\left[\beta Y R^{\theta}\right] + \exp\left[s_c R^{d}\right]} \tag{1.11}$$

$$p_{\text{out}}(R) = \frac{Z_{\text{out}}}{Z_{\text{sphere}}} = \frac{\exp\left[s_c R^{d}\right]}{\exp\left[\beta Y R^{\theta}\right] + \exp\left[s_c R^{d}\right]} \tag{1.12}$$

The role of the so-called "entropic driving force" and of the surface tension generated by the pinning field are now clear: according to equation (1.11), $Y(T)$ is the force trying to keep the sphere in the original state, according to equation (1.12), $s_c(T)$ is the reason to get out of the original state. This writing also allows to give a clear interpretation to the mosaic length ξ, introduced in RFOT by the equation (1.8). In this framework, a typical length-scale ξ can be defined as the length such that the two probabilities balance:

$$\xi = \left(\frac{Y(T)}{T s_c(T)}\right)^{\frac{1}{\theta - d}} \quad . \tag{1.13}$$

For small values of R, $R < \xi$, the surface tension term dominates, and we have

$$p_{\text{in}} \sim 1 \quad , \tag{1.14}$$

$$p_{\text{out}} \sim 0 \tag{1.15}$$

so that the sphere has a very small probability to change state due to the overwhelming effect of the pinning field at the interface. On the other hand, for $R > \xi$ we have the opposite,

$$p_{\text{in}} \sim 0 \quad , \tag{1.16}$$

$$p_{\text{out}} \sim 1 \tag{1.17}$$

and the sphere is found in a different state with probability one: the pinning field and the surface energy are thermodynamically overwhelmed by the configurational entropy.

1.2.4 Point-to-set correlation functions

The discussion of RFOT theory exposed in section 1.2.3 gives a protocol to measure the mosaic length in glass-former. The protocol is the following:

- Consider an equilibrium configuration C in a glass former.
- Divide the system in two regions delimited by a sphere of radius R.
- Freeze the particles outside the sphere and let the particle inside the sphere free to relax to a configuration C'.
- Introduce a notion of "similarity" between the configuration C and C' *in the center* of the sphere.
- According to the previous discussion, we expect that, for small R, the boundary conditions are strong and keep C' close to C. For large R, the boundary becomes less efficient and the system is free to rearrange.
- Define a static correlation length l_s, for example as the smallest value of R such that the similarity between C and C' becomes smaller than a preassigned value ϵ.

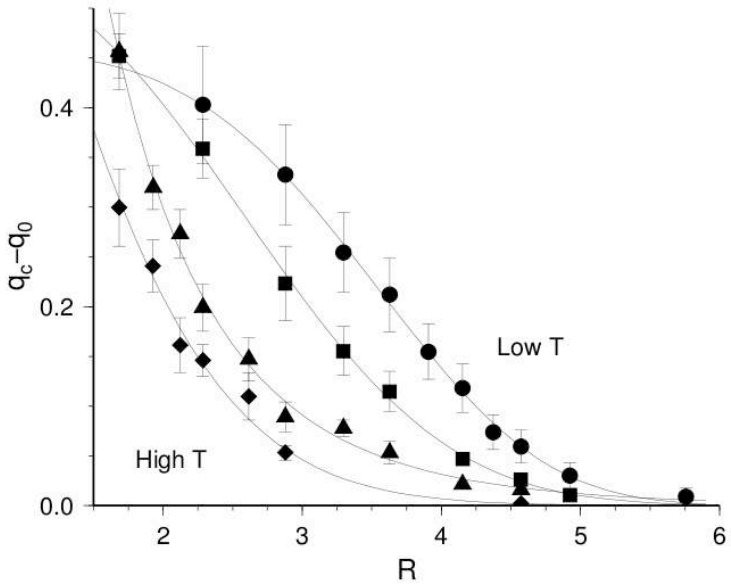

Figure 1.2: Plot of measured *point-to-set* correlation function in the soft-spheres numerical experiment performed in [66].

- Mean over different equilibrium realizations of C and C'.

Let us stress that the "similarity" between different configurations must be defined in the center of the sphere. This is one of the main ingredients in the definition of *point-to-set* correlation functions. Rigorous analytical results have been obtained in [65]. In this work, a time scale τ and a *point-to-set* length scale l are defined according to the previous description. They satisfy the following inequalities:

$$C_1 l \leq \tau \leq \exp\{C_2 l^d\} \tag{1.18}$$

where C_1 and C_2 are model dependent constants and d is the dimension of the system. The bounds between τ and l show that the growth of the relaxation time τ must be accompanied by the growth of a static correlation length l, if this is properly defined in terms of point-to-set correlation functions. This result sheds light on the conundrum of the existence of a static signature of the glass transition. A static signature exists, but, in order to be identified, we need a correct tool. Point-to-set correlation functions are one of these correct tools. Also other frameworks have been recently proposed [72, 73, 74]. On the contrary, point-to-point correlation functions are featureless near the glass transition.

The numerical study of soft-sphere particles – a model of interacting particles which presents features of a fragile glass-forming liquid – in bounded geometry has been a good background to test the predictions of this section. The protocol introduced above was implemented with Monte Carlo simulations in [75, 66]. This led to the measure of the growth of a static correlation length in a glass forming-linquid as the temperature was lowered, see figure (1.2).

In the following section we will introduce a spin-glass model with Kac interactions which allowed to calculate analytically point-to-set correlation functions.

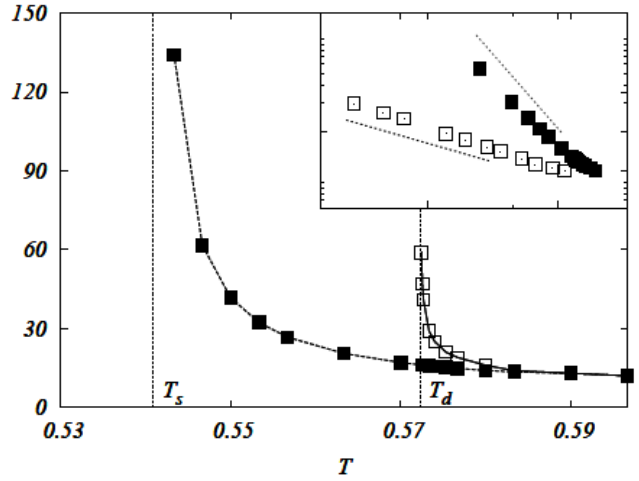

Figure 1.3: Static (filled squares) and dynamic (empty squares) lengths l_s and l_d. The vertical lines correspond to the dynamic and thermodynamic glass transition: $T_d \simeq 0.575$ and $T_s \simeq 0.541$. The lengths behave respectively as $l_s \sim (T - T_s)^{-1}$ and $l_d \sim (T - T_d)^{-1/4}$, as depicted in the inset of the figure. The figure is reprinted from [50].

1.3 Kac Spin-Glass models

Kac models are classical tools of statistical physics to study the relationship between finite dimensional systems and their mean-field counterparts. Variables interacting through a potential of range r_0 are considered in these models. For any finite values of r_0 the general properties of finite dimensional systems, such as convexity of free-energy and absence of infinite life metastable states, hold. These properties break down in mean-field theory, which can be recovered in the case of r_0 scaling as the linear system size L and both lengths tend to infinity together. The relation between the two regimes can be understood studying the so-called Kac limit, where one considers a large interaction range $r_0 \to \infty$ after having performed the thermodynamic limit $L \to \infty$. The resulting theory is an improved mean-field theory that incorporate spatial dimensions [76, 77, 78, 79, 80, 81, 82, 50, 83], see [84] for a recent review.

1.3.1 The model

We consider a finite-dimensional version of the spherical p-spin model, defined on a d-dimensional cubic lattice Λ of linear size L, whose elementary degrees of freedom are spins $S_i \in \mathbb{R}$ with $i \in \Lambda$. We introduce the interaction range $\gamma^{-1} > 0$ and a non negative rapidly decreasing function $\psi(x)$ normalized by: $\int \mathrm{d}^d x \psi(|x|) = 1$. We define the local overlap of two configurations S^1 and S^2 as:

$$Q_{S^1 S^2}(i) = \gamma^d \sum_{j \in \Lambda} \psi(\gamma |i - j|) S^1_j S^2_j \ . \tag{1.19}$$

We impose that configurations are subjected to the local spherical constraint: $Q_{S^1 S^1}(i) = 1$ $\forall i \in \Lambda$. We then introduce the finite-range p-spin Hamiltonian:

$$H_p[S,J] = - \sum_{i_1,\ldots,i_p} J_{i_1,\ldots,i_p} S_{i_1} \ldots S_{i_p} \tag{1.20}$$

where the couplings $J_{i_1,\dots,i_p}$ are i.i.d. random variables with zero mean and variance:

$$\mathbb{E}\left[J^2_{i_1,\dots,i_p}\right] = \gamma^{pd}\sum_{k\in\Lambda}\psi(\gamma|i_1-k|)...\psi(\gamma|i_p-k|)\ . \tag{1.21}$$

γ^{-1} is the interaction range since only variables located at vertices i and j such that $|i-j| < \gamma^{-1}$ really interact. This also implies that the Hamiltonian is a random variable with zero mean and variance:

$$\mathbb{E}\left[H[S^1,J]H[S^2,J]\right] = \sum_{i\in\Lambda} f(Q_{S^1S^2}(i))\ , \tag{1.22}$$

where $f(x)$ is a polynomial with positive coefficients, for example $f(x) = x^p$, if we consider a pure p-spin model. The model can be analyzed in the Kac limit: $L, \gamma^{-1} \to \infty$ with $L \gg \gamma^{-1}$.

1.3.2 Point-to-set correlation functions

Point-to-set correlation functions can be suitably defined in Kac-glass models. In this section we will introduce the definition and the results obtained by Franz and Montanari in [50]. A more detailed physical analysis will be presented in chapter 2.

In order to define a point-to-set correlation function, we fix a reference configuration S^α drawn from the equilibrium Boltzmann measure and we consider a second configuration S that is constrained to be close to S^α outside a sphere $B(l)$ of radius l. Configurations S are then sampled with Boltzmann weight inside $B(l)$ with the boundary condition determined by S^α. We define a static point-to-set correlation length l_s to the smallest value of l such that the correlation between S^α and S decays below a preassigned value ϵ. Let us be more precise in the following lines.

Let us consider an observable $\mathcal{O}$ of the system. Given a configuration S^α, in order to sample with Boltzmann weight configurations S which must be close to S^α outside of the sphere $B(l)$ we introduce the constrained Boltzmann measure $\langle\cdot\rangle_\alpha(l)$, given by:

$$\langle\mathcal{O}\rangle_\alpha(l) \equiv \ \tfrac{1}{Z[S^\alpha]}\int \mathrm{d}S\mathcal{O}(S)e^{-\beta H[S,J]}\prod_{i\in B(l)}\delta(Q_{S^\alpha S}(i)-\bar{q}) \tag{1.23}$$

where $\int$ denotes integration over configurations satisfying the local spherical constraint and $\bar{q} \le 1$. The partition function is:

$$Z[S^\alpha] \equiv \ \int \mathrm{d}S e^{-\beta H[S,J]}\prod_{i\in B(l)}\delta(Q_{S^\alpha S}(i)-\bar{q})\ .$$

Since the local overlap is a measure of the the similarity between S and the reference configuration S^α, a point-to-set correlation function can be defined by:

$$G(l) \equiv \mathbb{E}\left\{\mathbb{E}_{S^\alpha}[\langle Q_{S^\alpha S}(0)\rangle_\alpha(l)]\right\} \tag{1.24}$$

where $\mathbb{E}$ and $\mathbb{E}_{S^\alpha}$ denotes the mean over the disorder and over the reference configuration S^α. The static length scale l_s is:

$$l_s \equiv \min\{l|G(l) < \epsilon\}\ . \tag{1.25}$$

In figure (1.3) we plot the results obtained in [50] concerning the calculation of point-to-set length scale in the p-spin Kac model. We see that a static critical temperature T_s, where l_s diverges, can be identified.

A dynamical correlation length can also be defined. Let us consider a system initialized by setting $S(t = 0) = S^\alpha$ and constrained to remain close to S^α outside the sphere $B(l)$ at all subsequent times, and let $\tau(l)$ the shortest time such that the correlation function $\langle S_0(0) S_=(t) \rangle_{\text{conn}}$ decays below ϵ. We can define a dynamic correlation length l_d by the property that $\tau(l)$ is exponentially divergent as $\gamma \to 0$ for $l < l_d$, and stays bounded for $l > l_d$. In figure (1.3) we see that this analysis allows to identify a dynamical critical temperature T_d where the dynamical correlation length l_d diverges.

Chapter 2

Kac-glass models in sandwich geometry

2.1 Motivations

We have seen that point-to-set correlation functions have been introduced in the context of RFOT in order to measure the amorphous overlap between different states. We have also seen that they can be suitably defined and analytically calculated in Kac-glass models. The very definition of point-to-set correlation functions relies on a spherical geometry. It can be interesting to test if the physical picture presented above is peculiar of the spherical geometry, or if it is a quite general phenomenon independent of the geometry of the system. To this aim, we have studied the behaviour of Kac-glass models in the so called *sandwich*-geometry [41].

The sandwich-geometry is implemented by considering three regions of the lattice Λ: $A^+(l)$, $A^-(l)$ and a box $B(l)$, Figure (2.1). In this geometry point-to-set correlation functions can be defined as before, considering the system free to evolve in the central region $B(l)$, with the boundary conditions imposed by the fixed reference configuration in $A^+(l)$ and $A^-(l)$. Let us stress that the main difference between the spherical and the sandwich geometry is the fact that the first one is bounded, while the second one is unbounded. We will see that, in the context of Kac-glass models, point-to-set correlation functions behave exactly the same in the two geometries. Some time after our work, Gradenigo et al. [85] analyzed the same problem in the framework of numerical simulations on a soft-spheres glass model. In the same work, also the RFOT in sandwich geometry has been studied.

The main assumption of RFOT is that a supercooled liquid is composed of different

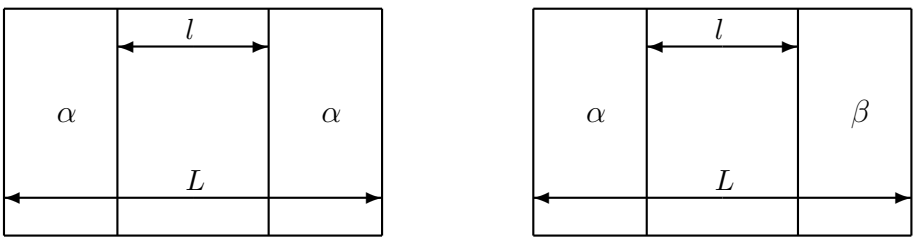

Figure 2.1: The *sandwich*-geometry for a system $\alpha\alpha$ (left) and $\alpha\beta$ (right). The box $B(l)$ is the central region, $A^+(l)$ and $A^-(l)$ are the lateral ones.

metastable states which are in contact. Mosaic length scales can be determined by the competition of a surface-tension cost between different states and and entropic gain. The interfaces between different metastable states are usually referred to as "amorphous domain walls". In recent numerical experiments, Cammarota et al. [86] measured the energy paid to put different metastable states in contact. The procedure is the following: freeze two states α and β, exchange a sphere of the state α with a sphere of the state β and let the system evolve. We can show that a spherical – or in general a bounded – geometry is not the good framework to measure the energy cost to put different metastable states in contact. In order to do this, let us consider, for simplicity, a Ising-like model described by an Hamiltonian H. We freeze a configuration S^α in a region A of the system. We study the thermodynamic considering only configurations S constrained to be close to S^α is A:

$$Z[S^\alpha] = \sum_S e^{-\beta H[S]} \chi_A[S,S^\alpha] \ , \tag{2.1}$$

where

$$\chi_A[S^1,S^2] = \begin{cases} 1 & \text{if } \ \mathrm{S}_\mathrm{i}^1 = \mathrm{S}_\mathrm{i}^2 \qquad \forall i \in A \\ 0 & \text{otherwise} \end{cases} \ . \tag{2.2}$$

The thermodynamic average of an observable $\mathcal{O}$ of the system is obtained by averaging with constrained Boltzmann measure the configurations inside the sphere and with Boltzmann measure the configurations S^α:

$$\langle \mathcal{O} \rangle = \sum_{S^\alpha} \frac{e^{-\beta H[S^\alpha]}}{Z} \sum_S \chi_A[S,S^\alpha] \frac{e^{-\beta H[S]}}{Z[S^\alpha]} \mathcal{O}(S) \ . \tag{2.3}$$

This average coincides with the usual thermodynamical one: $\frac{1}{Z}\sum_S e^{-\beta H[S]}\mathcal{O}(S)$. This simple fact has deep implications: in the case in which A is a sphere of radius R, on average, the energy per degree of freedom is independent of R. If, for typical choices of the position of the sphere, one finds that two thermodynamic states coexist for a well defined value of R, they will have the same energy.

The same argument may not be true if we consider a different geometry, i.e. the sandwich geometry. In that geometry, a good prescription, in order to measure energetic cost to put different metastable states in contact, is to fix a reference configuration S^α in $A^+(l)$, a different reference configuration S^β in $A^-(l)$, and let the system in $B(l)$ free to evolve with the boundary conditions imposed by the fixed reference configurations. This analysis will be presented in detail in the following sections. The same experiment has been carried in the context of numerical simulations of soft spheres by Gradenigo et al. in [85].

2.2 Definitions

In the following we will consider a system in the sandwich geometry. As introduced before, we can consider two kinds of systems:

- system $\alpha\alpha$: we fix a configuration S^α drawn from the Boltzmann equilibrium measure. We consider the thermodynamics of configurations S constrained to be close to S^α both in $A^+(l)$ and in $A^-(l)$;

- system $\alpha\beta$: we fix two configurations S^α and S^β drawn from the Boltzmann equilibrium measure. We consider the thermodynamics of configurations S constrained to be close to S^α in $A^+(l)$ and to S^β in $A^-(l)$.

Let be $\mathcal{O}$ an observable of the system and $\bar{q} \leq 1$. For a system $\alpha\beta$, we can define the constrained Boltzmann measure $\langle\cdot\rangle_{\alpha\beta}(l)$ by:

$$\begin{aligned}\langle\mathcal{O}\rangle_{\alpha\beta}(l) \equiv & \frac{1}{Z[S^{\alpha}_{A^+},S^{\beta}_{A^-}]} \int \mathrm{d}S\mathcal{O}(S)e^{-\beta H[S,J]} \\ & \times \prod_{i\in A^-} \delta(Q_{S^{\alpha}S}(i)-\bar{q}) \prod_{i\in A^+} \delta(Q_{S^{\beta}S}(i)-\bar{q})\end{aligned} \tag{2.4}$$

where $\int$ denotes integration over configurations satisfying the local spherical constraint. The partition function is:

$$\begin{aligned}Z[S^{\alpha}_{A^+},S^{\beta}_{A^-}] \equiv & \int \mathrm{d}S e^{-\beta H[S,J]} \\ & \times \prod_{i\in A^-} \delta(Q_{S^{\alpha}S}(i)-\bar{q}) \prod_{i\in A^+} \delta(Q_{S^{\beta}S}(i)-\bar{q}) \ .\end{aligned} \tag{2.5}$$

For a system $\alpha\alpha$, the constrained Boltzmann measure $\langle\cdot\rangle_{\alpha\alpha}(l)$ is obtained by imposing the constraint $\prod_{i\in A^+\cup A^-} \delta(Q_{S^{\alpha}S}(i)-\bar{q})$.

Let us define some observables we are interested in. In the following, the symbol $\mathbb{E}$ represents the average over both the distribution of fixed configurations S^{α} and S^{β} and the disorder. The free energy $F_{\alpha\beta}(l)$ is:

$$F_{\alpha\beta}(l,T) \equiv -\frac{1}{\beta}\ \mathbb{E}\left[\ln Z[S^{\alpha}_{A^+},S^{\beta}_{A^-}]\right] \ . \tag{2.6}$$

The internal energy $U_{\alpha\beta}(l,T)$:

$$U_{\alpha\beta}(l,T) \equiv \mathbb{E}\left[\langle H[S,J]\rangle_{\alpha\beta}(l)\right] = \mathbb{E}\left[-\frac{\partial}{\partial\beta}\ln Z[S^{\alpha}_{A^+},S^{\beta}_{A^-}]\right] \ .$$

The same quantities can be straightforwardly be defined for a system $\alpha\alpha$. We are interested to measure

$$Y(l,T) \equiv \lim_{\gamma\to 0}\lim_{L\to\infty} \frac{F_{\alpha\beta}(l,T)-F_{\alpha\alpha}(l,T)}{L^{d-1}} \ . \tag{2.7}$$

$Y(l,T)$ can be interpreted as a free-energy cost per unit area to put different metastable states at a distance l, then an effective, distance-dependent, surface tension. On the other hand, the energy cost to put different metastable states in contact can be written as:

$$K(l,T) \equiv \lim_{\gamma\to 0}\lim_{L\to\infty} \frac{U_{\alpha\beta}(l,T)-U_{\alpha\alpha}(l,T)}{L^{d-1}} \ . \tag{2.8}$$

We will see in the following section that all these quantities can be calculated in the Kac limit.

2.3 Some calculations

In this section we will briefly present how the quantities defined before can be calculated in the Kac limit. Let us consider a system $\alpha\beta$ and compute the free energy $F_{\alpha\beta}(l,T)$. The average of the partition function over $\mathbb{E}$ can be taken by introducing replicas along the lines of [78, 50]:

$$\begin{aligned}F_{\alpha\beta}(l,T) &\equiv -\frac{1}{\beta}\mathbb{E}\left[\ln Z[S^{\alpha}_{A^+},S^{\beta}_{A^-}]\right] \\ &= -\frac{1}{\beta}\lim_{m,n\to 0}\frac{1}{n}\mathbb{E}_J\left[Z^{m-2}\int \mathrm{d}S^{\alpha}\mathrm{d}S^{\beta}\exp\left[-\beta(H[S^{\alpha},J]+H[S^{\beta},J])\right]Z^{n}[S^{\alpha}_{A^+},S^{\beta}_{A^-}]\right]\end{aligned}$$

Performing the mean over the disorder $\mathbb{E}_J[\cdots]$ we obtain:

$$F_{\alpha\beta}(l,T) = -\frac{1}{\beta}\lim_{m,n\to 0}\frac{1}{n}\int\prod_{a=1}^{m+n}\mathrm{d}S^a\mathcal{C}(l)\exp\left[\frac{\beta^2}{2}\sum_{i\in\Lambda}\sum_{1\le a,b\le n}f(Q_{ab}(i))\right]$$

where $\mathcal{C}(l)$ is the constraint:

$$\mathcal{C}(l) = \prod_{a=m+1}^{m+n}\left[\prod_{i\in A^+}\delta(Q_{s^{m-1}s^a}(i)-\bar{q})\prod_{i\in A^-}\delta(Q_{s^m s^a}(i)-\bar{q})\right] .$$

Integrals over spin variables are then treated for an $(m+n)\times(m+n)$ matrix order parameter $q_{ab}(i)$:

$$F_{\alpha\beta}(l,T) = -\frac{1}{\beta}\lim_{m,n\to 0}\frac{1}{n}\int\prod_{i\in\Lambda}\prod_{a,b=1}^{m+n}q_{ab}(i)\mathcal{C}(l)\exp\left[\sum_{i\in\Lambda}\left(\frac{\beta^2}{2}\sum_{1\le a,b\le n}f(q_{ab}(i)))+\frac{1}{2}\log\det q(i)\right)\right] .$$

Performing the coarse graining – rescaling the position to define $x = i\gamma \in [-\hat{L},\hat{L}]^d$, $\hat{L}\equiv\gamma L$ – we obtain:

$$F_{\alpha\beta}(\hat{l},T) = -\frac{1}{\beta}\lim_{m,n\to 0}\frac{1}{n}\int[\mathrm{d}q_{ab}]\exp\left[\frac{1}{\gamma^d}\int\mathrm{d}x\left(\frac{\beta^2}{2}\sum_{1\le a,b\le n}f((\psi*q)_{ab}(x)))+\frac{1}{2}\log\det q(x)\right)\right]\mathcal{C}(\hat{l}) .$$

We introduce the following notation:

$$F_{\alpha\beta}(\hat{l},T) = -\frac{1}{\beta}\lim_{m,n\to 0}\frac{1}{n}\int[\mathrm{d}q_{ab}]e^{-\frac{1}{\gamma^d}\mathcal{S}_{\alpha\beta}(q_{ab})} . \tag{2.9}$$

The dependency upon γ is now completely explicit and, for $\gamma\to 0$, the functional integral can be performed using the saddle-point method. We look for a replica symmetric saddle point $q^{\mathrm{RS}}_{ab}(x)$. This is characterized by three scalar functions $p_1(x)$, $p_2(x)$ and $q(x)$; p_1 and p_2 are the local overlap between the constrained configuration and the reference configuration S^α and S^β respectively and q is the local overlap of two constrained configurations when they belong to the same metastable state (see Appendix 2.6 for more details). Using this ansatz we obtain that $\mathcal{S}_{\alpha\beta}(q_{ab}) = n\int\mathcal{L}_{\alpha\beta}\mathrm{d}^dx + O(n^2)$, where:

$$\begin{aligned}\mathcal{L}_{\alpha\beta}(x) = \; & -\tfrac{\beta^2}{2}[f(1)+2f((\psi*p_1)(x))+2f((\psi*p_2)(x))-f((\psi*q)(x))]+\\ & +\tfrac{1}{2}\left[\log(1-q(x))-\tfrac{p_1^2(x)+p_2^2(x)-q(x)}{1-q(x)}\right]\end{aligned} \tag{2.10}$$

with:

$$(\psi*q)(x) = \int\mathrm{d}^dy\psi(|y-x|)q(y) . \tag{2.11}$$

The constraint enforcing S to be close to S^α in $A^-(\hat{l})$ and to S^β in $A^+(\hat{l})$ is fulfilled by setting $p_1(x)=\bar{q}$ for $x\in A^-(\hat{l})$ and $p_2(x)=\bar{q}$ for $x\in A^+(\hat{l})$. We obtain $F_{\alpha\beta}(\hat{l},T)$ by evaluating the fields $p_1(x)$, $p_2(x)$ and $q(x)$ in the saddle point of the action $\mathcal{S}^0_{\alpha\beta}=\int\mathrm{d}^dx\mathcal{L}_{\alpha\beta}(x)$. The internal energy $U_{\alpha\beta}(\hat{l},T)$ can be calculated in the same lines (see Appendix 2.7 for more details) and expressed in terms of the saddle point fields $p_1(x)$, $p_2(x)$ and $q(x)$:

$$U_{\alpha\beta}(\hat{l},T) = -\beta\int\mathrm{d}x\,[1+f((\psi*p_1)(x))+f((\psi*p_2)(x))-f((\psi*q)(x))] . \tag{2.12}$$

We introduce a simplification in the Lagrangians: we expand the terms of the form $f((\psi*q)(x))$ in gradient of $q(x)$ and we truncate to the second order obtaining $f(q(x))-cf''(q(x))(\nabla q)^2(x)$ where $c=\frac{1}{2d}\int z^2\psi(|z|)\mathrm{d}z^d$ (in our running example $c=1$). We find the saddle-point fields iterating numerically the Euler-Lagrange equations of (2.10).

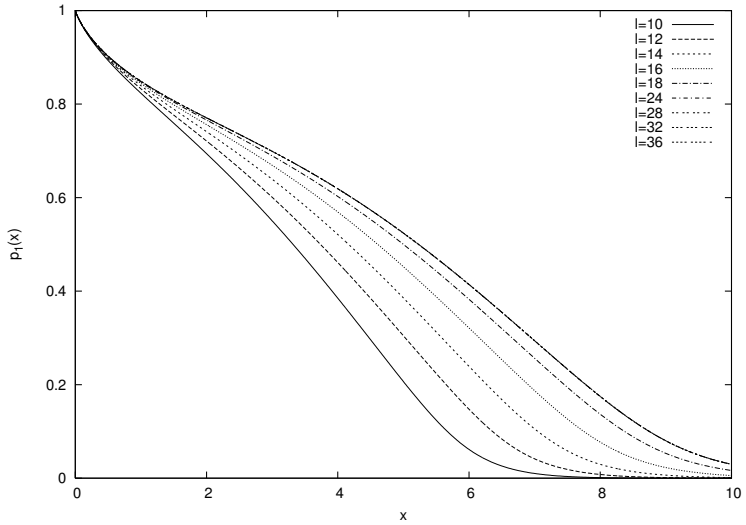

Figure 2.2: Plot of the profiles of the saddle-point field $p_1(x)$ for a system $\alpha\beta$ at temperature $T = 0.8$ for different values of the box $\hat{l}$. At this temperature $\hat{\xi}_s \sim 24$.

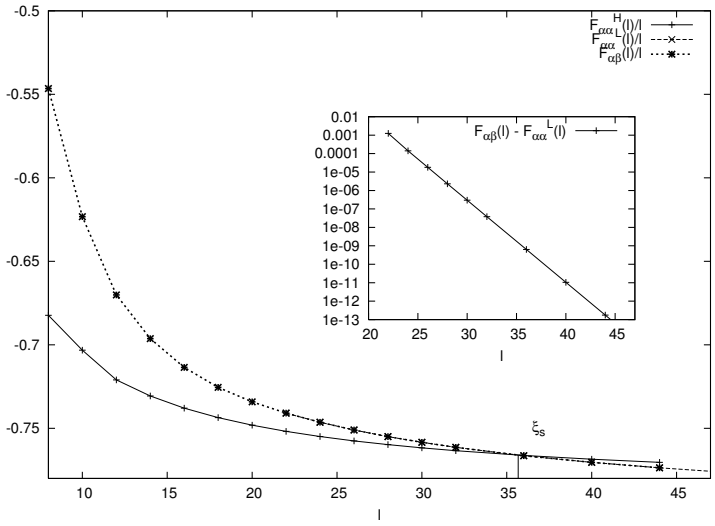

Figure 2.3: Main figure: Plot of the sub-extensive part of the free energy divided by the size as a function of $\hat{l}$ for a system at a temperature $T = 0.7874$ of: high-overlap minimum of a system $\alpha\alpha$, $\hat{F}^H_{\alpha\alpha}(\hat{l})/\hat{l}$; low-overlap minimum of a system $\alpha\alpha$, $\hat{F}^L_{\alpha\alpha}(\hat{l})/\hat{l}$; unique minimum of a system $\alpha\beta$, $\hat{F}_{\alpha\beta}(\hat{l})/\hat{l}$. The static correlation length $\hat{\xi}_s$ is pointed out. Using this scale $\hat{F}^L_{\alpha\alpha}(\hat{l})$ and $\hat{F}_{\alpha\beta}(\hat{l})$ are indistinguishable. Inset: the difference $\hat{F}^L_{\alpha\alpha}(\hat{l}) - \hat{F}_{\alpha\beta}(\hat{l})$ in logarithmic scale.

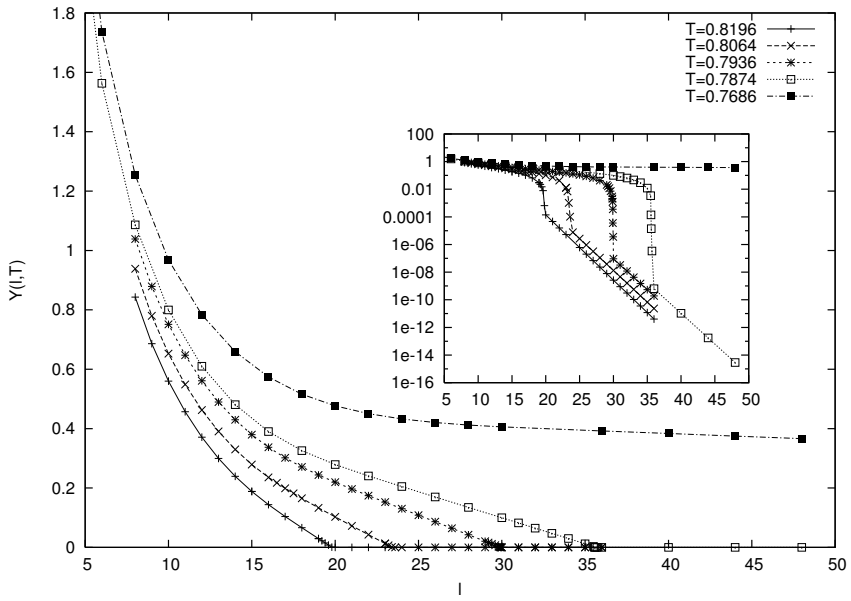

Figure 2.4: Plot of $Y(l,T)$ for different temperatures as a function of the width of the box $\hat{l}$. We remember that $T_s \approx 0.766287$ and $T_d \approx 0.813526$.

2.4 Results

The overlap profiles

The system $\alpha\alpha$ has been studied in spherical geometry in [50]. We have verified that the physical picture of the $\alpha\alpha$ system does not depend on the geometry: the saddle point equations for the fields $p(x)$ and $q(x)$ are the same in spherical and sandwich geometry. We can thus borrow some results from [50]. Two critical temperatures characterize the system: $T_s \approx 0.766287$ and $T_d \approx 0.813526$.

Setting the temperature of the system $T \gtrsim T_d$, we identify two lengths: $\hat{l}_0(T)$ and $\hat{\xi}_d(T)$, such that, for widths of the box $\hat{l} \in [\hat{l}_0(T), \hat{\xi}_d(T)]$, the action $\mathcal{S}^0_{\alpha\alpha}$ has two local minima. A minimum is characterized by a saddle-point field $p(x)$ rapidly decaying to zero in the interior of the box: we name this low-overlap minimum. The other minimum is characterized by a saddle-point field $p(x)$ everywhere large: we name this high-overlap minimum. For $\hat{l} > \hat{\xi}_d$ ($\hat{l} < \hat{l}_o$) only the low-(high-)overlap minimum exists. $\hat{\xi}_s(T)$ is defined as the minimum value of $\hat{l}$ such that the low-overlap minimum is the global minimum of the action. Within this picture we can identify two characteristic length scales: a dynamic length scale $\hat{\xi}_d(T)$ and a static length scale $\hat{\xi}_s(T)$. The interpretation of these length scales has been given in section 1.3.2. The critical temperatures T_s and T_d are defined as the temperatures at which $\hat{\xi}_s(T)$ and $\hat{\xi}_d(T)$ respectively diverge.

On the other hand, in the case of a system $\alpha\beta$, the action $\mathcal{S}^0_{\alpha\beta}$ has always a single minimum. Profiles of the saddle-point field $p_1(x)$ can be seen in Figure 2.2.

The free energy

We present in Figure 2.3 the plot of the sub-extensive part of the free energy of high-(low-)overlap minimum $\hat{F}^H_{\alpha\alpha}(\hat{l})$ ($\hat{F}^L_{\alpha\alpha}(\hat{l})$) divided by the size $\hat{l}$ for a system at a temperature $T_s < T < T_d$. $\hat{\xi}_s(T)$ is the value of $\hat{l}$ where $\hat{F}^L_{\alpha\alpha}(\hat{l})$ and $\hat{F}^H_{\alpha\alpha}(\hat{l})$ cross. We name the global free energy of a system $\alpha\alpha$ $F_{\alpha\alpha}(\hat{l}) = \min\left\{F^L_{\alpha\alpha}(\hat{l}), F^H_{\alpha\alpha}(\hat{l})\right\}$.

The sub-extensive part of the free energy of the unique minimum $\hat{F}_{\alpha\beta}(\hat{l})/\hat{l}$ for a temperature $T_s < T < T_d$ is also plotted in Figure 2.3. At all temperatures and values of $\hat{l}$ that we have studied, the sub-extensive part of the free energy of a system $\alpha\beta$ $\hat{F}_{\alpha\beta}(\hat{l})$ is close to the sub-extensive part of the low-overlap free energy of a system $\alpha\alpha$ $\hat{F}_{\alpha\alpha}(\hat{l})$, as can be seen in the inset of Figure 2.3.

In Figure 2.4 we follow the evolution of $\hat{l}$-dependent surface tension $Y(\hat{l},T)$ for systems at different temperatures $T > T_s$. We note that the static correlation length $\hat{\xi}_s(T)$ separates two regimes. For $\hat{l} < \hat{\xi}_s(T)$, $Y(\hat{l},T)$ has a power-law followed by a linear decrease. For $\hat{l} > \hat{\xi}_s(T)$, as we see in the inset of Figure 2.4, the decrease becomes exponential:

$$Y(\hat{l},T) \sim C\ e^{-\hat{l}/\tilde{l}}, \tag{2.13}$$

with $\tilde{l}$ weakly dependent on the temperature and showing no evident relation with $\hat{\xi}_s$. This shows that the surface tension $Y(\hat{l},T)$ is sensibly different from zero only for $\hat{l} \lesssim \hat{\xi}_s$. A similar result has been obtained in [87]. In that case the interface free energy has been obtained changing the boundary conditions along one direction, from periodic to anti-periodic.

Particular attention must be spent in the case $T = T_s$. At T_s, the static correlation length $\hat{\xi}_s$ diverges. This means that the high-overlap minimum is the global minimum of the action

$\mathcal{S}^0_{\alpha\alpha}$ for all the values of $\hat{l}$. We see in Figure 2.4 that, for T approaching T_s, the profile of $Y(\hat{l},T)$ takes the shape of a plateau. Consequently, at the critical temperature T_s, in the limit $\hat{l} \to \infty$, the surface tension $Y(\hat{l},T_s)$ does not fall to zero and takes a limiting value $Y(T_s)$. Arguably, the value $Y(T)$ is different from zero for temperatures $T < T_s$.

According to phenomenological arguments [68], the static correlation length $\hat{\xi}_s(T)$ can be interpreted as the typical size of metastable states of a system at a temperature T. Following this idea, in a system $\alpha\beta$ we are freezing a patchwork of metastable states of size $\hat{\xi}_s(T)$ outside the box and letting the system free to rearrange inside the box. If the width of the box is larger than the typical metastable-state size, $\hat{l} \gg \hat{\xi}_s(T)$, the system inside the box has enough space to rearrange in many different metastable states. On the contrary, when the width of the box is smaller than the metastable-state size, $\hat{l} < \hat{\xi}_s$, since there is not enough space to create metastable states on the interior, the frozen states are in contact and "repel" each other. This explains why the surface tension $Y(\hat{l},T)$ is significantly different from zero only for $\hat{l} < \hat{\xi}_s(T)$ and why the overlap profiles $p_1(x)$ and $p_2(x)$ between frozen metastable states and the interior of the box decrease faster for small boxes. At the critical temperature T_s the size of metastable states diverges. Consequently, the surface tension takes a finite value also in the limit $\hat{l} \to \infty$.

The internal energy and the entropy

We verified that for a system $\alpha\alpha$ the high-overlap and the low-overlap phases have the same internal energy $U_{\alpha\alpha}(\hat{l},T)$, as motivated in section 2.1. In Figure 2.5 we follow the evolution of the sub-extensive part of $U_{\alpha\beta}(\hat{l}) - U_{\alpha\alpha}(\hat{l})$ for different temperatures of the system. In this case, we note a power-law followed by a an exponential decrease.

We also computed the configurational entropy Σ as a function of the size $\hat{l}$ of the box, Figure 2.6. For a system $\alpha\alpha$ only the low-overlap phase presents a configurational entropy $\Sigma_{\alpha\alpha}$ different from zero. As noticed in [50], for $\hat{l} < \hat{l}^{1RSB}$ the replica-symmetric solution is incorrect since it gives a negative entropy. We found that the same is true for a system $\alpha\beta$. In the inset of Figure 2.6 we plot the difference between the configurational entropy of the two systems. We note that this quantity is a decreasing function of the size $\hat{l}$ of the system. This is consistent with the observation that the system loses memory of the frozen exterior for large sizes of the box.

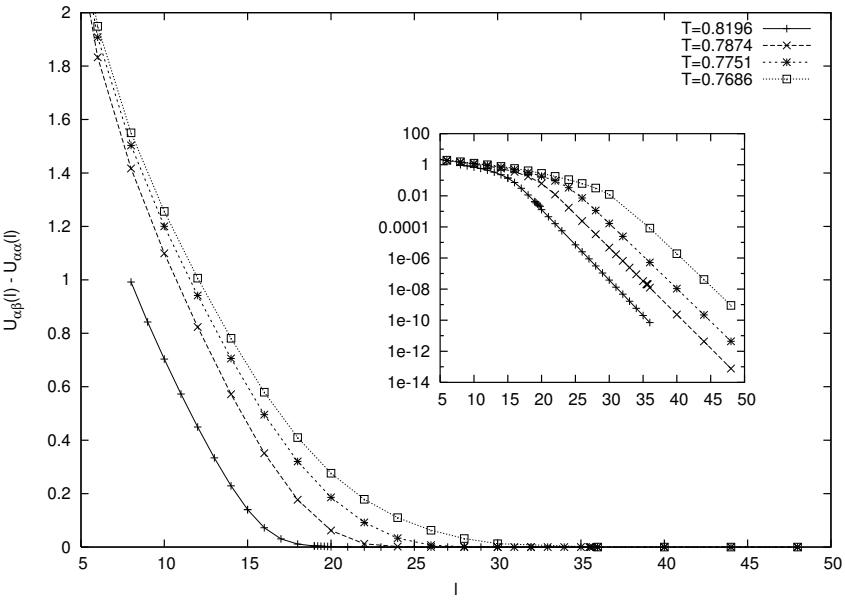

Figure 2.5: Plot of $U_{\alpha\beta}(\hat{l}) - U_{\alpha\alpha}(\hat{l})$ for different temperatures as a function of the width of the box $\hat{l}$. We remember that $T_s \approx 0.766287$ and $T_d \approx 0.813526$.

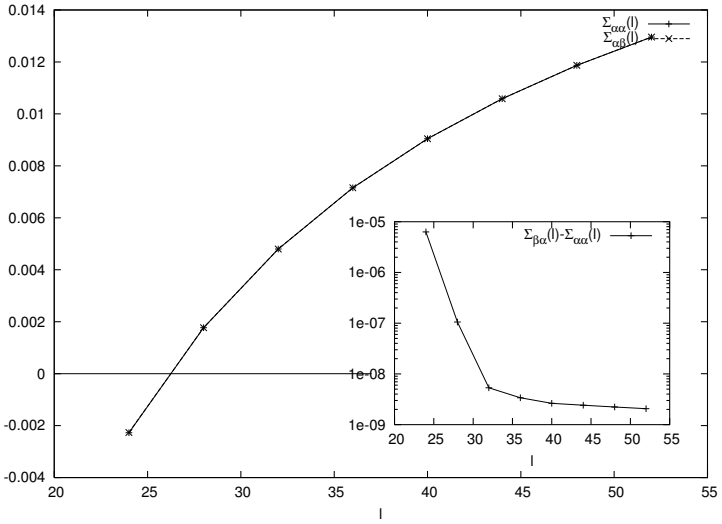

Figure 2.6: Main figure: The configurational entropy $\Sigma_{\alpha\alpha}(l)$ in function of l for a system $\alpha\alpha$ and $\Sigma_{\alpha\beta}(l)$ for a system $\alpha\beta$ at a temperature $T = 0.8$. Inset: the difference $\Sigma_{\alpha\beta}(l) - \Sigma_{\alpha\alpha}(l)$.

2.5 Conclusions and perspectives

In this chapter we have investigated the behaviour of a Kac spin-glass model in the so-called *sandwich* geometry. This particular geometry gives us the correct framework in which the energy cost to put different metastable states in contact can be measured. In the lines of our work, numerical experiments have been performed by the group of Cavagna in Rome [85]. A good qualitative agreement between the analytical and numerical results has been found. Within the sandwich-geometry framework it has been also possible to measure the free-energy cost to put metastable states in contact, that can be interpreted as a distance-dependent surface tension, one of the main ingredients of the Random First Order Theory Transition for the glass transition.

Given the recent numerical experiments of Cavagna, it would be interesting to consider the analytical and numerical results in a unifying framework which is able to correctly describe the physical behaviour of a glassy system in confined geometry.

2.6 Appendix: The overlap matrix

We give an explicit formulation of the overlap matrix in the replica symmetric ansatz $q_{ab}^{\mathrm{RS}}(x)$; the overlap matrix is an $(m+n)\times(m+n)$ matrix with m and n real numbers; if we take r and n integer, we can visualize the matrix in the following way:

$$q^{\mathrm{RS}} = \begin{bmatrix} A & B \\ B^T & C \end{bmatrix} . \tag{2.14}$$

The $n \times n$ matrix C is the overlap matrix between configuration that are taken with constrained Boltzmann measure and subjected to local spherical constraint; the replica symmetric ansatz imposes that $C_{ab} = q(x)$ for all $a \neq b$ and the spherical constraint that $C_{aa} = 1$; then C can be written in the form:

$$C = \begin{bmatrix} 1 & q(x) & q(x) & \dots & q(x) \\ q(x) & 1 & q(x) & \dots & q(x) \\ \dots & \dots & \dots & \dots & \\ q(x) & q(x) & q(x) & \dots & 1 \end{bmatrix} . \tag{2.15}$$

The $m \times m$ A matrix is the overlap matrix between configuration that are taken with Boltzmann measure and subjected to local spherical constraint; we impose the out of diagonal elements equal to zero, then we obtain that A is the identity matrix: $A = 1$.

The $m \times n$ B matrix is the overlap matrix between configuration that are taken with Boltzmann measure and configuration that are taken with constrained Boltzmann measure; we impose all the elements of this matrix equal to zero, except the last two lines that are equal to $p_1(x)$ and to $p_2(x)$; then A can be written in the form:

$$B = \begin{bmatrix} 0 & 0 & \dots & 0 \\ 0 & 0 & \dots & 0 \\ \dots & \dots & \dots & \dots \\ p_1(x) & p_1(x) & \dots & p_1(x) \\ p_2(x) & p_2(x) & \dots & p_2(x) \end{bmatrix} . \tag{2.16}$$

2.7 Appendix: Calculation of the energy

The internal energy of a system $\alpha\beta$ is:

$$U_{\alpha\beta}(l) \equiv \mathbb{E}\left[\langle H[s,J]\rangle_{\alpha\beta}(l)\right] = \mathbb{E}\left[-\frac{\partial}{\partial\beta}\ln Z[s^{\alpha}_{A^+},s^{\beta}_{A^-}]\right]$$

We give an explicit derivation of $U_{\alpha\beta}(l)$; similar calculations allow to obtain the free energy $F_{\alpha\beta}(l)$. We introduce two different temperatures β_1 and β_2 and n and m replicas of the system;

$$\begin{aligned}
U_{\alpha\beta}(l) &= \mathbb{E}\left[\mathbb{E}_{s^\alpha}\left[\mathbb{E}_{s^\beta}\left[-\frac{\partial}{\partial\beta}\ln Z[s^{\alpha}_{A^+},s^{\beta}_{A^-}]\right]\right]\right] \\
&= -\frac{\partial}{\partial\beta_2}\mathbb{E}\left[\frac{1}{Z^2[\beta_1]}\int \mathrm{d}s^\alpha \mathrm{d}s^\beta \exp\left[-\beta_1\left(H[s^\alpha,J]+H[s^\beta,J]\right)\right]\ln Z[s^\alpha,s^\beta,\beta_2]\right] \\
&= \lim_{m,n\to 0}\frac{1}{n}\left(-\frac{\partial}{\partial\beta_2}\right) \\
&\quad \mathbb{E}\left[Z^{m-2}[\beta_1]\int \mathrm{d}s^\alpha \mathrm{d}s^\beta \exp\left[-\beta_1(H[s^\alpha,J]+H[s^\beta,J])\right]Z^n[s^\alpha,s^\beta,\beta_2]\right]
\end{aligned}$$

where:

$$\mathcal{C} = \prod_{a=m+1}^{m+n}\left[\prod_{i\in A^+}\delta(Q_{s^{m-1}s^a}(i)-\bar{q})\prod_{i\in A^-}\delta(Q_{s^m s^a}(i)-\bar{q})\right] .$$

Then performing the expectation value over the disorder, the derivative and reimposing equal the temperatures we obtain:

$$\begin{aligned}
U_{\alpha\beta}(l) = \lim_{m,n\to 0}\frac{-\beta}{n} \quad & \int\prod_{a=1}^{m+n}\mathrm{d}s^a\mathcal{C}\exp\left[\tfrac{\beta^2}{2}\textstyle\sum_{i\in\Lambda}\sum_{1\le a,b\le n}f(Q_{ab}(i)))\right] \\
& \times\textstyle\sum_{i\in\Lambda}\left[\sum_{a,b\in C}f(Q_{ab}(i))+\frac{1}{2}\sum_{a,b\in B}f(Q_{ab}(i))+\frac{1}{2}\sum_{a,b\in B^T}f(Q_{ab}(i))\right] .
\end{aligned}$$

Integrals over the spin variables are then traded for an $(m+n)\times(m+n)$ matrix order parameter $q_{ab}(i)$.

$$\begin{aligned}
U_{\alpha\beta} = \lim_{m,n\to 0}\frac{-\beta}{n} \quad & \int\textstyle\prod_{i\in\Lambda}\prod_{a,b=1}^{m+n}q_{ab}(i)\mathcal{C}\exp\left[\sum_{i\in\Lambda}\left(\frac{\beta^2}{2}\sum_{1\le a,b\le n}f(q_{ab}(i)))+\frac{1}{2}\log\det q(i)\right)\right] \\
& \times\textstyle\sum_{i\in\Lambda}\left[\sum_{a,b\in C}f(q_{ab}(i))+\frac{1}{2}\sum_{a,b\in B}f(q_{ab}(i))+\frac{1}{2}\sum_{a,b\in B^T}f(q_{ab}(i))\right] .
\end{aligned}$$

Performing the coarse graining:

$$\begin{aligned}
U_{\alpha\beta} = \lim_{m,n\to 0}\frac{-\beta}{n} \quad & \int[\mathrm{d}q_{ab}]\int\mathrm{d}x\left[\textstyle\sum_{a,b\in C}f((\psi*q)_{ab}(x))+\frac{1}{2}\sum_{a,b\in B,B^T}f((\psi*q)_{ab}(x))\right] \\
& \times\exp\left[\tfrac{1}{\gamma^d}\textstyle\int\mathrm{d}x\left(\frac{\beta^2}{2}\sum_{1\le a,b\le n}f((\psi*q)_{ab}(x)))+\frac{1}{2}\log\det q(x)\right)\right]\mathcal{C} .
\end{aligned}$$

Using the replica symmetric matrix presented in 2.6 we obtain:

$$U_{\alpha\beta} = \lim_{n\to 0}\frac{-\beta}{n}\int[\mathrm{d}q][\mathrm{d}p_1][\mathrm{d}p_2]\left[n\int\mathrm{d}x\mathcal{H}(x)+o(n^2)\right]\exp\left[-\frac{n}{\gamma^d}\int\mathrm{d}x\mathcal{L}(x)+o(n^2)\right]$$

where:

$$\mathcal{H}(x) = 1+f((\psi*p_1)(x))+f((\psi*p_2)(x))-f((\psi*q)(x)) ;$$

$$\begin{aligned}
\mathcal{L}(x) = \quad & \tfrac{\beta^2}{2}\left[1+2f((\psi*p_1)(x))+2f((\psi*p_2)(x))-f((\psi*q)(x))\right]+ \\
& +\tfrac{1}{2}\left[\log(1-q(x))-\tfrac{p_1^2(x)+p_2^2(x)-q(x)}{1-q(x)}\right] .
\end{aligned}$$

We evaluate the action $\mathcal{S}^0_{\alpha\beta} = \int\mathrm{d}^dx\mathcal{L}_{\alpha\beta}(x)$ in the saddle point fields p_1, p_2 and q and we obtain that:

$$U_{\alpha\beta}(\hat{l}) = -\beta\int\mathrm{d}x\mathcal{H}(x) . \tag{2.17}$$

Part II

Spin-glass models and Extreme Value Statistics

Chapter 3

The problem of fluctuations of pseudo-critical temperatures

The characterization of phase transitions in terms of a non-analytic behaviour of thermodynamic functions in the infinite-size limit has served as a milestone in the physical understanding of critical phenomena. In laboratory and numerical experiments the system size is always finite, therefore the divergences that would result from such a non-analytical behaviour are suppressed, and are replaced by smooth maxima occurring in the observation of physical quantities as a function of the temperature. In disordered systems the pseudo-critical temperature, defined e.g. as the temperature at which this maximum occurs, is a fluctuating quantity depending on the realization of the disorder. A question naturally arises: can the fluctuations of the pseudo-critical temperature be understood and determined on employing tools from probability theory?

In these chapters we shall attempt to answer this question, investigating the fluctuations of the pseudo-critical temperature in some spin-glass models via analytic and numerical approaches. We will show how Extreme Value Statistics, a branch of probability theory, plays a fundamental role in this problem.

3.1 Motivations

We have seen in the Introduction that spin-glass models are characterized by the presence of disorder in the Hamiltonian via random couplings. The value of a generic observable $\mathcal{O}(J)$ depends on the realization of the disorder J. At first glance, this fact may look problematic: should we expect different physical behaviours for every realization of the disorder? Fortunately the answer is negative, since spin-glass models are built in such a way that *self-averaging* holds. This means that, in the thermodynamic limit, the value of observables which are extensive quantities does not fluctuate. In a more formal way, the distribution of $\mathcal{O}(J)$ as a function of the realization of J converges to a delta function in the thermodynamic limit. This property allows to have tractable models and thus to average out the disorder in the physical description.

If the system size is finite, the fluctuations of physical observables due to disorder can be strong. It may be interesting to describe these fluctuations: their scaling with the system size and the possibility of a limiting distribution for them. Recently, some authors analyzed the problem of the fluctuations of the ground-state energy of the SK model and of other spin-glass

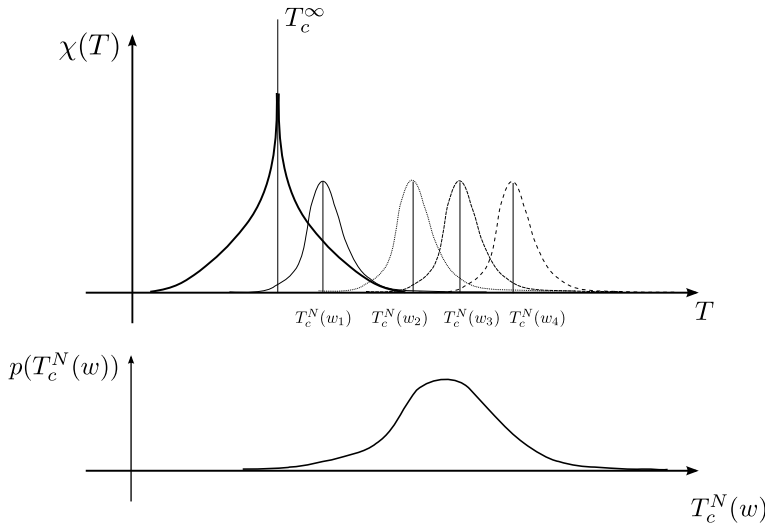

Figure 3.1: A pictorial representation of a possible definition of the pseudo-critical temperature $T_c^N(w)$ of a finite-size disordered model and its characterization in terms of its probability-distribution function $p(T_c^N(w))$

models [88, 89, 90]. This problem is also interesting from an Extreme-Value-Statistics point of view, since the the ground state is the minimum over an ensemble of correlated energies.

In this section we will consider the pseudo-critical temperature of a disordered system. It is well-known [91, 92, 93, 94] that criticality of a physical system can emerge only in the thermodynamic limit: at finite size the divergences of physical observables, characterizing the phase transition, are replaced by smooth maxima. In order to characterize the critical point of finite-size systems, a suitably-defined pseudo-critical temperature must be introduced, being the temperature at which such maxima occur. In pure systems the pseudo-critical temperature $T_c(N)$ is shifted with respect to the critical temperature T_c and, in the limit of large systems, $T_c(N)$ converges to T_c: $\lim_{N\to\infty} T_c(N) = T_c$. On the other hand, in disordered systems a pseudo-critical temperature $T_c(N,J)$ is a random variable depending on the realization of the disorder, as depicted in figure 3.1. We expect that, similarly to pure systems, in the limit of large size, the mean of a pseudo-critical temperature over the disorder converge to the infinite-size critical temperature: $\lim_{N\to\infty} \overline{T_c(N,J)} = T_c$. We also expect that, in some sense, the pseudo-critical temperature is a self-averaging quantity: its distribution converges to a delta in the large-size limit.

In the past, the characterization of the fluctuations of the pseudo-critical temperature of disordered system attracted a lot of attention from the physical community. The celebrated *Harris criterion* [95], for the behaviour of critical exponents in finite-dimensional disordered systems, relies on an argument about the local fluctuations of the critical temperature. More recently, several efforts have been put forward to study the fluctuations of the pseudo-critical temperature for disordered finite-dimensional systems [96, 97, 98, 99, 100, 101] and their physical implications. For instance, recently Sarlat et al. [102] showed that the theory of finite-size scaling, which is valid for pure systems, fails in a fully-connected disordered models because of strong sample-to-sample fluctuations of the critical temperature.

In this chapter we will introduce the tools that will allow us to study the problem of

fluctuations of the pseudo-critical temperature in spin-glass models in the following chapters. In section 3.2 we introduce the Random Matrix Theory (RMT). We show how some results of RMT have been used in the context of spin-glass models. In section 3.3 we introduce the TAP approach to spin-glass models. We analyze the TAP equations for the SK model and we present how some results of RMT theory allow to identify the critical temperature of the SK model. Finally, in section 3.4, we will introduce some results of Extreme Value Statistics, specifically the celebrated Tracy-Widom distribution, discovered in the context of RMT, and we present some physical applications of this ubiquitous distribution.

3.2 Some results of Random Matrix Theory

Ensembles of matrices with random entries have been systematically studied since the pioneering works of Wigner [103] and Dyson [104]. The purpose was to develop a statistical theory of energy levels of heavy nuclei, such that the unknown Hamiltonian (representing the complicated interactions among nucleons) is replaced by a statistical ensemble of random Hamiltonians satisfying minimal symmetry requirements. After the initial successes in Nuclear Physics, the field of random matrices has developed with countless applications in physics, mathematics and beyond. Let us mention number theory, in connection with Riemann's hypothesis [105], computational biology and genomics [106], quantum gravity [107] and multivariate data analysis and financial applications [108].

In order to define a Random Matrix Model, we have to consider an ensemble of $N \times N$ matrices X and the joint probability density function (jpdf) of the entries $P[X] := P(X_{11}, \ldots, X_{NN})$. We can require the following properties:

1. the entries are sampled independently from each other: $P[X] = \prod_{i,j} P_{ij}(X_{ij})$
2. there is a group of invariance for the probability density of entries: $P[GXG^{-1}] = P[X]$, where G is an element of the invariance group

The Gaussian ensemble is composed by square matrices having independent and normally distributed entries (real, complex or quaternion numbers), supplemented by an appropriate group invariance (orthogonal, unitary and symplectic respectively). These three ensembles are labelled by the Dyson's index $\beta = 1,2,4$ and are named Gaussian Orthogonal Ensemble (GOE), Gaussian Unitary Ensemble (GUE) and Gaussian Symplectic Ensemble (GSE) . The joint probability density of the entries can be written in the compact form:

$$P[X] = A_N \exp[-\beta \mathrm{tr}(X^2)/2] \tag{3.1}$$

where A_N is a normalization constant. Given the group invariance, the information encoded in the jpdf of entries is overabundant. The jpdf $P[X]$ in terms of N^2 independent elements can be traded for a jpdf in terms of the N real non-independent eigenvalues $\lambda_1, \ldots, \lambda_N$. For the Gaussian ensembles the jpdf of the eigenvalues takes the form:

$$P(\lambda_1, \ldots, \lambda_N) = B_N \exp\left[-\frac{\beta}{2}\left(\sum_{i=1}^{N} \lambda_i^2 - \sum_{i \neq j} \ln(|\lambda_i - \lambda_j|)\right)\right] \tag{3.2}$$

This joint law allows one to interpret the eigenvalues as the positions of charged particles, repelling each other via a 2-d Coulomb potential (logarithmic); they are confined on a 1-d line and each is subject to an external harmonic potential. The parameter β that characterizes the type of ensemble can be interpreted as the inverse temperature.

For a given Random Matrix Ensemble, one is interested in computing the density of eigenvalues $\rho(\lambda, N) \equiv \langle \sum_{i=1}^{N} \delta(\lambda - \lambda_i) \rangle / N$, where $\langle \dots \rangle$ stands for the average over the jpdf. In the limit $N \to \infty$, the density of eigenvalues can be easily calculated via the Coulomb gas analogy, introduced by Dyson [104]. On the other hand, it can be formally rewritten as:

$$\rho(\lambda, N) = \int_{-\infty}^{+\infty} \prod_{i=2}^{N} \mathrm{d}\lambda_i P(\lambda, \lambda_2, \dots, \lambda_N) \quad . \tag{3.3}$$

Wigner was able to compute this marginal and this is one of the central results in the random matrix theory, known as the celebrated Wigner semi-circular law:

$$\rho(\lambda, N) = \sqrt{\frac{2}{N\pi^2}} \left[1 - \frac{\lambda^2}{2N} \right]^{1/2} \tag{3.4}$$

which is true for every β and for N large. The semicircle has support in $[-\sqrt{2N}, \sqrt{2N}]$.

3.2.1 RMT and spin-glass models

Generally speaking, we can say that one of the main features of disordered systems, and thus of spin-glass models, is a corrugated energy (or free-energy) landscape. A corrugated energy landscape can be characterized by a huge number of local stationary points, which can be minima, maxima or saddles. If s are the local degrees of freedom of the model that we are considering, the stability of a stationary point s^* is encoded in the eigenvalues of the Hessian matrix $M_{ij} = \frac{\partial H[s]}{\partial s_i \partial s_j}\Big|_{s^*}$. Positive (negative) eigenvalues of the Hessian matrix correspond to stable (unstable) directions. A minimum is characterized by a positive definite spectrum of the Hessian matrix. In spin-glass models, given the presence of disorder, the Hessian matrix of a stationary point is a random matrix. In some cases, results form RMT can be used to study the stability of stationary points in spin-glass models. In the following sections we will study the stability of the paramagnetic minimum of the TAP free energy for the SK model. Since its Hessian matrix belongs to the GOE ensemble, we will see that the Wigner semicircle law allows to identify in a very elegant way the critical temperature of the model in the thermodynamic limit.

Let us give a further example. In the previous part we have discussed the phenomenology of the p-spin model. The energy landscape of this spin-glass model is corrugated and the number of stationary points with given energy $E \in [E_{min}, E_{max}]$ is exponential. One is able to compute [70] the average spectrum of the Hessian matrix of all minima with a given energy E, $\rho(\lambda; E)$, and see how it changes with E. Given the Gaussian nature of the disorder, $\rho(\lambda; E)$ is described by the Wigner semicircle law:

$$\rho(\lambda; E) = \frac{1}{2\pi} \sqrt{E_{th}^2 - (\lambda - E)^2} \tag{3.5}$$

where E_{th} is the so-called threshold energy, which depends on the parameters of the model. When $E < -|E_{th}|$ the semicircle is entirely contained in the positive semi-axis. At $E = |E_{th}|$ the semicircle touches the origin and for $E > |E_{th}|$ a part of the semicircle is contained in the negative axis, as depicted in figure 3.2. Therefore, at the threshold energy E_{th} a topological transition occurs between a region of the landscape mainly populated by stable minima ($E < -|E_{th}|$), and a region mainly populated by unstable saddles ($E > -|E_{th}|$). These results shade some light on the dynamical transition of the p-spin model. The energy of the minima visited by the system at the dynamical transition T_d is exactly equal to the threshold energy

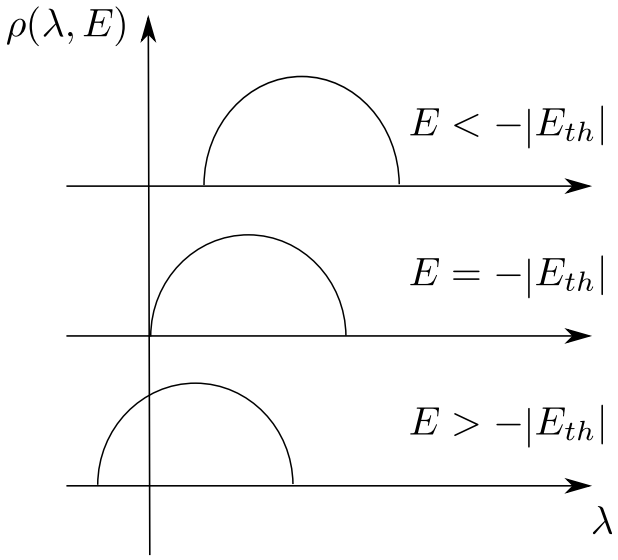

Figure 3.2: A pictorial representation of the averaged spectrum $\rho(\lambda,E)$ of the Hessian matrix of the stationary points of the energy of the p-spin model as a function of their energy. For $E < -|E_{th}|$ the spectrum is entirely contained in the positive semi-axis. At $E = |E_{th}|$ the spectrum touches the origin and for $E > |E_{th}|$ a part of the spectrum is contained in the negative axis.

E_{th}. As pointed out in [47], at equilibrium, for $T < T_d$, the system is trapped within minima of the energy, with all the eigenvalues of the Hessian larger than zero: ergodicity is broken. For $T > T_d$, on the contrary, the typical stationary point is a saddle, with a finite fraction of negative eigenvalues. Saddles do not trap the dynamics for infinite times, since, sooner or later, driven by thermal fluctuations, the system finds the negative modes and leaves the saddle: ergodicity is not broken. The thermal dynamical transition in the p-spin model can then be considered a manifestation of the topological one.

In order to go further in the comprehension of the phenomenology of the p-spin model, it can be interesting to evaluate the probability of finding a stationary point which is a saddle in the minima regime and vice versa. This problem has been firstly attached by Cavagna et al. in [109], where it has been shown that saddles exist in the regime dominated by minima, but the probability of these saddles to occur is exponentially small in N. The same problem can be formulated in RMT language by studying the distribution of the index of a Random Matrix. The fraction of positive eigenvalues $c = N_+/N$, or index, of a random matrix is a random variable whose distribution $P(c,N)$ was firstly studied by Cavagna et al. [110] and more recently exactly calculated by Majumdar et al. [111]. With Coulomb-gas techniques, the authors of [111] obtained that to leading order in N

$$P(c, N) \approx \exp\left[-\beta N^2 \phi(c)\right] \tag{3.6}$$

where the exact rate function $\phi(c)$ is symmetric around $c = 1/2$ and universal (independent of the Dyson index β). The symbol $\approx$ stands for the precise logarithmic law:

$$\lim_{N\to\infty} \frac{\log P(N_+ = cN)}{\beta N^2} = -\phi(c) \tag{3.7}$$

3.3 The TAP approach to spin-glass models

The aim of this section is to introduce the TAP approach to spin-glass models by paying particular attention to the SK model, along the lines of [112]. The TAP approach can be considered a generalization of the Curie-Weiss approach to ferromagnets: a free-energy function is constructed as a function of a local order parameter. Pure states of the system can be identified as the minima of this free energy. We will show that it is possible to obtain the critical temperature of the SK model in the thermodynamic limit by studying the stability of the high-temperature paramagnetic minimum.

3.3.1 Derivation of the TAP free energy

Let us consider a system described by local degrees of freedom $\vec{S}$ and by an Hamiltonian $H[\vec{S}]$. A general result of statistical mechanics [113] states that it is always possible to decompose the equilibrium Gibbs measure $P_G(\vec{S})$ as a sum over pure states:

$$P_G(\vec{S}) = \sum_\alpha w_\alpha P^\alpha(\vec{S}) \tag{3.8}$$

where α labels the pure states and w_α is such that $\sum_\alpha w_\alpha = 1$. A second result in finite-dimensional systems is the clustering property: connected correlation in a pure state vanishes at large distance. Since on complete graphs there is no notion of distance, for fully-connected models the clustering property translates in a factorization of the measure in a pure state:

$$P^\alpha(\vec{S}) = \prod_i P_i^\alpha(S_i) \ . \tag{3.9}$$

The single-spin probability distribution in a pure state α, $P_i^\alpha(S_i)$, is specified by the average magnetization of the spin S_i, $m_i^\alpha = \sum_{S_i} S_i P_i^\alpha(S_i)$. In the case of Ising spins we can rewrite $P_i^\alpha(S_i) = (1 + m_i^\alpha)/2$. We can conclude that, in a fully-connected model, a pure state α is completely identified by the set of magnetizations m_i^α. Let us finally remark that, if in finite-dimensional systems pure states can be selected via boundary conditions, in fully-connected models the only way to select pure states is via external fields. If in the ferromagnetic Ising model the two pure ferromagnetic states are identified by a global magnetization, in the SK model, for every realization of the disorder $\{J_{ij}\}$ each state is characterized by a local amorphous magnetization. The TAP approach to the SK model aims at constructing a free-energy function as a function of the local magnetization $\vec{m}$ such that pure states can be identified with the local minima of the free energy. In their original work [40], Thouless, Anderson and Palmer presented as "a fait accompli" the so called TAP free energy: they added the Onsager reaction term to the mean-field free energy. In the following we follow the approach of Yedidia and Georges [114] which allows to obtain a systematic derivation of the free energy. The same approach was introduced some years before by Plefka [115]. The idea is the following.

The free energy of a system of spins $\vec{S}$ described by an Hamiltonian $H[\vec{S}]$ with a local external field $\vec{b}$ is:

$$-\beta F[\beta, \vec{b}] = \log \left[\sum_{\vec{S}} \exp \left[-\beta H[\vec{S}] + \beta \sum_i S_i b_i \right] \right] \tag{3.10}$$

and the local magnetization $m_i[\beta, \vec{b}] = -\frac{\mathrm{d}}{\mathrm{d}b_i} F[\beta, \vec{b}]$. If we consider the Legendre transform of $F[\beta, \vec{b}]$ we obtain a free energy as function of the local magnetic fields $\vec{m}$:

$$-\beta \Gamma[\beta, \vec{m}] = -\beta \max_{\vec{b}} \left[F[\beta, \vec{b}] + \sum_i b_i m_i[\beta, \vec{b}] \right] \ . \tag{3.11}$$

In this way the local fields $\vec{b} = \vec{b}[\beta, \vec{m}]$ are fixed to enforce the magnetization $\vec{m}$. By construction $\Gamma[\beta, \vec{m}]$ is a concave function of $\vec{m}$. In order to construct a free-energy function such that the minima can be identified with the pure states, we are interested to calculate the high-temperature expansion of $\Gamma[\beta, \vec{b}]$. In the Yedidia–Georges approach [114] the following free-energy function is considered:

$$-\beta G[\beta, \vec{m}] = \log \left[\sum_{\vec{S}} \exp \left[-\beta H[\vec{S}] + \beta \sum_i \lambda_i(\beta)(S_i - m_i) \right] \right] \tag{3.12}$$

where the local fields $\lambda_i(\beta)$ are that to ensure $\langle S_i - m_i \rangle = 0$ for every temperature β. The free-energy function is then expanded around $\beta = 0$, an high-temepratrue expansion:

$$-\beta G[\beta, \vec{m}] = -\beta G[0, \vec{m}] - \left. \frac{\partial(\beta G[\beta, \vec{m}])}{\partial \beta} \right|_{\beta=0} \beta + \left. \frac{\partial^2(\beta G[\beta, \vec{m}])}{\partial \beta^2} \right|_{\beta=0} \frac{\beta^2}{2} + \dots \tag{3.13}$$

Developing at $\beta = 0$ we have reduced our problem to a problem of independent spins. For a system described by an Hamiltonian

$$H[\vec{S}] = -\sum_{(i,j)} J_{ij} S_i S_j \ , \tag{3.14}$$

where (i,j) means the sum over different pairs, the expansion of $\beta G[\beta, \vec{m}]$ until order 4 in β is:

$$\begin{aligned} -\beta G[\beta, \vec{m}] = & -\sum_i \left[\frac{1+m_i}{2} \ln \left(\frac{1+m_i}{2} \right) + \frac{1-m_i}{2} \ln \left(\frac{1-m_i}{2} \right) \right] \qquad (3.15) \\ & + \beta \sum_{(i,j)} J_{ij} m_i m_j \\ & + \frac{\beta^2}{2} \sum_{(i,j)} J_{ij}^2 \ (1 - m_i^2)(1 - m_j^2) \\ & + \frac{2\beta^3}{3} \sum_{(i,j)} J_{ij}^3 \ m_i (1 - m_i^2) m_j (1 - m_j^2) \\ & + \beta^3 \sum_{(i,j,k)} J_{ij} J_{jk} J_{ki} (1 - m_i^2)(1 - m_j^2)(1 - m_k^2) \\ & - \frac{\beta^4}{12} \sum_{(i,j)} J_{ij}^4 (1 - m_i^2)(1 - m_j^2)(1 + 3m_i^3 + 3m_j^3 - 15 m_i^2 m_j^2) \\ & + 2\beta^4 \sum_{(ijk)} J_{ij}^2 J_{jk} J_{ki} m_i (1 - m_i^2) m_j (1 - m_j^2)(1 - m_k^2) \\ & + \beta^4 \sum_{(ijkl)} J_{ij} J_{jk} J_{kl} J_{li} (1 - m_i^2)(1 - m_j^2)(1 - m_k^2)(1 - m_l^2) \\ & + \dots \qquad (3.16) \end{aligned}$$

where the notation (i,j), (i,j,k) and (i,j,k,l) means that one has to sum over all the distinct pairs, triplets and quadruplets of spins. Unfortunately Feynman rules for a fully diagrammatic expansion have not been found. We note that the first two terms of the expansion are the terms that would be recovered via the mean-field approximation, which is correct for infinite-ranged ferromagnetic models. The term of order β^2 is the so called Onsager reaction term, introduced by Thouless, Anderson and Palmer in their original work [40]. This

high-temperature expansion, known as Plefka or Yedidia-Georges expansion, is a systematic method for deriving TAP equations for different class of models and has been extensively used in several different contexts in physics, from classical disordered systems [116, 117, 118] to general quantum systems [119, 120, 121, 122].

3.3.2 Analysis of TAP equations in the thermodynamic limit

Let us consider the Hamiltonian of a model on a complete graph:

$$H[S] = \sum_{i \neq j} J_{ij} S_i S_j \ . \tag{3.17}$$

For this model, the stationary conditions

$$\frac{\mathrm{d}}{\mathrm{d}m_i} \left[-\beta G(\beta, \vec{m}) \right] = 0 \tag{3.18}$$

become:

$$-\text{arctanh}\ (m_i) + \beta \sum_{j(\neq i)} J_{ij} m_j - \beta^2 m_i \sum_{j(\neq i)} J_{ij}^2 (1 - m_j^2) + O(\beta^3) = 0 \tag{3.19}$$

which are the so-called TAP equations for $i = 1, \ldots, N$. In the case of fully connected ferromagnetic model ($J_{ij} = 1/N$ for all (i,j)) we expect that at the minimum of the free energy the magnetizations are all equal, $m_i = m$. In this case the terms $O(\beta^n)$ with $n \geq 2$ vanish for $N \to \infty$ and we recover the stationary equation of the mean-field approach. In the SK model J_{ij} are Gaussian random variables with zero mean and variance $\overline{J_{ij}^2} = J^2/N$, then the terms $O(\beta^2)$ in the TAP free energy are now relevant, but for N large we can replace the J_{ij}^2 with their average. Still, the terms $O(\beta^3)$ can be neglected as they vanish for $N \to \infty$. At high temperature these equations have only the paramagnetic solution $m_i = 0$. It can be interesting to study the stability of the paramagnetic solution as a function of the temperature. We introduce the Hessian matrix of the paramagnetic minimum M_{ij}:

$$\beta M_{ij} = \left. \frac{\mathrm{d}\left[-\beta G(\beta, \vec{m}) \right]}{\mathrm{d}m_i \mathrm{d}m_j} \right|_{\vec{m}=0} = (1 + \beta^2 J^2)\delta_{ij} - \beta J_{ij} \ . \tag{3.20}$$

Since the coupling matrix J_{ij} belongs to the GOE ensemble, we can exploit results of RMT and obtain that its spectrum, in the thermodynamic limit, is described by the Wigner semicircle with support in $[-2J, 2J]$. Consequently the spectrum of M_{ij}, i.e. $\rho(\lambda, \beta)$, has support on $[(1-\beta J)^2, (1+\beta J)^2]$, as depicted in figure 3.3. The minimal eigenvalue of the spectrum is $\lambda_{min} = (1-\beta J)^2$. We obtain that in the high-temperature regime, $\rho(\lambda, \beta)$ has support in the positive region, the paramagnetic minimum is stable. At $\beta = 1/J$, the minimal eigenvalue vanishes and the semicircle touches 0: zero modes appear suggesting that for $\beta > 1/J$ the paramagnet becomes unstable. Contrary, according to TAP equations for $\beta > 1/J$, it seems that the paramagnet is stable for all temperatures. This strange result is in fact incorrect: the paramagnet becomes indeed unstable at low temperature. In fact, it can be shown that the TAP equations do not make sense for the paramagnet at $\beta > 1/J$ [123]. Since M_{ij} corresponds to the inverse susceptibility matrix χ_{ij}^{-1}, at $\beta = 1$, the susceptivity matrix presents a diverging mode: $\beta = 1$ can be considered the critical temperature of the SK model. This result is consistent with the one obtained by Parisi via the replica approach [113].

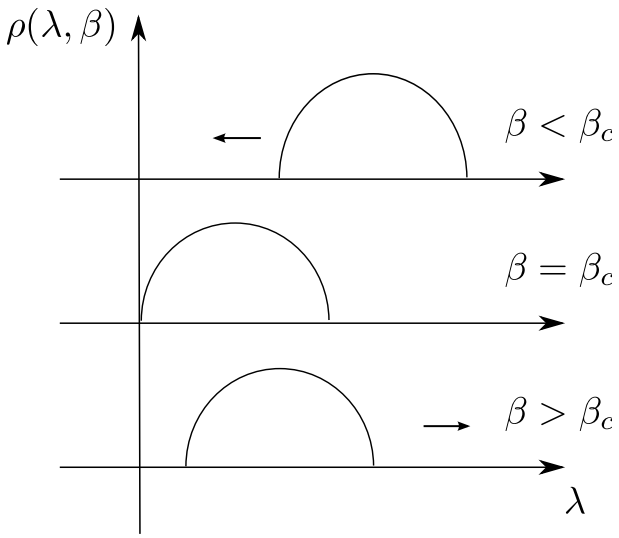

Figure 3.3: Pictorial representation of the averaged spectrum $\rho(\lambda,T)$ of the Hessian matrix of the paramagnetic minimum of the TAP free energy of the SK model as a function of the temperature T. The critical temperature of the SK model can be identified by the vanishing of the minimal eigenvalue, i.e. the spectrum touching the origin.

3.4 Extreme Value Statistics

The aim of Extreme Value Statistics (EVS) theory is to describe properties of atypical realizations of on ensemble of random variables: events which lie in the tails of distributions. Let us consider the maximum X_n over an ensemble of n random variables $(x_1, x_2, \ldots, x_n)$, defined via:

$$X_n = \max(x_1, x_2, \ldots, x_n) \quad . \tag{3.21}$$

Given the probability distribution $P(x_1, x_2, \ldots, x_n)$, we are interested in characterizing the probability distribution of X_n. This characterization can help solving practical problems. In 1709 Nicolas Bernoulli tried to answer the question: given an ensemble of n people dying randomly in a lapse of t years, what is the typical mean-life of the last survived person? The same kind of problems can also be found extreme events in hydrology [124] – water-flood of rivers – or geology [125] – earthquakes. More recently, EVS drew the attention of the financial community in the evaluation of risk [126]. One of the roles of financial markets is actually to allow different actors in the economic world to trade their risks, which requires pricing them. Let us suppose that the price of a stock in a market at day t x_t changes daily randomly:

$$x_{t+1} = x_t + \eta \tag{3.22}$$

where η is a random variable. What is the probability that the biggest loss is larger than a value Λ in a period of n days?

A complete presentation of the theory of EVS can be found in the book of Gumbell [127], but let also cite the first articles on this topic [128, 129, 130, 131]. In this section we will introduce the results of the theory of EVS for independent and identically distributed (iid) random variables and some recent results of physical interest on the case of correlated random variables.

3.4.1 Extreme Value Statistics for iid random variables

Let us consider an ensemble of independent and identically distributed (iid) random variables $(x_1, x_2, \ldots, x_n)$ with $p(x)$ the probability density function (pdf) of every random variable. The joint pdf of $(x_1, x_2, \ldots, x_n)$ is:

$$P(x_1, x_2, \ldots, x_n) = \prod_{i=1}^{n} p(x_i) \ . \tag{3.23}$$

We define $X_n = \max(x_1, x_2, \ldots, x_n)$ and we introduce the scaling variable

$$z = \frac{X_n - a_n}{b_n} \ . \tag{3.24}$$

The non-universal coefficients a_n and b_n - depending on the pdf $p(x)$ - are such that the following limit exists:

$$\lim_{n\to\infty} P\left[\frac{X_n - a_n}{b_n} < z\right] = F_k(z) \ . \tag{3.25}$$

In the case of iid random variables the theorem [131] assures the existence of a pair of sequences (a_n, b_n) such that the limit of equation 3.25 converges to one of the following distributions:

$$\text{Gumbel}: \quad F_I(z) = \exp(-e^{-z}) \tag{3.26}$$

$$\text{Frechet}: \quad F_{II}(z) = \begin{cases} 0 & \text{if } z \le 0 \\ \exp(-z^{-\gamma}) & \text{if } z > 0 \end{cases} \quad (\gamma > 1) \tag{3.27}$$

$$\text{Weibull}: \quad F_{III}(z) = \begin{cases} \exp(-|z|^{\gamma}) & \text{if } z \le 0 \\ 1 & \text{if } z > 0 \end{cases} \quad (\gamma > 1) \ . \tag{3.28}$$

For pdf $p(x)$ decreasing more rapidly than any power-law for $x \to \infty$, the limiting distribution of z is Gumbel. The Frechet distribution is the limiting distribution of z for power-law pdf $p(x) \sim 1/x^{\gamma+1}$ for $x \to \infty$. In the case the support of the pdf $p(x)$ is limited on a domain $[I, S]$ or $]-\infty, S]$ and near the right bound S $p(x)$ behaves as $(S-x)^{\gamma-1}$, the limiting distribution of z is Weibull.

3.4.2 The Tracy–Widom Distribution

We have seen that for independent random variables the limiting distribution of extreme values belong to three universality classes. Fewer results are known in the theory of EVS in the case of non-independent random variables. A natural question is: what are the universality classes when the random variables are correlated? Recently there has been an attempt at identifying universality classes with the different schemes of replica-symmetry breaking introduced in spin-glass theory [132]. A breakthrough in the field has been achieved by Tracy and Widom [133, 134, 135, 136]. Tracy and Widom were able to calculate analytically the limiting distribution of the largest eigenvalue of some classes of random matrices. Quite remarkably, in the following years it has been found that this new distribution had evident connections with other physical and mathematical models. In this section we will present how the Tracy–Widom distribution has been introduced and some applications of physical interest.

We have seen in the previous sections that the eigenvalues of a Gaussian random matrix are correlated random variables. The jpdf is:

$$P(\lambda_1, \ldots, \lambda_N) = B_N \exp\left[-\frac{\beta}{2}\left(\sum_{i=1}^{N} \lambda_i^2 - \sum_{i\neq j} \ln(|\lambda_i - \lambda_j|)\right)\right] \tag{3.29}$$

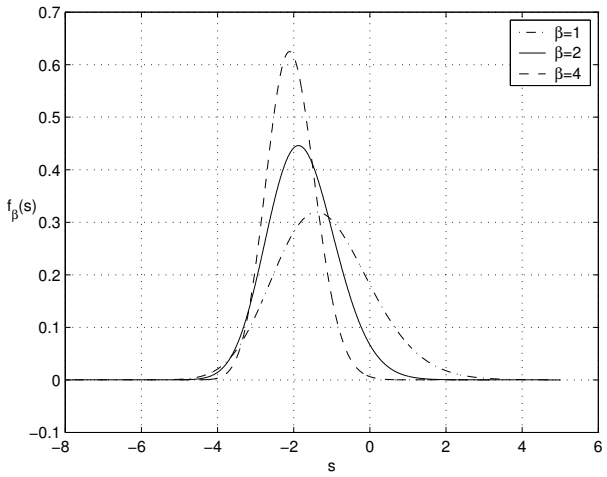

Figure 3.4: The Tracy-Widom distribution for $\beta = 1, 2, 4$. Image taken from [137].

Let us now concentrate on the largest eigenvalue of a gaussian random matrix $\lambda_{\max}$. From the Wigner semicircle law it is clear that $\lim_{N\to\infty}\langle\lambda_{\max}\rangle/\sqrt{2N} = 1$. If we consider N large but finite, this quantity has sample-to-sample fluctuations around its infinite-size mean $\sqrt{2N}$. It can be interesting to characterize the scaling in N of these fluctuations and the limiting distribution for N large but finite. This has been done quite recently by Tracy and Widom. They showed that the random variable $\xi = \sqrt{2}N^{1/6}[\lambda_{\max} - \sqrt{2N}]$, in the limit of large N, has a non-trivial limiting N-independent probability distribution

$$\lim_{N\to\infty} \text{Prob}[\xi < z] = F_\beta(z) \tag{3.30}$$

whose form depends on the value of the Dyson's index β. The function $F_\beta(z)$, called the Tracy-Widom (TW) distribution function, can be computed as a solution of a nonlinear Painlevé differential equation. Let us reproduce its limits in the case $\beta = 2$:

$$F_2(x) = \begin{cases} 1 - O(\exp[-4z^{3/2}/3]) & \text{as } z \to \infty \\ \exp[-|z|^3/12] & \text{as } z \to -\infty \end{cases} .$$

The probability density function $f_\beta(x) = \frac{\mathrm{d}F_\beta(x)}{\mathrm{d}x}$ thus has highly asymmetric tails. The density is depicted in figure 3.4. A convenient way to express these typical fluctuations of $\lambda_{\max}$ around its mean $\sqrt{2N}$ is to write, for large N:

$$\lambda_{\max} = \sqrt{2N} + \frac{\chi}{\sqrt{2}N^{1/6}} \tag{3.31}$$

where the random variable χ is distributed according the TW distribution.

We want to stress that the TW distribution is very robust. It has been shown that it is the limiting distribution of the largest eigenvalue of matrices drawn from a larger class of ensembles, e.g. when the entries are independent and identically distributed random variables drawn from an arbitrary distribution with all moments finite [138]. Fluctuations of the largest eigenvalue of the adjacency matrix of a random regular graph are described by the TW distribution [139]. Interested in financial applications, Biroli, Bouchaud and Potters [140] extended these results to the case of a random matrices where each entry is drawn independently from a power-law distribution [141].

It is quite remarkable that the fluctuations of observables of a wide range of models are described by the TW distribution, as pedagogically presented in the lecture notes of Majumdar [142]. The TW distribution is the limiting distribution of the length of the Longest Increasing Subsequence of random permutations [143], and in the Longest Common Subsequence problem [144] of biological inspiration. In physical models, the TW distribution appeared in a range of models describing growth processes of interfaces. In order to give an example of the growth process of an interface, consider the propagation of water on a sheet of paper when a glass of water falls accidentally on the table. In order to understand this kind of physical phenomena, discrete and continuous growth models have been introduced. Let us consider the class of discrete models which directed polymers [145], polynuclear growth models [146] and ballistic deposition models [144] belong to. It has been numerically tested that this class of models share the same universal exponents of continuous non-linear Kardar-Parisi-Zhang equation [147] describing the evolution of an interface. Recently, it has been also shown that all these discrete growth models share the same common scaled height distribution (Tracy-Widom). This finding allows to put the universality on a much stronger basis, going beyond just the second moment of the distribution. On the other hand, for flat and droplet initial condition, it has been shown that the limiting distribution of the height fluctuations of the KPZ equation is described by the TW distribution [148, 149]. Despite several mathematical efforts, the experimental evidence for the appearance of the KPZ universality class is quite elusive. Let us cite the recent experimental work on turbulent liquid crystal growth [150, 151] where the KPZ behaviour has been identified and the full distribution of the height fluctuations measured, showing a good agreement with the TW distribution. Quite interestingly, the TW distribution has been found to describe also the conductance fluctuations in two- and three- dimensional Anderson insulators [152, 153] and has been measured in coupled random lasers [154].

Chapter 4

Fluctuations of the pseudo-critical temperature in SK model: an analytical approach

4.1 Motivations

In this chapter we will focus on the problem of fluctuations of a suitably-defined pseudo-critical temperature of the SK model due to the presence of disorder. We will use an analytical approach in order to investigate this problem. The problem of fluctuations of the pseudo-critical temperature relies on a definition of pseudo-critical temperature. This definition is subject to some arbitrariness, but some features must be verified in order to be consistent with the thermodynamic limit. First of all, the probability distribution of this quantity must shrink to a delta function centered on β_c^∞ if the system size tends to infinity, $N \to \infty$. On the other hand, we can expect that, for large but finite N, the fluctuations of the pseudo-critical temperature follow the scaling form:

$$\beta_c^N(w) = \beta_c^\infty + a\frac{\varphi(w)}{N^\alpha} \tag{4.1}$$

where $\varphi(w)$ is a random variable distributed according to a limiting size-independent distribution $p(\varphi)$ and α a scaling exponent.

In chapter 3 we have considered the TAP approach to the SK model. The TAP approach is well suited in order to describe disorder sample-to-sample fluctuations of a physical observable, since the TAP free energy is constructed for every single realization of the disorder and not averaged over the disorder distribution. We have seen that the critical temperature can be identified studying the stability of the paramagnetic minimum of the TAP free energy in the high-tempertature phase in the thermodynamic limit. The stability of the paramagnetic minimum is encoded in the spectrum of its Hessian matrix. The Hessian matrix is a random matrix, depending on the realization of the disorder, drawn from the GOE ensemble of Gaussian Random Matrices. In the thermodynamic limit, its spectrum is described by the Wigner semicircle law and has positive support in the high-temperature phase, so that the paramagnet is stable. The critical temperature can be identified by the vanishing of the minimal eigenvalue of the Hessian matrix, corresponding to an instability of the paramagnetic minimum and to a diverging susceptivity. In the present chapter we want to generalize this approach to systems of finite but large size N. In this case, we can exploit the results by

Tracy and Widom (TW) concerning the fluctuation of the minimal eigenvalue of a random matrix in the GOE ensemble. In order to do that, we have to perform a careful analysis of the Plefka-Yedidia-Georges expansion. The results of this work have been published in [42].

4.2 The Model

Let us write the Hamiltonian of the SK model in the following form:

$$H[\{S_i\},\{x_{ij}\}] = -\frac{J}{N^{1/2}} \sum_{i\neq j=1}^{N} x_{ij} S_i S_j + \sum_{i=1}^{N} h_i S_i \tag{4.2}$$

where $S_i = \pm 1$ and the couplings $\{x_{ij}\}_{i\neq j=1,\cdots,N} \equiv \{x\}$ are distributed according to normal distribution with zero mean and unit variance, and J is a parameter fixing the strength of the interaction energy between spins. We have seen in chapter 3 that the TAP free energy can be obtained as an expansion in powers of the parameter

$$\alpha \equiv \frac{\beta J}{N^{1/2}},$$

where β is the inverse temperature of the model, as shown by Plefka [115] and Yedidia and Georges [114]. It is a general fact that, if the model is on a complete graph, the Plefka expansion truncates to a finite order in α, because the terms of higher order should vanish in the thermodynamic limit. In particular, for the SK model the orders of the expansion larger than three vanish [155] in the limit $N \to \infty$, in such a way that the expansion truncates, and one is left with the first three orders of the α-series, which read:

$$\begin{aligned} -\beta f(\{m_i\},\beta) = \quad & -\sum_i \left[\frac{1+m_i}{2} \ln\left(\frac{1+m_i}{2}\right) + \frac{1-m_i}{2} \ln\left(\frac{1-m_i}{2}\right) \right] \\ & +\alpha \sum_{(ij)} x_{ij} m_i m_j \\ & +\alpha^2 \sum_{(ij)} x_{ij}^2 (1-m_i^2)(1-m_j^2), \end{aligned} \tag{4.3}$$

where (ij) means the sum over all distinct pairs and $m_i \equiv \langle S_i \rangle$ is the local magnetization, i. e. the thermal average $\langle \cdots \rangle$ of the spin S_i performed with the Boltzmann weight given by Eq. (4.2) at fixed disorder $\{x\}$. In the thermodynamic limit, $N \to \infty$, for temperatures $T > T_c$, the only minimum of TAP free energy of the SK model is the paramagnetic minimum $m_i = 0\ \forall i$. Below the critical temperature, the TAP free energy presents exponentially-many different minima, the system is in the glassy phase. The Hessian matrix of f is defined by:

$$\beta H_{ij} \equiv \beta \frac{\partial h_i}{\partial m_j} = \frac{\partial^2 (\beta f)}{\partial m_i \partial m_j}, \tag{4.4}$$

and evaluated in the paramagnetic minimum at leading order in N is:

$$\beta H_{ij} = (1+\beta^2 J^2)\delta_{ij} - \alpha x_{ij} \quad . \tag{4.5}$$

The rest of this chapter is structured as follows. In Section 4.3, we generalize Eq. (4.5) to finite sizes, in the simplifying assumption that the Plefka expansion can be truncated up to order α^2, which is known as the TAP approximation. We then study the finite-size fluctuations of the minimal eigenvalue λ of the susceptibility matrix, and find them to be governed by the TW distribution. In Section 4.4, we extend this simplified approach by taking into account the full Plefka expansion, by an infinite re-summation of the series. Hence, in Section 4.5, we give a suitable definition of a finite-size pseudo-critical temperature, and show the fluctuations of the latter to be governed by the TW distribution.

4.3 Finite-size analysis of the Hessian matrix in the TAP approximation

In this Section we study the finite-size fluctuations due to disorder of the minimal eigenvalue of the Hessian matrix βH_{ij} of the paramagnetic minimum $m_i = 0\,\forall i$, by considering the free energy f in the TAP approximation, Eq. (4.3). Back to the TAP equations (4.3), the inverse susceptibility matrix in the paramagnetic minimum for finite N reads:

$$\begin{aligned} \beta H_{ij} &= -\alpha x_{ij} + \delta_{ij}\left(1 + \alpha^2 \sum_{k\neq i} x_{ki}^2\right) \\ &= -\alpha x_{ij} + \delta_{ij}\left(1+\beta^2 J^2\right) + \delta_{ij}\frac{(\beta J)^2}{\sqrt{N}} z_2^i, \end{aligned} \tag{4.6}$$

where

$$z_2^i \equiv \sqrt{N}\left(\frac{1}{N}\sum_{k\neq i} x_{ki}^2 - 1\right). \tag{4.7}$$

According to Eq. (4.7), z_2^i is given by the sum of $N-1$ independent identically-distributed random variables x_{ij}^2. By the central limit theorem, at leading order in N the variable z_2^i is distributed according to a Gaussian distribution with zero mean and variance 2

$$p_N(z_2^i = z) \overset{N\to\infty}{\to} \frac{1}{\sqrt{4\pi}} \mathrm{e}^{-z^4/4}, \tag{4.8}$$

where $p_N(z_2^i = z)$ denotes the probability that z_2^i is equal to z at finite size N. We set

$$\beta H_{ij} \equiv \delta_{ij}\left(1+\beta^2 J^2\right) + \alpha M_{ij} \quad . \tag{4.9}$$

According to Eq. (4.7), the diagonal elements of M_{ij} are random variables correlated to out-of-diagonal elements. The statistical properties of the spectrum of a random matrix whose entries are correlated to each other has been studied heretofore only in some cases. For instance, Staring et al. [156] studied the mean eigenvalue density for matrices with a constraint implying that the row sum of matrix elements should vanish, and other correlated cases have been investigated both from a physical [157] and mathematical [158] point of view.

For $\beta J = 1$ if z_2^i were independent on $\{x\}$, the matrix M_{ij} would belong to the GOE ensemble. In that case, for N large but finite, we know that the fluctuations of the minimal eigenvalue λ of the Hessian matrix βH_{ij} due to the disorder would be described by the scaling form:

$$\lambda = \frac{1}{N^{2/3}}\phi, \tag{4.10}$$

where ϕ is a random variable distributed according to the TW distribution $p_{\mathrm{GOE}}(\phi)$. As shown in Appendix 4.7, this is indeed the case for z_2^i, which can be treated, at leading order in N, as a random variable independent on x_{ij}. The general idea is that z_2^i is given by the sum of $N-1$ terms all of the same order of magnitude, and only one amongst them depends on x_{ij}. It follows that at leading order in N, z_2^i can be considered as independent on x_{ij}. Since in Eq. (4.6) z_2^i is multiplied by a sub-leading factor $1/\sqrt{N}$, in Eq. (4.6) we can consider z_2^i at leading order in N, and treat it as independent on x_{ij}. To test this independence property, we set $\beta J = 1$, generate numerically $S \gg 1$ samples of the $N \times N$ matrix βH_{ij}, and compute the average density of eigenvalues of βH_{ij}, together with the distribution of the

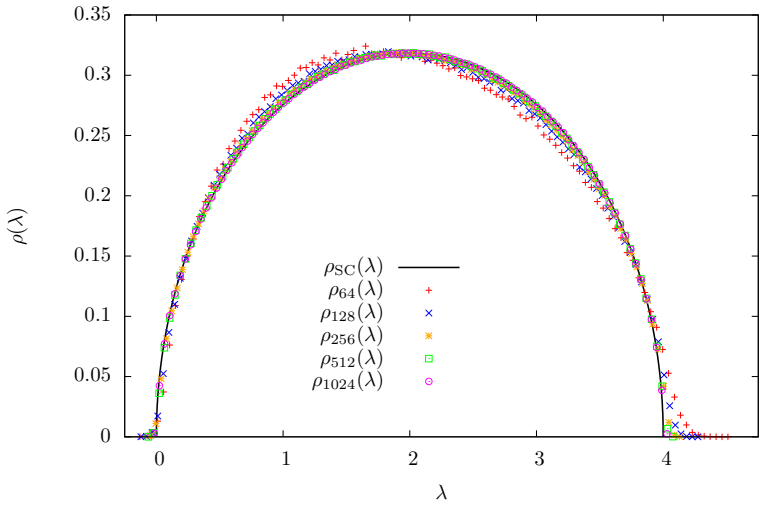

Figure 4.1: Density of eigenvalues $\rho_N(\lambda)$ of the matrix $\beta\chi^{-1}$ for $N = 64,128,256,512,1024$ (in red, blue, yellow, green, violet respectively), $\beta J = 1$ and $S = 16 \times 10^3$, and Wigner semicircular law $\rho_{SC}(\lambda) = 1/(2\pi)\sqrt{4-(2-\lambda)^2}$ (black) as a function of λ. $\rho_N(\lambda)$ approaches $\rho_{SC}(\lambda)$ as N is increased.

minimal eigenvalue λ for several sizes N. The averaged eigenvalue distribution $\rho_N(\lambda)$ as a function of λ is depicted in Fig. 4.1, and tends to the Wigner semicircle as N is increased, showing that the minimal eigenvalue λ tends to 0 as $N \to \infty$. The finite-size fluctuations of λ around 0 are then investigated in Fig. 4.2. Defining ϕ in terms of λ by Eq. (4.10), in Fig. 4.2 we depict the distribution $p_N(\phi)$ of the variable ϕ for several sizes N, and show that for increasing N, $p_N(\phi)$ approaches the TW distribution $p_{GOE}(\phi)$. Let us introduce the central moments

$$\begin{aligned} \mu_1^N &\equiv \mathbb{E}_N[\phi], \\ \mu_i^N &\equiv \mathbb{E}_N[(\phi - \mathbb{E}_N[\phi])^i] \; \forall i > 1 \end{aligned}$$

of $p_N(\phi)$, and the central moments

$$\begin{aligned} \mu_1^{GOE} &\equiv \mathbb{E}_{GOE}[\phi], \\ \mu_i^{GOE} &\equiv \mathbb{E}_{GOE}[(\phi - \mathbb{E}_{GOE}[\phi])^i] \; \forall i > 1 \end{aligned}$$

of the TW distribution, where

$$\begin{aligned} \mathbb{E}_N[\cdot] &\equiv \int d\phi \, p_N(\phi) \cdot , \\ \mathbb{E}_{GOE}[\cdot] &\equiv \int d\phi \, p_{GOE}(\phi) \cdot . \end{aligned}$$

In the inset of Fig. 4.2 we depict μ_i^N for several sizes N and μ_i^{GOE} as a function of i, showing that μ_i^N converges to μ_i^{GOE} as N is increased. In Figure 4.3 this convergence is clarified by depicting $\Delta\mu_i^N \equiv (\mu_i^N - \mu_i^{GOE})/\mu_i^{GOE}$ for several values of $i > 1$ as a function of N. $\Delta\mu_i^N$ is found to converge to 0 for large N. In the inset of Fig. 4.3 we depict $\Delta\mu_1^N$ as a function of N, showing that the convergence of the first central moment with N is much slower than that of the other central moments. It is interesting to observe that a slowly-converging first moment has been recently found also in experimental [150] and numerical [159] data of models of growing interfaces where the TW distribution appears.

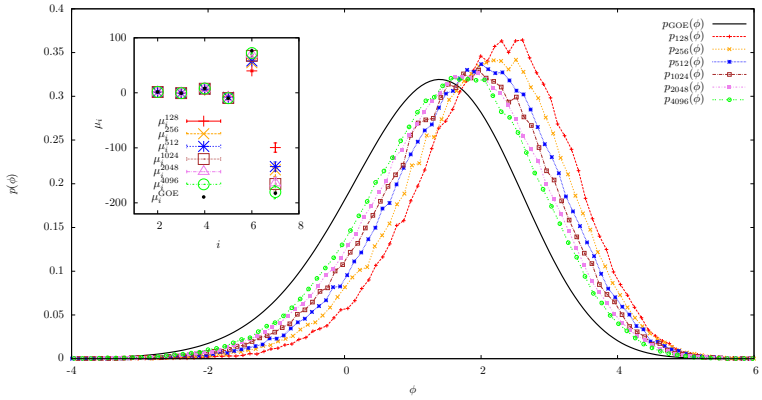

Figure 4.2: Distribution $p_N(\phi)$ for $N = 128, 256, 512, 1024, 2048, 4096$ (in red, yellow, blue, brown, violet, green respectively) and $10^5 \leq S \leq 4 \times 10^5$ samples, and the Tracy-Widom distribution $p_{\mathrm{GOE}}(\phi)$ for the GOE ensemble (black), as a function of ϕ. For increasing N, $p_N(\phi)$ approaches $p_{\mathrm{GOE}}(\phi)$, confirming the asymptotic independence of the diagonal elements (**??**) by each of the off-diagonal elements x_{ij} for large N. Inset: μ_i^N for sizes $N = 128, 256, 512, 1024, 2048, 4096$ (in red, yellow, blue, brown, violet, green respectively), $10^5 \leq S \leq 4 \times 10^5$, and μ_i^{GOE} (black) as a function of $i > 1$.

The analytical argument proving the independence property of z_2^i has been thus confirmed by this numerical calculation. Hence, the main result of this Section is that the finite-size fluctuations of the minimal eigenvalue of the Hessian matrix βH_{ij} in the TAP approximation for $\beta J = 1$ are of order $N^{-2/3}$ and are distributed according to the TW law. These fluctuations have already been found to be of order $N^{-2/3}$ in a previous work [160], and more recently reconsidered [161], following an independent derivation based on scaling arguments, even though the distribution has not been worked out. Our approach sheds some light on the nature of the scaling $N^{-2/3}$, which is non-trivial, since it comes from the $N^{-1/6}$-scaling of the TW distribution, which is found to govern the fluctuations of λ.

We now recall that both the derivation of this Section and the previously-developed analysis of Bray and Moore [160] rely on the TAP approximation, i. e. neglect the terms of the Plefka expansion (4.11) of order larger than 2 in α. As we will show in the following Section, these terms give a non-negligible contribution to the finite-size corrections of the TAP equations, and so to the finite-size fluctuations of the critical temperature, and thus must be definitely taken into account in a complete treatment.

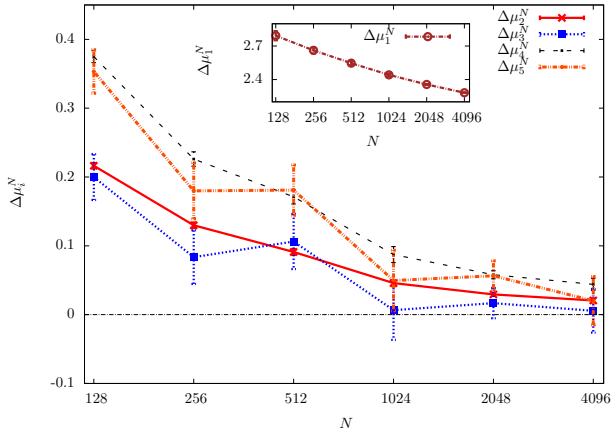

Figure 4.3: Relative difference $\Delta\mu_i^N$ between the central moments μ_i^N of the distribution $p_N(\phi)$ for $10^5 \leq S \leq 4\times10^5$, and the central moments μ_i^{GOE} of the Tracy-Widom distribution as a function of $N = 128, 256, 512, 1024, 2048, 4096$, for $i = 2, 3, 4, 5$ (in red, blue, black, orange respectively). For increasing N, μ_i^N approaches μ_i^{GOE}, confirming the asymptotic independence of z_2^i by each of the off-diagonal elements x_{ij} for large N. Inset: relative difference of the first central moment $\Delta\mu_1^N$ as a function of N (brown). $\Delta\mu_1^N$ approaches 0 very slowly as N is increased.

4.4 Finite-size analysis of the Hessian matrix within the full Plefka expansion

In this Section we compute the Hessian matrix βH_{ij} for a system of large but finite size N by taking into account all the terms of the Plefka expansion, in the effort to go beyond the TAP approximation of Section 4.3. Notwithstanding its apparent difficulty, here we show that this task can be pursued by a direct inspection of the terms of the expansion. Indeed, let us formally write the free-energy f as a series in α,

$$f(\{m\},\beta) = \sum_{n=0}^{\infty} \alpha^n f_n(\{m\},\beta). \tag{4.11}$$

For $n < 3$, the f_ns are given by Eq. (4.3). For $n > 3$, f_n is given by the sum of several different addends, which proliferate for increasing n, as shown in chapter 3. It is easy to show that at leading order in N, there is just one term contributing to f_n, and that such term can be written explicitly as

$$\begin{aligned} f_n(\{m\},\beta) \overset{N\to\infty}{\approx} & \sum_{i_1>\cdots>i_{n-1}} x_{i_1 i_2} x_{i_2 i_3} \cdots x_{i_{n-1} i_1} \\ & \times (1-m_{i_1}^2) \times \cdots \times (1-m_{i_{n-1}}^2). \end{aligned} \tag{4.12}$$

It follows that by plugging Eq. (4.12) in Eq. (4.11) and computing the Hessian matrix βH_{ij} for $m_i = 0$, one obtains a simple expression:

$$\begin{aligned} \beta H_{ij} &= -\alpha x_{ij} + \delta_{ij}\left(1 + \alpha^2 \sum_{k\neq i} x_{ki}^2 + 2\sum_{n=3}^{\infty} \alpha^n \sum_{i_1>\cdots>i_{n-1}} x_{i i_1} x_{i_1 i_2} \cdots x_{i_{n-1} i}\right) \\ &= -\alpha x_{ij} + \delta_{ij}\left(1+\beta^2 J^2\right) + \delta_{ij}\frac{1}{\sqrt{N}}\left[(\beta J)^2 z_2^i + 2\sum_{n=3}^{\infty} \frac{(\beta J)^n}{\sqrt{(n-1)!}} z_n^i\right]. \end{aligned} \tag{4.13}$$

where

$$z_n^i \equiv \frac{\sqrt{(n-1)!}}{N^{\frac{n-1}{2}}} \times \times \sum_{i_1>\cdots>i_{n-1}} x_{ii_1}x_{i_1i_2}\cdots x_{i_{n-1}i}, \forall n>2. \tag{4.14}$$

According to Eq. (4.14), one has that at leading order in N

$$\begin{aligned} \mathbb{E}_x[z_n^i] &= 0\,\forall n>2, \\ \mathbb{E}_x[(z_n^i)^2] &= 1\,\forall n>2, \end{aligned} \tag{4.15}$$

where in the second line of Eq. (4.15) the multiple sum defining z_n^i has been evaluated at leading order in N.

We observe that the random variables z_n^i and x_{jk} in Eq. (4.13) are not independent, since each z_n^i depends on the bond variables $\{x\}$. Following an argument similar to that given in Section 4.3 for z_2^i, we observe that, by Eq. (4.14) and at leading order in N, z_n^i is given by a sum of $O(N^{n-1})$ terms which are all of the same order of magnitude. Each term is given by the product of $n-1$ bond variables $x_{ii_1}x_{i_1i_2}\cdots x_{i_{n-1}i}$ forming a loop passing by site i. For any fixed i,j,k and n, only $O(N^{n-2})$ terms amongst the $O(N^{n-1})$ terms of z_n^i are entangled with the random bond variable x_{jk}. It follows that at leading order in N, z_n^i can be considered as independent by x_{jk}. Since the sum in the second line of Eq. (4.13) has a $1/\sqrt{N}$ factor multiplying each of the z_n^is, we can consider the z_n^i at leading order in N. Hence, in Eq. (4.13) we can consider each of z_n^is as independent on x_{jk}. In Appendix 4.8 we show that at leading order in N the distribution of z_n^i is a Gaussian with zero mean and unit variance for every i and $n>2$, while in Appendix 4.9 we show that at leading order in N the variables $\{z_n^i\}_{n,i}$ are mutually independent. Both these predictions are confirmed by numerical tests, illustrated in Appendix 4.8 and 4.9 respectively.

Hence, at leading order in N the term in square brackets in Eq. (4.13) is nothing but the sum of independent Gaussian variables, and is thus equal to a random variable $\sigma\times\zeta_i$, where ζ_i is Gaussian with zero mean and unit variance, and

$$\begin{aligned} \sigma^2 &= 2(\beta J)^4 + 4\sum_{n=3}^{\infty}\frac{(\beta J)^{2n}}{(n-1)!} \\ &= 2(\beta J)^2\{2(e^{(\beta J)^2}-1)-(\beta J)^2\} \end{aligned}$$

It follows that Eq. (4.13) becomes

$$\begin{aligned} \beta H_{ij} &= -\alpha x_{ij} + \delta_{ij}\left(1+\beta^2J^2+\frac{\sigma}{\sqrt{N}}\zeta_i\right) \\ &= -\alpha x'_{ij} + \delta_{ij}\left(1+\beta^2J^2\right), \end{aligned} \tag{4.16}$$

where

$$x'_{ij} \equiv x_{ij} - \delta_{ij}\frac{\sigma}{\beta J}\zeta_i. \tag{4.17}$$

Because of the additional diagonal term in Eq. (4.17), the matrix x'_{ij} does not belong to the GOE ensemble, but it falls in the class of Wigner matrices. It has been shown by Soshnikov[138] that the presence of the diagonal elements in Eq. (4.17) does not alter the universal distribution of the maximal eigenvalue of x'_{ij}, which is still distributed according to

the TW law. Hence, we have that, for N large but finite, the fluctuations of the the minimal eigenvalue λ of the Hessian matrix in the paramagnetic minimum βH_{ij} due to the disorder are described by the relation:

$$\lambda = (1 - \beta J)^2 + \frac{\beta J}{N^{2/3}} \phi_{\mathrm{GOE}}, \tag{4.18}$$

where ϕ_{GOE} is a random variable depending on the disorder sample x_{ij}, and distributed according to the TW law.

To summarize, in this Section we have calculated the Hessian matrix βH_{ij}, by considering the full Plefka expansion. In this framework additional diagonal terms are generated. These terms were not present in the TAP approximation. For large but finite N, all these additional terms can be handled via a resummation to all orders in the Plefka expansion. As a result, we obtain that the fluctuations of the minimal eigenvalue λ of the Hessian matrix are still governed by the TW law, as in the TAP case treated in Section 4.3.

4.5 Finite size fluctuations of the pseudo-critical temperature

We can now define a finite-size critical temperature, and investigate its finite-size fluctuations due to disorder.

In the previous Sections we have shown that for a large but finite size N, the minimal eigenvalue of the Hessian matrix of $\beta f(\{m\}, \beta)$ evaluated in the paramagnetic minimum $m_i = 0$, is a function of the temperature and of a quantity ϕ_{GOE}, which depends on the realization of the disorder $\{x\}$. Since the TW law, i. e. the distribution of ϕ_{GOE}, has support for both positive and negative values of ϕ_{GOE}, the subleading term in Eq. (4.18) can be positive or negative. Accordingly, for samples $\{x\}$ such that $\phi_{\mathrm{GOE}} < 0$, there exists a value of $\beta J \approx 1$ such that $\lambda(\beta J) = 0$. Since the Hessian matrix is by definition equal to to inverse susceptivity matrix, a vanishing mode of the Hessian matrix implies that the spin-glass susceptibility in the paramagnetic minimum diverges. This fact is physically meaningless, since there cannot be divergences in physical quantities at finite size. This apparent contradiction can be easily understood by observing that if $\lambda(\beta J) = 0$, the true physical susceptibility is no more the paramagnetic one, but must be evaluated in the low-lying non-paramagnetic minima of the free-energy, whose appearance is driven by the emergent instability of the paramagnetic minimum.

According to this discussion, in the following we will consider only samples $\{x\}$ such that $\phi_{\mathrm{GOE}} > 0$. For these samples, the spectrum of the Hessian matrix at the paramagnetic minimum has positive support for every temperature: the paramagnetic solution is always stable. We define a pseudo-inverse critical temperature $\beta_c J$ as the value of βJ such that λ has a minimum at $\beta_c J$, as depicted in figure 4.4

$$\begin{aligned} \left.\frac{d\lambda}{d\beta J}\right|_{\beta J = \beta_c J} &\equiv 0 \\ &= -2(1 - \beta_c J) + \frac{1}{N^{2/3}} \phi_{\mathrm{GOE}} \end{aligned} \tag{4.19}$$

where in the second line of Eq. (4.19), Eq. (4.18) has been used. This definition of pseudo-critical temperature has a clear physical interpretation: the stability of the paramagnetic

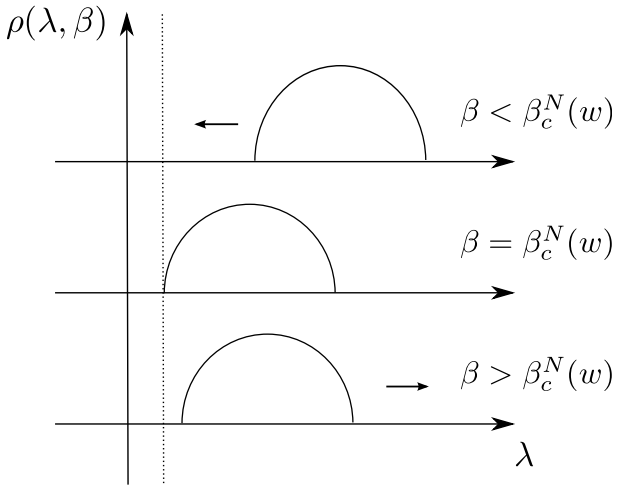

Figure 4.4: A pictorial representation of the definition of the pseudo-critical temperature given in Eq. (4.19).

minimum, which is encoded into the spectrum of the Hessian matrix βH_{ij}, has a minimum at $\beta = \beta_c$.

According to Eq. (4.19), the finite-size critical temperature β_c is given by

$$\beta_c J = 1 - \frac{1/2}{N^{2/3}} \phi_{\mathrm{GOE}}, \tag{4.20}$$

where ϕ_{GOE} depends on the sample $\{x\}$, and is distributed according to the TW law.

Eq. (4.20) shows that the pseudo-critical temperature of the SK model, defined via Eq. (4.19), is a random variable depending on the realization of the quenched disorder: finite-size fluctuations of the pseudo-critical temperature are of order $N^{-2/3}$, and are distributed according to the TW law. This has to be considered the main result of this chapter.

4.6 Conclusions and perspectives

In this section we have studied the problem of fluctuations of a finite-size pseudo-critical temperature of a spin-glass model on a complete graph, the Sherrington-Kirkpatrik model. We have performed a finite-size analysis of the TAP free energy and studied the stability of the paramagnetic minimum in the high-temperature phase. A definition of pseudo-critical temperature was introduced, and, exploiting results from Extreme Value Statistics in the context of Random Matrix Theory, we have shown that the fluctuations of the pseudo-critical temperature due to the disorder are described by the relation:

$$\beta_c^N(\{x\}) J = 1 - \frac{1/2}{N^{2/3}} \phi_{\mathrm{GOE}}(\{x\}), \tag{4.21}$$

where $\phi_{\mathrm{GOE}}(\{x\})$ is a random variable depending on the realization of the disorder and distributed according to the Tracy-Widom distribution. To our knowledge, this is the first time that the fluctuations of the pseudo-critical temperature of the SK model are studied. We consider this result interesting since this is also the first time that the ubiquitous Tracy-Widom distribution plays a role in spin-glass models.

This result opens several perspectives. First of all, it could be interesting to introduce a definition of pseudo-critical temperature which can be measured in numerical experiments since it is not possible to use the present one. It could be interesting then to test with numerical simulations which features of the present result are definition-dependent and which are universal. Numerical simulations can then be extended to other spin-glass models, like the Edward-Anderson model, for which the present analysis can not be pursued. This analysis has been done and the results will be presented in chapter 5.

In recent years, we have witnessed a growing interest for spin-glass models for which the coupling strengths are drawn from a Lévy distribution [162, 163, 164, 165]. The main featere of these distributions are power-law tails resulting in diverging moments. On the other hand some insight on the spectral theory of random matrices with Lévy-distributed entries have been achieved [166, 140]. In the light of these results, it could be interesting to investigate the fluctuations of the pseudo-critical for the Lévy-spin-glass models.

On the other hand, it could be interesting to consider spin-glass models in the 1RSB universality class, which present a dynamical critical temperature, like the p-spin model, and study the fluctuations of the pseudo-critical temperature in that case. We have seen that results from Random Matrix Theory allowed to obtain information about the dynamical critical temperature in the context of the topological transition of the p-spin model, according to the discussion introduced in Chapter 3. Is it possible to exploit the results of Tracy and Widom in order to characterize the fluctuations of a pseudo-critical temperature also in this context?

4.7 Appendix: Proof of the asymptotic independence of x_{ij} and z_2^i

Here we show that at leading order in N the variables x_{ij} and z_2^i are independent, i. e. that at leading order in N

$$p_N(x_{ij} = x, z_2^i = z) = p_N(x_{ij} = x) \times p_N(z_2^i = z). \tag{4.22}$$

Let us explicitly write the left-hand size of Eq. (4.22) as

$$\begin{aligned} p_N(x_{ij} = x, z_2^i = z) &= \mathbb{E}_{\{x_{ik}\}_{k\neq i}}[\delta(x_{ij} - x)\delta(z_2^i - z)], \\ &= \mathbb{E}_{x_{ij}}\left[\delta(x_{ij} - x)\mathbb{E}_{\{x_{ik}\}_{k\neq i,k\neq j}}\left[\delta\left(\sqrt{N}\left(\frac{1}{N}\sum_{k\neq i,k\neq j} x_{ki}^2 - 1\right) - \bar{z}_2^{ij}\right)\right]\right] \end{aligned} \tag{4.23}$$

where $\mathbb{E}_{x_{lm},x_{no},\cdots}$ denotes the expectation value with respect to the probability distributions of the variables $x_{lm}, x_{no}, \cdots$, δ denotes the Dirac delta function, and

$$\bar{z}_2^{ij} \equiv z - \frac{x_{ij}^2}{\sqrt{N}}. \tag{4.24}$$

Proceeding systematically at leading order in N, the second expectation value in the second line of Eq. (4.23) is nothing but the probability that the variable $\sqrt{N}(\frac{1}{N}\sum_{k\neq i,k\neq j} x_{ki}^2 - 1)$ is equal to $\bar{z}_2^{ij}$. We observe that according to the central limit theorem, at leading order in N

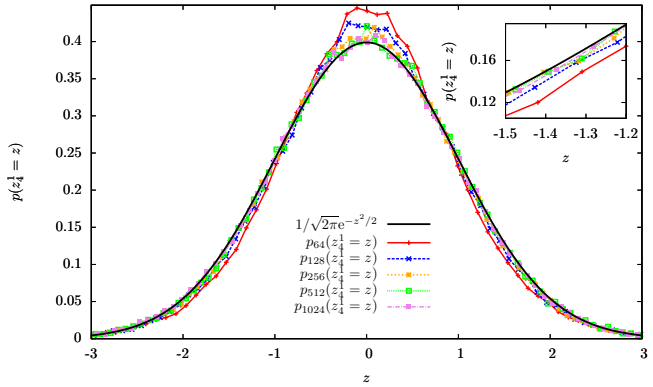

Figure 4.5: Probability distribution $p_N(z_4^1 = z)$ for $S = 10^5$ and different values of N = 64,128,256,512,1024 (in red, blue, yellow, green, violet respectively) together with a Gaussian distribution $1/\sqrt{2\pi}e^{-z^2/2}$ with zero mean and unit variance (black), as a function of z. As N is increased $p_N(z_4^1 = z)$ converges to $1/\sqrt{2\pi}e^{-z^2/2}$, as predicted by the analytical calculation, Eq. (4.30). Inset: zoom of the above plot explicitly showing the convergence of $p_N(z_4^1 = z)$ to $1/\sqrt{2\pi}e^{-z^2/2}$ as N is increased.

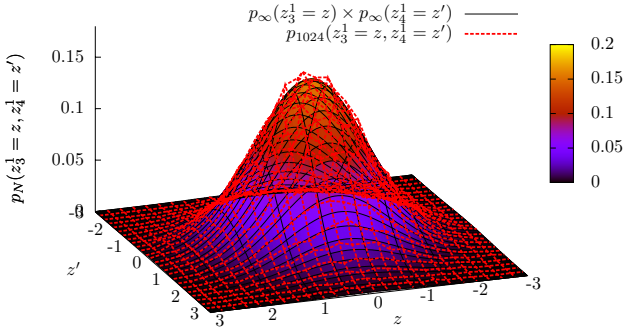

Figure 4.6: $p_{1024}(z_3^1 = z, z_4^1 = z')$ for $S = 10^5$ samples (red), and the $N \to \infty$-limit of the right-hand side of Eq. (4.33) (black), as a function of z,z'. For large N, $p_N(z_3^1 = z, z_4^1 = z')$ equals $p_N(z_3^1 = z) \times p_N(z_4^1 = z')$, as predicted by Eq. (4.33). Hence, at leading order in N the variables z_3^1 and z_4^1 are independent.

this probability is given by

$$\mathbb{E}_{\{x_{ik}\}_{k\neq i,k\neq j}}\left[\delta\left(\sqrt{N}\left(\frac{1}{N}\sum_{k\neq i,k\neq j}x_{ki}^2 - 1\right) - \overline{z}_2^{ij}\right)\right] = \frac{1}{\sqrt{4\pi}}e^{-\frac{\left(\overline{z}_2^{ij}\right)^2}{4}}. \tag{4.25}$$

By plugging Eq. (4.25) into Eq. (4.23) and using Eq. (4.24), one has

$$\begin{aligned} p_N(x_{ij}=x, z_2^i=z) &= \frac{1}{\sqrt{4\pi}}\int dx_{ij} P(x_{ij})\delta(x_{ij}-x)\times \\ &\quad \times \mathrm{e}^{-\frac{\left(z-x_{ij}^2/\sqrt{N}\right)^2}{4}} \\ &= P(x)\frac{1}{\sqrt{4\pi}}\mathrm{e}^{-\frac{\left(z-x^2/\sqrt{N}\right)^2}{4}} \\ &= p_N(x_{ij}=x)\times p_N(z_2^i=z), \end{aligned} \tag{4.26}$$

where in the first line Eq. (4.26) we explicitly wrote the expectation value with respect to x_{ij} in terms of the probability distribution $P(x_{ij})$, while in the third line proceeded at leading order in N, and used Eq. (4.8).

4.8 Appendix: Computation of the probability distribution of z_n^i

Here we compute the probability distribution of z_n^i at leading order in N . Let us define a super index $L \equiv \{i_1, \ldots, i_{n-1}\}$, where L stands for 'loop', since L represents a loop passing by the site i. Let us also set $X_L \equiv x_{ii_1}x_{i_1i_2}\cdots x_{i_{n-1}i}$. By Eq. (4.14) one has

$$z_n^i = \frac{\sqrt{(n-1)!}}{N^{\frac{n-1}{2}}}\sum_L X_L, \forall n > 2. \tag{4.27}$$

We observe that the probability distribution of X_L is the same for every L. Hence, according to Eq. (4.27), z_n^i is given by the sum of equally distributed random variables. Now pick two of these variables, $X_L, X_{L'}$. For some choices of L, L', X_L and $X_{L'}$ are not independent, since they can depend on the same bond variables x_{ij}. If one picks one variable X_L, the number of variables appearing in the sum (4.27) which are dependent on X_L are those having at least one common edge with the edges of X_L. The number of these variables, at leading order in N, is $O(N^{n-2})$, since they are obtained by fixing one of the $n-1$ indexes $i_1, \cdots, i_{n-1}$. The latter statement is equivalent to saying that if one picks at random two variables $X_L, X_{L'}$, the probability that they are correlated is

$$O(N^{n-2}/N^{n-1}) = O(N^{-1}). \tag{4.28}$$

Hence, at leading order in N we can treat the ensemble of the variables $\{X_L\}_L$ as independent. According to the central limit theorem, at leading order in N the variable

$$\frac{\sqrt{(n-1)!}}{N^{\frac{n-1}{2}}} z_n^i = \frac{1}{\frac{N^{n-1}}{(n-1)!}}\sum_L X_L$$

is distributed according to a Gaussian distribution with mean $\mathbb{E}_x[X_L] = 0$ and variance

$$\mathbb{E}_x\left[\left(\frac{\sqrt{(n-1)!}}{N^{\frac{n-1}{2}}} z_n^i\right)^2\right] = \frac{\mathbb{E}_x[X_L^2]}{\frac{N^{n-1}}{(n-1)!}} = \frac{1}{\frac{N^{n-1}}{(n-1)!}}, \tag{4.29}$$

where in Eq. (4.29) Eq. (**??**) has been used. It follows that at leading order in N, z_n^i is distributed according to a Gaussian distribution with zero mean and unit variance

$$p_N(z_n^i = z) \overset{N\to\infty}{\to} \frac{1}{\sqrt{2\pi}}\mathrm{e}^{-\frac{z^2}{2}}, \tag{4.30}$$

where $p_N(z_n^i = z)$ is defined as the probability that z_n^i is equal to z at size N.

Eq. (4.30) has been tested numerically for the first few values of n: $p_N(z_n^i = z)$ has been computed by generating $S \gg 1$ samples of $\{x\}$, and so of z_n^i. For $n = 3,4$, the resulting probability distribution $p_N(z_n^i = z)$ converges to a Gaussian distribution with zero mean and unit variance as N is increased, confirming the result (4.30). This convergence is shown in Fig. 4.5, where $p_N(z_4^1 = z)$ is depicted for different values of N together with the right-hand side of Eq. (4.30), as a function of z.

4.9 Appendix: Independence of the z_n^is at leading order in N

Let us consider two distinct variables z_n^i, z_m^j, and proceed at leading order in N.

Following the notation of Appendix 4.8, we write Eq. (4.14) as

$$z_n^i = \frac{\sqrt{(n-1)!}}{N^{\frac{n-1}{2}}} \sum_L X_L, \tag{4.31}$$

$$z_m^j = \frac{\sqrt{(m-1)!}}{N^{\frac{m-1}{2}}} \sum_{L'} X_{L'}, \tag{4.32}$$

where L,L' represent a loop of length n,m passing by the site i,j respectively. Some of the variables X_L depend on some of the variables $X_{L'}$, because they can depend on the same bond variables x_{ij}. Let us pick at random one variable X_L appearing in z_n^i, and count the number of variables $X_{L'}$ in z_m^j that are dependent on X_L. At leading order in N, these are given by the number of $X_{L'}$ having at least one common bond with X_L, and are $O(N^{m-2})$. Hence, if one picks at random two variables $X_L, X_{L'}$ in Eqs. (4.31), (4.32) respectively, the probability that $X_L, X_{L'}$ are dependent is

$$O(N^{m-2}/N^{m-1}) = O(N^{-1}).$$

It follows that z_n^i and z_m^j are independent at leading order in N, i. e. for $N \to \infty$

$$p_N(z_n^i = z, z_m^j = z') = p_N(z_n^i = z) \times p_N(z_m^j = z'), \tag{4.33}$$

where $p_N(z_n^i = z, z_m^j = z')$ denotes the joint probability that z_n^i equals z and z_m^j equals z', at fixed size N.

Eq. (4.33) has been tested numerically for $n = 3$,$m = 4$: $p_N(z_3^1 = z, z_4^1 = z')$ has been computed by generating a number $S \gg 1$ of samples of $\{x\}$, and so of z_3^1, z_4^1. As a result, the left-hand side of Eq. (4.33) converges to the right-hand side as N is increased, confirming the predictions of the above analytical argument. This is shown in Fig. 4.6, where $p_{1024}(z_3^1 = z, z_4^1 = z')$ is depicted together with the $N \to \infty$-limit of the right-hand side of Eq. (4.33) (see Eq. (4.30)), as a function of z,z'.

Chapter 5

Fluctuations of pseudo-critical temperatures in spin-glass models: a numerical study

5.1 Motivations

In chapter 3 we have introduced the problem of fluctuations of a pseudo-critical temperature in a finite-size disordered system due to the presence of disorder. In chapter 4 we have presented an analytical approach to this problem, studying the stability of the paramagnetic minimum of the TAP free energy in the high-temperature phase, considering the full analysis of the Plefka expansion. A definition of pseudo-critical temperature has been introduced and, borrowing results from Random Matrix Theory and Extreme Values Statistics, we obtained that the fluctuations of such pseudo-critical temperature are distributed according to the Tracy-Widom (TW) distribution, at least in a given temperature range.

In order to get a better understanding of the role played by Extreme Value Statistics in connection with the fluctuations of physical observables in spin-glass models, we have investigated the fluctuations of the pseudo-critical temperatures by means of numerical simulations. Generally speaking, the presence for disorder and frustration, which are responsible of a corrugated (free) energy landscape, renders the numerical investigation of spin-glass models a daunting task. Sophisticated computational methods, like parallel tempering and multi-spin coding, allow to simulate efficiently these models.

First, in order to investigate numerically the fluctuations of a pseudo-critical temperature, one must introduce a definition of such a temperature. Unfortunately, observables which present a sharp peak as a function of the temperature in the critical region, which can play the role of a pseudo-critical temperature, do not exist in spin-glass models. On the other hand, we know, by the full-RSB scheme introduced in the Introduction, that the variance of the overlap distribution, i.e. $\langle q^2 \rangle$, is an indicator of the spin-glass transition. The spin-glass susceptibility $\chi_{SG} = N\langle q^2 \rangle$ is a quantity that diverges in all the spin-glass phase and stays finite in the paramagnetic phase. We have decided to consider these observables in our numerical simulations. A precise definition of the pseudo-critical temperature will be given in the following.

In our numerical simulations we have considered two fully-connected spin-glass models: the Sherrington-Kirpatrick model with gaussian and binary couplings, and a short-range spin-glass model, the Edward-Anderson model with binary couplings. The binary nature of interactions of some of these models allows to implement the fast multi-spin coding simulation

technique. We observe that the features of fluctuations of the pseudo-critical temperature are quite similar in the SK model with both gaussian and binary couplings, described by the same scaling exponent and by the same limiting distribution, once again the TW distribution. On the other hand, we observe that for the EA model the fluctuations are described with good accuracy by the Gumbel distribution. These two results put in evidence a strong link between the fluctuations of a physical observable in spin-glass models and the theory of Extreme Value Statistics. If the features of the fluctuations of the pseudo-critical temperature of the SK model, in some sense, can be explained by the analysis presented in chapter 4, the features concerning the EA model are, to our eyes, quite unexpected. We propose a tentative argument in order to understand our observations. The results presented in this chapter have been published in [43].

5.2 Models and the observables

Let us firstly introduce the models and the physical observables that we have considered in our numerical simulations. We consider a system of N spins $S_i = \pm 1$ located at the vertices of a graph, interacting via the Hamiltonian

$$H[\vec{S}] = -\sum_{(i,j)} J_{ij} S_i S_j, \tag{5.1}$$

where the sum runs over the interacting spin pairs (i,j). We consider:

- **GSK**: Sherrington-Kirpatrick model with Gaussian couplings [4]. The underlying graph of the model is a complete graph: the interacting spin-pairs are all the distinct pairs. The couplings J_{ij} are independent identically distributed (i.i.d.) Gaussian random variables with zero mean and variance $1/N$.
- **BSK**: Sherrington-Kirpatrick model with binary couplings [167]. The underlying graph of the model is a complete graph. The couplings J_{ij} are i.i.d. random variables equal to $\pm 1/\sqrt{N}$ with equal probability.
- **EA**: 3-d Edwards-Anderson model [3]. The underlying graph of the model is a three-dimensional cubic lattice with periodic boundary conditions: the interacting spin-pairs are the nearest-neighbors pairs. The couplings J_{ij} are i.i.d. random variables equal to ± 1 with equal probability.

Let us now define the physical observables used to carry on the numerical analysis of the problem. Given two real spins replicas $\vec{S}^1, \vec{S}^2$, their mutual overlap

$$q \equiv \frac{1}{N} \sum_{i=1}^{N} S_i^1 S_i^2 \tag{5.2}$$

is a physical quantity characterizing the spin glass-transition in the thermodynamic limit [5, 31]:

$$\overline{\langle q^2 \rangle_{\mathcal{J}}(\beta)} = \begin{cases} 0 & \beta < \beta_c \\ > 0 & \beta > \beta_c \end{cases} \tag{5.3}$$

where $\langle \cdots \rangle_{\mathcal{J}}$ denotes the thermal average performed with the Boltzmann weight defined by the Hamiltonian $H[\vec{S}]$, $\beta \equiv 1/T$ is the inverse temperature, and $\overline{\cdots}$ stands for the average over quenched disorder $\mathcal{J} \equiv \{J_{ij}\}_{ij}$. The spin-glass susceptivity χ_{GS} is related to the second moment of the overlap probability distribution $P(q)$ by:

$$\chi_{SG}(\beta) = N \overline{\langle q^2 \rangle_{\mathcal{J}}(\beta)} \ . \tag{5.4}$$

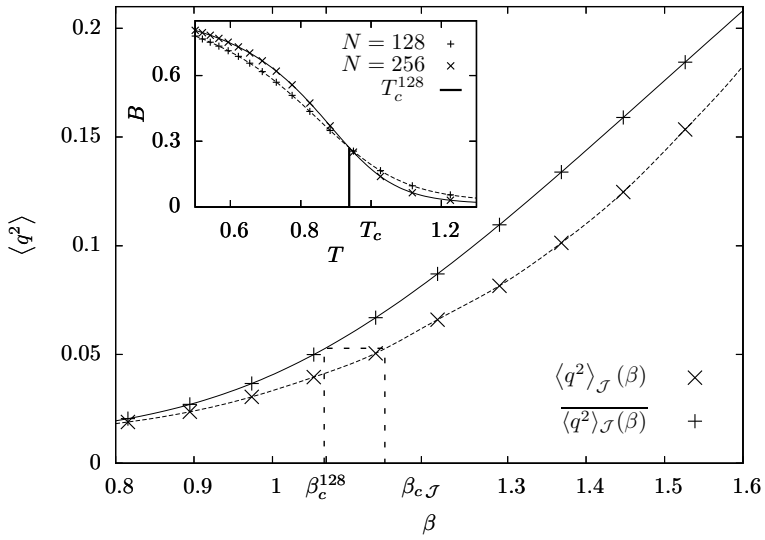

Figure 5.1: Square value of the overlap $\langle q^2 \rangle_{\mathcal{J}}$ for a sample $\mathcal{J}$ (dashed curve) for the BSK model with $N = 128$, its average $\overline{\langle q^2 \rangle_{\mathcal{J}}}$ over the samples $\mathcal{J}$ (solid curve) as a function of the inverse-temperature β, and critical temperatures β_c^N and $\beta_{c\mathcal{J}}$. The dashed vertical lines depict the definition (5.6) of $\beta_{c\mathcal{J}}$. This graphical representation allows for a clear physical interpretation of Eq. (5.6): $\beta_{c\mathcal{J}}$ is the temperature at which the sample $\mathcal{J}$ becomes critical, i. e. its mean square overlap equals the critical value $\overline{\langle q^2 \rangle_{\mathcal{J}}(\beta_{c\,N})}$. Roughly speaking, samples $\mathcal{J}$ such that $\langle q^2 \rangle_{\mathcal{J}}(\beta_{c\,N}) < \overline{\langle q^2 \rangle_{\mathcal{J}}(\beta_{c\,N})}$, as the one depicted in the Figure, are less critical than average, because their square mean overlap at $\beta_{c\,N}$ is smaller than the above critical value. Accordingly, their pseudo-critical temperature $\beta_{c\mathcal{J}}$ satisfies $\beta_{c\mathcal{J}} > \beta_{c\,N}$, because lower-than-average values of the temperature are needed to bring the sample to a critical value of the overlap. The same argument holds in the case $\langle q^2 \rangle_{\mathcal{J}}(\beta_{c\,N}) > \overline{\langle q^2 \rangle_{\mathcal{J}}(\beta_{c\,N})}$. Inset: Binder parameter B as a function of the temperature T for $N = 128$,256 and average pseudo-critical temperature T_c^{128}.

A further observable is the Binder parameter

$$B(T) \equiv \frac{1}{2}\left(3 - \frac{\overline{\langle q^4\rangle_{\mathcal{J}}}}{(\overline{\langle q^2\rangle_{\mathcal{J}}})^2}\right), \tag{5.5}$$

measuring the deviation of the overlap probability distribution $P(q)$ [113] from a Gaussian distribution. People usually define an average finite-size pseudo-critical temperature T_c^N, which depends on the system size N, as the temperature at which the Binder parameter of a system of size $2N$ crosses the Binder parameter of a system of size N [168].

We are now in a position to define a finite-size critical temperature $T_{c\mathcal{J}} = 1/\beta_{c\mathcal{J}}$, and study its fluctuations with respect to quenched disorder. We consider as observable $\langle q^2\rangle_{\mathcal{J}}$ as a function of the temperature T for several samples of the quenched disorder $\mathcal{J}$. In analogy with Eq. (5.3), we define the critical temperature $\beta_{c\mathcal{J}}$ as the value of β such that $\langle q^2\rangle_{\mathcal{J}}(\beta_{c\mathcal{J}})$ *significantly differs from zero*, i. e. is critical. Since a typical critical value of the square overlap at size N is $\overline{\langle q^2\rangle_{\mathcal{J}}(\beta_{cN})}$, the above qualitative definition is easily cast into the quantitative relation

$$\langle q^2\rangle_{\mathcal{J}}(\beta_{c\mathcal{J}}) = \overline{\langle q^2\rangle_{\mathcal{J}}(\beta_{cN})}\ . \tag{5.6}$$

Both for the GSK and BSK model, β_c^N is chosen to be the average critical temperature at size N, which is defined as the temperature at which the Binder parameter, Eq. (5.5), of a system of size N equals the Binder parameter of a system of size $2N$. For the EA model we simply take β_{cN} to be equal to the infinite-size critical temperature $\beta_c = 0.855$ [169], because in this case the Binder parameters cross at a temperature which is very close to the infinite-size critical temperature β_c. The definition of the pseudo-critical temperature given by Eq. (5.6) is qualitatively depicted in Fig. 5.1.

The distribution of $\beta_{c\mathcal{J}}$ can be characterized by its mean $\overline{\beta_{c\mathcal{J}}}$, its variance $\sigma_N^2 \equiv \overline{\beta_{c\mathcal{J}}^2} - \overline{\beta_{c\mathcal{J}}}^2$ and by the PDF $p_N(x_{\mathcal{J}})$ of the natural scaling variable

$$x_{\mathcal{J}} \equiv (\beta_{c\mathcal{J}} - \overline{\beta_{c\mathcal{J}}})/\sigma_N\ . \tag{5.7}$$

We can expect that, to leading order in N, $\sigma_N \sim N^{-\phi}$ and that, for large N, $p_N(x_{\mathcal{J}})$ converges to a nontrivial limiting PDF $p_\infty(x_{\mathcal{J}})$.

5.3 Some details on numerical methods

The observables of the SK and the EA model have been computed with MC simulations, which have been performed with the Parallel Tempering (PT) algorithm [170, 171, 172]. As explained in a recent review [173], the general idea of parallel tempering is to simulate M replicas of the system, each replica at a different temperature. The high-temperature systems are generally able to sample large volumes of phase space, whereas low-temperature systems, whilst having precise sampling in a local region of phase space, may become trapped in local energy minima during the timescale of a typical computer simulation. Parallel tempering achieves good sampling by allowing the systems at different temperatures to exchange complete configurations. Thus, the inclusion of higher temperature systems ensures that the lower temperature systems can access a representative set of low-temperature regions of phase space.

The multispin-coding technique [31] has been implemented for the studied models with binary couplings. In the simulation of a system with binary variables, only one bit is required for storing the information of a single spin, then a computer word can store the information

of several spins at the same time. The Monte Carlo spin flip process can then be implemented with the logical commands. This technique allows to reduce both storage and cpu times.

In table 5.1 we report the parameters used in our numerical simulations for the three models considered: the GSK, the BSK and the EA. N is the system size, i.e. the number of spins, $N_{replica}$ is the number of replicas used in the parallel tempering algorithm, β_{min} and β_{max} define the thermal window investigated in our simulations and $N_{samples}$ is the number of disorder samples simulated at a given system size and at given temperature. The large number of samples investigated allows to have a good statistics in the estimation of the distribution of the pseudo-critical temperature. Also larger sizes for the BSK model have been investigated (N = 1024,2048,4096) but the small number of samples, compared to the number of samples of smaller sizes, does not allow to investigate the probability distribution of the pseudo-critical temperature. On the other hand, these sizes allowed us to have a better estimation of the scaling exponent ϕ.

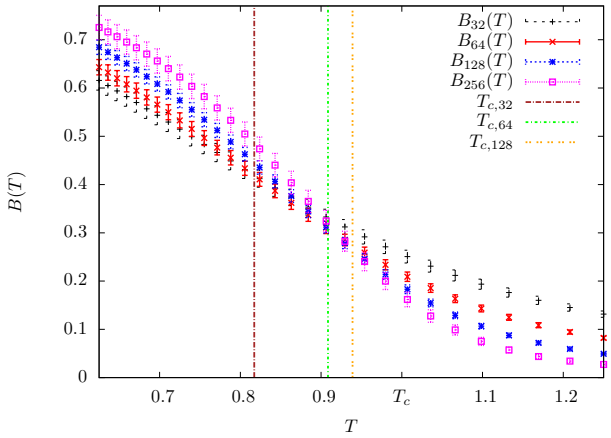

Figure 5.2: Binder parameter $B(T)$ as a function of the temperature T for $N = 32, 64, 128, 256$ (in black, red, blue, violet respectively), $2.8\times10^3 \leq S \leq 2.5\times10^4$, and $T_{c\,N}$ for $N = 32,64,128$ (brown, green, orange respectively), and the infinite-size critical temperature T_c. Error bars on $B(T)$ are an estimate of sample-to-sample fluctuations.

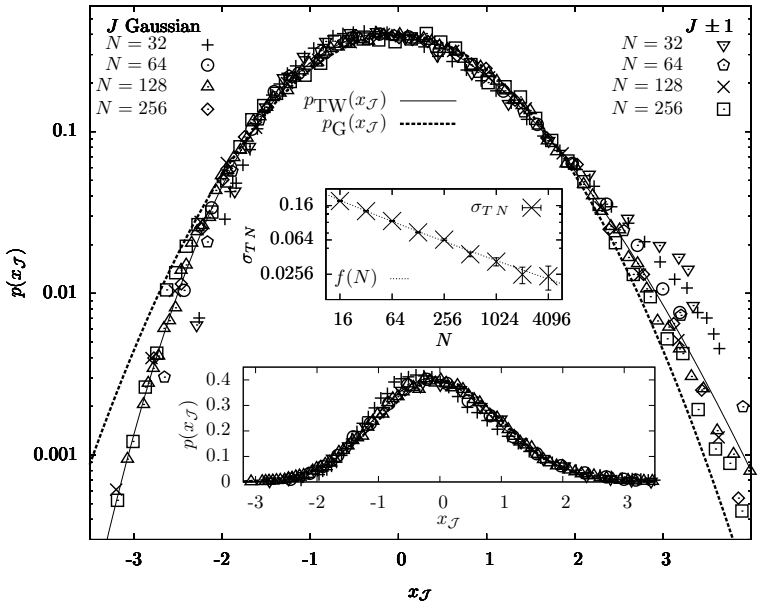

Figure 5.3: Distribution of the pseudo-critical point both for the SK model with Gaussian couplings (GSK) and for the SK model with binary couplings (BSK). PDF $p_N(x_{\mathcal{J}})$ of the rescaled critical temperature $x_{\mathcal{J}}$ for systems sizes $N = 32,64,128,256$ with $1.6 \times 10^4 \leq S \leq 4.7 \times 10^4$ (GSK) and $2.9 \times 10^4 \leq S \leq 9.8 \times 10^4$ (BSK) disorder samples, Tracy-Widom distribution $p_{\rm TW}(x_{\mathcal{J}})$ (solid curve) and Gaussian distribution $p_{\rm G}(x_{\mathcal{J}})$ (dashed curve), both with zero mean and unit variance. The plot has no adjustable parameters, and is in logarithmic scale to highlight the behaviour of the distributions on the tails. Top inset: width $\sigma_{T\,N}$ as a function of N and fitting function $f(N) = aN^{-\phi} + bN^{-2\phi}$, yielding $\phi = 0.34 \pm 0.05$. Bottom inset: same plot as in the main plot in linear scale.

5.4 Numerical results for the SK model

Monte Carlo simulations for the GSK and BSK model allowed for a numerical computation of $\langle q^2 \rangle_{\mathcal{J}}$, of the Binder parameter $B(T)$ and so of $\beta_{c\mathcal{J}}$ for several disorder samples $\mathcal{J}$.

In figure 5.2 we plot the Binder parameter for the GSK model for the investigated sizes and temperatures. Let us now concentrate on the investigation of the fluctuations of the pseudo-critical temperature. Data show that as the system size N is increased, $\overline{\beta_{c\mathcal{J}}}$ approaches β_c. Setting $T_{c\mathcal{J}} \equiv 1/\beta_{c\mathcal{J}}$, $\sigma^2_{T\,N} \equiv \overline{T^2_{c\mathcal{J}}} - \overline{T_{c\mathcal{J}}}^2 \sim N^{-\phi}$, the power law fit of $\sigma_{T\,N}$ shown in Fig. 5.3 gives the value of the scaling exponent $\phi = 0.31 \pm 0.07$ (GSK) and $\phi = 0.34 \pm 0.05$ (BSK). These values of ϕ are both consistent with the value $\phi = 1/3$ that one would expect from scaling arguments by considering the variable $y \equiv N^{1/3}(T - T_c)$ introduced in [174]. On the other hand, the measured value of the scaling exponent ϕ is also consistent with other measures performed by another group [175], while our work was being achieved.

The PDF p_N of the rescaled variable $x_{\mathcal{J}}$ is depicted in Fig. 5.3. The curves $p_N(x_{\mathcal{J}})$ collapse quite satisfyingly indicating that we are close to the asymptotic regime $N \to \infty$. Even though one could naively expect the fluctuations of the pseudo-critical point to be Gaussian, Fig. 5.3 shows that this is not the case. In fact we find that the limiting distribution describing the fluctuations of the pseudo-critical temperature, defined via equation (5.6), is described with a good accuracy by the Tracy-Widom distribution, at least in the high-temperature phase $\beta_{c\mathcal{J}} < 1$. It is then interesting to compare this result with the one obtained by the analytic approach presented in chapter 4. We observe that within the two approaches, the analytical and the numerical one, notwithstanding we are forced to introduce two different definition of pseudo-critical temperature, it seems that the limiting distribution, i.e. the Tracy-Widom distribution, is in some sense universal, with respect to the distribution of the disorder (BSK and GSK) and to the choice of the definition. On the other hand, since the scaling exponent ϕ measured in this section is not compatible with the one obtained via the analytic approach $\phi = 2/3$, we can conclude that the scaling exponent is definition-dependent.

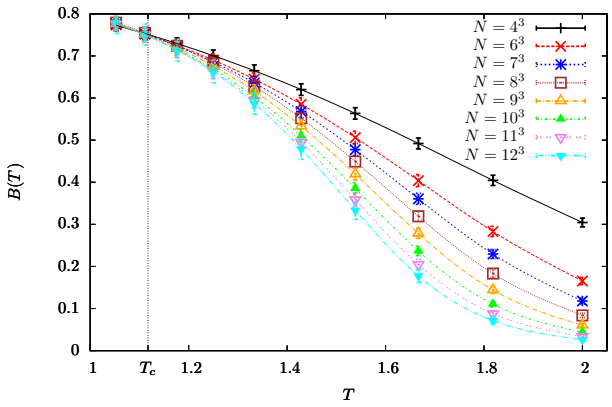

Figure 5.4: Binder parameter B as a function of the temperature T for $N = 4^3$,6^3, 7^3, 8^3, 9^3, 10^3,11^3, 12^3 (in black, red, blue, brown, yellow, green, violet, cyan respectively) and $2.5 \times 10^3 \leq S \leq 3.2 \times 10^4$, and estimate of critical temperature T_c in the infinite-size limit (gray). The continuous lines are just a guide for the eye. Error bars on $B(T)$ are an estimate of sample-to-sample fluctuations.

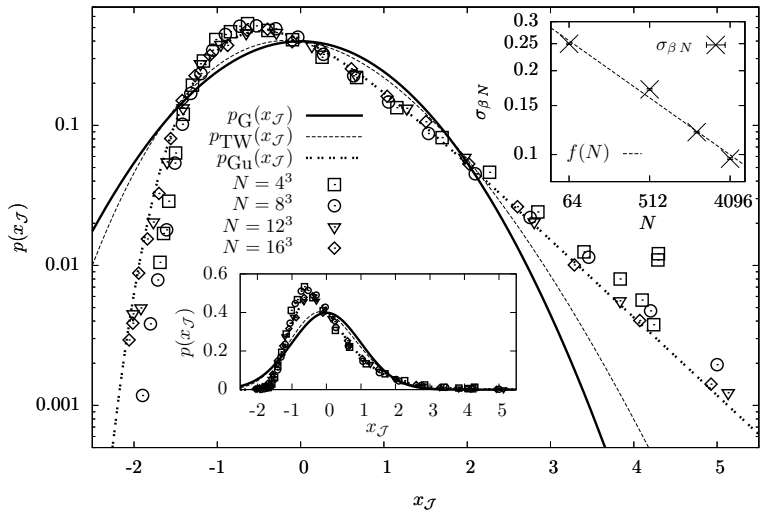

Figure 5.5: Distribution of the pseudo-critical point for the EA model. PDF $p_N(x_{\mathcal{J}})$ of the rescaled variable $x_{\mathcal{J}}$ for systems sizes $N = 4^3$,8^3,12^3,16^3 with $2.4{\times}10^4 \leq S \leq 3.2{\times}10^4$ disorder samples, Gaussian distribution $p_{\mathrm{G}}(x_{\mathcal{J}})$ (solid curve), Tracy-Widom distribution $p_{\mathrm{TW}}(x_{\mathcal{J}})$ (dashed curve) and Gumbel distribution $p_{\mathrm{Gu}}(x_{\mathcal{J}})$ (dotted curve), all with zero mean and unit variance. The plot has no adjustable parameters, and is in logarithmic scale to highlight the behaviour of the distributions on the tails. Top inset: width $\sigma_{\beta N}$ as a function of N, and fitting function $f(N) = a\, N^{-\phi}$, with scaling exponent $\phi = 0.23 \pm 0.03$. Bottom inset: same plot as in the main plot in linear scale.

5.5 Numerical results for the 3-d EA model

Monte Carlo simulations for the EA model allowed for a numerical computation of $\langle q^2 \rangle_{\mathcal{J}}$, of the Binder parameter $B(T)$ and so of $\beta_{c\,\mathcal{J}}$ for several disorder samples $\mathcal{J}$.

In figure 5.4 we plot the Binder parameter for the GSK model for the investigated sizes and temperatures. Let us now concentrate on the investigation of the fluctuations of the pseudo-critical temperature. Similarly to the SK model, the width $\sigma_{\beta\,N}$ of the distribution of the pseudo-critical point $\beta_{c\,\mathcal{J}}$ shrinks to zero as the system size N is increased: a power law fit $\sigma_{\beta\,N} = a\,N^{-\phi}$ gives the value of the scaling exponent $\phi = 0.23 \pm 0.03$ (inset of Fig. 5.5). The PDFs $p_N(x_{\mathcal{J}})$ of the rescaled critical temperature seem to approach a limiting distribution as N is increased, as depicted in Fig. 5.5, coinciding with the Gumbel distribution.

Both ϕ and the PDF have the following interesting features. As far as the exponent ϕ is concerned, we recall [96] that for systems known to be governed by a random fixed point like the EA model it was predicted that the scaling exponent satisfies $1/\phi = d\nu$, where d is the dimensionality of the system. The value of the critical exponent $\nu = 1.8 \pm 0.2$ for the EA model is known from numerical simulations [31], yielding a value of $\phi = 0.19 \pm 0.02$ which is compatible with that measured from the fluctuations of the critical temperature.

As far as the limiting distribution $p_\infty(x_{\mathcal{J}})$ is concerned, we recall that [176] a disordered system like the EA behaves as an ensemble of independent sub-systems $\mathcal{S}_1, \ldots, \mathcal{S}_M$, where each sub-system $\mathcal{S}_i$ has a random local critical temperature β_c^i, the local critical temperatures $\{\beta_c^i\}_i$ being IID random variables depending on the *local* realization of the disorder. We can argue that, for a single realization of the disorder $\mathcal{J}$, the pseudo-critical temperature $\beta_{c\,\mathcal{J}}$ results from the fact that β has to be taken large enough to bring all of the sub-systems $\{\mathcal{S}_i\}_i$ to criticality. Thus, $\beta_{c\,\mathcal{J}}$ is the maximum over the ensemble of the local critical temperatures $\beta_{c\,\mathcal{J}} = \max_i \beta_c^i$. If this picture is correct, $\beta_{c\,\mathcal{J}}$ is distributed according to one of the the EVS limiting distributions of independent variables: the Gumbel, Fréchet, or Weibull distribution. Assuming that the distribution of β_c^i decays exponentially for large β_c^i, the distribution of $\beta_{c\,\mathcal{J}}$ is the Gumbel one. We want to stress that this argument would not hold for the SK model, where there is no geometric structure.

GSK			
N	$\beta_{min} \leq \beta \leq \beta_{max}$	$N_{replica}$	$N_{samples}$
32	$0.2 \leq \beta \leq 2.2$	30	46911
64	$0.8 \leq \beta \leq 1.6$	30	19946
128	$0.8 \leq \beta \leq 1.6$	30	25135
256	$0.8 \leq \beta \leq 1.6$	30	15545
BSK			
N	$\beta_{min} \leq \beta \leq \beta_{max}$	$N_{replica}$	$N_{samples}$
32	$0.2 \leq \beta \leq 2.2$	20	98950
64	$0.5 \leq \beta \leq 2$	20	33392
128	$0.5 \leq \beta \leq 2$	20	79104
256	$0.5 \leq \beta \leq 2$	20	28993
512	$0.5 \leq \beta \leq 2$	20	3393
EA			
N	$\beta_{min} \leq \beta \leq \beta_{max}$	$N_{replica}$	$N_{samples}$
4^3	$0.5 \leq \beta \leq 2$	16	27367
8^3	$0.5 \leq \beta \leq 2$	16	32419
12^3	$0.5 \leq \beta \leq 2$	16	24001
16^3	$0.5 \leq \beta \leq 2$	16	24513

Table 5.1: Simulation parameters for the GSK, BSK and EA models. N is the system size, i.e. the number of spins, $N_{replica}$ is the number of replicas used in the parallel tempering algorithm, β_{min} and β_{max} define the thermal window investigated in our simulations and $N_{samples}$ is the number of disorder samples simulated at a given system size and a given temperature.

5.6 Conclusions and perspectives

In this chapter we have investigated the fluctuations of a suitably-defined pseudo-critical temperature due to the presence of disorder in fully-connected and nearest-neighbours spin-glass models via numerical simulations. In the case of the fully-connected Sherrington-Kirkpatrick model we find that such fluctuations, for large system size, are described by a limiting distribution which coincides with the Tracy-Widom distribution, introduced in chapter 3 in the context of the fluctuations of the largest eigenvalue of gaussian random matrices. To our knowledge, this is the first time that the ubiquitous Tracy-Widom distribution plays a role in the description of the fluctuations of a physical observable in spin-glass-models context. This connection has been suggested by the analytical approach to the same problem presented in chapter 4.

On the other hand we have investigated the fluctuations of the pseudo-critical temperature in nearest-neighbours Edward-Anderson model. In this case, we find that the limiting distribution describing the fluctuation of the pseudo-critical temperature coincides with the Gumbel distribution. A tentative argument, based on the local fluctuations of the quenched disorder, to explain this result has been proposed. These two results shed some light on the important role played by the Extreme Value Statistics theory in connection with the description of spin-glass models.

The present work opens several perspectives. As far as the SK model is concerned, we

recall that the TW distribution describes typical fluctuations of the maximal eigenvalue of a Gaussian Orthogonal Ensemble random matrix, while the large deviations regime of these fluctuations has been studied only recently [177]. It would be interesting to study numerically the large deviations regime of the fluctuations of the critical temperature, where the distribution of the pseudo-critical point should be described by the large deviations function derived in [177].

Moreover, in order to bridge the gap between a mean-field and a short-range interactions regime, it could be interesting to investigate the fluctuations of the pseudo-critical temperature in spin-glass models with tunable long-range interactions, like those introduced in [178].

As far as the EA model is concerned, it would be interesting to test experimentally the scenario found here in $Fe_{0.5}Mn_{0.5}TiO_3$ [179] or $Eu_{0.5}Ba_{0.5}MnO_3$ [180] spin-glass materials. Indeed, ac-susceptibility measurements in these systems show [179] that the spin-glass critical temperature can be identified as the temperature where the susceptibility develops a cusp. Accordingly, the pseudo-critical point could be easily identified and measured, and one could test whether the resulting rescaled pseudo-critical point distribution converges to the Gumbel distribution as the system size is increased.

Part III

Interdisciplinary Applications

Chapter 6

Financial Crisis, Systemic Risk and Stress Tests

Financial crisis are usually followed by long periods of recession of economy. How to explain this fact? According to the point of view of Friedman and Schwartz [181], financial crises raise the cost of intermediation and restrict credit, which in turns restrain the level of activity in the real sector and ultimately can lead to periods of low growth and recession. Financial crises occur quite often if compared to other crises. This suggests that the financial sector is unusually susceptible to shocks. Moreover, shocks that initially affect only some financial institutions easily propagate to larger sectors of the financial system and then infect the whole system. The risk that contagion can spread from small parts of the financial system to the whole system, is usually referred to as Systemic Risk.

Governments and international organizations are increasingly worried about systemic risk, under which "the world's financial system can collapse like a row of dominoes" [182]. One of the main purposes of financial supervisory authorities and central banks is to maintain systemic financial stability, thus a correct evaluation of Systemic Risk becomes mandatory. Given the enormous social cost of financial crisis, authorities have often decided to bail out troubled financial institutions rather than risking that their default might provoke the failure of other institutions.

The banking system is considered a fundamental framework in which financial contagion can take place. Troubled banks may default on their interbank liabilities and hence cause other banks to default triggering a domino effect. The stability of a banking system is constantly monitored by financial supervisory authorities. Stress Test are commonly used tools to quantify Systemic Risk in financial networks [183].

6.1 Introduction: the fear of contagion

6.1.1 The 2008-09 financial crisis

The financial crisis of 2008-09 had its origins in the housing market. Problems in a relatively small portion of the home mortgage market triggered the most severe financial crisis in the United States since the Great Depression. Some authors [184] stress the central role played by the presence of Systemic Risk in the propagation of the crisis. Let us resume in few lines the main steps of the crisis. In the second half of 2007 banks and other financial

firms realized significant losses in their investments in home mortgages and home-mortgages securities. Some authors [185] relate these events to the high proliferation of sub-prime loans and to the burst of the housing bubble. This provoked the failure and near-failure of some major financial firms: Bear Stearns, IndyMac Federal Bank, the Federal National Mortgage Association (Fannie Mae), the Federal Home Loan Mortgage Corporation (Freddie Mac), Lehman Brothers, American International Group (AIG) and Citigroup. International financial markets realized significant losses in much of 2008 and 2009. According to [184], "Systemic risk concerns were at the heart of the Federal Reserve's decision to facilitate the acquisition of Bear Stearns by JPMorgan Chase in March 2008 and the U.S. Department of the Treasury's decisions to place Fannie Mae and Freddie Mac into conservatorship and to assume control of AIG in September 2008". In other words, some financial institutions have been "saved", since they have been considered "too-big-to-fail", to prevent the risk that the shock of failures would propagate inside the financial network. In a speech at the Federal Deposit Insurance Corporation's Forum in 2008 [186] , the Federal Reserve Chairmen Ben Bernanke explained:

> Our analyses persuaded us [...] that allowing Bear Stearns to fail so abruptly at a time when the financial markets were already under considerable stress would likely have had extremely adverse implications for the financial system and for the broader economy. In particular, Bear Stearns' failure under those circumstances would have seriously disrupted certain key secured funding markets and derivatives markets and possibly would have led to runs on other financial firms.

6.1.2 When genius failed: Long-Term Capital Management

The history of Long-Term Capital Management (LTCM) is vividly described in the book of Roger Lowenstein: "When Genius Failed: The Rise and Fall of Long-Term Capital Management" [187]. LTCM was a prominent U.S. hedge found founded in March 1994 by John Meriwether, with a small group of associates, most notably economists Robert Merton and Myron Scholes, who received the Nobel Prize in economics in 1997. LTCM was very successful: by the end of 1997 it had achieved annual rates of return of around 40 percent and had nearly tripled its investors' money. A temporary market irrationality in bond pricing affected markets during august 1998. In the same month Russian government devalued the ruble and defaulted on its bonds. LTCM lost hundred of millions of dollars and approached a default. The Governors of U.S. Federal Reserve was concerned that the default of LTCM can trigger a domino effect on financial markets. In the speech of William McDonough, President of Fed. Reserve Bank of New York [188]:

> Had Long-Term Capital been suddenly put into default, its [derivatives] counterparties would have immediately "closed out" their positions. If counterparties would have been able to close-out their positions at existing market prices, losses, if any, would have been minimal. However, if many firms had rushed to close-out hundreds of billions of dollars in transactions simultaneously, they would have been unable to liquidate collateral or establish offsetting positions at the previously-existing prices. Markets would have moved sharply and losses would have been exaggerated.

A group consisting of banks and insurance-holding company offered to buy out the shareholders of LTCM for $250 million and put $3.75 billion into the fund as new capital.

6.2 Systemic Risk in banks networks

In financial literature a common definition of Systemic Risk is still unsettled. According to Schwarcz [182], a common factor in the various definitions of systemic risk is that "a trigger event, such as an economic shock or institutional failure, causes a chain of bad economic consequences – sometimes referred to as a domino effect. These consequences could include (a chain of) financial institution and/or market failures. Less dramatically, these consequences might include (a chain of) significant losses to financial institutions or substantial financial-market price volatility". In this section we will consider networks of banks. We will present the reasons why the banking system is considered so fragile and the channels which the shocks can propagate through inside the system.

6.2.1 The "fragility" of the banking system

In public policy, banks' failures are feared for the risk that wave of failure can propagate to other banks, then to the whole banking system and even beyond to financial system or to domestic economy. The same fear is not perceived if we consider the failure of other firms, e.g. airline companies or steel factories or grocery stores. On the contrary, in these fields, the surviving firms benefits from the failure of a competitor: they can expand their market. What makes the banking sector peculiar? Two reasons are identified to make the banking system so "fragile":

- Interconnectedness. Banks are closely interconnected with each other through lending to and borrowing from each other. Via the payment clearing system, it is believed that the failure of bank can quickly propagate to the others.

- High leverage. Compared to most non financial firms, banks, and other financial institutions, have a low capital-to-assets ratio, which means that they are highly leveraged. In order to give an example concerning the 2008-09 crisis: "Investment banks were especially highly leveraged before the crisis, with debt-to-equity ratios of approximately 25 to 1. That is, for every dollar of equity, investment banks issued an average of $25 of debt. By comparison, commercial banks, which are subject to minimum capital requirements, had leverage ratios of approximately 12 to 1.14 High leverage means that financial firms enjoyed high rates of return on equity when times were good but also a high risk of failing when markets turned against them" [184].

6.2.2 The channels of contagion

Different channels of contagion can be identified. In our analysis we will concentrate on the Systemic Risk arising from interbank lending. Stress tests to evaluate Systemic Risk on this channel of contagion rely on the following mechanism. A bank or a group of banks are assumed to default: they are not able to pay back their borrowings in the loan market. This provokes losses to their creditor banks. If the losses of creditor banks exceed their capital, also creditor banks default. Since every default weakens the surviving banks, this could lead to a cascade of bank failures. Other channels of contagion can be identified. Contagion can take place if an institution does not meet its obligations in payments systems [189]. In the following lines we will present another way of contagion, deriving from deposit withdrawals, also know as "bank run".

6.2.3 Bank run

The classic example of systemic risk in the context of financial network is a "bank run". The inability of a bank to satisfy withdrawal-demands causes its failure, in turn causing other banks or their creditors to fail. The triggering event can be considered exogenous to the system, i.e. the panic of depositors that "run" to the bank to quickly withdraw their money. Because banks keep only a small fraction of their deposits on hand as cash reserves, a bank may have insufficient cash to pay all withdrawal-demands, causing it to default. The interconnectedness of the banking system then becomes the channel of propagation of the shock: one bank's default on an obligation to another may adversely affect that other bank's ability to meet its obligations to yet other banks. The shock of failures can propagate and the domino effect takes place.

As pointed out in [182], "This scenario is most graphically illustrated by the Great Depression. In response to the stock market downturn of August 1929 and the crash of October 1929, depositors en masse attempted to convert their bank deposits into cash. Many banks were unable to satisfy all of these demands, causing them to fail and contracting the money supply. These failures, in turn, caused many otherwise solvent banks to default, and many companies, deprived of liquidity, were forced into bankruptcy. During the height of the Great Depression, from 1930 to 1933, there were approximately two thousand bank failures yearly".

6.3 Theoretical framework for interbank lending

Let us consider an ensemble $\mathcal{B} = \{b_0, \dots, b_{N-1}\}$ of N banks, in which each bank in $\mathcal{B}$ may borrow to or lend money from other banks in $\mathcal{B}$. This structure is encoded in the so-called liability matrix L, an $N \times N$ non-symmetric matrix describing the instantaneous state of a credit network [‡1]. Each element L_{ij} denotes the funds that bank $j \in E$ borrowed from bank $i \in \mathcal{B}$ (regardless of the maturity of the debt). We fix the convention that $L_{ij} \geq 0$ $\forall (i,j) \in \mathcal{B} \times \mathcal{B}$, $L_{ii} = 0$ $\forall i \in \mathcal{B}$. With this definition, the expression $r_i = \sum_j L_{ij}$ represents the total credit which the institution i possesses against the system, while $c_j = \sum_i L_{ij}$ represents the total debt owed by the institution j to the environment.[‡2] This matrix contains information about the instantaneous state of a credit network, and it is sufficient to estimate the risk of contagion in many cases of practical relevance.

$$
L_{ij} = \begin{array}{c}
\left[\begin{array}{ccccc}
0 & L_{12} & L_{13} & \dots & L_{1N} \\
L_{21} & 0 & L_{23} & \dots & L_{2N} \\
L_{31} & L_{32} & 0 & \dots & L_{0N} \\
\dots & \dots & \dots & \dots & \dots \\
L_{N1} & L_{N2} & L_{N3} & \dots & 0
\end{array}\right]
\begin{array}{c}
\rightarrow \\ \rightarrow \\ \rightarrow \\ \rightarrow \\ \rightarrow
\end{array}
\begin{array}{c}
r_1 \\ r_2 \\ r_3 \\ \dots \\ r_N
\end{array} \\
\begin{array}{ccccc}
\downarrow & \downarrow & \downarrow & \downarrow & \downarrow \\
c_1 & c_2 & c_3 & \dots & c_N
\end{array}
\end{array}
$$

The construction of the liability matrix L depends on the informations that we have about bilateral exposures between banks. These informations can be obtained from credit registers and supervisory report of banks or by balance data sheets of banks. We can distinguish beween two cases:

- **Complete information**: in some countries, for instance in Italy, Hungary, and Mexico, using credit registers and supervisory reports, one is able to obtain informations about

[‡1] The network topology can also be studied, see [190, 191]

[‡2] Without loss of generality we consider a closed economy ($\sum_i r_i = \sum_j c_j$), by using bank b_0 as a placeholder to take into account flows of money external to the system.

all the bilateral exposures between banks. Then the liability matrix elements L_{ij} can be fully identified.

- **Incomplete information**: in some countries, from credit registers and supervisory reports, one is able to obtain only partial information about the liability exposures between banks. Credit registers or supervisory reports cover only exposures exceeding a threshold that is defined either in terms of the absolute amount of the exposure or as a fraction of the lender's capital. This allows to identify only some elements of the liability matrix L. An alternative source of information that is widely available is banks' balance sheets, which only contain information on total interbank lending and borrowing of the reporting institution, from which one is able to identify the vectors r_i and c_i.

In the case of incomplete information, one is left with the problem of reconstructing the liability matrix from partial informations. This case will be extensively discussed in the following chapter. Let us now suppose that one owns the liability matrix of banking network. Widely used tools to asses the stability of the network to shocks and then to evaluate Systemic Risk are stress tests.

6.4 Stress Tests: how to measure Systemic Risk

A widely used measure of vulnerability in financial literature is the stress-test introduced by Furfine [192], which is a sequential algorithm to simulate contagion. Suppose that the liability matrix L is given and let us define C_z the initial capital of a bank z in the system $\mathcal{B}$. The idea of the algorithm is simple: suppose that such bank z of the ensemble $\mathcal{B}$ fails due to exogenous reasons. Then it is assumed that any bank $i \in \mathcal{B}$ loses a quantity of money equal to its exposure versus z (L_{iz}) multiplied by an exogenously given parameter $\alpha \in [0,1]$ for loss-given-default. Then if the loss of the bank i exceeds its capital C_i, bank i fails. This procedure is then iterated until no more banks fail, and the total number of defaults is recorded.

The procedure described above can be formally rephrased in the following steps:

Step 0: A bank $z \in B$ fails for external reasons. Let us define $D_0 = \{z\}$, $S_0 = \mathcal{B}\backslash\{z\}$. For the banks $i \in S_0$ we set $C_i^0 = C_i$.

Step t: The capital C_i^{t-1} at step $t-1$ of banks $i \in S_{t-1}$ is updated according to

$$C_i^t = C_i^{t-1} - \alpha \sum_{j \in D^{t-1}} L_{ij}$$

with $\alpha \in [0,1]$. A bank $i \in S_{t-1}$ fails at time t if $C_i^t < 0$. Let us define D_t, the ensemble of all the banks $i \in S_{t-1}$ that failed at time t and $S_t = S_{t-1}\backslash D_t$ the ensemble of banks survived at step t.

Step t_{stop}: The algorithm stops at time t_{stop} such that $D_{t_{stop}} = \varnothing$.

We want to stress the importance of the loss-given-default parameter α in order to estimate the extent of contagion. The parameter α is considered fixed for every step of the algorithm. In literature we can find different estimations of the values of the loss-given-default parameter. According to James [193] the typical losses on assets of a failing bank including

the cost of resolution are around 40%. According to Kaufman [194], creditor banks are able to recover the 95% of their exposures. When authors perform Stress Tests, given the small knowledge about the loss-given-default-parameter, they usually try a large range of values. Some authors also tried to endogenise the loss-given-default parameter in the Stress-Test model [195] introducing a clearing mechanism. As explained by Upper [183], this requires a series of assumptions that are far from harmless. In literature, Stress Tests are usually performed considering the failure of a single institution, as introduced by Furfine. This assumption is reasonable if we suppose that the failing bank, hit by a shock, has a completely different risk profile than other banks. But, as seen in the case of financial crisis of 2008-09, external shocks can hit several banks simultaneously. In that case, the Stress-Test algorithm must be modified considering groups of banks failing simultaneously.

In his original work [192], Furfine has investigated the contagion in the U.S. banking system using the Federal Reserve's large-value transfer system (Fedwire) data during February and March 1998. Using a search algorithm, he was able to identify all the transactions between the 719 financial institutions that have been conducted via Fedwire. Exposures obtained via the analysis of Fedwire represent only a small fraction of U.S. total interbank exposures (approximately 14 % [192]). This work also provides evidence that smaller banks generally have larger funds exposures relative to their capital level.

In financial literature the stability of the banking system of different countries has been studied. Let us cite the works of Angelini, Maresca and Russo [189] and Mistrulli [196] for the Italian system , Sheldon and Maurer for the Swiss system [197], Furfine for the U.S. system [192], Degryse and Nguyen for the Belgian system [198], Wells for the U.K. system [199] and Upper and Worms for the German system [200]. A complete review on the topic is given by Upper in [183]. Given the differences on the structures of the banking systems in different countries and of methodologies used to analyze data, it is difficult to give a unified picture of the stability of the banking systems in different countries. As a broad picture [183] we can conclude that the results of the literature seem to suggest that contagion due to exposures in the interbank loan market is an unlikely event, in the sense that it happens in only a small number of scenarios considered, but that it could have substantial effects on the health of the banking system of many countries if it does occur.

Chapter 7

Advanced financial network reconstruction for the estimation of systemic risk

7.1 Motivations

In the previous chapter we have shown that banking system is considered a fundamental framework in which financial contagion can take place. Troubled banks may default on their interbank liabilities and hence cause other banks to default triggering a domino effect. We have also seen that detailed data on banks bilateral exposures are not always available. Institutions are often left with the problem of assessing the resilience of a system to financial shocks by relying on an incomplete information set.

In this framework the reconstruction of bilateral exposures becomes a central issue for the estimation of risk. The so called *entropy-maximization method* is a commonly used tool to reconstruct financial networks from incomplete information [189, 197, 198, 199, 200]. The main limitation of this procedure is that it assumes a market structure which can be quite different from the actual one: it tends to spread the debt as evenly as possible.

Allen and Gale [201] were the first authors to point out the crucial role that the "architecture" of the financial network can play in connection with the extent of the spread of the contagion. Complete networks have been shown to be more robust than incomplete networks, see also [202]. In the lines with this thesis, we expect that the reconstruction of the liability matrix via the entropy-maximization method leads to an undervaluation of the extent of contagion. This thesis has been tested by Mistrulli [196] in the context of the Italian banking system, where complete informations on the interbank exposures are available. Stress-Test simulations have been performed on real bilateral exposures and on reconstructed bilateral via entropy-maximisation method. The comparison shows that, depending on the structure of interbank linkages, entropy-maximisation method can lead both to undervaluation and to overvaluation of the risk of contagion, concluding that the maximum-entropy approach may not be very reliable in the evaluation of the severity of contagion.

In order to have a correct, or at least a more reliable, evaluation of risk of contagion, reconstruction procedures which allows to consider different network architectures must be considered. In a recent work [44], we have introduced a message-passing algorithm which allows to tune the sparsity of the reconstructed network.

7.2 Framework

Let us consider a set of N banks $\mathcal{B} = \{b_0, \ldots, b_{N-1}\}$, in which each bank in $\mathcal{B}$ may borrow to or lend money from other banks in $\mathcal{B}$. This structure is encoded in the so-called liability matrix L, an $N \times N$ weighted, directed adjacency matrix describing the instantaneous state of a credit network. Each element L_{ij} denotes the funds that bank $j \in \mathcal{B}$ borrowed from bank $i \in \mathcal{B}$ (regardless of the maturity of the debt). We fix the convention that $L_{ij} \geq 0$ $\forall (i,j) \in \mathcal{B} \times \mathcal{B}$, $L_{ii} = 0$ $\forall i \in \mathcal{B}$. With this definition, the expression $L_i^{\rightarrow} = \sum_j L_{ij}$ represents the total credit which the institution i possesses against the system (also known as out-strength), while $L_j^{\leftarrow} = \sum_i L_{ij}$ represents the total debt owed by the institution j to the environment (in-strength).[‡1] This matrix contains information about the instantaneous state of a credit network, and it is sufficient to estimate the risk of contagion in many cases of practical relevance. Indeed one is often unable to obtain from empirical data the complete expression for the matrix L. Data are typically extracted by a bank balance sheets or by institutional databases [190], and partial informations have to be coherently integrated into a list of plausible liability matrices. In the following discussion, we will suppose that three different types of informations about L are available, as typically reported in the literature [200]:

1. All the debts larger than a certain threshold θ are known. This allows us to rescale all the elements of L by θ, so that we consider without loss of generality liability matrices for which all the unknown elements are bound to be in the interval [0,1]. We assume to have at most order N elements exceeding such threshold.

2. We assume a certain set of entries (which we take to be of order N) to be known. This corresponds to banks or bank sectors for which some particular position needs to be disclosed by law.

3. The total credit $L_i^{\rightarrow}$ and the total debit $L_j^{\leftarrow}$ of each bank are known. Acceptable candidates for liability matrices need to satisfy a set of $2N$ linear constraints, whose rank is in general $\mathcal{R} \leq 2N - 1$ (due to the closed economy condition).

We remark that we have defined a set of constraints of order N elements, which is too small to single out a unique candidate for the true unknown liability matrix. The possible solutions compatible with the observations define a space Λ, whose members we denote with $\hat{L}$. Let U be the set of not directly known (i.e. non-fixed by to constraints of type (1) and (2)) entries of the liabilities matrix. Then those entries of the liability matrix (whose number is $M = |U|$) are real numbers subject to domain constraints (they must be in [0,1]) and linear algebraic constraints (the sum on the rows and on the columns must be respected). The ratio $M/\mathcal{R} \geq 1$ controls the degree of underdetermination of the network, and is typically much larger than one.

7.3 Dense reconstruction

A possible procedure to study the robustness of a financial network when the complete information about the liability matrix is not uniquely specified, is to pick from the set of candidate matrices Λ a representative matrix, and to test the stability uniquely for the network specified by such $\hat{L}$. In this case a criteria has to be chosen to select a particular matrix out of the Λ space, including some assumptions about the structure of the true L_{ij}. A choice which

[‡1] Without loss of generality we consider a closed economy ($\sum_i L_i^{\rightarrow} = \sum_j L_j^{\leftarrow}$), by using bank b_0 as a placeholder to take into account flows of money external to the system.

is commonly adopted [189, 197, 198, 199, 200] is based on the maximum-entropy criteria, which assumes that banks spread their lending as evenly as possible. The problem in this case amounts to finding a vector $\vec{L} = \{L_\alpha\}_{\alpha \in U}$ (the unknown entries of the liability matrix) whose entries comply with the algebraic and domain constraints and minimize the distance from the uniform vector $\vec{M} = \{M_\alpha\}_{\alpha \in \mathcal{U}}$ (such that $\forall \alpha \quad M_\alpha = 1$), where the distance is quantified by the Kullback-Leibler divergence:

$$D_{KL}(\vec{L}, \vec{M}) = \sum_\alpha L_\alpha \log \frac{L_\alpha}{M_\alpha}$$

The minimization of such function is a standard convex optimization problem, that can be solved efficiently in polynomial time. In financial literature this algorithm is known with the name of Maximal Entropy (ME) reconstruction, for some details see [203]. We remark that no entry is exactly set to zero unless this is required by the algebraic constraints.

7.4 Sparse reconstruction: a statistical-mechanics approach

As we have seen in the Introduction, statistical physics (and in particular statistical mechanics of spin-glass models) has been increasingly successful in analyzing and solving complex problems coming from graph theory and theoretical computer science [204]. For some NP-complete problems, using a statistical mechanics approach, it was possible to obtain results which had not been found before using classical mathematical methods. Concerning graph theory, let us cite the statistical mechanics approach to a NP-complete problem, the vertex-cover problem, studied in [205]. In the present section, we present how typical tools of statistical mechanics of spin-glass models and theoretical computer science, e.g. the belief-propagation algorithm, can be used to face the problem introduced in this chapter, namely the problem of the reconstruction of sparse banks liability networks.

ME might not be a particularly good description of reality since the number of counterparties of a bank is expected to be limited and much smaller than N, while ME tends to produce completely connected structures. In the case of real networks the degree of market concentration can be higher than suggested by ME. This systematically leads to an underestimation of risk, as a structure in which the debt is distributed homogeneously among the nodes is generally known to be able to absorb shocks more effectively than a system in which few nodes dominate the network [196]. In order to be closer to reality and to estimate more accurately the risk contagion it is then necessary to reconstruct liability matrices whose degree of sparsity (i.e. the fraction of zero entries of $\hat{L}$) can be tuned, and eventually taken to be as big as possible. This corresponds to the choice of topologies for the interbank networks in which the number of links can be explicitly regulated by means of a control parameter. We present in this section an algorithm which, given the fraction $\hat{\lambda}$ of entries which are expected to be exactly zero, is able to reconstruct a sample of network structures compatible with this requirement, and to find a λ_{max} which bounds the maximum possible degree of sparsity. We focus the discussion on the generic case in which topological properties of the original credit network such as the sparsity parameter λ or the number of counter parties of each bank are not known, without imposing any specific type of null model. The purpose of the algorithm is to provide an efficient mean to explore the space Λ, and to illustrate how the result of the stress-testing procedures may vary according to the density of zeroes of the matrix $\hat{L}$ which is assumed.

To be more specific, let us define the notion of *support* of a liability matrix as follows: given

an $N \times N$ weighted, directed adjacency matrix L, we define its support $a \in \{0,1\}^{N^2}$ as the $N \times N$ adjacency matrix such that

$$a_{i,j}(L) = \begin{cases} 1 & \text{if} \quad L_{ij} > 0 \\ 0 & \text{otherwise} \end{cases} .$$

The *sparsity* λ associated with a specific network structure a is defined as $\lambda\{a_{i,j}\} = 1 - (\sum_{ij} a_{i,j})/N(N-1)$. Finally, given a network structure $\hat{a}$ and a set of liability matrices Λ, we say that $\hat{a}$ is *compatible* with Λ if there exists at least a matrix $\hat{L} \in \Lambda$ such that $a_{i,j}(\hat{L}) = \hat{a}_{i,j}$. Now we consider a liability matrix L which is partially unknown in the sense of section 7.2, and address the following issues: (i) is it possible to fix a fraction $\hat{\lambda}$ of the unknown entries to zero without violating the domain and the algebraic constraints? More formally, this corresponds to ask whether it exists a matrix $\hat{L} \in \Lambda$ such that $\hat{\lambda} = \lambda(a(\hat{L}))$. More generally, (ii) how many supports $\hat{a}$ with fixed sparsity $\hat{\lambda}$ are compatible with Λ? The algorithm solves this problems by sampling from the space of all compatible supports $a(\Lambda)$ potential candidates whose degree of sparsity is constrained to be $\hat{\lambda}$, and by evaluating the volume of such support sub-space. As one can easily expect, there will be a range of $[\lambda_{min}, \lambda_{max}]$ of fractions of fixed zeros compatible with the constraints: trivially $\lambda_{min} = 0$ corresponds to the dense network, which always admits a compatible solution, but we are able to find a non-trivial λ_{max} which corresponds to the maximally sparse network of banks. A plot of the logarithm of the number of possible supports as a function of $\hat{\lambda}$ is given in figure 7.1 ($\times$ signs) for a network as the ones described in section 7.5. Once a support is given, the liability matrix elements can easily be reconstructed via ME.[‡2]

The algorithm that we use to sample the candidate network structures $\hat{a}$ employs a message-passing technique which is able to overcome the problem of explicitly inspecting the compatibility of each network. The main idea is that we want to associate to each adjacency matrix a a sampling probability $P_0\{a_{i,j}\}$, that is strictly zero for non-compatible supports and is otherwise finite. Sampling uniformly from the space of compatible supports would correspond to the choice that $P_0\{a_{i,j}\} = 1/|a(\Lambda)|$ iff $a_{i,j} \in a(\Lambda)$ and zero otherwise. Indeed, to fix the required degree of sparsity of the network $\hat{\lambda}$ one can consider the modified sampling probability

$$P_0\{a_{i,j}\} = \frac{1}{Z} \begin{cases} z^{\sum_{ij} a_{i,j}} & \text{if} \quad a \in a(\Lambda) \\ 0 & \text{otherwise} \end{cases} ,$$

where Z is a normalization constant and the *fugacity* z controls the average degree of sparsity of the sampled network, and is fixed in order to recover $\hat{\lambda} = \sum_a P_0\{a_{i,j}\} \sum_{i \neq j} (1 - a_{i,j})$. The variable $\log z$ is analogous to a chemical potential in physics, in the sense that it is used to select denser or sparser sub-graphs (i.e. tuning the $\hat{\lambda}$ parameter). The probability distribution $P_0\{a_{i,j}\}$ can also be seen as the $\beta \to \infty$ limit of

$$P_0\{a_{i,j}\} = \frac{1}{Z} e^{-\beta \mathcal{H}_0\{a_{i,j}\}} z^{\sum_{ij} a_{i,j}} , \tag{7.1}$$

where we introduce the formal cost function $\mathcal{H}_0\{a_{i,j}\}$ which vanishes for $a \in a(\Lambda)$ and is 1 otherwise. Probability distributions of the form (7.1) are typically hard to compute explicitly due to the presence of the normalization constant Z, but their approximate marginals can be

[‡2] As shown in figure 7.2 and 7.3, ME tends to underestimate the risk of contagion even in the case in which the true support $a(L)$ is known, thus suggesting that other reconstruction algorithms should be employed for the estimation of the non-zero entries of a partially known liability matrix. Indeed, it is clear from those same simulations that inferring the support corresponding to the original network is a significant first step towards a more correct estimation of the risk of contagion.

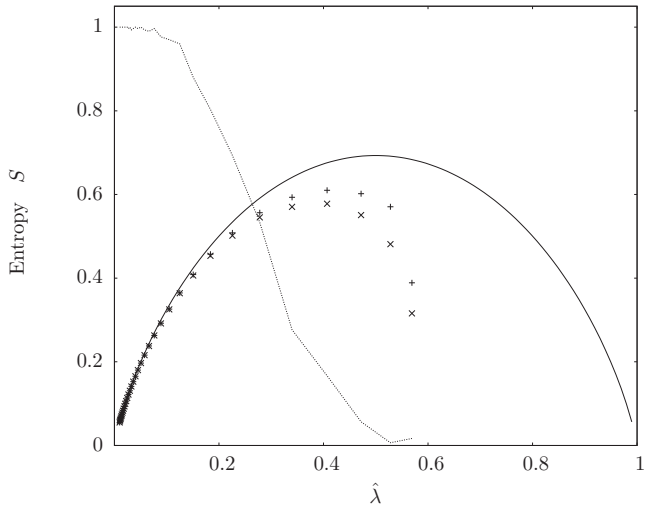

Figure 7.1: Entropy S of the space of compatible configurations $a_{i,j}$ at fixed sparsity $\hat{\lambda}$ with the energy $\mathcal{H}(a_{i,j})$ (+ sign) and true energy $\mathcal{H}_0(a_{i,j})$ ($\times$ sign) for the examples discussed in the text. S is defined as the logarithm of the number of configurations $\{a_{i,j}\}$ with $\mathcal{H} = 0$ (or $\mathcal{H}_0$), divided by the number M of possibly non-zero entries $a_{i,j}$. The solid line plotted for comparison is the entropy of a system of independent links $a_{i,j}$ with the same density (i.e. number of non-zero links). The probability for a solution of $\mathcal{H}_0(a_{i,j})$ to be also a solution of $\mathcal{H}(a_{i,j})$ is also plotted on the same graph (dashed line).

estimated efficiently (i.e. within a time scaling linearly in the number of unknown variables M) by means of the iterative algorithms such as the one described in the appendix. The solution that one obtains for the marginals

$$p_{0\,i,j} = \sum_a P_0\{a_{i,j}\}\delta(a_{i,j} = 1) \tag{7.2}$$

corresponds to the probability that the entry $a_{i,j}$ is equal to one in the ensemble of network structures which (i) are compatible with Λ and (ii) have an average degree of sparsity $\hat{\lambda}$. Being able to compute those marginals allow to sample efficiently the space of solution by employing procedures such as the *decimation* one described in the appendix, in which at each step the most biased variable (i,j) is fixed to $a_{i,j} = 1$ with probability $p_{i,j}$, and a reduced problem in which such $a_{i,j}$ is held fixed is successively solved. Once all variables are fixed, an adjacency matrix $a_{i,j}$ is selected out of the space of solutions and can be used as a candidate network structure.

Unfortunately, the energy function $\mathcal{H}_0$ is hard to manipulate, and we need to resort to an approximate energy function $\mathcal{H}$, whose structure is derived in the following paragraph. Suppose that a liability matrix with unknown entries is given, together with of the vectors of total credit ($L_i^{\rightarrow}$) and the one of total liabilities ($L_i^{\leftarrow}$). Then without loss of generality one can assume the known entries to be equal to zero, as the values of the known entries can always be absorbed into a rescaled value of the $L_i^{\rightarrow}$ and $L_i^{\leftarrow}$, and the problem can be restricted just to the unknown entries of the matrix. Under this assumption we can define the set of banks $\mathbf{B} \subseteq \mathcal{B}$ which are linked to the unknown entries of the liability matrix. Each node of $\mathbf{B}$ is a bank and the directed edges are the elements of U. For each node i of $\mathbf{B}$ the sum of the incoming entries $L_i^{\rightarrow} = \sum_j L_{ij}$ and of the outgoing entries $L_j^{\leftarrow} = \sum_i L_{ij}$ is known. Let $k_i^{\leftarrow}$ ($k_i^{\rightarrow}$) be the number of incoming (outgoing) links in the subset of edges where $L_{i,j} > 0$. Since

$L_{i,j} \leq 1$, the number $k_i^{\leftarrow}$ ($k_i^{\rightarrow}$) of incoming (outgoing) links is at least the integer part of $L_i^{\leftarrow}$ ($L_i^{\leftarrow}$) plus one. Therefore, one can define a cost function[‡3]

$$\mathcal{H}\{a_{i,j}\} = \sum_i \left[\theta\left(L_i^{\rightarrow} - k_i^{\rightarrow}\right) + \theta\left(L_i^{\leftarrow} - k_i^{\leftarrow}\right)\right] \tag{7.3}$$

over the dynamical variables $a_{i,j} = 0,1$ which identify the subset of edges, with

$$k_i^{\rightarrow} = \sum_j a_{i,j}, \qquad k_i^{\leftarrow} = \sum_j a_{j,i}\ .$$

Then we can construct the probability function

$$P\{a_{i,j}\} = \frac{1}{Z} e^{-\beta\,\mathcal{H}\{a_{i,j}\}} z^{\sum_{ij} a_{i,j}} \tag{7.4}$$

which we employ to sample the space of candidate network structures. Notice that all subgraphs $a_{i,j}$ with $\mathcal{H} = 0$ are feasible candidates for the support of solutions $L_{i,j} > 0$ to the problem. In general, the constraints are $2N$ linear equations and, as long as the number on non-zero elements $L_{i,j}$ is larger than $2N$ solutions exist, but it is not granted that they have $L_{i,j} \in [0,1]$ for al i,j. In other words, all the compatible solutions have to satisfy the constraint $\mathcal{H} = 0$, but the converse is not true (as shown in figure 7.1), because some support $a_{i,j}$ may not admit a solution with $L_{i,j} \in [0,1]$ for al i,j. Equivalently, the cost function $\mathcal{H}_0\{a_{i,j}\}$ involves constraints that the approximate $\mathcal{H}$ is not able to capture.
Message passing algorithms can be derived along the lines of Refs. [206] to solve efficiently the problem of sampling the space of solutions of (7.3) as described in detail in appendix. In particular we propose a generalization the algorithm employed in Ref. [206], in which we consider hard constraints enforced by inequalities rather than equalities and add a fugacity parameter z in order to control the density of links of the solutions.

7.5 Application to synthetic data

In this section we will show how our algorithm of reconstruction of the liability matrix L_{ij} (presented in section 7.4) gives more realistic stress-test results if compared with ME reconstruction algorithm (presented in section 7.3).
We choose to present the results obtained for specific ensembles of artificial matrices, whose structure should capture some of the relevant features of real credit networks[‡4]. The first case that we analyze is the simplest possible network with a non-trivial topology, namely the one in which every entrance of the liability matrix L_{ij} with $i \neq j$ is set to zero with probability λ, and otherwise is a random number uniformly chosen in [0,1]. We set the banks initial capital C_i to random numbers uniformly chosen in $[C_{min}, C_{max}]$. We impose the threshold $\theta = 1$, which means that all the entrance of the liability matrix are unknown (a worst-case scenario). We then reconstruct the liability matrix via ME algorithm and via our algorithm trying to fix the fraction $\hat{\lambda}$ of zeroes equal to λ. Then we stress-test via the Furfine algorithm the three liability matrices: the true one, the one reconstructed via ME algorithm one and the reconstructed by means of our message-passing algorithm, varying the loss-given-default α in [0,1]. The results of our simulations are shown in figure 7.2. We clearly show that the

[‡3] Here $\theta(x) = 0$ for $x < 0$ and $\theta(x) = 1$ otherwise is the Heaviside step function.

[‡4] Our attempts to obtain data on real financial networks, such as those in Refs. [196, 190], from central banks were unsuccessful. We focus on ensembles of homogeneous networks (i.e. non-scale free). This is appropriate since the unknown part of the financial network concerns small liabilities, and there is no a priory reason to assume a particularly skewed distribution of degrees for the unknown part of the financial newtork.

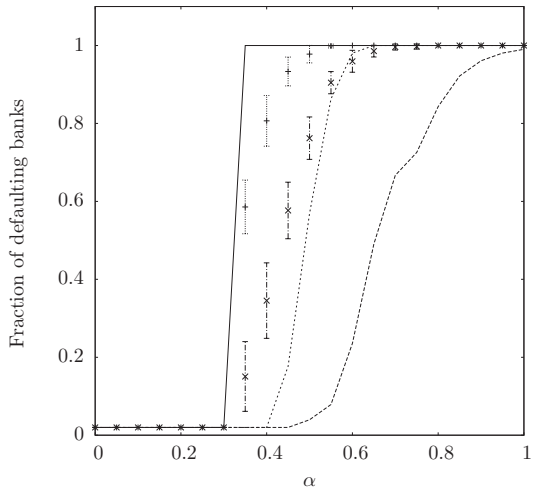

Figure 7.2: Plot of mean fraction of failed banks vs loss-given-default parameter α. The mean is done by averaging over the defaulting bank which starts the contagion. Results are obtained by considering: true liability matrix (solid line), reconstructed via ME algorithm liability matrix (thick dashed line) and the maximally sparse matrix (+ signs). Plots were obtained for a network of $N = 50$ banks with entries uniform in [0,1], where the link probability was fixed to 0.3 and the initial capital was set to $C_i = C = 0.3$. One can easily see that a better estimation of the true risk of contagion is obtained if the reconstruction of the liability matrix is done by enforcing the correct sparsity of the network rather than with the ME algorithm: the results obtained by putting the *correct* support (soft dashed line), corresponding to the original network structure $a(L_{ij})$, are also plotted, as well as the ones obtained by using a *typical* support ($\times$ signs), corresponding to the choice of a random, compatible support $a_{i,j}$ whose degree of sparsity matches the one of the original network. Errors bars refer to the fluctuations of the default ratio associated with the choice of a specific support out of the ensemble the compatible ones at fixed degree of sparsity.

ME algorithm underestimates the risk of contagion, while more realistic results are obtained if the original degree of sparsity λ is assumed.

Notice that even when the degree of sparsity is correctly estimated, stress tests on the reconstructed matrix still underestimate systemic risk. This is because the weights L_α on the reconstructed sub-graph are assigned again using the ME algorithm. This by itself produces an assignment of weights which is much more uniform than a random assignment of L_{ij} on the sub-graph, which satisfies the constraints. As a result, the propagation of risk is much reduced in the ME solution.

The second ensemble that we consider is a simple extension of the first one, in which the only modification that we have introduced implements heterogeneity in the size of the liabilities L_{ij}. In particular we consider matrix elements distributed according to

$$p(L_{ij}) \sim (b + L_{ij})^{-\mu-1} \, .$$

Also in this case we can show (figure 7.3) that a more accurate estimation of the default probability is achieved by enforcing the sparsity parameter of the reconstructed network to be the correct one. In this case the maximally sparse curve is less informative than in the uniform case. This is easily understood as due to the fact that the typical element $L_{ij} \sim 10^{-2}$ is much smaller than the threshold $\theta = 1$, so that a number of zero entries substantially larger than the original one can be fixed without violating the hard constraints.

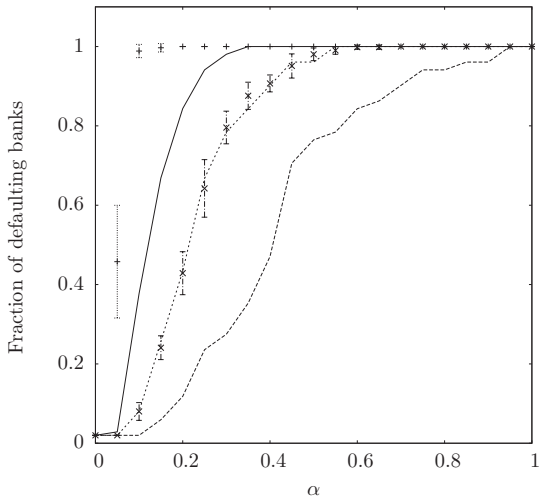

Figure 7.3: A plot analogous to the one in figure 7.2 for the case of power-law distributed entries of the liability matrix. This plots was obtained for a network of size $N = 50$, where the link probability was fixed to $1/2$. The parameters for the distribution of the entries were set to $b = 0.01$ and $\mu = 2$, while the capital of each bank was fixed to $C_i = C = 0.02$.

In both cases, when the true sparsity of the network is unknown, focusing on the sparsest possible graph likely over-estimates systemic cascades, thereby providing a more conservative measure for systemic risk than the one obtained by employing ME alone.

7.6 The role of the threshold

In the discussion above we disregarded the role of the threshold θ above which an exposure L_{ij} has to be made publicly available to regulators by setting it equal to 1. Indeed the problem of setting such threshold is a central problem to build a regulatory policy, hence the discussion of the reliability of the reconstruction algorithm varying θ while keeping fixed the true L is in practice particularly relevant. An appropriate way to address this issue is the following: given a network ensemble (such as the ones described in previous section) and a threshold θ, how many network structures are there with a compatible support? In particular, we remark that among all such compatible supports the maximally sparse one can be used to bound from above the maximum amount of risk given a policy for the thresholding. In particular for each value of θ, we empirically find that $\lambda_{max}[\theta]$ enjoys the following properties:

1. The maximum sparsity $\lambda_{max}(\theta)$ is a decreasing function of θ. In particular for $\theta \to 0$ one has $\lambda_{max}(\theta) \to \lambda$;

2. The entropy $S(\hat{\lambda}(\theta)) \to 0$ when the threshold goes to 0.

An example of this behavior for an ensemble of networks with power-law distributed weights is represented in figure 7.4, while in 7.5 we plot the entropy $S(\lambda_{max})$ structures as a function of θ. Therefore the algorithm described in section 7.4 provides quantitative measures for the uncertainty induced by the choice of a given threshold θ on network reconstruction. Ideally θ should be chosen so that maximally sparse structures are close to the true ones, and that the space of compatible structures is not too large (small entropy).

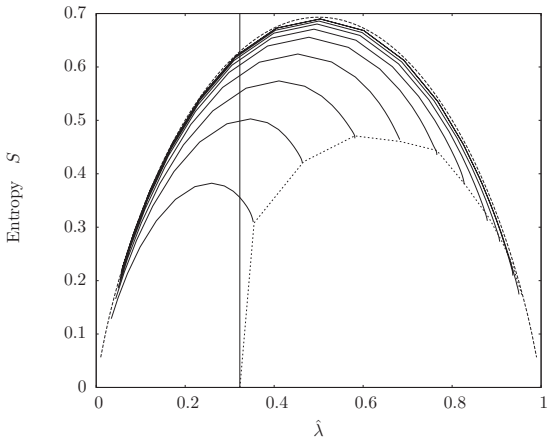

Figure 7.4: We plot the entropy of the space of compatible distributions (i.e. of the solutions of $\mathcal{H}\{a_{i,j}\}$) as a function of the sparsity parameter $\hat{\lambda}$ by varying the threshold θ from 1 (top curve) to 0.01 (bottom curve). The dashed line signals the transition point where solutions cease to exist. We consider power-law distributed entries for the true network ($D = 30$, $\lambda \approx 0.3$, $b = 0.01$ and $\mu = 2$). This shows how the volume of the space is reduced by a change of the threshold and how λ_{max} gets closer to λ by lowering θ.

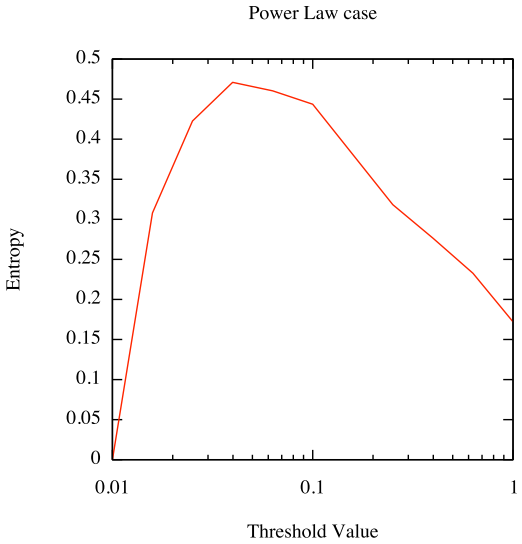

Figure 7.5: The entropy of the space of solutions $\mathcal{H}\{a_{i,j}\}$ as a function of the threshold for the same network as the one depicted in figure 7.4.

7.7 Conclusions and perspectives

In this chapter we have shown how it is possible to estimate the robustness of a financial network to exogenous crashes by using partial information. In particular we analyzed how the results of such estimation crucially depend on the topological properties of the underlying network, and showed that the number of links in a credit network dramatically control its resilience: connected networks can in most cases spread the response to external shocks more evenly than sparse ones.

We have also proposed an efficient message-passing algorithm for the reconstruction of the topology of partially unknown credit networks, in order to estimate with more accuracy their robustness. Such algorithm allows (i) to sample the space of possible network structures, which is assumed to be trivial in many algorithms commonly employed for network reconstruction, and (ii) to produce typical credit networks, respecting the topological constraint on the total number of links.

Finally, we test our algorithms on ensembles of synthetic credit networks which incorporate some of the main features of real credit networks (sparsity and heterogeneity), and find that the quality of the stress-test when only partial information is available critically depends on the assumptions about the network topology. In particular we find that ME underestimates the risk of contagion if the sparsity of the real ensemble is big enough, while with our algorithm we are able to estimate it more correctly. We remark that a worst case analysis of the topology is possible using this message-passing algorithm, as we are able to produce the maximally sparse (hence, maximally fragile) possible structure for the network.

Further developments of this work are indeed possible, in particular the identification and the reconstruction of other relevant topological features of credit networks would be relevant for a more accurate estimation of the contagion risk.

On the other hand, it would be interesting to test the algorithm on real data, as the ones used in financial literature to test the stability of banking systems of different countries. Unfortunately (or fortunately) it is not an easy task to gain access to bilateral exposures of banking systems. If our algorithm would produce plausible reconstructions of financial network, it can be directly implemented by regulators or monitors of financial stability.

7.8 Appendix: The message-passing algorithm

We describe here the algorithm which we use to sample the solution space of the energy function

$$\mathcal{H}\{a_{i,j}\} = \sum_i \left[\theta\left(L_i^{\rightarrow} - k_i^{\rightarrow}\right) + \theta\left(L_i^{\leftarrow} - k_i^{\leftarrow}\right)\right]$$

which we derived along the line of [206]. Specifically, given as an input an incomplete liability matrix, whose information is encoded into a set of N in-strength $L_i^{\leftarrow}$, N out-strength $L_i^{\rightarrow}$ and a set of U unknown entries of cardinality $M = |U|$), we provide an algorithm which for any positive value of the fugacity z returns an adjacency matrices $a_{i,j}$ sampled according to the probability distribution (7.4)

$$P\{a_{i,j}\} = \frac{1}{Z} e^{-\beta\,\mathcal{H}\{a_{i,j}\}} z^{\sum_{ij} a_{i,j}} .$$

The procedure that we describe can further be separated in two main tasks: (i) given a probability distribution of the form (7.4), finding an efficient mean to calculate marginals $p_{i,j}$

defined analogously to (7.2) and (ii) given a fast algorithm to calculate marginals, using them to find an adjacency matrix $a_{i,j}$ distributed according to $P\{a_{i,j}\}$.

7.8.1 Calculation of the marginals

The structure of the problem admits a graphical representation as a factor graph, in which $|U|$ variable nodes are associated to the $a_{i,j}$ degrees of freedom, while the constraints are represented as factor nodes. In particular, there are $2N$ function nodes, labeled $a \in \{i \rightarrow , \leftarrow i,\ i = 1,\dots,N\}$ each with k_a variable nodes attached. Let the variables be denoted $x_{a,b} = x_{b,a} = 0{,}1$ with a,b and let ∂a be the set of neighbors of node a. Let $M = \frac{1}{2}\sum_a |\partial a|$ be the total number of variables. For each variable $x_{a,b}$ we define the *message* $\mu_{a\to b}$ as the reduced marginal

$$\mu_{a\to b} = \sum_x P\{x_{a,b}|\ \not{b}\}\delta(x_{a,b} = 1)\ ,$$

where $P\{x_{a,b}|\ \not{b}\}$ denotes the restriction of the probability measure (7.4) to a problem in which the function node b is absent. Such messages need to fulfill self-consistent relations (BP equations) [20] which can be written in terms of the statistical weights[‡5]

$$V^m_{S\to a} = \sum_{U\in S:|U|=m} \prod_{b\in U} \mu_{b\to a} \prod_{c\in S\setminus U} (1-\mu_{c\to a})$$

and they read

$$\begin{aligned} \mu_{a\to b} &= \frac{\sum_{m=L_a-1}^{k_a-1} z^{m+1} V^m_{\partial a\setminus b\to a}}{\sum_{m=L_a-1}^{k_a-1} z^{m+1} V^m_{\partial a\setminus b\to a} + \sum_{m=L_a}^{k_a-1} z^m V^m_{\partial a\setminus b\to a}} \qquad (7.5)\\ &= \frac{V^{L_a-1}_{\partial a\setminus b\to a} + zW_{\partial a\setminus b\to a}}{V^{L_a-1}_{\partial a\setminus b\to a} + (1+z)W_{\partial a\setminus b\to a}} \\ W_{\partial a\setminus b\to a} &= \sum_{m=L_a}^{k_a-1} z^{m-L_a} V^m_{\partial a\setminus b\to a}\ . \qquad (7.6) \end{aligned}$$

Here z is the fugacity of links, and controls the average degree of sparsity $\hat{\lambda}$ of the supports in the solution space. For $z \to 0$ we obtain the equation for the sparsest possible graph

$$\mu_{a\to b} = \frac{V^{L_a-1}_{\partial a\setminus b\to a}}{V^{L_a-1}_{\partial a\setminus b\to a} + V^{L_a}_{\partial a\setminus b\to a}}\ ,$$

whereas for $z \to \infty$ we recover the maximally connected graph $\mu_{a\to b} = 1$ for all a and $b \in \partial a$.

Once the fixed point of Eqs. (7.5,7.6) is found by iteration, for a given z, one can compute the marginals

$$p_{a,b} = \frac{\mu_{a\to b}\mu_{b\to a}}{\mu_{a\to b}\mu_{b\to a} + (1-\mu_{a\to b})(1-\mu_{b\to a})}$$

[‡5]Since k_a can be as large as N, the direct computation of $V^m_{S\to a}$ involved in principle 2^{k_a} terms, which may be very large. A faster way to compute it is to use the recursion relation

$$V^m_{S\to a} = (1-\mu_{b\to a})V^m_{S\setminus b\to a} + \mu_{b\to a}V^{m-1}_{S\setminus b\to a}, \qquad \forall b \in S\ .$$

In practice this allows one to build $V^m_{S\to a}$ adding one at a time the nodes in S. This procedure involves of order $m^2 \le k_a^2$ operations.

that link (a,b) is present, and the entropy

$$S(z) = \sum_a \log \sum_{m=L_a}^{k_a} V^m_{\partial a \to a} - \frac{1}{2} \sum_a \sum_{b \in \partial a} \log \left[\mu_{a\to b}\mu_{b\to a} + (1-\mu_{a\to b})(1-\mu_{b\to a}) \right]$$

To plot the number of solutions (or of different supports) as a function of the sparsity parameter $\hat{\lambda}$, and the associated entropy $\Sigma(\hat{\lambda})$ one should use the fact that:

$$e^{MS(z)} = \int_0^1 d\hat{\lambda}\, e^{M\Sigma(\hat{\lambda}) + M(1-\hat{\lambda})\log z}$$

and hence perform the back-Legendre transform.

7.8.2 Decimation

We describe in the following a *decimation* procedure to generate the configurations $a_{i,j}$ once that the problem of computing marginals $p_{i,j}$ is controlled. For simplicity we choose to present a simple version of the algorithm, while more detailed description of this procedure and a discussion of its efficient variants can be found in reference [20].

Step 0: Define the set $U^{(0)} = U$, and the in- and out-strengths $L_a^{(0)} = L_a$. The candidate network structure is defined as $a_{i,j}^{(0)} = 0$ if $(i,j) \in U$ and $a_{i,j}^{(0)} = a(L_{ij})$ otherwise.
Step $t+1$: Find the marginals $p_{i,j}^{(t)}$ corresponding of the probability distribution $P^{(t)}\{a_{i,j}\}$ associated to the reduced problem defined by the incomplete matrix of unknown entries $U^{(t)}$ and in- and out-strengths $L_a^{(t)}$. Select the most biased variable $(i^\star,j^\star) = \text{argmin}_{(i,j)\in U^{(t)}} \min[p_{i,j}^{(t)}, 1-p_{i,j}^{(t)}]$ and set:

$$\begin{aligned}
a_{i^\star,j^\star}^{(t+1)} &= 1 \text{ with prob. } p_{i^\star,j^\star} \\
U^{(t+1)} &= U^{(t)} \setminus (i^\star,j^\star) \\
L_i^{\rightarrow\,(t+1)} &= L_i^{\rightarrow\,(t)} - a_{i^\star,j^\star} \\
L_i^{\leftarrow\,(t+1)} &= L_i^{\leftarrow\,(t)} - a_{i^\star,j^\star}
\end{aligned}$$

Step t_{stop}: The algorithm stops at time t_{stop} such that $U^{(t_{stop})} = \varnothing$. The candidate support $a_{i,j} = a_{i,j}^{(t_{stop})}$ so-obtained is distributed according to the probability distribution (7.4).

Conclusions

This thesis is devoted to the study of statistical mechanics of disordered systems. We paid attention both to fundamental problems of spin-glass theory and to more direct applications of statistical mechanics tools to problems of interdisciplinary interest, like financial problems.

The spin-glass models considered in our work are the 'classical' models introduced in 1975 by Edward and Anderson and by Sherrington and Kirkpatrick. On the one hand, the spin-glass phase of the SK model has been deeply understood thanks to the inspired works of Parisi. This phase presents an interesting range of features and new non-standard tools of statistical mechanics are needed to characterize them. Undoubtedly, the study of this model has led to the discovery of a new, exciting and challenging branch of physics, that nowadays we would call the 'spin-glass physics'. On the other hand, the correct physical picture of the EA model is still an open question. Long debates took place in the spin-glass community concerning the validity of the SK framework also for the EA model. Other competing theories have been proposed. Nowadays a definitive answer is still missing. In our work we investigated the problem of the characterization of the fluctuations of the pseudo-critical temperature in spin-glass models, by means of an analytic approach, for the SK model, and by numerical simulations for both models. We find an interesting connection with Extreme Value Statistic Theory for correlated and independent random variables. The ubiquitous Tracy-Widom and Gumbel distributions have been shown to describe these fluctuations. If it is true what Italo Calvino said about classics: 'A classic is a book that has never finished saying what it has to say.', we can safely say that the spin-glass models considered in these works certainly deserve to be regarded as classics within spin-glass theory.

Our attention was also devoted to the study of spin-glass models in connection with the physics of supercooled liquids. If the introduction of *point-to-set* correlation functions in spherical geometry can be considered a fundamental step forward in the detection of the elusive amorphous order of supercooled liquids near the glass transition, spin-glass models with Kac interactions provided a framework in which these new ideas can be analytically measured and studied. We devoted our attention to the study of Kac-glass models in the so-called sandwich geometry. This unbounded geometry gives us a correct framework in which main ingredients of the Random First Order Transition Theory can be measured, like the energy and the free energy cost to put different metastable states in contact. The approach we have proposed can be easily implemented in numerical experiments of glass-forming liquids. This has been done by the group of Cavagna in Rome. A good qualitative agreement between analytic and numerics has been found.

In order to widen our horizons of research, we have finally focused on problems coming

from a non-physical domain, i.e. finance, that can investigated via tools of statistical mechanics. The recent financial crisis sharpened the perceived fear by economic institutions that the financial default of a single state can provoke a European or worst a global chain of defaults. We say that a financial network in which shocks affecting a single or a small number of institutions can easily propagate to all the network is affected by systemic risk. In this context, we speculated that statistical physics may give a correct framework to understand this problem. In financial literature it is a common belief that the interbank lending network is a fundamental channel in which financial contagion can take place. Financial regulators constantly monitor the stability of financial networks by means of stress-tests, but are often left with the problem of evaluating this stability from incomplete data sets, e.g. incomplete interbank lending liabilities matrices. The correct reconstruction of this incomplete information becomes then mandatory in order to have a truthful estimation of systemic risk. We introduced a message-passing algorithm to investigate this problem. Message-passing algorithms have been extensively applied to problems in computer science and spin-glass theory. Our algorithm allows to tune the sparsity of the reconstructed financial network. This ingredient is completely missed by algorithms so far presented in the literature, e.g. the maximum entropy algorithm. This fact typically leads to a severe under-estimation of the risk of contagion. In order to quantify these ideas we tested our algorithm on synthetic data.

Before concluding, it is appropriate to give a list of open problems and directions for future research that may stem from the present thesis:

- the study of fluctuations of the pseudo-critical temperature in spin-glass models has been limited to the static critical temperature of the EA and the SK model, characterized by a distribution of the disorder with finite variance. In this context it would be interesting to extend this analysis considering other distributions of the disorder, like second-moment diverging Lévy distributions. In a numerical approach this would require more refined simulations techniques [163]. On the other hand, our investigations was limited to typical fluctuations, while a step forward in the comprehension of the subject would be to characterize the large deviations regime. Recent results in the context of Random Matrix Theory provided universal functions that we expect to describe this regime. Also in this case, improved simulations techniques must be implemented [207]. The analysis can also be extended to the study of the fluctuations of the dynamical critical temperature in 1RSB spin-glass models. The topological phase transition of the p-spin model gives us some hints that the ubiquitous Tracy-Widom distribution could play an important role also in the description of this model.

- in the context of Kac-glass models in connection with the glass transition, we have already pointe out that numerical simulations on glass-forming liquids models have been performed by the group of Cavagna in Rome. It would be very interesting to provide a unified framework for the problem of glass formers in sandwich geometry. The analytic approach of Kac-spin glass models combined with numerical simulations results and phenomenological arguments of RFOT could lead to a better comprehension of the role that this particular geometry plays in connection with the glass transition.

- the algorithm that we proposed for a correct evaluation of systemic risk has been tested on synthetic data. The real aim of this work is to test the algorithm on real data, but, unfortunately, this kind of information is very difficult to obtain from banks or financial institutions.

  Various algorithmic improvements can also be implemented in order to simulate more realistic scenarios. First of all, in financial literature, it has been shown that, for

historical reasons, banks belonging to lending networks are clusterised in sectors [208]. An improved algorithm capable of taking into account this fact would surely be able to give a more truthful estimation of risk. On the other hand the parameter which tunes the sparsity of the reconstructed network is freely adjusted in the actual development of the algorithm. We can tune from maximally connected network to a worst-case scenario of maximally sparse networks. An optimal criterion to rely upon for identifying the correct heterogeneity of the network is very much called for.

The end of this manuscript is also the end of these three years devoted to research in fundamental physics. Since we believe that physics can progress only thanks to pleasure and amusement on doing it, we want to conclude this manuscript with a citation of Isaac Asimov:

The most exciting phrase to hear in science,
the one that heralds new discoveries,
is not "Eureka!" (I found it!) but "That's funny..."

Isaac Asimov

Article 1

Journal of Statistical Mechanics: Theory and Experiment
An IOP and SISSA journal

Surface tension in Kac glass models

Elia Zarinelli and Silvio Franz

Laboratoire de Physique Théorique et Modèles Statistiques, CNRS and Université Paris-Sud, UMR8626, Bat. 100, 91405 Orsay, France
E-mail: elia.zarinelli@lptms.u-psud.fr and silvio.franz@lptms.u-psud.fr

Received 17 December 2009
Accepted 11 March 2010
Published 8 April 2010

Online at stacks.iop.org/JSTAT/2010/P04008
doi:10.1088/1742-5468/2010/04/P04008

Abstract. In this paper we study a distance-dependent surface tension, defined as the free-energy cost for putting metastable states at a given distance. This will be done in the framework of a disordered microscopic model with Kac interactions that can be solved in the mean-field limit.

Keywords: spin glasses (theory), structural glasses (theory)

ArXiv ePrint: 0912.2764

J. Stat. Mech. (2010) P04008

Contents

1. Introduction

The introduction of *point-to-set* correlation functions [1]–[5] allowed important progress in understanding the growth of static correlations in supercooled liquids near the glass transition. These non-standard correlation functions measure how deeply the effect of amorphous boundary conditions penetrates within a system. In order to introduce them, let us consider a large ensemble of interacting particles becoming glassy at low temperature. We assume that the liquid is trapped in a metastable state. We freeze the motion of all the particles outside a sphere of radius R. Then we let the particles inside the sphere be free to move and eventually to rearrange in a different metastable state. The effect of the external particles is to create a pinning field favouring internal configurations which best match the frozen exterior. For small radius R, the effect of the pinning field on the interior of the sphere is strong. In that case the sphere remains in the same state. In contrast, for large radius R, the effect becomes weak and the sphere can be found in a different state. Roughly speaking, a *point-to-set* correlation function measures the overlap between the initial state and the one reached after the rearrangement of the system. It has been found in numerical experiments that on lowering the temperature the effect of the amorphous boundary conditions propagates deeper into the region [3, 4].

A standard random first-order transition (RFOT) [6, 1] assumes that the competition between an entropy-rich state with high energy and an entropy-poor state with low energy can explain the transition from high-overlap to low-overlap metastable states of the previous system, as the radius of the sphere is increased. As we are going to show, such a mechanism has to be reconsidered. In order to do this, let us consider, for simplicity, an Ising-like model described by a Hamiltonian H. We freeze a configuration S^α in a region A of the system. We study the thermodynamics considering only configurations S constrained to be close to S^α in A:

$$Z[S^\alpha] = \sum_S \mathrm{e}^{-\beta H[S]} \chi_A[S, S^\alpha] \tag{1}$$

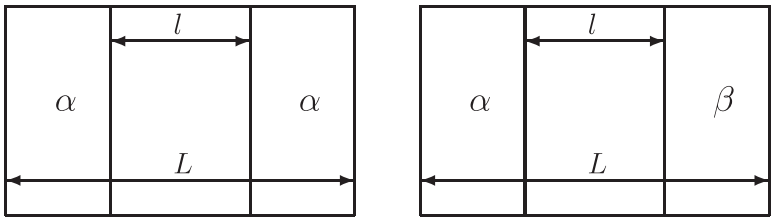

Figure 1. The *sandwich* geometry for a system $\alpha\alpha$ (left) and $\alpha\beta$ (right). The box $B(l)$ is the central region; $A^+(l)$ and $A^-(l)$ are the lateral ones.

where

$$\chi_A[S^1, S^2] = \begin{cases} 1 & \text{if } S_i^1 = S_i^2 \quad \forall i \in A \\ 0 & \text{otherwise.} \end{cases} \tag{2}$$

The thermodynamic average of an observable $\mathcal{O}$ of the system is obtained by averaging with a constrained Boltzmann measure the configurations inside the sphere and with a Boltzmann measure the configurations S^α:

$$\langle \mathcal{O} \rangle = \sum_{S^\alpha} \frac{\mathrm{e}^{-\beta H[S^\alpha]}}{Z} \sum_S \chi_A[S, S^\alpha] \frac{\mathrm{e}^{-\beta H[S]}}{Z[S^\alpha]} \mathcal{O}(S). \tag{3}$$

This average coincides with the usual thermodynamical one: $(1/Z)\sum_S \mathrm{e}^{-\beta H[S]}\mathcal{O}(S)$. This simple fact has deep implications: in the case in which A is a sphere of radius R, on average, the energy per degree of freedom is independent of R. If, for typical choices of the position of the sphere, one finds that two thermodynamic states coexist for a well defined value of R, they will have the same energy. Possible mechanisms for coexistence should therefore have a purely entropic origin [7].

In recent numerical experiments [8] the energy cost of putting different metastable states in contact has been measured. The procedure is the following: freeze two states α and β, exchange a sphere of the state α with a sphere of the state β and let the system evolve. Inspired by this idea, in the present work we want to introduce a different *point-to-set* correlation function defined as the free-energy cost for putting different metastable states at distance l. In order to do that, we consider a *sandwich* geometry: two regions of the space divided by a box of width l, and then freeze different metastable states at opposite sides of the box; figure 1. This system is well suited for study in the framework of a p-spin model with Kac interaction [5], [9]–[13].

The paper is organized as follows. In section 2 we introduce the model that we consider and the basic definitions; in section 3 we briefly illustrate how to obtain the free energy of the system; more details on these calculations can be found in the appendices A and in B; in section 4 we present our results and in section 5 we draw our conclusions.

2. The model

We consider a finite-dimensional version of the spherical p-spin model, defined on a d-dimensional cubic lattice Λ of linear size L, whose elementary degrees of freedom are spins $S_i \in \mathbb{R}$ with $i \in \Lambda$. We introduce the interaction range $\gamma^{-1} > 0$ and a non-negative

J. Stat. Mech. (2010) P04008

rapidly decreasing function $\psi(x)$ normalized by $\int \mathrm{d}^d x\, \psi(|x|) = 1$. We define the local overlap of two configurations S^1 and S^2 as

$$Q_{S^1S^2}(i) = \gamma^d \sum_{j\in\Lambda} \psi(\gamma|i-j|) S^1_j S^2_j. \tag{4}$$

We impose that configurations are subject to the local spherical constraint: $Q_{S^1S^1}(i) = 1\ \forall i \in \Lambda$. We then introduce the finite-range p-spin Hamiltonian:

$$H_p[S,J] = -\sum_{i_1,\ldots,i_p} J_{i_1,\ldots,i_p} S_{i_1}\cdots S_{i_p} \tag{5}$$

where the couplings $J_{i_1,\ldots,i_p}$ are i.i.d. random variables with zero mean and variance:

$$\mathbb{E}\left[J^2_{i_1,\ldots,i_p}\right] = \gamma^{pd} \sum_{k\in\Lambda} \psi(\gamma|i_1-k|)\cdots\psi(\gamma|i_p-k|). \tag{6}$$

γ^{-1} is the interaction range, since only variables located at vertices i and j such that $|i-j| < \gamma^{-1}$ really interact. This also implies that the Hamiltonian is a random variable with zero mean and variance:

$$\mathbb{E}\left[H[S^1,J]H[S^2,J]\right] = \sum_{i\in\Lambda} f(Q_{S^1S^2}(i)), \tag{7}$$

where $f(x)$ is a polynomial with positive coefficients, for example $f(x) = x^p$, if we consider a pure p-spin model; in the following we will consider $f(x) = \frac{1}{10}x^2 + x^4$, where the quartic term ensures having a regular gradient expansion of the free-energy density.

We analyse the model in the Kac limit: $L, \gamma^{-1} \to \infty$ with $L \gg \gamma^{-1}$, where the model can be solved by means of the saddle-point approximation.

The sandwich geometry is implemented by considering three regions of the lattice Λ: $A^+(l)$, $A^-(l)$ and a box $B(l)$; figure 1. In order to put the same or different states at opposites sides of the box, we introduce two different systems, that we call $\alpha\alpha$ and $\alpha\beta$:

- system $\alpha\alpha$: we fix a configuration S^α drawn from the Boltzmann equilibrium measure; we consider the thermodynamic of configurations S constrained to be close to S^α both in $A^+(l)$ and in $A^-(l)$;
- system $\alpha\beta$: we fix two configurations S^α and S^β drawn from the Boltzmann equilibrium measure; we consider the thermodynamics of configurations S constrained to be close to S^α in $A^+(l)$ and to S^β in $A^-(l)$.

We consider a system $\alpha\beta$. Let $\mathcal{O}$ be an observable of the system and $\bar{q} \le 1$. The constrained Boltzmann measure $\langle\cdot\rangle_{\alpha\beta}(l)$ is

$$\langle\mathcal{O}\rangle_{\alpha\beta}(l) \equiv \frac{1}{Z[S^\alpha_{A^+}, S^\beta_{A^-}]} \int \mathrm{d}S\, \mathcal{O}(S) \mathrm{e}^{-\beta H[S,J]} \prod_{i\in A^-} \delta(Q_{S^\alpha S}(i) - \bar{q}) \prod_{i\in A^+} \delta(Q_{S^\beta S}(i) - \bar{q}) \tag{8}$$

where $\int$ denotes integration over configurations satisfying the local spherical constraint. The partition function is

$$Z[S^\alpha_{A^+}, S^\beta_{A^-}] \equiv \int \mathrm{d}S\, \mathrm{e}^{-\beta H[S,J]} \prod_{i\in A^-} \delta(Q_{S^\alpha S}(i) - \bar{q}) \prod_{i\in A^+} \delta(Q_{S^\beta S}(i) - \bar{q}). \tag{9}$$

J. Stat. Mech. (2010) P04008

The symbol $\mathbb{E}$ represents the average over both the distributions of fixed configurations S^α and S^β and the disorder; the free energy of the system $F_{\alpha\beta}(l)$ is then

$$F_{\alpha\beta}(l,T) \equiv -\frac{1}{\beta}\mathbb{E}[\ln Z[S^\alpha_{A^+}, S^\beta_{A^-}]]. \tag{10}$$

For a system $\alpha\alpha$, the constrained Boltzmann measure $\langle\cdot\rangle_{\alpha\alpha}(l)$ is obtained by imposing the constraint $\prod_{i\in A^+\cup A^-}\delta(Q_{S^\alpha S}(i)-\bar{q})$; then $F_{\alpha\alpha}(l,T)\equiv -(1/\beta)\mathbb{E}[\ln Z[S^\alpha_{A^+\cup A^-}]]$

As we will see in the following, $F_{\alpha\beta}(l,T)$ and $F_{\alpha\alpha}(l,T)$ can be calculated in the Kac limit, $\gamma\to 0$ taken after $L\to\infty$. This allows us to measure the free-energy cost per unit area for putting different metastable states at a distance l:

$$Y(l,T)\equiv \lim_{\gamma\to 0}\lim_{L\to\infty}\frac{F_{\alpha\beta}(l,T)-F_{\alpha\alpha}(l,T)}{L^{d-1}}; \tag{11}$$

this quantity can be interpreted as an effective, distance-dependent, surface tension.

3. Calculations

In the following we consider a system $\alpha\beta$; a system $\alpha\alpha$ can be treated in the same way. In order to calculate $F_{\alpha\beta}$, the average $\mathbb{E}$ can be taken by introducing replicas along the lines of [12, 13] (more details on calculations can be found in appendix B). Integrals over spin variables are then treated for an $(m+n)\times(m+n)$ matrix order parameter $q_{ab}(i)$. We rescale the position to define $x=\mathrm{i}\gamma\in[-\hat{L},\hat{L}]^d$, $\hat{L}\equiv\gamma L$ to get

$$F_{\alpha\beta}(\hat{l}) = -\frac{1}{\beta}\lim_{m,n\to 0}\int[\mathrm{d}q_{ab}]\mathrm{e}^{-(1/\gamma^d)\mathcal{S}_{\alpha\beta}(q_{ab})}. \tag{12}$$

The dependence upon γ is now completely explicit and, for $\gamma\to 0$, the functional integration can be performed using the saddle-point method. We look for a replica symmetric saddle point $q^{\mathrm{RS}}_{ab}(x)$. This is characterized by three scalar functions $p_1(x)$, $p_2(x)$ and $q(x)$; p_1 and p_2 are the local overlaps between the constrained configuration and the reference configuration S^α and S^β respectively and q is the local overlap of two constrained configurations when they belong to the same metastable state (see appendix A for more details). Using this ansatz we obtain that $\mathcal{S}_{\alpha\beta}(q_{ab})=n\int\mathcal{L}_{\alpha\beta}\,\mathrm{d}^dx+\mathrm{O}(n^2)$, where

$$\begin{aligned}\mathcal{L}_{\alpha\beta}(x) = &-\frac{\beta^2}{2}[f(1)+2f((\psi*p_1)(x))+2f((\psi*p_2)(x))-f((\psi*q)(x))]\\ &+\frac{1}{2}\left[\log(1-q(x))-\frac{p_1^2(x)+p_2^2(x)-q(x)}{1-q(x)}\right]\end{aligned} \tag{13}$$

with

$$(\psi*q)(x)=\int\mathrm{d}^dy\,\psi(|y-x|)q(y). \tag{14}$$

The constraint forcing S to be close to S^α in $A^-(\hat{l})$ and to S^β in $A^+(\hat{l})$ is fulfilled by setting $p_1(x)=\bar{q}$ for $x\in A^-(\hat{l})$ and $p_2(x)=\bar{q}$ for $x\in A^+(\hat{l})$. We obtain $F_{\alpha\beta}(\hat{l})$ by evaluating the fields $p_1(x)$, $p_2(x)$ and $q(x)$ in the saddle point of the action $\mathcal{S}^0_{\alpha\beta}=\int\mathrm{d}^dx\,\mathcal{L}_{\alpha\beta}(x)$. The resulting free energy will present an extensive part $\mathrm{O}(L^d)$ which will be the same for a system $\alpha\alpha$ and for a system $\alpha\beta$. Then, in the calculation of the surface tension

$Y(\hat{l},T)$, the extensive part of the free energy will be erased and contributions will come only from the sub-leading order $\mathrm{O}(L^{d-1})$; the resulting form of the surface tension is $Y(\hat{l},T)=\hat{F}_{\alpha\beta}(\hat{l},T)-\hat{F}_{\alpha\alpha}(\hat{l},T)$, where $\hat{F}_{\alpha\beta}(\hat{l},T)=(1/\beta)\int_0^{\hat{l}}\mathrm{d}x\,\mathcal{L}_{\alpha\beta}(x)$.

We introduce a simplification in the Lagrangians: we expand the terms of the form $f((\psi*q)(x))$ in the gradient of $q(x)$ and we truncate to the second order, obtaining $f(q(x))-cf''(q(x))(\nabla q)^2(x)$ where $c=(1/2d)\int z^2\psi(|z|)\,\mathrm{d}z^d$ (in our running example, $c=1$). We find the saddle-point fields by numerically iterating the Euler–Lagrange equations of (13).

4. Results

The system $\alpha\alpha$ has been studied in spherical geometry [5]; we verified that in the sandwich geometry the behaviour does not change with respect to the spherical case. Two critical temperatures characterize the system: $T_\mathrm{s}\approx 0.766\,287$ and $T_\mathrm{d}\approx 0.813\,526$.

Setting the temperature of the system $T\gtrsim T_\mathrm{d}$, we find two lengths: $\hat{l}_0(T)$ and $\hat{\xi}_\mathrm{d}(T)$, such that, for widths of the box $\hat{l}\in[\hat{l}_0(T),\hat{\xi}_\mathrm{d}(T)]$, the action $\mathcal{S}^0_{\alpha\alpha}$ has two local minima. A minimum is characterized by a saddle-point field $p(x)$ rapidly decaying to zero in the interior of the box; we name this the low-overlap minimum. The other minimum is characterized by a saddle-point field $p(x)$ everywhere large; we name this the high-overlap minimum. For $\hat{l}>\hat{\xi}_\mathrm{d}$ ($\hat{l}<\hat{l}_0$) only the low-overlap (high-overlap) minimum exists. $\hat{\xi}_\mathrm{s}(T)$ is defined as the minimum value of $\hat{l}$ such that the low-overlap minimum is the global minimum of the action. The critical temperatures T_s and T_d are defined as the temperatures at which $\hat{\xi}_\mathrm{s}(T)$ and $\hat{\xi}_\mathrm{d}(T)$ respectively diverge.

For a better comprehension, we present in figure 3 the plot of the sub-extensive part of the free energy of the high-overlap (low-overlap) minimum $\hat{F}^\mathrm{H}_{\alpha\alpha}(\hat{l})$ ($\hat{F}^\mathrm{L}_{\alpha\alpha}(\hat{l})$) divided by the size $\hat{l}$ for a system at a temperature $T_\mathrm{s}<T<T_\mathrm{d}$. $\hat{\xi}_\mathrm{s}(T)$ is then the value of $\hat{l}$ where $\hat{F}^\mathrm{L}_{\alpha\alpha}(\hat{l})$ and $\hat{F}^\mathrm{H}_{\alpha\alpha}(\hat{l})$ cross. Then the global free energy of a system $\alpha\alpha$ is $F_{\alpha\alpha}(\hat{l})=\min\{F^\mathrm{L}_{\alpha\alpha}(\hat{l}),F^\mathrm{H}_{\alpha\alpha}(\hat{l})\}$.

On the other hand, in the case of a system $\alpha\beta$, the action $\mathcal{S}^0_{\alpha\beta}$ always has a single minimum. Profiles of the saddle-point field $p_1(x)$ can be seen in figure 2. The sub-extensive part of the free energy of the unique minimum $\hat{F}_{\alpha\beta}(\hat{l})/\hat{l}$ for a temperature $T_\mathrm{s}<T<T_\mathrm{d}$ is also plotted in figure 3. At all temperatures and values of $\hat{l}$ that we have studied, the sub-extensive part of the free energy of a system $\alpha\beta\hat{F}_{\alpha\beta}(\hat{l})$ is close to the sub-extensive part of the low-overlap free energy of a system $\alpha\alpha\hat{F}_{\alpha\alpha}(\hat{l})$, as can be seen in the inset of figure 3.

In figure 4 we follow the evolution of $\hat{l}$-dependent surface tension $Y(\hat{l},T)$ for systems at different temperatures $T>T_\mathrm{s}$. We note that the static correlation length $\hat{\xi}_\mathrm{s}(T)$ separates two regimes. For $\hat{l}<\hat{\xi}_\mathrm{s}(T)$, $Y(\hat{l},T)$ has a power law followed by a linear decrease. For $\hat{l}>\hat{\xi}_\mathrm{s}(T)$, as we see in the inset of figure 4, the decrease becomes exponential:

$$Y(\hat{l},T)\sim C\mathrm{e}^{-\hat{l}/\tilde{l}}, \tag{15}$$

with $\tilde{l}$ weakly dependent on the temperature and showing no evident relation with $\hat{\xi}_\mathrm{s}$. This shows that the surface tension $Y(\hat{l},T)$ is appreciably different from zero only for $\hat{l}\lesssim\hat{\xi}_\mathrm{s}$. A similar result has been obtained in [14]; in that case the interface free energy

J. Stat. Mech. (2010) P04008

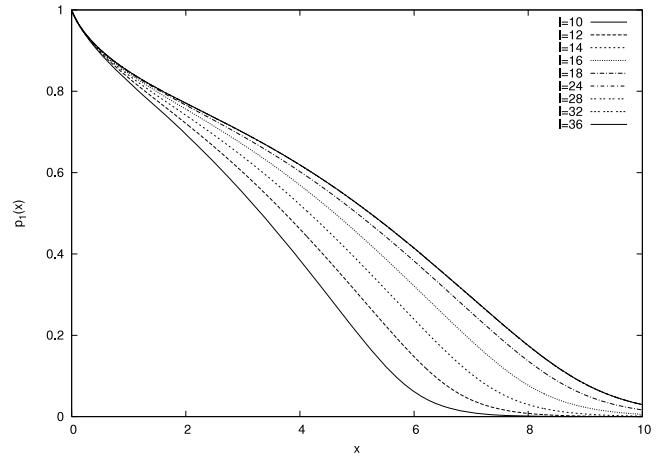

Figure 2. Plot of the profiles of the saddle-point field $p_1(x)$ for a system $\alpha\beta$ at temperature $T = 0.8$ for different values of the box $\hat{l}$. At this temperature, $\hat{\xi}_{\rm s} \sim 24$.

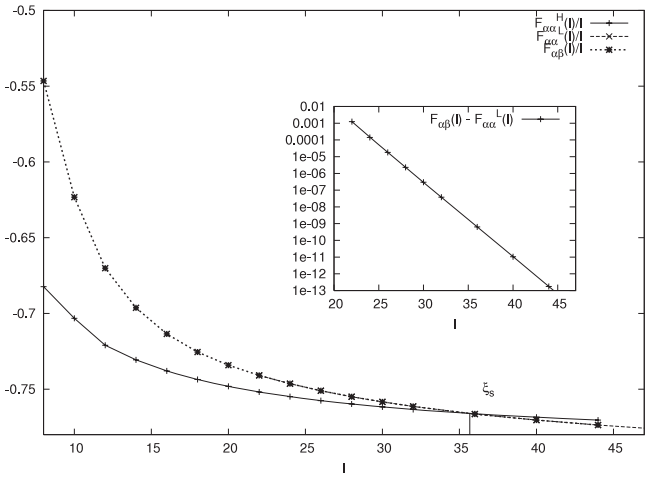

Figure 3. Main figure: plot of the sub-extensive part of the free energy divided by the size as a function of $\hat{l}$ for a system at a temperature $T = 0.7874$ of: the high-overlap minimum of a system $\alpha\alpha$, $\hat{F}^{\rm H}_{\alpha\alpha}(\hat{l})/\hat{l}$; the low-overlap minimum of a system $\alpha\alpha$, $\hat{F}^{\rm L}_{\alpha\alpha}(\hat{l})/\hat{l}$; the unique minimum of a system $\alpha\beta$, $\hat{F}_{\alpha\beta}(\hat{l})/\hat{l}$. The static correlation length $\hat{\xi}_{\rm s}$ is pointed out. Using this scale $\hat{F}^{\rm L}_{\alpha\alpha}(\hat{l})$ and $\hat{F}_{\alpha\beta}(\hat{l})$ are indistinguishable. Inset: the difference $\hat{F}^{\rm L}_{\alpha\alpha}(\hat{l}) - \hat{F}_{\alpha\beta}(\hat{l})$ on a logarithmic scale.

has been obtained by changing the boundary conditions along one direction, from periodic to anti-periodic.

Particular attention must be paid to the case $T = T_{\rm s}$. At $T_{\rm s}$, the static correlation length $\hat{\xi}_{\rm s}$ diverges. This means that the high-overlap minimum is the global minimum of the action $\mathcal{S}^0_{\alpha\alpha}$ for all the values of $\hat{l}$. We see in figure 4 that, for T approaching $T_{\rm s}$, the profile of $Y(\hat{l}, T)$ takes the shape of a plateau. Consequently, at the critical temperature $T_{\rm s}$, in the limit $\hat{l} \to \infty$, the surface tension $Y(\hat{l}, T_{\rm s})$ does not fall to zero and takes a

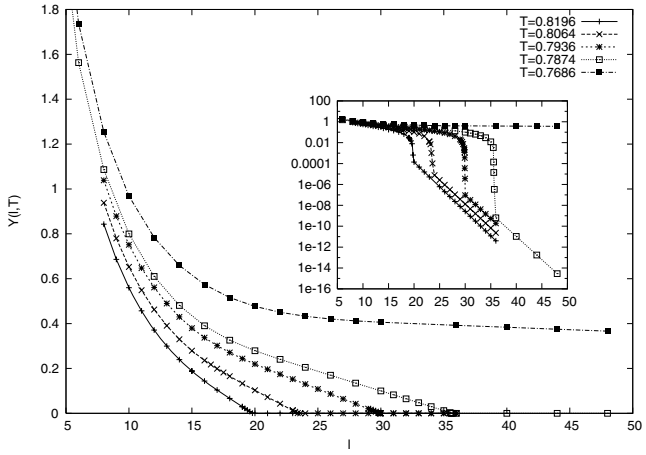

Figure 4. Plot of $Y(l,T)$ for different temperatures as a function of the width of the box $\hat{l}$. We recall that $T_s \approx 0.766\,287$ and $T_d \approx 0.813\,526$.

limiting value $Y(T_s)$. Arguably, the value $Y(T)$ is different from zero for temperatures $T < T_s$.

According to phenomenological arguments [1], the static correlation length $\hat{\xi}_s(T)$ can be interpreted as the typical size of metastable states of a system at a temperature T. Following this idea, in a system $\alpha\beta$ we are freezing a patchwork of metastable states of size $\hat{\xi}_s(T)$ outside the box and letting the system be free to rearrange inside the box. If the width of the box is larger than the typical metastable-state size, $\hat{l} \gg \hat{\xi}_s(T)$, the system inside the box has enough space to rearrange in many different metastable states. In contrast, when the width of the box is smaller than the metastable-state size, $\hat{l} < \hat{\xi}_s$, since there is not enough space to create metastable states on the interior, the frozen states are in contact and then 'repel' each other. This explains why the surface tension $Y(\hat{l},T)$ is significantly different from zero only for $\hat{l} < \hat{\xi}_s(T)$ and why the overlap profiles $p_1(x)$ and $p_2(x)$ between frozen metastable states and the interior of the box decrease faster for small boxes. At the critical temperature T_s the size of the metastable states diverges. Consequently, the surface tension takes a finite value also in the limit $\hat{l} \to \infty$.

Other observables of the system have been considered. We studied the internal energy U. We verified that for a system $\alpha\alpha$ the high-overlap and the low-overlap phases have the same energy, as motivated in section 1. In figure 5 we follow the evolution of $U_{\alpha\beta}(\hat{l}) - U_{\alpha\alpha}(\hat{l})$ for different temperatures of the system. A detailed derivation of this quantity can be found in appendix B. In this case, we note a power law followed by an exponential decrease.

We also computed the configurational entropy Σ as a function of the size $\hat{l}$ of the box; figure 6. For a system $\alpha\alpha$ only the low-overlap phase presents a configurational entropy $\Sigma_{\alpha\alpha}$ different from zero. As noticed in [5], for $\hat{l} < \hat{l}^{1RSB}$ the replica symmetric solution is incorrect since it gives a negative entropy. We found that the same is true for a system $\alpha\beta$. In the inset of figure 6 we plot the difference between the configurational entropies of the two systems. We note that this quantity is a decreasing function of the size $\hat{l}$ of the system. This is consistent with the observation that the system loses memory of the frozen exterior for large sizes of the box.

J. Stat. Mech. (2010) P04008

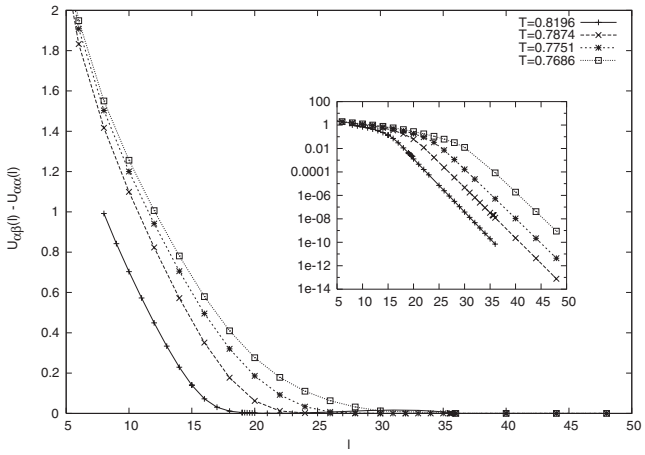

Figure 5. Plot of $U_{\alpha\beta}(\hat{l}) - U_{\alpha\alpha}(\hat{l})$ for different temperatures as a function of the width of the box $\hat{l}$. We recall that $T_{\rm s} \approx 0.766\,287$ and $T_{\rm d} \approx 0.813\,526$.

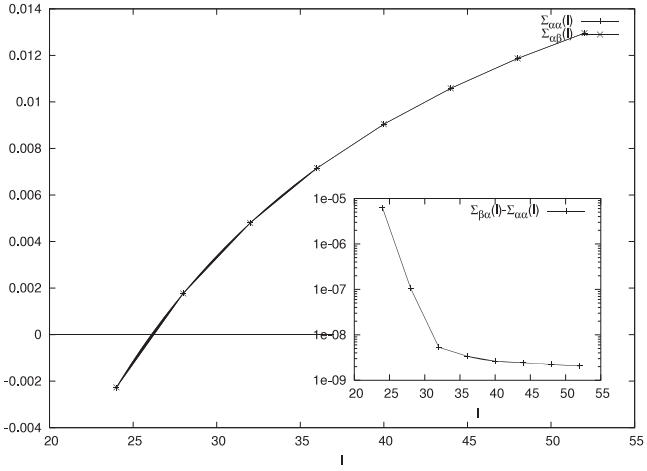

Figure 6. Main figure: the configurational entropy $\Sigma_{\alpha\alpha}(l)$ as a function of l for a system $\alpha\alpha$ and $\Sigma_{\alpha\beta}(l)$ for a system $\alpha\beta$ at a temperature $T = 0.8$. Inset: the difference $\Sigma_{\alpha\beta}(l) - \Sigma_{\alpha\alpha}(l)$.

5. Conclusions

In this paper we have studied a distance-dependent surface tension, defined as the free-energy cost for putting metastable states at a given distance. This has been done in the framework of a disordered microscopic model with Kac interactions that can be solved in the mean-field limit. We have found that the surface tension is appreciably different from zero only for distances between metastable states smaller than the static correlation length of the system. A description of this behaviour in terms of a phenomenological droplet argument has been proposed. Other observables, like the internal energy and the configurational entropy, have been studied. The behaviour of the configurational entropy allowed us to identify under which size the replica symmetric ansatz becomes incorrect and a 1-RSB solution must be considered.

doi:10.1088/1742-5468/2010/04/P04008

J. Stat. Mech. (2010) P04008

Acknowledgments

It is a pleasure to thank D Fichera, M Castellana and G Biroli for interesting discussions.

Appendix A

We give an explicit formulation of the overlap matrix in the replica symmetric ansatz $q^{\mathrm{RS}}_{ab}(x)$; the overlap matrix is an $(m+n)\times(m+n)$ matrix with m and n real numbers; if we take r and n integer, we can visualize the matrix in the following way:

$$q^{\mathrm{RS}} = \begin{bmatrix} A & B \\ B^{\mathrm{T}} & C \end{bmatrix}. \tag{A.1}$$

The $n\times n$ matrix C is the matrix of overlap between configurations that are taken with constrained Boltzmann measure and subject to the local spherical constraint; the replica symmetric ansatz imposes that $C_{ab} = q(x)$ for all $a \neq b$ and the spherical constraint that $C_{aa} = 1$; then C can be written in the form

$$C = \begin{bmatrix} 1 & q(x) & q(x) & \dots & q(x) \\ q(x) & 1 & q(x) & \dots & q(x) \\ \dots & \dots & \dots & \dots & \\ q(x) & q(x) & q(x) & \dots & 1 \end{bmatrix}. \tag{A.2}$$

The $m\times m$ A matrix is the matrix of overlap between configurations that are taken with Boltzmann measure and subject to the local spherical constraint; we impose that the out of diagonal elements are equal to zero, and then we obtain that A is the identity matrix: $A = 1$.

The $m\times n$ B matrix is the matrix of overlap between configurations that are taken with Boltzmann measure and configurations that are taken with constrained Boltzmann measure; we impose that all the elements of this matrix are equal to zero, except the last two lines that are equal to $p_1(x)$ and to $p_2(x)$; then A can be written in the form

$$B = \begin{bmatrix} 0 & 0 & \dots & 0 \\ 0 & 0 & \dots & 0 \\ \dots & \dots & \dots & \dots \\ p_1(x) & p_1(x) & \dots & p_1(x) \\ p_2(x) & p_2(x) & \dots & p_2(x) \end{bmatrix}. \tag{A.3}$$

Appendix B

The internal energy of a system $\alpha\beta$ is

$$U_{\alpha\beta}(l) \equiv \mathbb{E}\left[\langle H[s,J]\rangle_{\alpha\beta}(l)\right] = \mathbb{E}\left[-\frac{\partial}{\partial\beta}\ln Z[s^{\alpha}_{A^+}, s^{\beta}_{A^-}]\right].$$

We give an explicit derivation of $U_{\alpha\beta}(l)$; similar calculations allow us to obtain the free energy $F_{\alpha\beta}(l)$. We introduce two different temperatures β_1 and β_2 and n and m replicas

of the system:

$$
\begin{aligned}
U_{\alpha\beta}(l) &= \mathbb{E}\left[\mathbb{E}_{s^\alpha}\left[\mathbb{E}_{s^\beta}\left[-\frac{\partial}{\partial\beta}\ln Z[s^\alpha_{A^+}, s^\beta_{A^-}]\right]\right]\right] \\
&= -\frac{\partial}{\partial\beta_2}\mathbb{E}\left[\frac{1}{Z^2[\beta_1]}\int \mathrm{d}s^\alpha\,\mathrm{d}s^\beta\,\exp\left[-\beta_1\left(H[s^\alpha, J] + H[s^\beta, J]\right)\right]\ln Z[s^\alpha, s^\beta, \beta_2]\right] \\
&= \lim_{m,n\to 0}\frac{1}{n}\left(-\frac{\partial}{\partial\beta_2}\right) \\
&\quad\times\ \mathbb{E}\left[Z^{m-2}[\beta_1]\int \mathrm{d}s^\alpha \mathrm{d}s^\beta \exp\left[-\beta_1(H[s^\alpha, J] + H[s^\beta, J])\right] Z^n[s^\alpha, s^\beta, \beta_2]\right]
\end{aligned}
$$

where

$$
\mathcal{C} = \prod_{a=m+1}^{m+n}\left[\prod_{i\in A^+}\delta(Q_{s^{m-1}s^a}(i) - \bar{q})\prod_{i\in A^-}\delta(Q_{s^m s^a}(i) - \bar{q})\right].
$$

Then taking the expectation value over the disorder, the derivative, and reimposing equal temperatures we obtain

$$
\begin{aligned}
U_{\alpha\beta}(l) = \lim_{m,n\to 0}\frac{-\beta}{n}\int\prod_{a=1}^{m+n}\mathrm{d}s^a\,\mathcal{C}\exp\left[\frac{\beta^2}{2}\sum_{i\in\Lambda}\sum_{1\le a,b\le n} f(Q_{ab}(i))\right] \\
\times\ \sum_{i\in\Lambda}\left[\sum_{a,b\in C} f(Q_{ab}(i)) + \frac{1}{2}\sum_{a,b\in B} f(Q_{ab}(i)) + \frac{1}{2}\sum_{a,b\in B^{\mathrm{T}}} f(Q_{ab}(i))\right].
\end{aligned}
$$

Integrals over the spin variables are then traded for an $(m+n)\times(m+n)$ matrix order parameter $q_{ab}(i)$:

$$
\begin{aligned}
U_{\alpha\beta} = \lim_{m,n\to 0}\frac{-\beta}{n}\int\prod_{i\in\Lambda}\prod_{a,b=1}^{m+n} q_{ab}(i)\mathcal{C}\exp\left[\sum_{i\in\Lambda}\left(\frac{\beta^2}{2}\sum_{1\le a,b\le n} f(q_{ab}(i)) + \frac{1}{2}\log\det q(i)\right)\right] \\
\times\ \sum_{i\in\Lambda}\left[\sum_{a,b\in C} f(q_{ab}(i)) + \frac{1}{2}\sum_{a,b\in B} f(q_{ab}(i)) + \frac{1}{2}\sum_{a,b\in B^{\mathrm{T}}} f(q_{ab}(i))\right].
\end{aligned}
$$

Performing the coarse graining,

$$
\begin{aligned}
U_{\alpha\beta} = \lim_{m,n\to 0}\frac{-\beta}{n}\int[\mathrm{d}q_{ab}]\int\mathrm{d}x\left[\sum_{a,b\in C} f((\psi * q)_{ab}(x)) + \frac{1}{2}\sum_{a,b\in B,B^{\mathrm{T}}} f((\psi * q)_{ab}(x))\right] \\
\times\ \exp\left[\frac{1}{\gamma^d}\int\mathrm{d}x\left(\frac{\beta^2}{2}\sum_{1\le a,b\le n} f((\psi * q)_{ab}(x)) + \frac{1}{2}\log\det q(x)\right)\right]\mathcal{C}.
\end{aligned}
$$

Using the replica symmetric matrix presented in appendix A we obtain

$$
U_{\alpha\beta} = \lim_{n\to 0}\frac{-\beta}{n}\int[\mathrm{d}q][\mathrm{d}p_1][\mathrm{d}p_2]\left[n\int\mathrm{d}x\,\mathcal{H}(x) + o(n^2)\right]\exp\left[-\frac{n}{\gamma^d}\int\mathrm{d}x\,\mathcal{L}(x) + o(n^2)\right]
$$

J. Stat. Mech. (2010) P04008

where

$$\mathcal{H}(x) = 1 + f((\psi * p_1)(x)) + f((\psi * p_2)(x)) - f((\psi * q)(x));$$

$$\mathcal{L}(x) = \frac{\beta^2}{2}\left[1 + 2f((\psi * p_1)(x)) + 2f((\psi * p_2)(x)) - f((\psi * q)(x))\right] + \frac{1}{2}\left[\log(1 - q(x)) - \frac{p_1^2(x) + p_2^2(x) - q(x)}{1 - q(x)}\right].$$

We evaluate the action $\mathcal{S}^0_{\alpha\beta} = \int \mathrm{d}^d x\, \mathcal{L}_{\alpha\beta}(x)$ in the saddle-point fields p_1, p_2 and q and we obtain that

$$U_{\alpha\beta}(\hat{l}) = -\beta \int \mathrm{d}x\, \mathcal{H}(x). \tag{B.1}$$

References

[1] Biroli G and Bouchaud J P, *On the Adam–Gibbs–Kirkpatrick–Thirumalai–Wolynes scenario for the viscosity increase in glasses*, 2004 *J. Chem. Phys.* **121** 7347

[2] Montanari A and Semerjian G, *Rigorous inequalities between length and time scales in glassy systems*, 2006 *J. Stat. Phys.* **125** 23

[3] Cavagna A, Grigera T S and Verrocchio P, *Mosaic multi-state scenario versus one-state description of supercooled liquids*, 2007 *Phys. Rev. Lett.* **98** 187801

[4] Biroli G, Bouchaud J P, Cavagna A, Grigera T S and Verrocchio P, *Thermodynamic signature of growing amorphous order in glass-forming liquids*, 2008 *Nat. Phys.* **4** 771

[5] Franz S and Montanari A, *Analytic determination of dynamical and mosaic length scales in a Kac glass model*, 2007 *J. Phys. A: Math. Theor.* **40** F251

[6] Kirkpatrick T R, Thirumalai D and Wolynes P G, *Scaling concepts for the dynamics of viscous liquids near an ideal glassy state*, 1989 *Phys. Rev.* A **40** 1045

[7] Franz S and Semerjian G, *Analytical approaches to time and length scales in models of glasses*, 2010 at press

[8] Cammarota C, Cavagna A, Gradenigo G, Grigera T S and Verrocchio P, *Evidence for a spinodal limit of amorphous excitations in glassy systems*, 2009 *J. Stat. Mech.* L12002

[9] Franz S and Toninelli F L, *The Kac limit for finite-range spin glasses*, 2004 *Phys. Rev. Lett.* **92** 030602

[10] Franz S and Toninelli F L, *Finite-range spin glasses in the Kac limit: free energy and local observables*, 2004 *J. Phys. A: Math. Gen.* **37** 7433

[11] Franz S and Toninelli F L, *A field-theoretical approach to the spin-glass transition: models with long but finite*, 2005 *J. Stat. Mech.* P01008

[12] Franz S, *First steps of a nucleation theory in disordered systems*, 2005 *J. Stat. Mech.* P04001

[13] Franz S, *Metastable states, relaxation times and free-energy barriers in finite-dimensional glassy systems*, 2006 *Europhys. Lett.* **73** 492

[14] Moore M A, *Interface free energies in p-spin glass models*, 2006 *Phys. Rev. Lett.* **96** 137202

J. Stat. Mech. (2010) P04008

Article 2

PHYSICAL REVIEW B **84**, 144417 (2011)

Role of Tracy-Widom distribution in finite-size fluctuations of the critical temperature of the Sherrington-Kirkpatrick spin glass

Michele Castellana[1,2,*] and Elia Zarinelli[1,†]
[1]*LPTMS, CNRS and Université Paris-Sud, UMR8626, Bât. 100, F-91405 Orsay, France*
[2]*Dipartimento di Fisica, Università di Roma 'La Sapienza', I-00185 Rome, Italy*
(Received 20 April 2011; published 10 October 2011)

We investigate the finite-size fluctuations due to quenched disorder of the critical temperature of the Sherrington-Kirkpatrick spin glass. In order to accomplish this task, we perform a finite-size analysis of the spectrum of the susceptibility matrix obtained via the Plefka expansion. By exploiting results from random matrix theory, we obtain that the fluctuations of the critical temperature are described by the Tracy-Widom distribution with a nontrivial scaling exponent 2/3.

DOI: 10.1103/PhysRevB.84.144417 PACS number(s): 64.70.Q−, 75.10.Nr, 02.50.−r

I. INTRODUCTION

The characterization of phase transitions in terms of a nonanalytic behavior of thermodynamic functions in the infinite-size limit has served as a milestone[1–5] in the physical understanding of critical phenomena. In laboratory and numerical experiments, the system size is always finite so that the divergences that would result from such a nonanalytic behavior are suppressed, and are replaced by smooth maxima occurring in the observation of physical quantities as a function of the temperature. In disordered systems, the pseudocritical temperature, defined as the temperature at which this maximum occurs, is a fluctuating quantity depending on the realization of the disorder. A question naturally arises: Can the fluctuations of the pseudocritical temperature be understood and determined with tools of probability theory? Several efforts have been made to study the fluctuations of the pseudocritical temperature for disordered finite-dimensional systems[6–9] and their physical implications. For instance, recently Sarlat *et al.*[10] showed that the theory of finite-size scaling, which is valid for pure systems, fails in fully-connected disordered models because of strong sample-to-sample fluctuations of the critical temperature.

The extreme value statistics of independent random variables is a well-established problem with a long history dating from the original work of Gumbel,[11] while less results are known in the case where the random variables are correlated. The eigenvalues of a Gaussian random matrix are an example of strongly-correlated random variables.[12] Only recently, Tracy and Widom calculated[13–16] exactly the probability distribution of the typical fluctuations of the largest eigenvalue of a Gaussian random matrix around its infinite-size value. This distribution, known as Tracy-Widom distribution, appears in many different models of statistical physics, such as directed polymers[17,18] or polynuclear growth models,[19] showing profound links between such different systems. Conversely, to our knowledge no evident connections between the Tracy-Widom distribution and the physics of spin glasses have been found heretofore.[20]

The purpose of this work is to try to fill this gap. We consider a mean-field spin glass model, the Sherrington-Kirkpatrick (SK) model,[21] and propose a definition of finite-size critical temperature inspired by a previous analysis.[8] We investigate the finite-size fluctuations of this pseudocritical temperature in the framework of extreme value statistics and show that the Tracy-Widom distribution naturally arises in the description of such fluctuations.

II. THE MODEL

The SK model[21] is defined by the Hamiltonian

$$H[\{S_i\},\{x_{ij}\}] = -\frac{J}{N^{1/2}} \sum_{i>j=1}^{N} x_{ij} S_i S_j + \sum_{i=1}^{N} h_i S_i, \qquad (1)$$

where $S_i = \pm 1$, the couplings $\{x_{ij}\}_{i>j=1,\ldots,N} \equiv \{x\}$, $x_{ji} \equiv x_{ij} \forall i > j$ are distributed according to normal distribution with zero mean and unit variance

$$P(x) = \frac{1}{\sqrt{2\pi}} e^{-\frac{x^2}{2}}, \qquad (2)$$

and J is a parameter tuning the strength of the interaction energy between spins.

The low-temperature features of the SK model have been widely investigated in the past and are encoded in Parisi's solution,[22–27] showing that the SK has a finite-temperature spin glass transition at $T_c = J$ in the thermodynamic limit $N \to \infty$. The critical value T_c can be physically thought of as the value of the temperature where ergodicity breaking occurs and the spin glass susceptibility diverges.[25–27]

While Parisi's solution has been derived within the replica method framework, an alternative approach to study the SK model had been previously proposed by Thouless, Anderson, and Palmer (TAP).[28] Within this approach, the system is described in terms of a free energy at fixed local magnetization, and the physical features derived in terms of the resulting free-energy landscape. Later on, Plefka[29] showed that the TAP free energy can be obtained as the result of a systematic expansion in powers of the parameter

$$\alpha \equiv \frac{\beta J}{N^{1/2}},$$

where β is the inverse temperature of the model. This α expansion, known as Plefka expansion, has thus served as a method for deriving the TAP free energy for several classes of models, and has been extensively used in different contexts in physics, from classical disordered systems,[30–32] to general quantum systems.[33–36] It is a general fact that, if the model is

defined on a complete graph, the Plefka expansion truncates to a finite order in α, because higher-order terms should vanish in the thermodynamic limit. In particular, for the SK model, the orders of the expansion larger than three are believed[37] to vanish in the limit $N \to \infty$ in such a way that the expansion truncates, and one is left with the first three orders of the α series, which reads

$$-\beta f(\{m_i\},\beta) = -\sum_i \left[\frac{1+m_i}{2}\ln\left(\frac{1+m_i}{2}\right) + \frac{1-m_i}{2} \times \ln\left(\frac{1-m_i}{2}\right)\right] + \alpha \sum_{i>j} x_{ij} m_i m_j + \frac{\alpha^2}{2}\sum_{i>j} x_{ij}^2 \left(1-m_i^2\right)\left(1-m_j^2\right), \tag{3}$$

where $m_i \equiv \langle S_i \rangle$ is the local magnetization, i.e., the thermal average $\langle\rangle$ of the spin S_i performed with the Boltzmann weight given by Eq. (1) at fixed disorder $\{x\}$.

In the thermodynamic limit $N \to \infty$, for temperatures $T > T_c$, the only minimum of $\beta f(\{m\},\beta)$ is the paramagnetic one $m_i = 0\,\forall i$. Below the critical temperature, the TAP free energy has exponentially many different minima: the system is in a glassy phase. In this framework, the phase transition at T_c can be characterized by the inverse susceptibility matrix, which is also the Hessian of βf

$$\beta\chi^{-1}_{ij} \equiv \beta\frac{\partial h_i}{\partial m_j} = \frac{\partial^2(\beta f)}{\partial m_i \partial m_j}. \tag{4}$$

The inverse susceptibility matrix in the paramagnetic minimum at leading order in N is

$$\beta\chi^{-1}_{ij} = (1+\beta^2 J^2)\delta_{ij} - \alpha x_{ij}. \tag{5}$$

Random-matrix theory states that the average density of eigenvalues of x,

$$\rho_N(\lambda) \equiv \mathbb{E}_x\left[\frac{1}{N}\sum_{i=1}^{N}\delta(\lambda - \lambda_i(\{x\}))\right], \tag{6}$$

has a semicircular shape[38] on a finite support $[-2\sqrt{N}, 2\sqrt{N}]$, where $\mathbb{E}_x$ denotes expectation value with respect to the random bonds $\{x\}$, and $\lambda_i(\{x\})$ is the ith eigenvalue of x. Equation (6) is nothing but the density of eigenvalues of the Gaussian orthogonal ensemble (GOE) of Gaussian random matrices.[12,39]

Due to self-averaging properties, the minimal eigenvalue of $\beta\chi^{-1}$ in the paramagnetic minimum is $\lambda = (1-\beta J)^2$. This shows that, for $T > T_c$, λ is strictly positive and vanishes at T_c, implying the divergence[25] of the spin glass susceptibility $1/\beta^2 \mathrm{Tr}[\chi^2]$. Since λ is also the minimal eigenvalue of the Hessian matrix of βf in the paramagnetic minimum, we deduce that this is stable for $T > T_c$ and becomes marginally stable at T_c.

This analysis sheds some light on the nature of the spin glass transition of the SK model in terms of the minimal eigenvalue λ of the inverse susceptibility matrix (Hessian matrix) in the thermodynamic limit. In this paper we generalize such analysis to finite sizes, where no diverging susceptibility nor uniquely-defined critical temperature exists, and the minimal eigenvalue λ acquires fluctuations due to quenched disorder. We show that a finite-size pseudocritical temperature can be suitably defined and investigate its finite-size fluctuations with respect to disorder. As a result of this work, these fluctuations are found to be described by the Tracy-Widom distribution.

The rest of the paper is structured as follows. In Sec. III, we generalize Eq. (5) to finite sizes, in the simplifying assumption that the Plefka expansion can be truncated up to order α^2, which is known as the TAP approach. We then study the finite-size fluctuations of the minimal eigenvalue λ of the susceptibility matrix, and show that they are governed by the TW distribution. In Sec. IV, we extend this simplified approach by taking into account the full Plefka expansion, by performing an infinite re-summation of the series. Hence, in Sec. V, we give a suitable definition of a finite-size pseudocritical temperature, and show that its fluctuations are governed by the TW distribution. In Sec. VI, this result is discussed in the perspective of generalizing it to more realistic spin glass models.

III. FINITE-SIZE ANALYSIS OF THE SUSCEPTIBILITY IN THE TAP APPROXIMATION

In this section, we study the finite-size fluctuations due to disorder of the minimal eigenvalue of the inverse susceptibility matrix $\beta\chi^{-1}$ at the paramagnetic minimum $m_i = 0\,\forall i$, by considering the free energy f in the TAP approximation, Eq. (3). We want to stress the fact that large deviations of thermodynamics quantities of the SK model have been already studied heretofore. For example, Parisi *et al.* have studied[40,41] the probability distribution of large deviations of the free energy within the replica approach. The same authors studied the probability of positive large deviations of the free energy per spin in general mean-field spin-glass models,[42] and showed that such fluctuations can be interpreted in terms of the fluctuations of the largest eigenvalue of Gaussian matrices, in analogy with the lines followed in the present work.

Back to the TAP equations (3), the inverse susceptibility matrix in the paramagnetic minimum for finite N reads

$$\beta\chi^{-1}_{ij} = -\alpha x_{ij} + \delta_{ij}\left(1 + \alpha^2\sum_{k\neq i} x_{ki}^2\right) = -\alpha x_{ij} + \delta_{ij}(1+\beta^2 J^2) + \delta_{ij}\frac{(\beta J)^2}{\sqrt{N}} z_2^i, \tag{7}$$

where

$$z_2^i \equiv \sqrt{N}\left(\frac{1}{N}\sum_{k\neq i} x_{ki}^2 - 1\right). \tag{8}$$

According to Eq. (8), z_2^i is given by the sum of $N-1$ independent identically-distributed random variables x_{ij}^2. By the central limit theorem, at leading order in N the variable z_2^i is distributed according to a Gaussian distribution with zero mean and variance 2

$$p_N\left(z_2^i = z\right) \overset{N\to\infty}{\to} \frac{1}{\sqrt{4\pi}} e^{-z^2/4}, \tag{9}$$

where $p_N(z_2^i = z)$ denotes the probability that z_2^i is equal to z at finite size N.

We set

$$\beta\chi_{ij}^{-1} \equiv \delta_{ij}(1+\beta^2 J^2) + \alpha M_{ij}. \tag{10}$$

According to Eq. (8), the diagonal elements of M_{ij} are random variables correlated to out-of-diagonal elements. The statistical properties of the spectrum of a random matrix whose entries are correlated to each other has been studied heretofore only in some cases. For instance, Stäring *et al.*[43] studied the average eigenvalue density for matrices with a constraint implying that the row sum of matrix elements should vanish, and other correlated cases have been investigated both from a physical[44] and mathematical[45] point of view.

In recent years, a huge amount of results has been obtained on the distribution of the minimal eigenvalue of a $N \times N$ random matrix drawn from Gaussian ensembles, such as GOE. In particular, Tracy and Widom[13–16] deduced that for large N, small fluctuations of the minimal eigenvalue $\lambda_{\rm GOE}$ of a GOE matrix around its leading-order value $-2\sqrt{N}$ are given by

$$\lambda_{\rm GOE} = -2\sqrt{N} + \frac{1}{N^{1/6}}\phi_{\rm GOE}, \tag{11}$$

where $\phi_{\rm GOE}$ is a random variable distributed according to the Tracy-Widom (TW) distribution for the GOE ensemble $p_{\rm GOE}(\phi)$. It follows that for $\beta J = 1$ if z_2^i was independent on $\{x\}$, the matrix M_{ij} would belong to the GOE ensemble, and the minimal eigenvalue λ of $\beta\chi^{-1}$ would define a variable ϕ according to

$$\lambda = \frac{1}{N^{2/3}}\phi, \tag{12}$$

and ϕ would be distributed according to the TW distribution $p_{\rm GOE}(\phi)$.

As shown in Appendix A, this is indeed the case for z_2^i, which can be treated, at leading order in N, as a random variable independent on x_{ij}. The general idea is that z_2^i is given by the sum of $N-1$ terms all of the same order of magnitude, and only one amongst these $N-1$ terms depends on x_{ij}. It follows that at leading order in N, z_2^i can be considered as independent on x_{ij}. Since in Eq. (7) z_2^i is multiplied by a sub-leading factor $1/\sqrt{N}$, in Eq. (7) we can consider z_2^i at leading order in N, and treat it as independent on x_{ij}.

To test this independence property, we set $\beta J = 1$, generate numerically $S \gg 1$ samples of the $N \times N$ matrix $\beta\chi^{-1}$, and compute the average density of eigenvalues of $\beta\chi^{-1}$, defined as in Eq. (6), together with the distribution of the minimal eigenvalue λ for several sizes N. The eigenvalue distribution $\rho_N(\lambda)$ as a function of λ is depicted in Fig. 1, and tends to the Wigner semicircle as N is increased, showing that the minimal eigenvalue λ tends to 0 as $N \to \infty$.

The finite-size fluctuations of λ around 0 are then investigated in Fig. 2. Defining ϕ in terms of λ by Eq. (12), in Fig. 2 we depict the distribution $p_N(\phi)$ of the variable ϕ for several sizes N, and show that for increasing N, $p_N(\phi)$ approaches the TW distribution $p_{\rm GOE}(\phi)$. Let us introduce the central moments

$$\mu_1^N \equiv \mathbb{E}_N[\phi],$$
$$\mu_i^N \equiv \mathbb{E}_N[(\phi - \mathbb{E}_N[\phi])^i]\,\forall i > 1$$

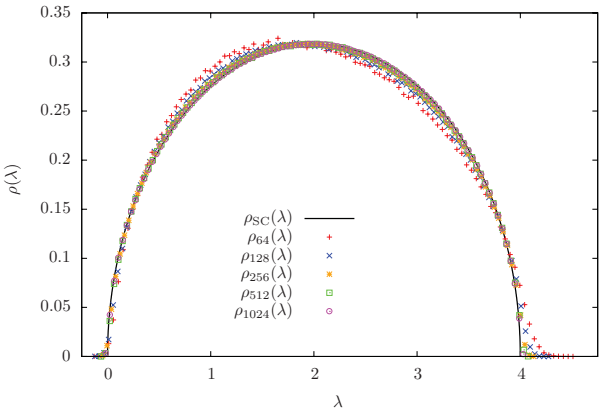

FIG. 1. (Color online) Density of eigenvalues $\rho_N(\lambda)$ of the matrix $\beta\chi^{-1}$ for $N = 64, 128, 256, 512, 1024$ (in red, blue, yellow, green, violet respectively), $\beta J = 1$ and $S = 16 \times 10^3$, and Wigner semicircular law $\rho_{\rm SC}(\lambda) = 1/(2\pi)\sqrt{4-(2-\lambda)^2}$ (black) as a function of λ. $\rho_N(\lambda)$ approaches $\rho_{\rm SC}(\lambda)$ as N is increased.

of $p_N(\phi)$, and the central moments

$$\mu_1^{\rm GOE} \equiv \mathbb{E}_{\rm GOE}[\phi],$$
$$\mu_i^{\rm GOE} \equiv \mathbb{E}_{\rm GOE}[(\phi - \mathbb{E}_{\rm GOE}[\phi])^i]\,\forall i > 1$$

of the TW distribution, where

$$\mathbb{E}_N[\cdot] \equiv \int d\phi\; p_N(\phi)\cdot,$$
$$\mathbb{E}_{\rm GOE}[\cdot] \equiv \int d\phi\; p_{\rm GOE}(\phi)\cdot.$$

In the inset of Fig. 2 we depict μ_i^N for several sizes N and $\mu_i^{\rm GOE}$ as a function of i, showing that μ_i^N converges to $\mu_i^{\rm GOE}$ as N is increased.

In Fig. 3, this convergence is clarified by depicting $\Delta\mu_i^N \equiv (\mu_i^N - \mu_i^{\rm GOE})/\mu_i^{\rm GOE}$ for several values of $i > 1$ as a function of N. $\Delta\mu_i^N$ is found to converge to 0 for large N. In the inset of Fig. 3, we depict $\Delta\mu_1^N$ as a function of N, showing that the convergence of the first central moment with N is much slower than that of the other central moments. It is interesting to observe that a slowly-converging first moment has been recently found also in experimental[46] and numerical[47] data of models of growing interfaces where the TW distribution appears.

The analytical argument proving the independence property of z_2^i has been thus confirmed by this numerical calculation. Hence, the main result of this section is that the finite-size fluctuations of the minimal eigenvalue of the susceptibility matrix $\beta\chi^{-1}$ in the TAP approximation for $\beta J = 1$ are of the order of $N^{-2/3}$ and are distributed according to the TW law. These fluctuations have already been found to be of the order of $N^{-2/3}$ in a previous work,[48] and more recently reconsidered,[49] following an independent derivation based on scaling arguments, even though the distribution has not been worked out. Our approach sheds some light on the nature of the scaling $N^{-2/3}$, which is nontrivial, since it comes from the $N^{-1/6}$ scaling of the TW distribution, which is found to govern the fluctuations of λ. Moreover, the fact that we find the same scaling as that found in such previous works can be considered as a consistency test of our calculation.

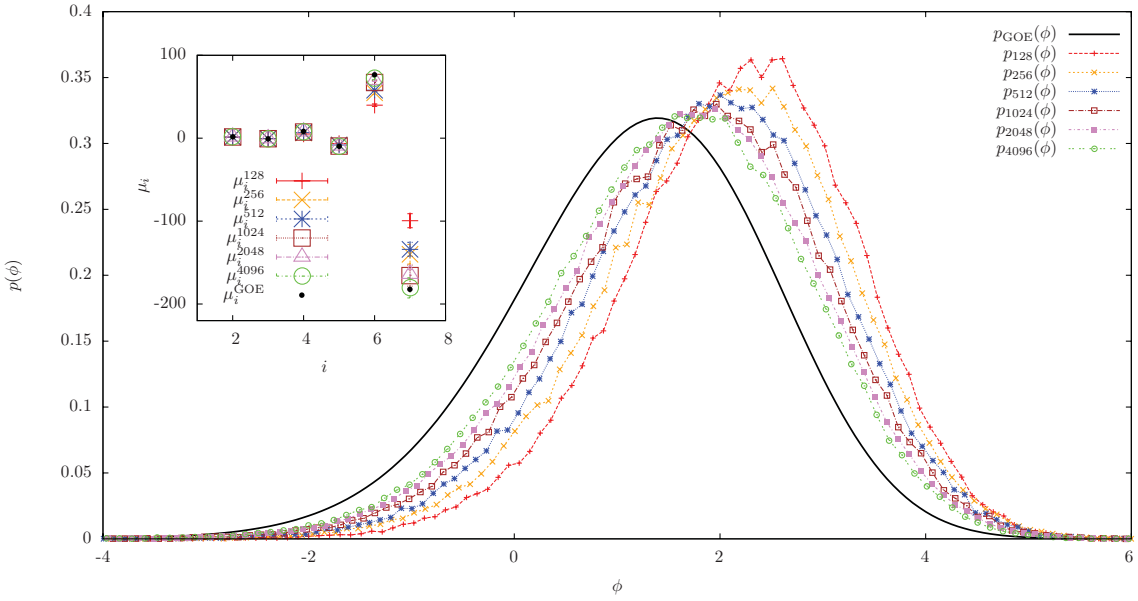

FIG. 2. (Color online) Distribution $p_N(\phi)$ for $N = 128,256,512,1024,2048,4096$ (in red, yellow, blue, brown, violet, green respectively) and $10^5 \leqslant S \leqslant 4 \times 10^5$ samples, and the Tracy-Widom distribution $p_{\rm GOE}(\phi)$ for the GOE ensemble (black), as a function of ϕ. For increasing N, $p_N(\phi)$ approaches $p_{\rm GOE}(\phi)$, confirming the asymptotic independence of the diagonal elements (11) by each of the off-diagonal elements x_{ij} for large N. Inset: μ_i^N for sizes $N = 128,256,512,1024,2048,4096$ (in red, yellow, blue, brown, violet, green respectively), $10^5 \leqslant S \leqslant 4 \times 10^5$, and $\mu_i^{\rm GOE}$ (black) as a function of $i > 1$.

We now recall that both the derivation of this section and the previously-developed analysis of Bray and Moore[48] rely on the TAP approximation, i.e., neglect the terms of the Plefka expansion (13) of order larger than 2 in α. As we will show in the following section, these terms give a non-negligible contribution to the finite-size corrections of the TAP equations, and so to the finite-size fluctuations of the critical temperature,

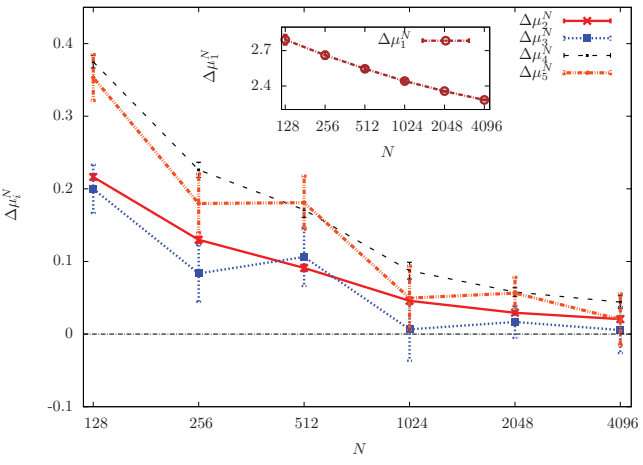

FIG. 3. (Color online) Relative difference $\Delta\mu_i^N$ between the central moments μ_i^N of the distribution $p_N(\phi)$ for $10^5 \leqslant S \leqslant 4 \times 10^5$, and the central moments $\mu_i^{\rm GOE}$ of the Tracy-Widom distribution as a function of $N = 128,256,512,1024,2048,4096$, for $i = 2,3,4,5$ (in red, blue, black, orange respectively). For increasing N, μ_i^N approaches $\mu_i^{\rm GOE}$, confirming the asymptotic independence of z_2^i by each of the off-diagonal elements x_{ij} for large N. Inset: relative difference of the first central moment $\Delta\mu_1^N$ as a function of N (brown). $\Delta\mu_1^N$ approaches 0 very slowly as N is increased.

and thus must be definitely taken into account in a complete treatment.

IV. FINITE-SIZE ANALYSIS OF THE SUSCEPTIBILITY WITHIN THE FULL PLEFKA EXPANSION

In this section, we compute the inverse susceptibility matrix $\beta\chi^{-1}$ by taking into account all the terms of the Plefka expansion, in the effort to go beyond the TAP approximation of Sec. III. Notwithstanding its apparent difficulty, here we show that this task can be pursued by a direct inspection of the terms of the expansion. Indeed, let us formally write the free-energy f as a series[29] in α,

$$f(\{m\},\beta) = \sum_{n=0}^{\infty} \alpha^n f_n(\{m\},\beta). \tag{13}$$

For $n < 3$, the f_n's are given by Eq. (3). For $n > 3$, f_n is given by the sum of several different addends,[37] which proliferate for increasing n.

It is easy to show that at leading order in N, there is just one term contributing to f_n, and that such a term can be written explicitly as

$$f_n(\{m\},\beta) \overset{N\to\infty}{\approx} \sum_{i_1>\cdots>i_{n-1}} x_{i_1 i_2} x_{i_2 i_3} \cdots x_{i_{n-1} i_1} \times \left(1 - m_{i_1}^2\right) \times \cdots \times \left(1 - m_{i_{n-1}}^2\right). \tag{14}$$

It follows that by plugging Eq. (14) into Eq. (13) and computing $\beta\chi^{-1}$ for $m_i = 0$, one obtains a simple expression for the inverse susceptibility at the paramagnetic solution

$$\begin{aligned}\beta\chi^{-1}_{ij} &= -\alpha x_{ij} + \delta_{ij}\Bigg(1 + \alpha^2 \sum_{k\neq i} x^2_{ki} + 2\sum_{n=3}^{\infty}\alpha^n \\ &\quad\times \sum_{i_1>\cdots>i_{n-1}} x_{ii_1}x_{i_1i_2}\cdots x_{i_{n-1}i}\Bigg) \\ &= -\alpha x_{ij} + \delta_{ij}(1+\beta^2J^2) + \delta_{ij}\frac{1}{\sqrt{N}} \\ &\quad\times\left[(\beta J)^2 z^i_2 + 2\sum_{n=3}^{\infty}\frac{(\beta J)^n}{\sqrt{(n-1)!}} z^i_n\right]. \end{aligned} \tag{15}$$

where

$$z^i_n \equiv \frac{\sqrt{(n-1)!}}{N^{\frac{n-1}{2}}} \sum_{i_1>\cdots>i_{n-1}} x_{ii_1}x_{i_1i_2}\cdots x_{i_{n-1}i}, \forall n > 2. \tag{16}$$

According to Eq. (16), one has that at leading order in N,

$$\begin{aligned}\mathbb{E}_x\left[z^i_n\right] &= 0\,\forall n > 2, \\ \mathbb{E}_x\left[\left(z^i_n\right)^2\right] &= 1\,\forall n > 2,\end{aligned} \tag{17}$$

where in the second line of Eq. (17) the multiple sum defining z^i_n has been evaluated at leading order in N.

We observe that the random variables z^i_n and x_{jk} in Eq. (15) are not independent, since each z^i_n depends on the bond variables $\{x\}$. Following an argument similar to that given in Sec. III for z^i_2, we observe that, by Eq. (16) and at leading order in N, z^i_n is given by a sum of $O(N^{n-1})$ terms which are all of the same order of magnitude. Each term is given by the product of $n-1$ bond variables $x_{ii_1}x_{i_1i_2}\cdots x_{i_{n-1}i}$ forming a loop passing by site i. For any fixed i, j, k, and n, only $O(N^{n-2})$ terms amongst the $O(N^{n-1})$ terms of z^i_n are entangled with the random bond variable x_{jk}. It follows that at leading order in N, z^i_n can be considered as independent by x_{jk}. Since the sum in the second line of Eq. (15) has a $1/\sqrt{N}$ factor multiplying each of the z^i_n's, we can consider the z^i_n at leading order in N. Hence, in Eq. (15) we can consider each of the z^i_n's as independent on x_{jk}.

In Appendix B we show that at leading order in N, the distribution of z^i_n is a Gaussian with zero mean and unit variance for every i and $n > 2$, while in Appendix C we show that at leading order in N the variables $\{z^i_n\}_{n,i}$ are mutually independent. Both these predictions are confirmed by numerical tests, illustrated in Appendix B and C respectively.

Hence, at leading order in N the term in square brackets in Eq. (15) is nothing but the sum of independent Gaussian variables, and is thus equal to a random variable $\sigma \times \zeta_i$, where ζ_i is Gaussian with zero mean and unit variance, and

$$\begin{aligned}\sigma^2 &= 2(\beta J)^4 + 4\sum_{n=3}^{\infty}\frac{(\beta J)^{2n}}{(n-1)!} \\ &= 2(\beta J)^2\{2(e^{(\beta J)^2} - 1) - (\beta J)^2\}.\end{aligned}$$

It follows that Eq. (15) becomes

$$\begin{aligned}\beta\chi^{-1}_{ij} &= -\alpha x_{ij} + \delta_{ij}\left(1 + \beta^2J^2 + \frac{\sigma}{\sqrt{N}}\zeta_i\right) \\ &= -\alpha x'_{ij} + \delta_{ij}(1+\beta^2J^2),\end{aligned} \tag{18}$$

where

$$x'_{ij} \equiv x_{ij} - \delta_{ij}\frac{\sigma}{\beta J}\zeta_i. \tag{19}$$

Because of the additional diagonal term in Eq. (19), the matrix x'_{ij} does not belong to the GOE ensemble. Notwithstanding this fact, it has been shown by Soshnikov[50] that the presence of the diagonal elements in Eq. (19) does not alter the universal distribution of the maximal eigenvalue of x'_{ij}, which is still distributed according to the TW law. Hence, denoting by λ the minimal eigenvalue of $\beta\chi^{-1}$, we have

$$\lambda = (1-\beta J)^2 + \frac{\beta J}{N^{2/3}}\phi_{\mathrm{GOE}}, \tag{20}$$

where ϕ_{GOE} is a random variable depending on the sample x_{ij}, and distributed according to the TW law.

In this section, we have calculated the inverse susceptibility matrix $\beta\chi^{-1}$, by considering the full Plefka expansion. In this framework, additional diagonal terms are generated that were not present in the TAP approximation. These additional terms can be handled via a resummation to all orders in the Plefka expansion. As a result, we obtain that the fluctuations of the minimal eigenvalue λ of the susceptibility $\beta\chi^{-1}$ are still governed by the TW law, as in the TAP case treated in Sec. III.

V. FINITE SIZE FLUCTUATIONS OF THE CRITICAL TEMPERATURE

We can now define a finite-size critical temperature, and investigate its finite-size fluctuations due to disorder. In the previous sections, we have shown that for a large but finite size N, the minimal eigenvalue of the inverse susceptibility matrix, i.e., the Hessian matrix of $\beta f(\{m\},\beta)$ evaluated in the paramagnetic minimum $m_i = 0$, is a function of the temperature and of a quantity ϕ_{GOE}, which depends on the realization of the disorder $\{x\}$. Since the TW law, i.e., the distribution of ϕ_{GOE}, has support for both positive and negative values of ϕ_{GOE}, the subleading term in Eq. (20) can be positive or negative. Accordingly, for samples $\{x\}$ such that $\phi_{\mathrm{GOE}} < 0$, there exists a value of $\beta J \approx 1$ such that $\lambda(\beta J) = 0$, in such a way that the spin-glass susceptibility in the paramagnetic minimum diverges. This fact is physically meaningless, since there cannot be divergences in physical quantities at finite size. This apparent contradiction can be easily understood by observing that if $\lambda(\beta J) = 0$, the true physical susceptibility is no more the paramagnetic one, but must be evaluated in the low-lying nonparamagnetic minima of the free energy, whose appearance is driven by the emergent instability of the paramagnetic minimum. According to this discussion, in the following we will consider only samples $\{x\}$ such that $\phi_{\mathrm{GOE}} > 0$.

For these samples, the spectrum of the Hessian matrix at the paramagnetic minimum has positive support for every temperature: The paramagnetic solution is always stable, and the paramagnetic susceptibility matrix χ is physical and finite. We define a pseudoinverse critical temperature $\beta_c J$ as the value of βJ such that λ has a minimum at $\beta_c J$:

$$\left.\frac{d\lambda}{d\beta J}\right|_{\beta J=\beta_c J} \equiv 0 = -2(1-\beta_c J) + \frac{1}{N^{2/3}}\phi_{\mathrm{GOE}}, \qquad (21)$$

where in the second line of Eq. (21), Eq. (20) has been used. This definition of pseudocritical temperature has a clear physical interpretation: The stability of the paramagnetic minimum, which is encoded into the spectrum of the Hessian matrix $\beta\chi^{-1}$, has a minimum at $\beta = \beta_c$. According to Eq. (21), the finite-size critical temperature β_c is given by

$$\beta_c J = 1 - \frac{1/2}{N^{2/3}}\phi_{\mathrm{GOE}}, \qquad (22)$$

where ϕ_{GOE} depends on the sample $\{x\}$, and is distributed according to the TW law.

Eq. (22) shows that the pseudocritical temperature of the SK model is a random variable depending on the realization of the quenched disorder. Finite-size fluctuations of the pseudocritical temperature are of the order of $N^{-2/3}$, and are distributed according to the TW law. This has to be considered the main result of this paper.

VI. DISCUSSION AND CONCLUSIONS

In this paper, the finite-size fluctuations of the critical temperature of the Sherrington-Kirkpatrick spin glass model have been investigated. The analysis is carried on within the framework of the Plefka expansion for the free energy at fixed local magnetization. A direct investigation of the expansion shows that an infinite resummation of the series is required to describe the finite-size fluctuations of the critical temperature. By observing that the terms in the expansion can be treated as independent random variables, one can suitably define a finite-size critical temperature. Such a critical temperature has a unique value in the infinite-size limit, while it exhibits fluctuations due to quenched disorder at finite sizes. These fluctuations with respect to the infinite-size value have been analyzed, and have been found to be of the order of $N^{-2/3}$, where N is the system size, and to be distributed according to the Tracy-Widom distribution.

The exponent $2/3$ describing the fluctuations of the pseudocritical temperature stems from the fact that the finite-size fluctuations of the minimal eigenvalue λ of the inverse susceptibility matrix are of the order of $N^{-2/3}$. Such a scaling for λ at the critical temperature had already been obtained in a previous work,[48] where it was derived by a completely independent method, by taking into account only the first three terms of the Plefka expansion. The present work shows that a more careful treatment, including an infinite resummation of the expansion, is needed to handle finite-size effects. The exponent $2/3$ derived by Bray and Moore[48] is here rederived by establishing a connection with recently-developed results in random matrix theory, showing that the scaling $N^{-2/3}$ comes from the scaling of the Tracy-Widom distribution, which was still unknown when the paper by Bray and Moore[48] was written.

As a possible development of the present work, it would be interesting to study the fluctuations of the critical temperature for a SK model where the couplings are distributed according to a power law. Indeed, in a recent work[52] the distribution of the largest eigenvalue λ of a random matrix M whose entries M_{ij} are power-law distributed as $p(M_{ij}) \sim M_{ij}^{-1-\mu}$ has been studied. The authors show that if $\mu > 4$, the fluctuations of λ are of the order of $N^{-2/3}$ and are given by the TW distribution, while if $\mu < 4$ the fluctuations are of the order of $N^{-2/\mu-1/2}$ and are governed by Fréchet's statistics. This result could be directly applied to a SK model with power-law distributed couplings. In particular, it would be interesting to see if there exists a threshold in the exponent μ separating two different regimes of the fluctuations of T_c.

Another interesting perspective would be to generalize the present approach to realistic spin glass models with finite-range interactions. For instance, a huge amount of results has been quite recently obtained for the three-dimensional Ising spin glass,[53–60] and for the short-range p-spin glass model in three dimensions,[61] yielding evidence for a finite-temperature phase transition. It would be interesting to try to generalize the present work to that systems, and compare the resulting fluctuations of the critical temperature with sample-to-sample fluctuations observed in these numerical works. Accordingly, the finite-size fluctuations deriving from the generalization of this work to the three-dimensional Ising spin glass could be hopefully compared with those observed in experimental spin glasses,[62] such as $Fe_{0.5}Mn_{0.5}TiO_3$.

Finally, a recent numerical analysis[63] inspired by the present work has investigated the sample-to-sample fluctuations of a given pseudocritical temperature for the SK model, which is different from that defined in this work. Even though the relatively small number of samples did not allow for a precise determination of the probability distribution of that pseudocritical point, the analysis yields a scaling exponent equal to $1/3$, which is different from that of the pseudocritical temperature defined here. As a consequence, the general scaling features of the pseudocritical temperature seem to depend on the actual definition of the pseudocritical point itself, even though different definitions of the pseudocritical temperature must all converge to the infinite-size pseudocritical temperature as the system size tends to infinity. As a future perspective, it would be interesting to investigate which amongst the features of the pseudocritical point are definition-independent, if any.

ACKNOWLEDGMENTS

We are glad to thank J. Rambeau and G. Schehr for interesting discussions and suggestions. We also acknowledge support from the D. I. computational center of University Paris Sud.

APPENDIX A: PROOF OF THE ASYMPTOTIC INDEPENDENCE OF x_{ij} AND z_2^i

Here we show that at leading order in N, the variables x_{ij} and z_2^i are independent, i.e., that at leading order in N

$$p_N\left(x_{ij}=x,z_2^i=z\right)=p_N(x_{ij}=x)\times p_N\left(z_2^i=z\right). \tag{A1}$$

Let us explicitly write the left-hand size of Eq. (A1) as

$$\begin{aligned}
&p_N\left(x_{ij}=x,z_2^i=z\right)\\
&=\mathbb{E}_{\{x_{ik}\}_{k\neq i}}\left[\delta(x_{ij}-x)\delta\left(z_2^i-z\right)\right],\\
&=\mathbb{E}_{x_{ij}}\Bigg[\delta(x_{ij}-x)\mathbb{E}_{\{x_{ik}\}_{k\neq i,k\neq j}}\\
&\quad\times\left\{\delta\left[\sqrt{N}\left(\frac{1}{N}\sum_{k\neq i,k\neq j}x_{ki}^2-1\right)-\bar{z}_2^{ij}\right]\right\}\Bigg],
\end{aligned} \tag{A2}$$

where $\mathbb{E}_{x_{lm},x_{no},\ldots}$ denotes the expectation value with respect to the probability distributions of the variables $x_{lm},x_{no},\ldots,\delta$ denotes the Dirac delta function, and

$$\bar{z}_2^{ij}\equiv z-\frac{x_{ij}^2}{\sqrt{N}}. \tag{A3}$$

Proceeding systematically at leading order in N, the second expectation value in the second line of Eq. (A2) is nothing but the probability that the variable $\sqrt{N}(\frac{1}{N}\sum_{k\neq i,k\neq j}x_{ki}^2-1)$ is equal to $\bar{z}_2^{ij}$. We observe that according to the central limit theorem, at leading order in N this probability is given by

$$\begin{aligned}
&\mathbb{E}_{\{x_{ik}\}_{k\neq i,k\neq j}}\left[\delta\left(\sqrt{N}\left(\frac{1}{N}\sum_{k\neq i,k\neq j}x_{ki}^2-1\right)-\bar{z}_2^{ij}\right)\right]\\
&=\frac{1}{\sqrt{4\pi}}e^{-\frac{(\bar{z}_2^{ij})^2}{4}}.
\end{aligned} \tag{A4}$$

By plugging Eq. (A4) into Eq. (A2) and using Eq. (A3), one has

$$\begin{aligned}
p_N\left(x_{ij}=x,z_2^i=z\right)&=\frac{1}{\sqrt{4\pi}}\int dx_{ij}\,P(x_{ij})\delta(x_{ij}-x)\\
&\quad\times e^{-\frac{(z-x_{ij}^2/\sqrt{N})^2}{4}}\\
&=P(x)\frac{1}{\sqrt{4\pi}}e^{-\frac{(z-x^2/\sqrt{N})^2}{4}}\\
&=p_N(x_{ij}=x)\times p_N\left(z_2^i=z\right),
\end{aligned} \tag{A5}$$

where in the first line we explicitly wrote the expectation value with respect to x_{ij} in terms of the probability distribution (2), while in the third line proceeded at leading order in N, and used Eq. (9).

APPENDIX B: COMPUTATION OF THE PROBABILITY DISTRIBUTION OF z_n^i

Here we compute the probability distribution of z_n^i at leading order in N. Let us define a super index $L\equiv\{i_1,\ldots,i_{n-1}\}$, where L stands for loop, since L represents a loop passing by the site i. Let us also set $X_L\equiv x_{ii_1}x_{i_1i_2}\cdots x_{i_{n-1}i}$. By Eq. (16) one has

$$z_n^i=\frac{\sqrt{(n-1)!}}{N^{\frac{n-1}{2}}}\sum_L X_L,\forall n>2. \tag{B1}$$

We observe that the probability distribution of X_L is the same for every L. Hence, according to Eq. (B1), z_n^i is given by the sum of equally distributed random variables. Now pick two of these variables, X_L and $X_{L'}$. For some choices of L,L', X_L and $X_{L'}$ are not independent, since they can depend on the same bond variables x_{ij}. If one picks one variable X_L, the number of variables appearing in the sum (B1) which are dependent on X_L are those having at least one common edge with the edges of X_L. The number of these variables, at leading order in N, is $O(N^{n-2})$, since they are obtained by fixing one of the $n-1$ indexes $i_1,\ldots,i_{n-1}$. The latter statement is equivalent to saying that if one picks at random two variables X_L and $X_{L'}$, the probability that they are correlated is

$$O(N^{n-2}/N^{n-1})=O(N^{-1}). \tag{B2}$$

Hence, at leading order in N, we can treat the ensemble of the variables $\{X_L\}_L$ as independent. According to the central limit theorem, at leading order in N, the variable

$$\frac{\sqrt{(n-1)!}}{N^{\frac{n-1}{2}}}z_n^i=\frac{1}{\frac{N^{n-1}}{(n-1)!}}\sum_L X_L$$

is distributed according to a Gaussian distribution with mean $\mathbb{E}_x[X_L]=0$ and variance

$$\mathbb{E}_x\left[\left(\frac{\sqrt{(n-1)!}}{N^{\frac{n-1}{2}}}z_n^i\right)^2\right]=\frac{\mathbb{E}_x\left[X_L^2\right]}{\frac{N^{n-1}}{(n-1)!}}=\frac{1}{\frac{N^{n-1}}{(n-1)!}}, \tag{B3}$$

where in Eq. (B3) Eq. (2) has been used. It follows that at leading order in N, z_n^i is distributed according to a Gaussian distribution with zero mean and unit variance

$$p_N\left(z_n^i=z\right)\overset{N\to\infty}{\to}\frac{1}{\sqrt{2\pi}}e^{-\frac{z^2}{2}}, \tag{B4}$$

where $p_N(z_n^i=z)$ is defined as the probability that z_n^i is equal to z at size N.

Eq. (B4) has been tested numerically for the first few values of n: $p_N(z_n^i=z)$ has been computed by generating $S\gg1$ samples of $\{x\}$, and so of z_n^i. For $n=3$ and 4, the resulting probability distribution $p_N(z_n^i=z)$ converges to a Gaussian distribution with zero mean and unit variance as N is increased, confirming the result (B4). This convergence is shown in Fig. 4, where $p_N(z_4^1=z)$ is depicted for different values of N together with the right-hand side of Eq. (B4), as a function of z.

APPENDIX C: INDEPENDENCE OF THE z_n^i's AT LEADING ORDER IN N

Let us consider two distinct variables z_n^i and z_m^j, and proceed at leading order in N. Following the notation of Appendix B, we write Eq. (16) as

$$z_n^i=\frac{\sqrt{(n-1)!}}{N^{\frac{n-1}{2}}}\sum_L X_L, \tag{C1}$$

$$z_m^j=\frac{\sqrt{(m-1)!}}{N^{\frac{m-1}{2}}}\sum_{L'} X_{L'}, \tag{C2}$$

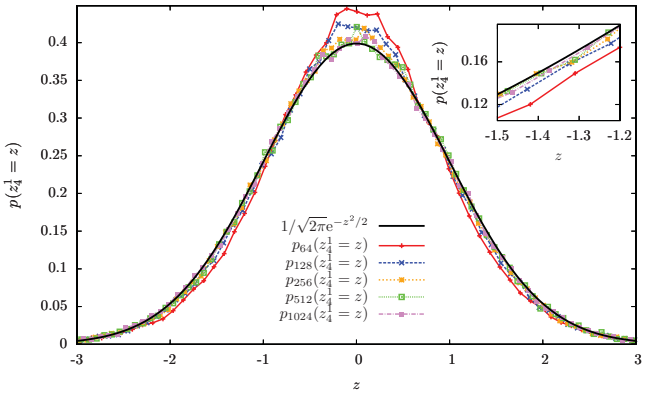

FIG. 4. (Color online) Probability distribution $p_N(z_4^1 = z)$ for $S = 10^5$ and different values of $N = 64,128,256,512,1024$ (in red, blue, yellow, green, violet respectively) together with a Gaussian distribution $1/\sqrt{2\pi}e^{-z^2/2}$ with zero mean and unit variance (black), as a function of z. As N is increased, $p_N(z_4^1 = z)$ converges to $1/\sqrt{2\pi}e^{-z^2/2}$, as predicted by the analytical calculation, Eq. (B4). Inset: zoom of the above plot explicitly showing the convergence of $p_N(z_4^1 = z)$ to $1/\sqrt{2\pi}e^{-z^2/2}$ as N is increased.

where L, L' represent a loop of length n, m passing by the site i, j respectively. Some of the variables X_L depend on some of the variables $X_{L'}$, because they can depend on the same bond variables x_{ij}. Let us pick at random one variable X_L appearing in z_n^i, and count the number of variables $X_{L'}$ in z_m^j that are dependent on X_L. At leading order in N, these are given by the number of $X_{L'}$ having at least one common bond with X_L, and are $O(N^{m-2})$. Hence, if one picks at random two variables $X_L, X_{L'}$ in Eqs. (C1), (C2) respectively, the probability that $X_L, X_{L'}$ are dependent is

$$O(N^{m-2}/N^{m-1}) = O(N^{-1}).$$

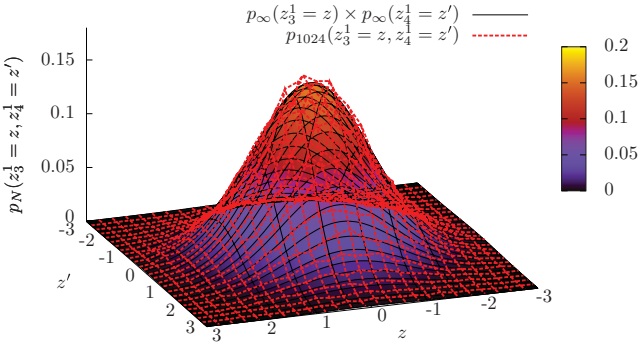

FIG. 5. (Color online) $p_{1024}(z_3^1 = z, z_4^1 = z')$ for $S = 10^5$ samples (red), and the $N \to \infty$ limit of the right-hand side of Eq. (C3) (black), as a function of z, z'. For large N, $p_N(z_3^1 = z, z_4^1 = z')$ equals $p_N(z_3^1 = z) \times p_N(z_4^1 = z')$, as predicted by Eq. (C3). Hence, at leading order in N, the variables z_3^1 and z_4^1 are independent.

It follows that z_n^i and z_m^j are independent at leading order in N, i.e., for $N \to \infty$

$$p_N\left(z_n^i = z, z_m^j = z'\right) = p_N\left(z_n^i = z\right) \times p_N\left(z_m^j = z'\right), \quad \text{(C3)}$$

where $p_N(z_n^i = z, z_m^j = z')$ denotes the joint probability that z_n^i equals z and z_m^j equals z', at fixed size N.

Eq. (C3) has been tested numerically for $n = 3, m = 4$: $p_N(z_3^1 = z, z_4^1 = z')$ has been computed by generating $S \gg 1$ samples of $\{x\}$, and so of z_3^1, z_4^1. As a result, the left-hand side of Eq. (C3) converges to the right-hand side as N is increased, confirming the predictions of the above analytical argument. This is shown in Fig. 5, where $p_{1024}(z_3^1 = z, z_4^1 = z')$ is depicted together with the $N \to \infty$ limit of the right-hand side of Eq. (C3) [see Eq. (B4)], as a function of z, z'.

*michele.castellana@lptms.u-psud.fr
†elia.zarinelli@lptms.u-psud.fr

[1] T. D. Lee and C. N. Yang, Phys. Rev. **87**, 410 (1952).
[2] C. Yang, Phys. Rev. **87**, 404 (1952).
[3] K. Huang, *Statistical mechanics* (Wiley, New York, 1987).
[4] M. Biskup, C. Borgs, J. T. Chayes, L. J. Kleinwaks, and R. Kotecký , Phys. Rev. Lett. **84**, 4794 (2000).
[5] D. Ruelle, Phys. Rev. Lett. **26**, 303 (1971).
[6] C. Monthus and T. Garel, J. Stat. Mech.: Theory Exp. **2005**, P12011.
[7] C. Monthus and T. Garel, Eur. Phys. J. B **48**, 393 (2005).
[8] F. Iglói, Y. C. Lin, H. Rieger, and C. Monthus, Phys. Rev. B **76**, 064421 (2007).
[9] C. Monthus and T. Garel, Phys. Rev. E **74**, 011101 (2006).
[10] T. Sarlat, A. Billoire, G. Biroli, and J. P. Bouchaud, J. Stat. Mech.: Theory Exp. **2009**, P08014.
[11] E. J. Gumbel, *Statistics of extremes* (Columbia University Press, New York, 1958).
[12] M. L. Mehta, *Random matrices* (Academic Press, Amsterdam, 2004).
[13] C. A. Tracy and H. Widom, *Distribution Functions for Largest Eigenvalues and Their Applications*, in *Proceedings of the International Congress of Mathematicians*, Vol. I, edited by LI Tatsien (Higher Education Press, Beijing, 2002), pp. 587–596.
[14] C. A. Tracy and H. Widom, Commun. Math. Phys. **177**, 727 (1996).
[15] C. A. Tracy and H. Widom, Commun. Math. Phys. **159**, 151 (1994).
[16] C. A. Tracy and H. Widom, Phys. Lett. B **305**, 115 (1993).
[17] K. Johansson, Commun. Math. Phys. **209**, 437 (2000).
[18] J. Baik and E. M. Rains, J. Stat. Phys. **100**, 523 (2000).
[19] M. Prähofer and H. Spohn, Phys. Rev. Lett. **84**, 4882 (2000).
[20] G. Biroli, J. P. Bouchaud, and M. Potters, J. Stat. Mech.: Theory Exp. **2007**, P07019.
[21] D. Sherrington and S. Kirkpatrick, Phys. Rev. Lett. **35**, 1792 (1975).
[22] G. Parisi, J. Phys. A: Math. Gen. **13**, 1101 (1980).
[23] G. Parisi, Phys. Rev. Lett. **50**, 1946 (1983).
[24] M. Talagrand, Comptes Rendus Mathematique **337**, 111 (2003).
[25] M. Mézard, G. Parisi, and M. A. Virasoro, *Spin Glass Theory and Beyond* (World Scientific, Singapore, 1987).
[26] M. Mézard and A. Montanari, *Information, Physics and Computation* (Oxford University Press, Oxford, 2009).
[27] H. Nishimori, *Statistical Physics of Spin Glasses and Information Processing: An Introduction* (Oxford University Press, Oxford, UK, 2001).

[28]D. J. Thouless, P. W. Anderson, and R. G. Palmer, Philos. Mag. **35**, 593 (1977).
[29]T. Plefka, J. Phys. A: Math. Gen. **15**, 1971 (1982).
[30]A. Georges, M. Mézard, and J. S. Yedidia, Phys. Rev. Lett. **64**, 2937 (1990).
[31]J. S. Yedidia and A. Georges, J. Phys. A: Math. Gen. **23**, 2165 (1990).
[32]T. Yokota, Phys. Rev. B **51**, 962 (1995).
[33]T. Plefka, Phys. Rev. E **73**, 016129 (2006).
[34]H. Ishii and T. Yamamoto, J. Phys. C **18**, 6225 (1985).
[35]L. De Cesare, K. L. Walasek, and K. Walasek, Phys. Rev. B **45**, 8127 (1992).
[36]G. Biroli and L. F. Cugliandolo, Phys. Rev. B **64**, 014206 (2001).
[37]J. S. Yedidia, in *Advanced Mean Field Methods: Theory and Practice* (MIT Press, Cambridge, MA, 2001), pp. 21–36.
[38]E. P. Wigner, The Annals of Mathematics **62**, 548 (1955).
[39]Y. V. Fyodorov, in *Recent Perspectives in Random Matrix Theory and Number Theory*, Vol. 322 (Cambridge Univ. Press, 2005), p. 31.
[40]G. Parisi and T. Rizzo, Phys. Rev. Lett. **101**, 117205 (2008).
[41]G. Parisi and T. Rizzo, Phys. Rev. B **79**, 134205 (2009).
[42]G. Parisi and T. Rizzo, Phys. Rev. B **81**, 094201 (2010).
[43]J. Stäring, B. Mehlig, Y. V. Fyodorov, and J. M. Luck, Phys. Rev. E **67**, 047101 (2003).
[44]P. Shukla, Phys. Rev. E **71**, 026226 (2005).
[45]Z. Bai and W. Zhou, Statistica Sinica **18**, 425 (2008).
[46]K. A. Takeuchi and M. Sano, Phys. Rev. Lett. **104**, 230601 (2010).
[47]J. Rambeau and G. Schehr (unpublished).
[48]A. J. Bray and M. A. Moore, J. Phys. C **12**, L441 (1979).
[49]T. Aspelmeier, A. Billoire, E. Marinari, and M. A. Moore, J. Phys. A: Math. Theor. **41**, 324008 (2008).
[50]A. Soshnikov, Commun. Math. Phys. **207**, 697 (1999).
[51]P. J. Forrester, S. N. Majumdar, and G. Schehr, Nucl. Phys. B **844**, 500 (2011).
[52]G. Biroli, J. P. Bouchaud, and M. Potters, Europhys. Lett. **78**, 10001 (2007).
[53]R. A. Banos, A. Cruz, L. A. Fernandez, J. M. Gil-Narvion, A. Gordillo-Guerrero, M. Guidetti, A. Maiorano, F. Mantovani, E. Marinari, V. Martin-Mayor *et al*., J. Stat. Mech.: Theory Exp. **2010**, P06026.
[54]M. Hasenbusch, A. Pelissetto, and E. Vicari, Phys. Rev. B **78**, 214205 (2008).
[55]R. Alvarez Baños *et al*., Phys. Rev. Lett. **105**, 177202 (2010).
[56]F. Belletti, A. Cruz *et al*., J. Stat. Phys. **135**, 1121 (2009).
[57]P. Contucci, C. Giardinà, C. Giberti, G. Parisi, and C. Vernia, Phys. Rev. Lett. **99**, 057206 (2007).
[58]P. Contucci, C. Giardinà, C. Giberti, G. Parisi, and C. Vernia, Phys. Rev. Lett. **103**, 017201 (2009).
[59]F. Krzakala and O. C. Martin, Phys. Rev. Lett. **85**, 3013 (2000).
[60]E. Marinari, G. Parisi, and J. J. Ruiz-Lorenzo, Phys. Rev. B **58**, 14852 (1998).
[61]M. Campellone, B. Coluzzi, and G. Parisi, Phys. Rev. B **58**, 12081 (1998).
[62]K. Gunnarsson, P. Svedlindh, P. Nordblad, L. Lundgren, H. Aruga, and A. Ito, Phys. Rev. B **43**, 8199 (1991).
[63]A. Billoire, L. A. Fernandez, A. Maiorano, E. Marinari, V. Martin-Mayor, and D. Yllanes, e-print arXiv:1108.1336.

Article 3

Extreme Value Statistics Distributions in Spin Glasses

Michele Castellana,[1,2,*] Aurélien Decelle,[1] and Elia Zarinelli[1]

[1]*LPTMS, CNRS and Université Paris-Sud, UMR8626, Bât. 100, 91405 Orsay, France*

[2]*Dipartimento di Fisica, Università di Roma "La Sapienza", 00185 Rome, Italy*

(Received 6 August 2011; published 27 December 2011)

We study the probability distribution of the pseudocritical temperature in a mean-field and in a short-range spin-glass model: the Sherrington-Kirkpatrick and the Edwards-Anderson (EA) model. In both cases, we put in evidence the underlying connection between the fluctuations of the pseudocritical point and the extreme value statistics of random variables. For the Sherrington-Kirkpatrick model, both with Gaussian and binary couplings, the distribution of the pseudocritical temperature is found to be the Tracy-Widom distribution. For the EA model, the distribution is found to be the Gumbel distribution. Being the EA model representative of uniaxial magnetic materials with quenched disorder like $Fe_{0.5}Mn_{0.5}TiO_3$ or $Eu_{0.5}Ba_{0.5}MnO_3$, its pseudocritical point distribution should be *a priori* experimentally accessible.

DOI: 10.1103/PhysRevLett.107.275701 PACS numbers: 64.70.Q−, 02.10.Yn, 02.50.−r

Disordered uniaxial magnetic materials having a glassy behavior like $Fe_{0.5}Mn_{0.5}TiO_3$ [1] and $Eu_{0.5}Ba_{0.5}MnO_3$ [2] have interested physicists for decades. Since the first pioneering work of Edwards and Anderson (EA) [3], these systems have been studied by means of spin-glass models with quenched disorder, which were later considered in their mean-field version by Sherrington and Kirkpatrick (SK) [4]. In the thermodynamic limit, Parisi's solution for the SK model [5] predicts a phase transition at a finite critical temperature separating a high-temperature paramagnetic phase from a low-temperature glassy phase. Differently, for the EA model there is no analytical solution and the existence of a finite-temperature phase transition relies entirely on numerical simulations [6].

Even though criticality in a physical system can emerge only in the thermodynamic limit [7,8], in laboratory and numerical experiments the system size is always finite: singularities of physical observables are smeared out and replaced by smooth maxima. In order to characterize the critical point of finite-size systems, a suitably defined pseudocritical temperature must be introduced, e.g., the temperature at which such maxima occur. In finite-size systems with quenched disorder, such a pseudocritical temperature is a random variable depending on the realization of the disorder. The characterization of the distribution of the pseudocritical point and of its scaling properties is still an open problem which has drawn the attention of physicists since the very first works of Harris [9–13]. Further studies of such distributions in spin glasses have been performed in a recent work [14], where some of the authors showed a connection between the fluctuations of the pseudocritical temperature of the SK model and the theory of extreme value statistics (EVS) of correlated random variables.

The EVS of independent identically distributed (IID) random variables is a well-established problem: a fundamental result [15] states that the limiting Probability Distribution Function (PDF) of the maximum of IID random variables belongs to three families of distributions: the Gumbel, Fréchet, or Weibull distribution. Much less is known about the EVS of correlated random variables. A noteworthy case of an EVS distribution of correlated random variables that has been recently discovered is the Tracy-Widom (TW) distribution [16], describing the fluctuations of the largest eigenvalue of a Gaussian random matrix. The TW distribution has been found to describe the fluctuations of observables of a broad number of physical and mathematical models, like the longest common sequence in a random permutation [17], directed polymers in disordered media [18], and polynuclear growth models [19], which can be described by the Kardar-Parisi-Zhang equation [20,21]. Recently the TW distribution has been found to describe the conductance fluctuations in two- and three- dimensional Anderson insulators [22,23] and has been measured in growing interfaces of liquid-crystal turbulence [24,25] experiments.

In this Letter we study the distribution of the pseudocritical temperature in the SK and in the EA model by means of numerical simulations. Our numerical findings show that the fluctuations of the pseudocirtical temperature of the SK model both with Gaussian and binary couplings are described by the TW distribution. This result suggests that the features of the fluctuations of the pseudocritical temperature are universal, i. e., stable with respect to the distribution of the disorder. To our knowledge, this is the first time that the ubiquitous TW distribution is shown to play a role in spin glasses. Moreover, our numerical analysis shows that the fluctuations of the pseudocritical point of the EA model are described by the Gumbel distribution. These two results shed light on the role played by EVS in spin glasses.

To pose the problem, let us consider a system of N spins $S_i = \pm 1$ located at the vertices of a graph, interacting via the Hamiltonian $H[\vec{S}] = -\sum_{(i,j)} J_{ij} S_i S_j$, where the sum runs over the interacting spin pairs (i, j). For the SK model

with Gaussian couplings (GSK) and for the SK model with binary couplings (BSK) the interacting spin pairs are all the distinct pairs. The couplings J_{ij} are IID Gaussian random variables with zero mean and variance $1/N$ for the GSK model [4], and are equal to $\pm 1/\sqrt{N}$ with equal probability for the BSK model [26]. For the EA model the interacting spin pairs are the nearest-neighbor pairs on a three-dimensional cubic lattice with periodic boundary conditions, and J_{ij} are IID random variables equal to ± 1 with equal probability [3]. For the BSK and EA model, the binary structure of the couplings allowed for the use of an efficient asynchronous multispin-coding simulation technique [6], yielding an extensive number of disorder samples and system sizes.

Let us now define the physical observables used to carry on the numerical analysis of the problem. Given two real spin replicas $\vec{S}^1$, $\vec{S}^2$, their mutual overlap $q \equiv \frac{1}{N}\sum_{i=1}^{N} S_i^1 S_i^2$ is a physical quantity characterizing the spin-glass transition in the thermodynamic limit [5,6]: $\overline{\langle q^2\rangle_{\mathcal{J}}(\beta)} = 0$ if $\beta < \beta_c$, $\overline{\langle q^2\rangle_{\mathcal{J}}(\beta)} > 0$ if $\beta > \beta_c$, where $\langle\cdots\rangle_{\mathcal{J}}$ denotes the thermal average performed with the Boltzmann weight defined by the Hamiltonian $H[\vec{S}]$, $\beta \equiv 1/T$ is the inverse temperature, and $\overline{\cdots}$ stands for the average over quenched disorder $\mathcal{J} \equiv \{J_{ij}\}_{ij}$. The finite-size inverse pseudocritical temperature $\beta_{c\,\mathcal{J}}$ of a sample with a realization $\mathcal{J}$ of the disorder can be defined as the value of β at which $\langle q^2\rangle_{\mathcal{J}}(\beta)$ *significantly differs from zero*, i. e., becomes critical. This qualitative definition is made quantitative by setting

$$\langle q^2\rangle_{\mathcal{J}}(\beta_{c\,\mathcal{J}}) = \overline{\langle q^2\rangle_{\mathcal{J}}(\beta_c^N)}. \tag{1}$$

Both for the GSK and BSK model, β_c^N is chosen to be the average critical temperature at size N, which is defined as the temperature at which the Binder ratio $B \equiv 1/2(3 - \overline{\langle q^4\rangle_{\mathcal{J}}}/\overline{\langle q^2\rangle_{\mathcal{J}}}^2)$ of a system of size N equals the Binder ratio of a system of size $2N$. For the EA model we simply take β_c^N to be equal to the infinite-size critical temperature $\beta_c = 0.855$ [27], because in this case the Binder ratios cross at a temperature which is very close to the infinite-size critical temperature β_c. The definition (1) and β_c^N are qualitatively depicted in Fig. 1. The distribution of $\beta_{c\,\mathcal{J}}$ can be characterized by its mean $\overline{\beta_{c\,\mathcal{J}}}$, its variance $\sigma_{\beta N}^2 \equiv \overline{\beta_{c\,\mathcal{J}}^2} - \overline{\beta_{c\,\mathcal{J}}}^2$, and by the PDF $p_N(x_{\mathcal{J}})$ of the natural scaling variable $x_{\mathcal{J}} \equiv (\beta_{c\,\mathcal{J}} - \overline{\beta_{c\,\mathcal{J}}})/\sigma_{\beta N}$. We can expect that, to leading order in N, $\sigma_{\beta N} \sim N^{-\phi}$, and that for large N, $p_N(x_{\mathcal{J}})$ converges to a nontrivial limiting PDF $p_\infty(x_{\mathcal{J}})$.

Sherrington-Kirkpatrick model.—Let us start discussing the distribution of $\beta_{c\,\mathcal{J}}$ for the GSK and BSK model. Monte Carlo (MC) simulations have been performed with parallel tempering for system sizes $N = 32, 64, 128, 256$ (GSK) and $N = 16, 32, 64, 128, 256, 512, 1024, 2048, 4096$ (BSK), allowing for a numerical computation of $\langle q^2\rangle_{\mathcal{J}}$ and so of $\beta_{c\,\mathcal{J}}$ for several samples $\mathcal{J}$. The data shows that as the system size N is increased, $\overline{\beta_{c\,\mathcal{J}}}$ approaches β_c. Setting $T_{c\,\mathcal{J}} \equiv 1/\beta_{c\,\mathcal{J}}$, $\sigma_{T\,N}^2 \equiv \overline{T_{c\,\mathcal{J}}^2} - \overline{T_{c\,\mathcal{J}}}^2 \sim N^{-\phi}$, the power law fit of $\sigma_{T\,N}$ shown in Fig. 2 gives the value of the scaling exponent $\phi = 0.31 \pm 0.07$ (GSK) and $\phi = 0.34 \pm 0.05$ (BSK). These values of ϕ are both consistent with the value $\phi = 1/3$ one would expect from scaling arguments by considering the variable $y \equiv N^{1/3}(T - T_c)$ [28].

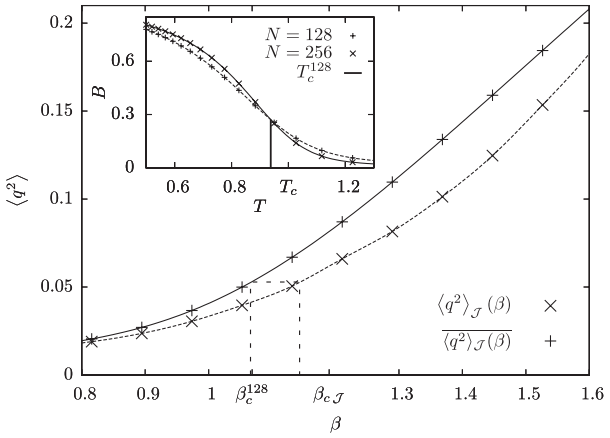

FIG. 1. Square value of the overlap $\langle q^2\rangle_{\mathcal{J}}$ for a sample $\mathcal{J}$ (dashed curve) for the binary Sherrington-Kirkpatrick model with $N = 128$, its average $\overline{\langle q^2\rangle_{\mathcal{J}}}$ over the samples $\mathcal{J}$ (solid curve) as a function of the inverse-temperature β, and critical temperatures β_c^N and $\beta_{c\,\mathcal{J}}$. The dashed vertical lines depict the definition (1) of $\beta_{c\,\mathcal{J}}$. Inset: Binder parameter B as a function of the temperature T for $N = 128$, 256, and average pseudocritical temperature T_c^{128}, with $T_c^N \equiv 1/\beta_c^N$.

The PDF p_N of the rescaled variable $x_{\mathcal{J}}$ is depicted in Fig. 2. The curves $p_N(x_{\mathcal{J}})$ collapse quite satisfyingly indicating that we are close to the asymptotic regime $N \to \infty$. Even though one could naively expect the fluctuations of the pseudocritical point to be Gaussian, Fig. 2 shows that this is not the case.

To understand this fact, let us recall the analysis proposed in a recent work [14] by some of the authors. In order to study the sample-to-sample fluctuations of the pseudocritical temperature one uses the Thouless-Anderson-Palmer approach for the SK model. In the TAP approach a free energy function of the local magnetization is built up for any sample $\mathcal{J}$ of the disorder, and its Hessian matrix H_{ij} calculated at the paramagnetic minimum is a random matrix in the Gaussian orthogonal ensemble. In the thermodynamic limit, the spectrum of H_{ij} is described by the Wigner semicircle, centered in $1 + \beta^2$ and with radius 2β. The critical temperature $\beta_c = 1$ of the SK model is identified as the value of β such that the minimal eigenvalue of H_{ij} vanishes. In [14] the fluctuations of the pseudocritical temperature are investigated in terms of the fluctuations of the minimal eigenvalue of H_{ij}. One introduces a definition of pseudocritical temperature $\hat{\beta}_{c\,\mathcal{J}}$, which is different from that considered in the present work. The finite-size fluctuations of $\hat{\beta}_{c\,\mathcal{J}}$ are found to be described by the relation

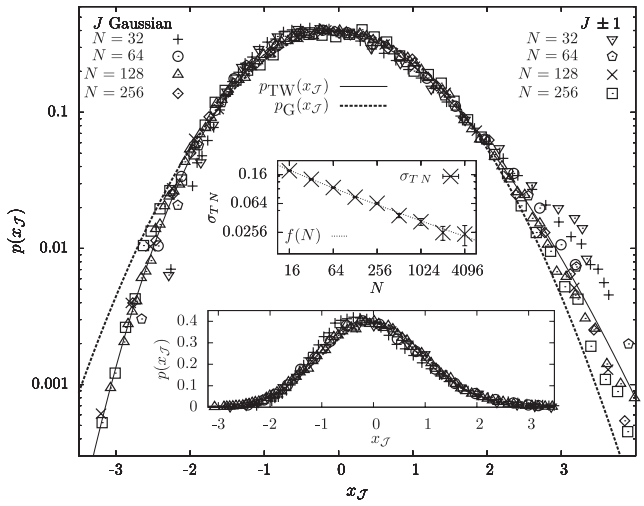

FIG. 2. Distribution of the pseudocritical point both for the Sherrington-Kirkpatrick (SK) model with Gaussian couplings (GSK) and for the SK model with binary couplings (BSK). PDF $p_N(x_{\mathcal{J}})$ of the rescaled critical temperature $x_{\mathcal{J}}$ for system sizes $N = 32$, 64, 128, 256 with $1.6 \times 10^4 \leq S \leq 4.7 \times 10^4$ (GSK) and $2.9 \times 10^4 \leq S \leq 9.8 \times 10^4$ (BSK) disorder samples, Tracy-Widom distribution $p_{\rm TW}(x_{\mathcal{J}})$ (solid curve) and Gaussian distribution $p_G(x_{\mathcal{J}})$ (dashed curve), both with zero mean and unit variance. The plot has no adjustable parameters, and is in logarithmic scale to highlight the behavior of the distributions on the tails. Top inset: width $\sigma_{T\,N}$ for the BSK as a function of N and fitting function $f(N) = aN^{-\phi} + bN^{-2\phi}$, yielding $\phi = 0.34 \pm 0.05$. Bottom inset: same plot as in the main plot in linear scale.

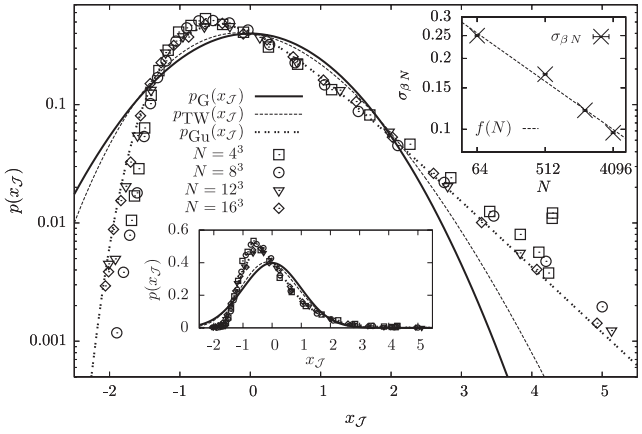

FIG. 3. Distribution of the pseudocritical point for the Edwards-Anderson model. PDF $p_N(x_{\mathcal{J}})$ of the rescaled critical temperature $x_{\mathcal{J}}$ for systems sizes $N = 4^3$, 8^3, 12^3, 16^3 with $2.4 \times 10^4 \leq S \leq 3.2 \times 10^4$ disorder samples, Gaussian distribution $p_G(x_{\mathcal{J}})$ (solid curve), Tracy-Widom distribution $p_{\rm TW}(x_{\mathcal{J}})$ (dashed curve), and Gumbel distribution $p_{\rm Gu}(x_{\mathcal{J}})$ (dotted curve), all with zero mean and unit variance. The plot has no adjustable parameters, and is in logarithmic scale to highlight the behavior of the distributions on the tails. Top inset: width $\sigma_{\beta\,N}$ as a function of N, and fitting function $f(N) = aN^{-\phi}$, with scaling exponent $\phi = 0.23 \pm 0.03$. Bottom inset: same plot as in the main plot in linear scale.

$\hat{\beta}_{c\,\mathcal{J}} = \beta_c - \chi_{\mathcal{J}}/(2N^{2/3})$, where $\chi_{\mathcal{J}}$ is distributed according to the TW distribution in the high-temperature region $\hat{\beta}_{c\,\mathcal{J}} < 1$. According to Fig. 2, MC simulations confirm this analysis: the limiting distribution of $p_N(x_{\mathcal{J}})$ is described with good accuracy by the TW distribution in the high-temperature regime $\beta_{c\,\mathcal{J}} < 1$ ($x_{\mathcal{J}} < 0$). The TW distribution is robust with respect to the choice of the disorder distribution and to the definition of pseudocritical temperature. On the other hand, since the exponent ϕ obtained from MC simulations is not compatible with the exponent $2/3$ of $\hat{\beta}_{c\,\mathcal{J}}$, we conclude that the scaling exponent is definition dependent [14,29].

Edwards-Anderson model.—The same analysis has been performed for the three-dimensional EA model. Physical observables have been computed with parallel tempering for system sizes $N = L^3$ with $L = 4, 8, 12, 16$. Similarly to the SK model, the width $\sigma_{\beta\,N}$ of the distribution of the pseudocritical point $\beta_{c\,\mathcal{J}}$ shrinks to zero as the system size N is increased: a power law fit $\sigma_{\beta\,N} = aN^{-\phi}$ gives the value of the scaling exponent $\phi = 0.23 \pm 0.03$ (inset of Fig. 3). The PDFs $p_N(x_{\mathcal{J}})$ of the rescaled critical temperature seem to have a finite limit as N is increased, as depicted in Fig. 3, and this limit coincides with the Gumbel distribution. Both ϕ and the PDF have the following interesting features. As far as the exponent ϕ is concerned, we recall [10] that for systems known to be governed by a random fixed point like the EA model, it was predicted that the scaling exponent satisfies $1/\phi = d\nu$, where d is the dimensionality of the system. The value of the critical exponent $\nu = 1.8 \pm 0.2$ for the EA model is known from numerical simulations [6], yielding a value of $\phi = 0.19 \pm 0.02$ which is compatible with that measured from the fluctuations of the critical temperature. As far as the limiting distribution $p_\infty(x_{\mathcal{J}})$ is concerned, we recall that [30] a disordered system like the EA behaves as an ensemble of independent subsystems $\mathcal{S}_1, \ldots, \mathcal{S}_M$, where each subsystem $\mathcal{S}_i$ has a random local critical temperature β_c^i, the local critical temperatures $\{\beta_c^i\}_i$ being IID random variables depending on the *local* realization of the disorder. We can argue that, for a single realization of the disorder $\mathcal{J}$, the pseudocritical temperature $\beta_{c\,\mathcal{J}}$ results from the fact that β has to be taken large enough to bring all of the subsystems $\{\mathcal{S}_i\}_i$ to criticality. Thus, $\beta_{c\,\mathcal{J}}$ is the maximum over the ensemble of the local critical temperatures $\beta_{c\,\mathcal{J}} = \max_i \beta_c^i$. If this picture is correct, $\beta_{c\,\mathcal{J}}$ is distributed according to one of the EVS limiting distributions of independent variables [15]: the Gumbel, Fréchet, or Weibull distribution. Assuming that the distribution of β_c^i decays exponentially for large β_c^i, the distribution of $\beta_{c\,\mathcal{J}}$ is the Gumbel one. We want to stress that this argument would not hold for the SK model, where there is no geometric structure.

Conclusions.—In this Letter, we have performed a numerical analysis of the distribution of the pseudocrtical

temperature in two mean-field spin glasses, the Sherrington-Kirkpatrick model with Gaussian couplings and with binary couplings, and in a short-range spin glass, the Edwards-Anderson model. The analysis for the Sherrington-Kirkpatrick models shows that the distribution of the pseudocritical temperature in the high-temperature phase is described with good accuracy by the Tracy-Widom distribution, as suggested by an analytical prediction previously published by some of the authors [14]. To our knowledge, this is the first time that the Tracy-Widom distribution is shown to play a role in spin glasses. The fact that both the Sherrington-Kirkpatrick model with Gaussian couplings and the Sherrington-Kirkpatrick model with binary couplings yield the Tracy-Widom distribution suggests that the Tracy-Widom distribution is universal with respect to the bonds' distribution.

The analysis pursued for the three-dimensional Edwards-Anderson model shows that the liming distribution of the pseudocritical temperature is the Gumbel distribution. An argument to understand this result has been proposed. These two numerical analyses put in evidence a connection between the critical regime of spin-glass models and the extreme value statistics theory which has never been proposed heretofore.

The present Letter opens several perspectives. As far as the Sherrington-Kirkpatrick model is concerned, we recall that the Tracy-Widom distribution describes typical fluctuations of the maximal eigenvalue of a Gaussian orthogonal ensemble random matrix, while the large deviations regime of these fluctuations has been studied only recently [31]. It would be interesting to study numerically the large deviations regime of the fluctuations of the critical temperature, where the distribution of the pseudocritical point could be described by the large deviations function derived in [31]. It would be also interesting to consider the case where the couplings J_{ij} are Gaussian with a positive bias J_0 [32]. Depending on the value of J_0, the Sherrington-Kirkpatrick model has a phase transition from a paramagnetic to a spin-glass phase or from a ferromagnetic to a mixed phase [32]: it would be interesting to investigate, both analytically and numerically, the fluctuations of these pseudocritical points. Moreover, in order to bridge the gap between a mean-field and a short-range interactions regime, it could be interesting to investigate the fluctuations of the pseudocritical temeperature in spin-glass models with tunable long-range interactions, like those introduced in [33]. As far as the Edwards-Anderson model is concerned, it would be interesting to test experimentally the scenario found here in $Fe_{0.5}Mn_{0.5}TiO_3$ [1] or $Eu_{0.5}Ba_{0.5}MnO_3$ [2] spin-glass materials. Indeed, ac-susceptibility measurements in these systems show [1] that the spin-glass critical temperature can be identified as the temperature where the susceptibility has a cusp. Accordingly, the pseudocritical point could be identified and measured, and one could test whether the resulting rescaled pseudocritical point distribution converges to the Gumbel distribution as the system size is increased.

We are glad to thank G. Parisi, A. Rosso and P. Vivo for interesting discussions and suggestions. We also acknowledge support from the D. I. computational center of University Paris Sud and from the LPTMS cluster.

*michele.castellana@lptms.u-psud.fr

[1] K. Gunnarsson *et al.*, Phys. Rev. B **43**, 8199 (1991).
[2] S. Nair and A. K. Nigam, Phys. Rev. B **75**, 214415 (2007).
[3] S. F. Edwards and P. W. Anderson, J. Phys. F **5**, 965 (1975).
[4] D. Sherrington and S. Kirkpatrick, Phys. Rev. Lett. **35**, 1792 (1975).
[5] M. Mézard, G. Parisi, and M. A. Virasoro, *Spin glass theory and beyond* (World Scientific, Singapore, 1987).
[6] M. Palassini and S. Caracciolo, Phys. Rev. Lett. **82**, 5128 (1999).
[7] T. D. Lee and C. N. Yang, Phys. Rev. **87**, 410 (1952).
[8] C. Yang, Phys. Rev. **87**, 404 (1952).
[9] A. Harris, J. Phys. C **7**, 1671 (1974).
[10] A. Aharony and A. B. Harris, Phys. Rev. Lett. **77**, 3700 (1996).
[11] S. Wiseman and E. Domany, Phys. Rev. Lett. **81**, 22 (1998).
[12] K. Bernardet, F. Pázmándi, and G. G. Batrouni, Phys. Rev. Lett. **84**, 4477 (2000).
[13] F. Iglói *et al.*, Phys. Rev. B **76**, 064421 (2007).
[14] M. Castellana and E. Zarinelli, Phys. Rev. B **84**, 144417 (2011).
[15] J. Galambos, *The asymptotic Theory of Extreme Order Statistics* (R. E. Krieger Publishing Co., Malabar, Florida, 1987).
[16] C. A. Tracy and H. Widom, in *Proc. International Congress of Mathematicians (Beijing, 2002)* (Higher Education Press, Beijing, 2002), Vol. 1.
[17] J. Baik, P. Deift, and K. Johansson, J. Am. Math. Soc. **12**, 1119 (1999).
[18] K. Johansson, Commun. Math. Phys. **209**, 437 (2000).
[19] M. Prähofer and H. Spohn, Phys. Rev. Lett. **84**, 4882 (2000).
[20] M. Kardar, G. Parisi, and Y. C. Zhang, Phys. Rev. Lett. **56**, 889 (1986).
[21] P. Calabrese and P. Le Doussal, Phys. Rev. Lett. **106**, 250603 (2011).
[22] A. M. Somoza, M. Ortuño, and J. Prior, Phys. Rev. Lett. **99**, 116602 (2007).
[23] C. Monthus and T. Garel, Phys. Rev. B **79**, 205120 (2009).
[24] K. A. Takeuchi and M. Sano, Phys. Rev. Lett. **104**, 230601 (2010).
[25] K. A. Takeuchi *et al.*, Sci. Rep. **1** (2011) 34.
[26] B. Coluzzi *et al.*, J. Phys. A **33**, 3851 (2000).
[27] T. Nakamura *et al.*, J. Phys. A **36**, 10895 (2003).

[28] G. Parisi *et al.*, J. Phys. A **26**, 247 (1993).
[29] A. Billoire *et al.*, J. Stat. Mech. (2011) P10019.
[30] T. Vojta, J. Phys. A **39**, R143 (2006).
[31] D. S. Dean and S. N. Majumdar, Phys. Rev. Lett. **97**, 160201 (2006).
[32] H. Nishimori, *Statistical Physics of Spin Glasses and Information Processing: An Introduction* (Oxford University Press, Oxford, UK, 2001).
[33] G. Kotliar, P. W. Anderson, and D. L. Stein, Phys. Rev. B **27**, 602 (1983).

Article 4

RECONSTRUCTION OF FINANCIAL NETWORKS FOR ROBUST ESTIMATION OF SYSTEMIC RISK

IACOPO MASTROMATTEO, ELIA ZARINELLI, AND MATTEO MARSILI

ABSTRACT. In this paper we estimate the propagation of liquidity shocks through interbank markets when the information about the underlying credit network is incomplete. We show that techniques such as Maximum Entropy currently used to reconstruct credit networks severely underestimate the risk of contagion by assuming a trivial (fully connected) topology, a type of network structure which can be very different from the one empirically observed. We propose an efficient message-passing algorithm to explore the space of possible network structures, and show that a correct estimation of the network degree of connectedness leads to more reliable estimations for systemic risk. Such algorithm is also able to produce maximally fragile structures, providing a practical upper bound for the risk of contagion when the actual network structure is unknown. We test our algorithm on ensembles of synthetic data encoding some features of real financial networks (sparsity and heterogeneity), finding that more accurate estimations of risk can be achieved. Finally we find that this algorithm can be used to control the amount of information regulators need to require from banks in order to sufficiently constrain the reconstruction of financial networks.

1. INTRODUCTION

The estimation of the robustness of a financial network to shocks and crashes is a topic of central importance to assess the stability of an economic system. Recent dramatic events evidenced the fragility of many economies, supporting the claim that "the worlds financial system can collapse like a row of dominoes" [1]. As a result, governments and international organizations became increasingly concerned about systemic risk. The banking system is thought to be a fundamental channel in the propagation of shocks to the entire economy: the economic distress of an insolvent bank can be transmitted to its creditors by interbank linkages, thus a shock can easily propagate to the whole network. Unfortunately detailed data on banks bilateral exposures is not always available, and institutions are often left with the problem of assessing the resilience of a system to financial shocks by exploiting an incomplete information set. In this framework the reconstruction of bilateral exposures becomes a central issue for the estimation of risk, and requires the application of sophisticated inference schemes to obtain reliable estimations. Among several methods, a commonly used tool for this task is the so called *entropy maximization method* [2, 3, 4, 5]. The main limitation of this procedure is that it assumes a market structure which can

The authors wish to thank F. Caccioli, F. Krzakala, Y. Sun, L. Zdeborova for very useful discussions. I.M. acknowledges support from GDRE 224 GREFI-MEFI CNRS-INdAM.

be quite different from the actual one: it tends to spread the debt as evenly as possible, without assuming any heterogeneity in the structure for the network [6]. Unfortunately these assumptions lead to an undervaluation of the extent of contagion, as the measure of the vulnerability to financial contagion depends crucially on the pattern of interbank linkages. Stress-tests used to quantitatively analyze this dependence confirm this results both for simulated and real data, as shown in figures 2, 3 and in reference [6].
In this paper we will introduce a message-passing algorithm to overcome this limitation, and to sample efficiently the space of possible structures for the network. This method can be used to propose plausible candidates for the real network structure, and to produce worst case scenarios for the spread of financial contagion. We remark that despite the huge number of possible network structures ($\sim 2^{N^2)}$) we are able to sample configuration from this space in a time which scales quadratically in the number of unknown entries of the liability matrix.

In section 2 we introduce the main concepts and define the problem of network reconstruction, while in 3 we present the Maximum Entropy (ME) algorithm, a commonly used procedure to infer credit networks from incomplete datasets. In section 4 we show the idea which allows our algorithm to explore the space of network structures and extend the validity of ME. Section 5 describes the stress-test which we employ to analyze the robustness of financial networks, and in section 6 we apply all these ideas to synthetic datasets. In section 7 we discuss the reliability of the reconstruction algorithm as a function of the policy adopted by regulatory institutions. Finally in section 8 we draw our last conclusions.

2. Framework

Let us consider an ensemble $\mathcal{B} = \{b_0, \dots, b_{N-1}\}$ of N banks, in which each bank in $\mathcal{B}$ may borrow to or lend money from other banks in $\mathcal{B}$. This structure is encoded in the so-called liability matrix L, an $N \times N$ non-symmetric matrix describing the instantaneous state of a credit network. Each element L_{ij} denotes the funds that bank $j \in \mathcal{B}$ borrowed from bank $i \in \mathcal{B}$ (regardless of the maturity of the debt). We fix the convention that $L_{ij} \geq 0$ $\forall (i,j) \in \mathcal{B}\times\mathcal{B}$, $L_{ii} = 0\ \forall i \in \mathcal{B}$. With this definition, the expression $L_i^{\rightarrow} = \sum_j L_{ij}$ represents the total credit which the institution i possesses against the system, while $L_j^{\leftarrow} = \sum_i L_{ij}$ represents the total debt owed by the institution j to the environment.[1] This matrix contains information about the instantaneous state of a credit network, and it is sufficient to estimate the risk of contagion in many cases of practical relevance. Indeed one is often unable to obtain from empirical data the complete expression for the matrix L. Data are typically extracted by a bank balance sheets or by institutional databases [7], and partial informations have to be coherently integrated into a list of plausible liability matrices. In the following discussion, we will suppose that three different types of informations about L are available, as typically reported in the literature [8]:

[1] Without loss of generality we consider a closed economy ($\sum_i L_i^{\rightarrow} = \sum_j L_j^{\leftarrow}$), by using bank b_0 as a placeholder to take into account flows of money external to the system.

(1) All the debts larger than a certain threshold θ are known. This allows us to rescale all the elements of L by θ, so that we consider without loss of generality liability matrices for which all the unknown elements are bound to be in the interval [0,1]. We assume to have at most order N elements exceeding such threshold.
(2) We assume a certain set of entries (which we take to be of order N) to be known. This corresponds to banks or bank sectors for which some particular position needs to be disclosed by law.
(3) The total credit $L_i^{\rightarrow}$ and the total debit $L_j^{\leftarrow}$ of each bank are known. Acceptable candidates for liability matrices need to satisfy a set of $2N$ linear constraints, whose rank is in general $\mathcal{R} \leq 2N - 1$.

We remark that we have defined a set of constraints of order N elements, which is too small to single out a unique candidate for the true unknown liability matrix. The possible solutions compatible with the observations define a space Λ, whose members we denote with $\hat{L}$. Let U be the set of not directly known (i.e. non-fixed by to constraints of type (1) and (2)) entries of the liabilities matrix. Then those entries of the liability matrix (whose number is $M = |U|$) are real numbers subject to domain constraints (they must be in $[0, 1]$) and linear algebraic constraints (the sum on the rows and on the columns must be respected). The ratio $M/\mathcal{R} \geq 1$ controls the degree of underdetermination of the network, and is typically much larger than one.

3. Dense reconstruction

A possible procedure to study the robustness of a financial network when the complete information about the liability matrix is not uniquely specified, is to pick from the set of candidate matrices Λ a representative matrix, and to test the stability uniquely for the network specified by such $\hat{L}$. In this case a criteria has to be chosen to select a particular matrix out of the Λ space, by doing some assumptions about the structure of the true L_{ij}. A choice which is commonly adopted [2, 3, 4, 5] is based on the maximum entropy criteria, which assumes that banks spread their lending as evenly as possible. The problem becomes in this case to finding a vector $\vec{L} = \{L_\alpha\}_{\alpha \in U}$ (the unknown entries of the liability matrix) whose entries respect the algebraic and domain constraints and minimize the distance with the uniform vector $\vec{Q} = \{Q_\alpha\}_{\alpha \in \mathcal{U}}$ (such that $\forall \alpha \quad Q_\alpha = 1$), where the distance is quantified by the Kullback-Leibler divergence:

$$D_{KL}(\vec{L}, \vec{Q}) = \sum_\alpha L_\alpha \log \frac{L_\alpha}{Q_\alpha}$$

The minimization of such function is a standard convex optimization problem, that can be solved efficiently in polynomial time. In financial literature this algorithm is known with the name of Maximal Entropy (ME) reconstruction. We remark that by using this

algorithm no entry is exactly put to zero unless it is forced by the algebraic constraints.[2]

4. Sparse reconstruction

ME might not be a particularly good description of reality since the number of counterparties of a bank is expected to be limited and much smaller than N, while ME tends to produce completely connected structures. In the case of real networks the degree of market concentration can be higher than suggested by ME. This systematically leads to an underestimation of risk, as a structure in which the debt is distributed homogeneously among the nodes is generally known to be able to absorb shocks more effectively than a system in which few nodes dominate the network [6]. In order to be closer to reality and to estimate more accurately the risk contagion it is than necessary to reconstruct liability matrices whose degree of sparsity can be tuned, and eventually taken to be as big as possible. We present in this section an algorithm which, given the fraction λ of entries which are expected to be exactly zero, is able to reconstruct a sample of network structures compatible with this requirement, and to find a λ_{max} which bounds the maximum possible sparsity. The issues that we want to solve are: (i) is it possible to fix a fraction λ of the unknown entires to zero without violating the domain and the algebraic constraints? (ii) For a given fraction λ, how many possible reconstructed liability matrices do exist? The algorithm solves this problems by sampling, for each given λ, the space of all possible supports for the reconstructed liability matrix such that the constraints are not violated, and by evaluating the volume of such support space. As one can easily expect, there will be a range of $[\lambda_{min}, \lambda_{max}]$ of fractions of fixed zeros compatible with the constraints: trivially $\lambda_{min} = 0$ corresponds to the dense network, which always admits a compatible solution, but we are able to find a non-trivial λ_{max} which corresponds to the maximally sparse network of banks. A plot of the logarithm of the number of possible supports as a function of λ is given in figure 1 ($\times$ signs) for a network as the ones described in section 6. Once a support is given, the liability matrix elements can easily be reconstructed via ME.

We briefly sketch here the idea behind the algorithm, relegating to the appendix the more technical parts. Suppose that a liability matrix with unknown entires is given, together with of the vectors of total credit ($L_i^{\rightarrow}$) and the one of total liabilities ($L_i^{\leftarrow}$). Then without loss of generality one can assume the known entries to be equal to zero, as the values of the known entries always can be absorbed into a rescaled value of the $L_i^{\rightarrow}$ and $L_i^{\leftarrow}$, and restrict the problem just to the unknown entries of the matrix. Under this assumption we can define the network $\mathcal{G}$ which is the support of the unknown entries of the liability matrix. Each node of $\mathcal{G}$ is a bank and the directed edges are the elements of U. For each node i of

[2] This algorithm is not the only possible choice to extract a representative matrix out from the set Λ. Indeed existing algorithms share with the ME the property of returning solutions located in the *interior* of Λ. On the other hand, when choosing a point at random in a compact set in very high dimension d, it is very likely that the point will be very close to the boundary (i.e. at a distance of order $1/d$). Hence, it is reasonable to expect that typical feasible liability matrices are located on or close the boundaries of Λ.

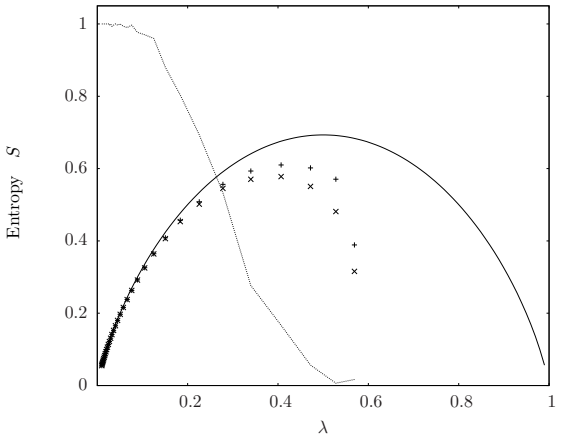

FIGURE 1. Entropy S of the space of compatible configurations $a_{i,j}$ at fixed magnetization $\hat{\lambda}$ with the energy $\mathcal{H}(a_{i,j})$ (+ sign) and true energy $\mathcal{H}_0(a_{i,j})$ ($\times$ sign) for the examples discussed in the text. S is defined as the logarithm of the number of configurations $\{a_{i,j}\}$ with $\mathcal{H} = 0$ (or $\mathcal{H}_0$), divided by the number M of possibly non-zero entries $a_{i,j}$. The solid line plotted for comparison is the entropy of a system of independent links $a_{i,j}$ with the same density (i.e. number of non-zero links). The probability for a solution of $\mathcal{H}_0(a_{i,j})$ to be also a solution of $\mathcal{H}(a_{i,j})$ is also plotted on the same graph (dashed line).

$\mathcal{G}$ the sum of the incoming entries $L_i^{\rightarrow} = \sum_j L_{ij}$ and of the outgoing entries $L_j^{\leftarrow} = \sum_i L_{ij}$ is known. Let $k_i^{\leftarrow}$ ($k_i^{\rightarrow}$) be the number of incoming (outgoing) links in the subset of edges where $L_{i,j} > 0$. Since $L_{i,j} \leq 1$, the number $k_i^{\leftarrow}$ ($k_i^{\rightarrow}$) of incoming (outgoing) links is at least the integer part of $L_i^{\leftarrow}$ ($L_i^{\leftarrow}$) plus one. Therefore, one can define a cost function[3]

$$\mathcal{H}\{a_{i,j}\} = \sum_i \left[\theta\left(L_i^{\rightarrow} - k_i^{\rightarrow}\right) + \theta\left(L_i^{\leftarrow} - k_i^{\leftarrow}\right)\right] \tag{1}$$

over the dynamical variables $a_{i,j} = 0, 1$ which identify the subset of edges, with

$$k_i^{\rightarrow} = \sum_j a_{i,j}, \qquad k_i^{\leftarrow} = \sum_j a_{j,i}.$$

All sub-graphs $a_{i,j}$ with $\mathcal{H} = 0$ are feasible candidates for the support of solutions $L_{i,j} > 0$ to the problem. In general, the constraints are $2N$ linear equations and, as long as the number on non-zero elements $L_{i,j}$ is larger than $2N$ solutions exist, but it is not granted that they have $L_{i,j} \in [0, 1]$ for al i, j. In other words, all the compatible solutions have to satisfy the constraint $\mathcal{H} = 0$, but the converse is not true (as shown in figure 1), because some support $a_{i,j}$ may not admit a solution with $L_{i,j} \in [0, 1]$ for al i, j. We distinguish

[3]Here $\theta(x) = 0$ for $x < 0$ and $\theta(x) = 1$ otherwise is the Heaviside step function.

these two cases by formally introducing a different cost function $\mathcal{H}_0\{a_{i,j}\}$ which vanishes only on the supports $a_{i,j}$ for which an admissible solution ofr $L_{i,j}$ exists. This cost function involves constraints that the approximate $\mathcal{H}$ is not able to capture.
Message passing algorithms can be derived along the lines of Refs. [9, 10] to solve efficiently the problem of sampling the space of solutions of (1) as described in detail in appendix. An additional variable (analogous to a chemical potential in physics) can be introduced in order to select denser or sparser sub-graphs (i.e. tuning the λ parameter). In particular, this allows one to find the maximally sparse subgraph compatible with the constraints.

5. Furfine stress-test

The aim of this section is to show that some measures of vulnerability of a banking system to financial contagion, also known with the name of stress-tests, are sensitive to the way in which the liability matrix is reconstructed. In particular the dense ME reconstruction typically underestimates the risk of contagion, while more realistic results are found if one employs a sparsification parameter λ controlling the density of links in a financial system.

A widely used measure of vulnerability in financial literature is the stress-test introduced by Furfine [11], which is a sequential algorithm to simulate contagion. Suppose that the liability matrix L is given and let us define C_z the initial capital of a bank z in the system $\mathcal{B}$. The idea of the algorithm is simple: suppose that a bank z of the ensemble $\mathcal{B}$ fails due to exogenous reasons. Then it is assumed that any bank $i \in \mathcal{B}$ loses a quantity of money equal to its exposure versus z (L_{iz}) multiplied by an exogenously given parameter $\alpha \in [0, 1]$ for loss-given-default. Than if the loss of the bank i exceeds its capital C_i, bank i fails. This procedure is then iterated until no more banks fail, and the total number of defaults is recorded.
The procedure described above can be formally rephrased in the following steps:

Step 0: A bank $z \in B$ fails for external reasons. Let us define $D_0 = \{z\}$, $S_0 = \mathcal{B}\backslash\{z\}$. For the banks $i \in S_0$ we set $C_i^0 = C_i$.

Step t: The capital C_i^{t-1} at step $t-1$ of banks $i \in S_{t-1}$ is updated according to

$$C_i^t = C_i^{t-1} - \alpha \sum_{j \in D^{t-1}} L_{ij}$$

with $\alpha \in [0, 1]$. A bank $i \in S_{t-1}$ fails at time t if $C_i^t < 0$. Let us define D_t, the ensemble of all the banks $i \in S_{t-1}$ that failed at time t and $S_t = S_{t-1}\backslash D_t$ the ensemble of banks survived at step t.

Step t_{stop}: The algorithm stops at time t_{stop} such that $D_{t_{stop}} = \varnothing$.

We remark that the capital C_i of each bank is exogenously given, and in principle it is not linked to the liability matrix L. The same holds for α, so that the result of a stress-test is understood as a curve quantifying the number of defaults as a function of the α parameter. Finally, the results of the stress-test depend on the first bank $z \in \mathcal{B}$ which defaults. Then one may choose either to consider the results of the stress-test dependent on the z which has been chosen or to average the outcome on all the banks in the system $\mathcal{B}$; we adopt this second type of measure, and consider the default of all the banks to be equally likely.

6. Application to synthetic data

In this section we will show how our algorithm of reconstruction of the liability matrix L_{ij} (presented in section 4) gives more realistic stress-test results if compared with ME reconstruction algorithm (presented in section 3).
We choose to present the results obtained for specific ensembles of artificial matrices, whose structure should capture the relevant features of real credit networks[4]. The first case that we analyze is the simplest possible network with a non-trivial topology, namely the one in which every entrance of the liability matrix L_{ij} with $i \neq j$ is set to zero with probability λ_{tr}, and otherwise is a random number uniformly chosen in $[0, 1]$. We set the banks initial capital C_i to random numbers uniformly chosen in $[C_{min}, C_{max}]$. We impose the threshold $\theta = 1$, which means that all the entrance of the liability matrix are unknown (a worst-case scenario). We than reconstruct the liability matrix via ME algorithm and via our algorithm trying to fix the fraction λ of zeroes equal to λ_{tr}. Then we stress-test via the Furfine algorithm the three liability matrices: the true one, the one reconstructed via ME algorithm one and the reconstructed by means of our message-passing algorithm, varying the loss-given-default α in $[0, 1]$. The results of our simulations are shown in figure 2. We clearly show that the ME algorithm underestimates the risk of contagion, while more realistic results are obtained if the correct degree of sparsity λ_{tr} is assumed.

Notice, that even with the correct estimate of the sparsity, stress tests on the reconstructed matrix still underestimate systemic risk. This is because the weights L_α on the reconstructed sub-graph are assigned again using the ME algorithm. This by itself produces an assignment of weights which is much more uniform than a random assignment of L_{ij} on the sub-graph, which satisfies the constraints (see footnote 2). As a result, the propagation of risk is much reduced in the ME solution.

The second ensemble that we consider is a simple extension of the first one, in which the only modification that we have introduced implements heterogeneity in the size of the liabilities L_{ij}. In particular we consider matrix elements distributed according to:

$$p(L_{ij}) \sim (b + L_{ij})^{-\mu-1}$$

[4]Our attempts to obtain data on real financial networks, such as those in Refs. [6, 7], from central banks were unsuccessful. We focus on ensembles of homogeneous networks (i.e. non-scale free). This is appropriate since the unknown part of the financial network concerns small liabilities, and there is no a priory reason to assume a particularly skewed distribution of degrees for the unknown part of the financial newtork.

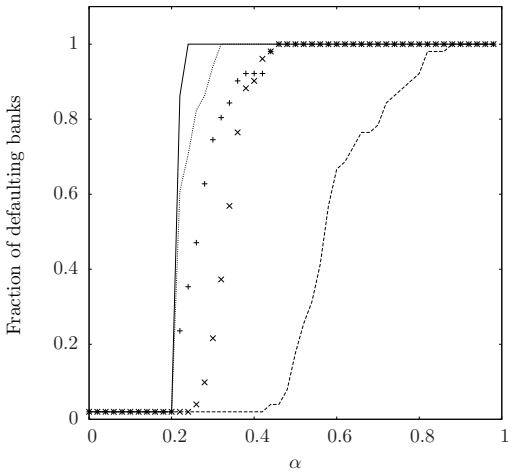

FIGURE 2. Plot of mean fraction of failed banks vs loss-given-default parameter α. The mean is done by averaging over the defaulting bank which starts the contagion. Results are obtained by considering: true liability matrix (solid line), reconstructed via ME algorithm liability matrix (thick dashed line) and the maximally sparse matrix (soft dashed line). Plots were obtained for a network of $N = 50$ banks with entries uniform in [0,1], where the link probability was fixed to $1/2$ and the initial capital was set to $C_i = C = 0.2$. One can easily see that a better estimation of the true risk of contagion is obtained if the reconstruction of the liability matrix is done by enforcing the correct sparsity of the network rather than with the ME algorithm: the results obtained by putting the *correct* support ($\times$ signs) are also plotted, as well as the ones obtained by using a *typical* support with a correctly tuned sparsity parameter (+ signs).

Also in this case we can show (figure 3) that a more correct estimation of the default probability is achieved by enforcing the sparsity parameter of the reconstructed network to be the correct one. In this case the maximally sparse curve is less informative than in the uniform case. This is easily understood as due to the fact that the typical element $L_{ij} \sim 10^{-2}$ is much smaller than the threshold $\theta = 1$, so that a number of zero entries substantially larger than the correct one can be fixed without violating the hard constraints.

In both cases, when the true sparsity of the network is unknown, focusing on the sparsest possible graph likely over-estimates systemic cascades, thereby providing a conservative measure for systemic risk.

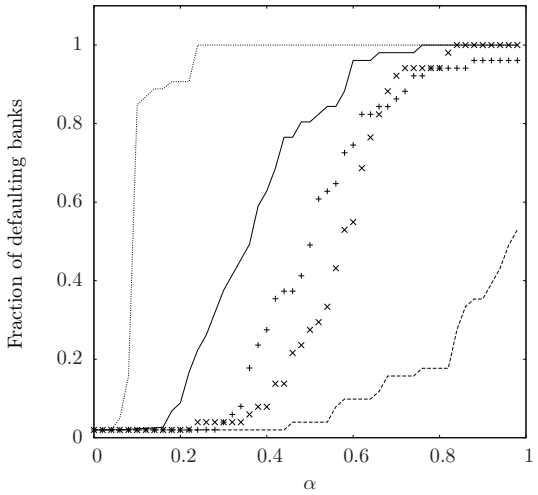

FIGURE 3. A plot analogous to the one in figure 2 for the case of power-law distributed entries of the liability matrix. This plots was obtained for a network of size $N = 50$, where the link probability was fixed to $1/2$. The parameters for the distribution of the entries were set to $b = 0.01$ and $\mu = 2$, while the capital of each bank was fixed to $C_i = C = 0.02$.

7. The role of the threshold

In the discussion above we disregarded the role of the threshold θ above which an exposure L_{ij} has to be made publicly available to regulators by setting it equal to 1. Indeed the problem of setting such threshold is a central problem to build a regulatory policy, hence the discussion of the reliability of the reconstruction algorithm varying θ while keeping fixed the true L is in practice particularly relevant. An appropriate way to address this issue is the following: given a network ensemble (such as the ones described in previous section) and a threshold θ, how many network structures are there with a compatible support? In particular, we remark that among all such compatible supports the maximally sparse one can be used to bound from above the maximum amount of risk given a policy for the thresholding. In particular for each value of θ, we empirically find that $\lambda_{max}[\theta]$ enjoys the following properties:

(1) The maximum sparsity $\lambda_{max}(\theta)$ is a decreasing function of θ. In particular for $\theta \to 0$ one has $\lambda_{max}(\theta) \to \lambda_{tr}$;
(2) The entropy $S(\lambda(\theta)) \to 0$ when the threshold goes to 0.

An example of this behavior for an ensemble of networks with power-law distributed weights is represented in figure 4, while in 5 we plot the entropy $S(\lambda_{max})$ structures as a function of θ. Therefore the algorithm described in section 4 provides quantitative measures for the uncertainty induced by the choice of a given threshold θ on network reconstruction.

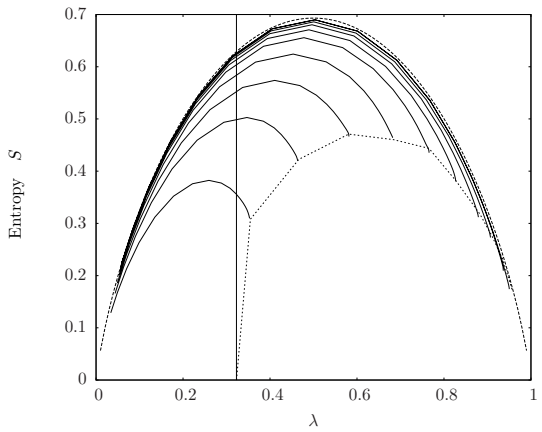

FIGURE 4. We plot the entropy of the space of compatible distributions (i.e. of the solutions of $\mathcal{H}\{a_{i,j}\}$) as a function of the sparsity parameter λ by varying the threshold θ from 1 (top curve) to 0.01 (bottom curve). The dashed line signals the transition point where solutions cease to exist. We consider power-law distributed entries for the true network ($D = 30$, $\lambda_{tr} \approx 0.3$, $b = 0.01$ and $\mu = 2$). This shows how the volume of the space is reduced by a change of the threshold and how λ_{max} gets closer to λ_{tr} by lowering θ.

Ideally θ should be chosen so that maximally sparse structures are close to the true ones, and that the space of compatible structures is not too large (small entropy).

8. Conclusions

We have shown how it is possible to estimate the robustness of a financial network to exogenous crashes by using partial information. We confirm [6] that systemic risk measures depend crucially on the topological properties of the underlying network, and we show that the number of links in a credit network controls in a critical manner its resilience: connected networks tend to absorb the response to external shocks more homogeneously than sparse ones. We have also proposed an efficient message-passing algorithm for the reconstruction of the topology of partially unknown credit networks, in order to estimate with more accuracy their robustness. Such algorithm allows (i) to sample the space of possible network structures, which is assumed to be trivial in Maximal Entropy algorithms commonly employed for network reconstruction, and (ii) to produce typical credit networks, respecting the topological constraint on the total number of links. Finally, we test our algorithms on ensembles of synthetic credit networks which incorporate some of the main features of real credit networks (sparsity and heterogeneity), and find that the quality of the stress-test when only partial information is available critically depends on the assumptions which are done about the network topology. In particular, we find that ME underestimates

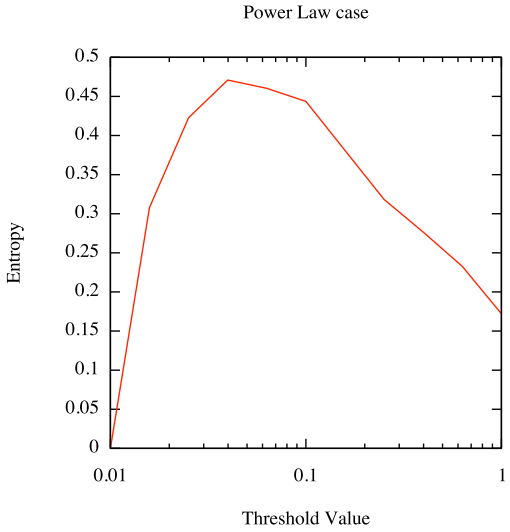

FIGURE 5. The entropy of the space of solutions $\mathcal{H}\{a_{i,j}\}$ as a function of the threshold for the same network as the one depicted in figure 4.

the risk of contagion if the sparsity of the real ensemble is big enough, while our algorithm provides less biased estimates. We remark that a worst case analysis of the topology is possible using the proposed algorithm, as we are able to produce the maximally sparse (hence, maximally fragile) possible structure for the network. Further developments of this work are indeed possible, in particular the identification and the reconstruction of other relevant topological features of credit networks would be relevant for a more accurate estimation of the contagion risk.

REFERENCES

[1] Schwarcz S. L., *Systemic Risk*, Duke Law School Legal Studies Paper No. 163
[2] Blavarg, M. and P. Nimander, Interbank Exposures and Systemic Risk, *Economic Review*, 2002, 2, 1945
[3] Wells S., Financial interlinkages in the United Kingdom's interbank market and the risk of contagion, 2004 *Bank of England* Working Paper No. 230
[4] Degryse H. and Nguyen G., Interbank Exposures: An Empirical Examination of Contagion Risk in the Belgian Banking System, 2007, *International Journal of Central Banking*, 3, 123-171.
[5] van Lelyveld I. P. P. and Liedorp F.R.,Interbank Contagion in the Dutch Banking Sector, 2006, *International Journal of Central Banking*, 2, 99-134.
[6] Mistrulli P.E., Assessing financial contagion in the interbank market: Maximum entropy versus observed interbank lending patterns, 2010 *Journal of Banking & Finance*
[7] Boss, M. and Elsinger, H. and Summer, M. and Thurner, S., Network topology of the interbank market, *Quant. Financ.*

[8] Upper C., Using counterfactual simulations to assess the danger of contagion in interbank markets, *BIS working papers* No 234
[9] Pretti, M. and Weigt, M., Sudden emergence of q-regular subgraphs in random graphs, *Europhysics Letters*, 75, 2008
[10] L. Zdeborová, M. Mézard, Constraint satisfaction problems with isolated solutions are hard *J. Stat. Mech.* 2008 P12004.
[11] Furfine, C. H., Interbank exposures: Quantifying the risk of contagion, *Journal of Money, Credit and Banking*, 2003

Appendix A. Message-passing algorithm

We describe here the algorithm which we use to sample the solution space of the energy function:

$$\mathcal{H}\{a_{i,j}\} = \sum_i \left[\theta\left(L_i^{\rightarrow} - k_i^{\rightarrow}\right) + \theta\left(L_i^{\leftarrow} - k_i^{\leftarrow}\right)\right]$$

which we derived along the line of [9]. The structure of the problem admits a graphical representation as a factor graph, in which $|U|$ variable nodes are associated to the $a_{i,j}$ degrees of freedom, while the constraints are represented as factor nodes. In particular, there are $2N$ function nodes, labeled $a \in \{i \rightarrow, \leftarrow i,\ i = 1, \dots, N\}$ each with k_a variable nodes attached. Let the variables be denoted $x_{a,b} = x_{b,a} = 0, 1$ with a, b and let ∂a be the set of neighbors of node a. Let $M = \frac{1}{2}\sum_a |\partial a|$ be the total number of variables. The messages can be written as

$$\mu_{a\to b} = P\{x_{a,b} = 1|\ \not{b}\}$$

where $\not{b}$ means "when the node b is removed". The BP equations are written in terms of the statistical weights[5]

$$V^m_{S\to a} = \sum_{U\in S:|U|=m} \prod_{b\in U} \mu_{b\to a} \prod_{c\in S\setminus U} (1-\mu_{c\to a})$$

and they read:

$$\mu_{a\to b} = \frac{\sum_{m=L_a-1}^{k_a-1} z^{m+1} V^m_{\partial a\setminus b\to a}}{\sum_{m=L_a-1}^{k_a-1} z^{m+1} V^m_{\partial a\setminus b\to a} + \sum_{m=L_a}^{k_a-1} z^m V^m_{\partial a\setminus b\to a}} = \frac{V^{L_a-1}_{\partial a\setminus b\to a} + z W_{\partial a\setminus b\to a}}{V^{L_a-1}_{\partial a\setminus b\to a} + (1+z) W_{\partial a\setminus b\to a}} \tag{2}$$

$$W_{\partial a\setminus b\to a} = \sum_{m=L_a}^{k_a-1} z^{m-L_a} V^m_{\partial a\setminus b\to a}. \tag{3}$$

[5]Since k_a can be as large as N, the direct computation of $V^m_{S\to a}$ involved in principle 2^{k_a} terms, which may be very large. A faster way to compute it is to use the recursion relation

$$V^m_{S\to a} = (1-\mu_{b\to a}) V^m_{S\setminus b\to a} + \mu_{b\to a} V^{m-1}_{S\setminus b\to a},\ \forall b \in S.$$

In practice this allows one to build $V^m_{S\to a}$ adding one at a time the nodes in S. This procedure involves of order $m^2 \le k_a^2$ operations.

Here z is the fugacity of links, and controls the degree of sparsity λ of the typical supports in the solution space. For $z \to 0$ we obtain the equation for the sparsest possible graph

$$\mu_{a\to b} = \frac{V_{\partial a\setminus b\to a}^{L_a-1}}{V_{\partial a\setminus b\to a}^{L_a-1} + V_{\partial a\setminus b\to a}^{L_a}}$$

whereas for $z \to \infty$ we recover the maximally connected graph $\mu_{a\to b} = 1$ for all a and $b \in \partial a$.

Once the fixed point of Eqs. (2,3) is found by iteration, for a given z, one can compute the probability

$$p_{a,b} = P\{x_{a,b} = 1\} = \frac{\mu_{a\to b}\mu_{b\to a}}{\mu_{a\to b}\mu_{b\to a} + (1-\mu_{a\to b})(1-\mu_{b\to a})}$$

that link (a, b) is present, and the entropy

$$S(z) = \sum_a \log \sum_{m=L_a}^{k_a} V_{\partial a\to a}^m - \frac{1}{2}\sum_a \sum_{b\in\partial a} \log\left[\mu_{a\to b}\mu_{b\to a} + (1-\mu_{a\to b})(1-\mu_{b\to a})\right]$$

To plot the number of solutions (or of different supports) as a function of the sparsity parameter λ, and the associated entropy $\Sigma(\lambda)$ one should use the fact that:

$$e^{MS(z)} = \int_0^1 d\lambda\, e^{M\Sigma(\lambda)+M(1-\lambda)\log z}$$

and hence perform the back-Legendre transform.

Iacopo Mastromatteo, *International School for Advanced Studies, via Beirut 2/4, 34014, Trieste, Italy*

Elia Zarinelli, *LPTMS, CNRS and Université Paris-Sud, UMR8626, Bât. 100, 91405 Orsay, France*

Matteo Marsili, *The Abdus Salam International Center for Theoretical Physics, Strada Costiera 11, 34014 Trieste, Italy*

Bibliography

[1] Boyer, C. & Merzbach, U. *A history of mathematics* (Wiley, 2011).

[2] Anderson, P. Spin glass i: A scaling law rescued. *Physics Today* **41**, 9 (1988).

[3] Edwards, S. F. & Anderson, P. W. Theory of spin-glasses. *J. Phys. F* **5**, 965–974 (1975).

[4] Sherrington, D. & Kirkpatrick, S. Solvable model of a spin-glass. *Phys. Rev. Lett.* **35**, 1792–1796 (1975).

[5] Parisi, G. The order parameter for spin glasses: A function on the interval 0-1. *Journal of Physics A: Mathematical and General* **13**, 1101 (1980).

[6] Parisi, G. Order parameter for spin-glasses. *Phys. Rev. Lett.* **50**, 1946–1948 (1983).

[7] Mézard, M., Parisi, G. & Virasoro, M. A. *Spin-Glass Theory and Beyond*, vol. 9 of *Lecture Notes in Physics* (World Scientific, Singapore, 1987).

[8] Derrida, B. Random-energy model: An exactly solvable model of disordered systems. *Physical Review B* **24**, 2613 (1981).

[9] Gross, D. & Mézard, M. The simplest spin glass. *Nuclear Physics B* **240**, 431–452 (1984).

[10] Kirkpatrick, T. & Wolynes, P. Connections between some kinetic and equilibrium theories of the glass transition. *Phys. Rev. A* **35**, 3072 (1987).

[11] Kirkpatrick, T. & Wolynes, P. Stable and metastable states in mean-field potts and structural glasses. *Physical Review B* **36**, 8552 (1987).

[12] Kirkpatrick, T. & Thirumalai, D. Mean-field soft-spin potts glass model: Statics and dynamics. *Physical Review B* **37**, 5342 (1988).

[13] Thirumalai, D. & Kirkpatrick, T. Mean-field potts glass model: Initial-condition effects on dynamics and properties of metastable states. *Physical Review B* **38**, 4881 (1988).

[14] Kirkpatrick, T., Thirumalai, D. & Wolynes, P. Scaling concepts for the dynamics of viscous liquids near an ideal glassy state. *Physical Review A* **40**, 1045 (1989).

[15] Dawson, K., Foffi, G., Sciortino, F., Tartaglia, P. & Zaccarelli, E. Mode-coupling theory of colloids with short-range attractions. *Journal of Physics: Condensed Matter* **13**, 9113 (2001).

[16] Mueller, M. & Ioffe, L. Glass transition and the coulomb gap in electron glasses. *Physical review letters* **93**, 256403 (2004).

[17] Angelani, L., Conti, C., Ruocco, G. & Zamponi, F. Glassy behavior of light. *Physical review letters* **96**, 65702 (2006).

[18] Mehta, A. *Granular Matter: an interdisciplinary approach* (Springer, 1994).

[19] Amit, D. *Modeling brain function: The world of attractor neural networks* (Cambridge Univ Pr, 1992).

[20] Mezard, M. & Montanari, A. *Information, physics, and computation* (Oxford University Press, USA, 2009).

[21] Monasson, R., Zecchina, R., Kirkpatrick, S., Selman, B. & Troyansky, L. Determining computational complexity from characteristic'phase transitions'. *Nature* **400**, 133–137 (1999).

[22] Kirkpatrick, S., Gelatt, C. & Vecchi, M. Optimization by simulated annealing. *science* **220**, 671 (1983).

[23] Mézard, M., Parisi, G. & Zecchina, R. Analytic and algorithmic solution of random satisfiability problems. *Science* **297**, 812 (2002).

[24] Hartmann, A., Rieger, H. & Wiley, J. *Optimization algorithms in physics*, vol. 2 (Wiley Online Library, 2002).

[25] Toulouse, G. Theory of the frustration effect in spin glasses: I. *Commun. Phys* **2**, 115–119 (1977).

[26] Ogielski, A. T. Dynamics of three-dimensional Ising spin glasses in thermal equilibrium. *Phys. Rev. B* **32**, 7384–7398 (1985).

[27] Bhatt, R. N. & Young, A. P. Numerical studies of Ising spin glasses in two, three, and four dimensions. *Physical Review B* **37**, 5606 (1988).

[28] Marinari, E., Parisi, G. & Ritort, F. On the 3d Ising spin glass, e-print: arxiv:cond-mat/9310041v2 URL http://lanl.arxiv.org/abs/cond-mat/9310041v2. cond-mat/9310041v2.

[29] Marinari, E., Parisi, G. & Ruiz-Lorenzo, J. J. Phase structure of the three-dimensional edwards-anderson spin glass. *Phys. Rev. B* **58**, 14852–14863 (1998).

[30] Mari, P. O. & Campbell, I. A. Ising spin glasses: Corrections to finite size scaling, freezing temperatures, and critical exponents. *Phys. Rev. E* **59**, 2653–2658 (1999).

[31] Palassini, M. & Caracciolo, S. Universal finite-size scaling functions in the 3-d Ising spin glass. *Phys. Rev. Lett.* **82**, 5128–5131 (1999).

[32] Ballesteros, H. G. *et al.* Critical behavior of the three-dimensional Ising spin glass. *Phys. Rev. B* **62**, 14237–14245 (2000).

[33] Katzgraber, H. G., Körner, M. & Young, A. P. Universality in three-dimensional Ising spin glasses: A monte carlo study. *Phys. Rev. B* **73**, 224432 (2006).

[34] Hasenbusch, M., Pelissetto, A. & Vicari, E. Critical behavior of three-dimensional Ising spin glass models. *Phys. Rev. B* **78**, 214205 (2008).

[35] Alvarez Baños, R. *et al.* Static versus dynamic heterogeneities in the $d = 3$ Edwards-Anderson-Ising spin glass. *Physical Review Letters* **105**, 177202 (2010).

[36] Belletti, F. *et al.* An in-depth view of the microscopic dynamics of Ising spin glasses at fixed temperature. *Journal of Statistical Physics* **135**, 1121–1158 (2009).

[37] Contucci, P., Giardinà, C., Giberti, C., Parisi, G. & Vernia, C. Ultrametricity in the Edwards-Anderson model. *Phys. Rev. Lett.* **99**, 057206 (2007).

[38] Contucci, P., Giardinà, C., Giberti, C., Parisi, G. & Vernia, C. Structure of correlations in three dimensional spin glasses. *Phys. Rev. Lett.* **103**, 017201 (2009).

[39] Krzakala, F. & Martin, O. C. Spin and link overlaps in three-dimensional spin glasses. *Phys. Rev. Lett.* **85**, 3013–3016 (2000).

[40] Thouless, D., Anderson, P. & Palmer, R. Solution of'solvable model of a spin glass'. *Philosophical Magazine* **35**, 593–601 (1977).

[41] Zarinelli, E. & Franz, S. Surface tension in kac glass models. *Journal of Statistical Mechanics: Theory and Experiment* **2010**, P04008 (2010).

[42] Castellana, M. & Zarinelli, E. Role of tracy-widom distribution in finite-size fluctuations of the critical temperature of the sherrington-kirkpatrick spin glass. *Physical Review B* **84**, 144417 (2011).

[43] Castellana, M., Decelle, A. & Zarinelli, E. Extreme value statistics distributions and spin glasses. *To be published in Physical Review Letters* (2011).

[44] Mastromatteo, I., Zarinelli, E. & Marsili, M. Reconstruction of financial network for robust estimation of systemic risk. *Arxiv preprint arXiv:1109.6210* (2011).

[45] Weintraub, H. *et al.* Through the glass lightly. *Science-AAAS-Weekly Paper Edition* **267**, 1609–1618 (1995).

[46] Debenedetti, P., Stillinger, F. *et al.* Supercooled liquids and the glass transition. *Nature* **410**, 259–267 (2001).

[47] Cavagna, A. Supercooled liquids for pedestrians. *Physics Reports* **476**, 51–124 (2009).

[48] Berthier, L. & Biroli, G. Theoretical perspective on the glass transition and amorphous materials. *Reviews of Modern Physics* **83**, 587 (2011).

[49] Biroli, G. & Bouchaud, J. The random first-order transition theory of glasses: a critical assessment. *Arxiv preprint arXiv:0912.2542* (2009).

[50] Franz, S. & Montanari, A. Analytic determination of dynamical and mosaic length scales in a kac glass model. *Journal of Physics A: Mathematical and Theoretical* **40**, F251 (2007).

[51] Sausset, F., Biroli, G. & Kurchan, J. Do solids flow? *Journal of Statistical Physics* **140**, 718–727 (2010).

[52] Kauzmann, W. The nature of the glassy state and the behavior of liquids at low temperatures. *Chemical Reviews* **43**, 219–256 (1948).

[53] Angell, C. Formation of glasses from liquids and biopolymers. *Science* **267**, 1924 (1995).

[54] Vogel, H. Das temperaturabhängigkeitsgesetz der viskosität von flüssigkeiten. *Phys. Z* **22**, 645–646 (1921).

[55] Fulcher, G. Analysis of recent measurements of the viscosity of glasses.—ii1. *Journal of the American Ceramic Society* **8**, 789–794 (1925).

[56] Tamman, V. & Hesse, H. Anorg allg che 1926, 19, 245. *Direct Link: Abstract PDF (575K) References* .

[57] Debenedetti, P. *Metastable liquids: concepts and principles* (Princeton Univ Pr, 1996).

[58] Angell, C. Structural instability and relaxation in liquid and glassy phases near the fragile liquid limit. *Journal of non-crystalline solids* **102**, 205–221 (1988).

[59] Goldstein, M. *J. Chem. Phys.* **51**, 3728 (1969).

[60] Ediger, M. Spatially heterogeneous dynamics in supercooled liquids. *Annual review of physical chemistry* **51**, 99–128 (2000).

[61] Donati, C., Glotzer, S. & Poole, P. Growing spatial correlations of particle displacements in a simulated liquid on cooling toward the glass transition. *Physical review letters* **82**, 5064–5067 (1999).

[62] Bennemann, C., Donati, C., Baschnagel, J. & Glotzer, S. Growing range of correlated motion in a polymer melt on cooling towards the glass transition. *Nature* **399**, 246–249 (1999).

[63] Franz, S. & Parisi, G. On non-linear susceptibility in supercooled liquids. *Journal of Physics: Condensed Matter* **12**, 6335 (2000).

[64] Donati, C., Franz, S., Glotzer, S. & Parisi, G. Theory of non-linear susceptibility and correlation length in glasses and liquids. *Journal of non-crystalline solids* **307**, 215–224 (2002).

[65] Montanari, A. & Semerjian, G. Rigorous inequalities between length and time scales in glassy systems. *Journal of statistical physics* **125**, 23–54 (2006).

[66] Biroli, G., Bouchaud, J., Cavagna, A., Grigera, T. & Verrocchio, P. Thermodynamic signature of growing amorphous order in glass-forming liquids. *Nature Physics* **4**, 771–775 (2008).

[67] Kirkpatrick, T. & Wolynes, P. Connections between some kinetic and equilibrium theories of the glass transition. *Physical Review A* **35**, 3072 (1987).

[68] Bouchaud, J. & Biroli, G. On the adam-gibbs-kirkpatrick-thirumalai-wolynes scenario for the viscosity increase in glasses. *The Journal of chemical physics* **121**, 7347 (2004).

[69] Gross, D., Kanter, I. & Sompolinsky, H. Mean-field theory of the potts glass. *Physical review letters* **55**, 304–307 (1985).

[70] Castellani, T. & Cavagna, A. Spin-glass theory for pedestrians. *Journal of Statistical Mechanics: Theory and Experiment* **2005**, P05012 (2005).

[71] Bouchaud, J., Cugliandolo, L., Kurchan, J. & Mézard, M. Mode-coupling approximations, glass theory and disordered systems. *Physica A: Statistical Mechanics and its Applications* **226**, 243–273 (1996).

[72] Kurchan, J. & Levine, D. Order in glassy systems. *Journal of Physics A: Mathematical and Theoretical* **44**, 035001 (2011).

[73] Sausset, F. & Levine, D. Characterizing order in amorphous systems. *Physical Review Letters* **107**, 45501 (2011).

[74] Cammarota, C. & Biroli, G. Ideal glass transitions by random pinning. *Arxiv preprint arXiv:1106.5513* (2011).

[75] Cavagna, A., Grigera, T. & Verrocchio, P. Mosaic multistate scenario versus one-state description of supercooled liquids. *Physical review letters* **98**, 187801 (2007).

[76] Franz, S. & Toninelli, F. Kac limit for finite-range spin glasses. *Physical review letters* **92**, 30602 (2004).

[77] Franz, S. & Toninelli, F. Finite-range spin glasses in the kac limit: free energy and local observables. *Journal of Physics A: Mathematical and General* **37**, 7433 (2004).

[78] Franz, S. & Toninelli, F. A field-theoretical approach to the spin glass transition: models with long but finite interaction range. *Journal of Statistical Mechanics: Theory and Experiment* **2005**, P01008 (2005).

[79] Franz, S. First steps of a nucleation theory in disordered systems. *Journal of Statistical Mechanics: Theory and Experiment* **2005**, P04001 (2005).

[80] Franz, S. Metastable states, relaxation times and free-energy barriers in finite-dimensional glassy systems. *EPL (Europhysics Letters)* **73**, 492 (2006).

[81] Franz, S. & Parisi, G. Local spin glass order in 1d. *EPL (Europhysics Letters)* **75**, 385 (2006).

[82] Franz, S. On the dynamics of kac p-spin glasses. *Journal of Statistical Physics* **126**, 765–780 (2007).

[83] Franz, S. Spin glass models with kac interactions. *The European Physical Journal B-Condensed Matter and Complex Systems* **64**, 557–561 (2008).

[84] Franz, S. & Semerjian, G. Analytical approaches to time-and length scales in models of glasses. *Dynamical Heterogeneities in Glasses, Colloids, and Granular Media* 407 (2011).

[85] Gradenigo, G. & Cavagna, A. To be published .

[86] Cammarota, C., Cavagna, A., Gradenigo, G., Grigera, T. & Verrocchio, P. Surface tension fluctuations and a new spinodal point in glass-forming liquids. *Arxiv preprint arXiv:0904.1522* (2009).

[87] Moore, M. Interface free energies in p-spin glass models. *Physical review letters* **96**, 137202 (2006).

[88] Palassini, M. Ground-state energy fluctuations in the sherrington-kirkpatrick model. *Arxiv preprint cond-mat/0307713* (2003).

[89] Bouchaud, J., Krzakala, F. & Martin, O. Energy exponents and corrections to scaling in ising spin glasses. *Physical Review B* **68**, 224404 (2003).

[90] Andreanov, A., Barbieri, F. & Martin, O. Large deviations in spin-glass ground-state energies. *The European Physical Journal B-Condensed Matter and Complex Systems* **41**, 365–375 (2004).

[91] Lee, T. D. & Yang, C. N. Statistical theory of equations of state and phase transitions. II. Lattice gas and Ising model. *Phys. Rev.* **87**, 410–419 (1952).

[92] Yang, C. Statistical theory of equations of state and phase transitions. I. theory of condensation. *Phys. Rev.* **87**, 404–409 (1952).

[93] Biskup, M., Borgs, C., Chayes, J., Kleinwaks, L. & Koteckỳ, R. General theory of Lee-Yang zeros in models with first-order phase transitions. *Physical Review Letters* **84**, 4794–4797 (2000).

[94] Ruelle, D. Extension of the Lee-Yang circle theorem. *Physical Review Letters* **26**, 303–304 (1971).

[95] Harris, A. Effect of random defects on the critical behaviour of ising models. *J. Phys. C* **7**, 1671 (1974).

[96] Aharony, A. & Harris, A. Absence of self-averaging and universal fluctuations in random systems near critical points. *Phys. Rev. Lett.* **77**, 3700–3703 (1996).

[97] Wiseman, S. & Domany, E. Finite-size scaling and lack of self-averaging in critical disordered systems. *Phys. Rev. Lett.* **81**, 22–25 (1998).

[98] Monthus, C. & Garel, T. Delocalization transition of the selective interface model: distribution of pseudo-critical temperatures. *Journal of Statistical Mechanics: Theory and Experiment* **2005**, P12011 (2005).

[99] Monthus, C. & Garel, T. Distribution of pseudo-critical temperatures and lack of self-averaging in disordered Poland-Scheraga models with different loop exponents. *The European Physical Journal B-Condensed Matter and Complex Systems* **48**, 393–403 (2005).

[100] Iglói, F., Lin, Y., Rieger, H. & Monthus, C. Finite-size scaling of pseudocritical point distributions in the random transverse-field Ising chain. *Phys. Rev. B* **76**, 064421 (2007).

[101] Monthus, C. & Garel, T. Freezing transition of the directed polymer in a 1+ d random medium: Location of the critical temperature and unusual critical properties. *Physical Review E* **74**, 011101 (2006).

[102] Sarlat, T., Billoire, A., Biroli, G. & Bouchaud, J. P. Predictive power of MCT: numerical testing and finite size scaling for a mean field spin glass. *Journal of Statistical Mechanics: Theory and Experiment* **2009**, P08014 (2009).

[103] Wigner, E. On the statistical distribution of the widths and spacings of nuclear resonance levels. In *Proc. Cambridge Philos. Soc*, vol. 47, 790–798 (Cambridge Univ Press, 1951).

[104] Dyson, F. Statistical theory of the energy levels of complex systems. i. *Journal of Mathematical Physics* **3** (1962).

[105] Keating, J. & Snaith, N. Random matrices and l-functions. *Journal of Physics A: Mathematical and General* **36**, 2859 (2003).

[106] Eisen, M., Spellman, P., Brown, P. & Botstein, D. Cluster analysis and display of genome-wide expression patterns. *Proceedings of the National Academy of Sciences* **95**, 14863 (1998).

[107] Ambjørn, L. *et al.* Matrix model calculations beyond the spherical limit. *Nuclear Physics B* **404**, 127–172 (1993).

[108] Muirhead, R. *Aspects of multivariate statistical theory* (Wiley Online Library, 1982).

[109] Cavagna, A., Giardina, I. & Parisi, G. Stationary points of the thouless-anderson-palmer free energy. *Physical Review B* **57**, 1123612–11257 (1998).

[110] Cavagna, A., Garrahan, J. & Giardina, I. Index distribution of random matrices with an application to disordered systems. *Physical Review B* **61**, 3960 (2000).

[111] Majumdar, S., Nadal, C., Scardicchio, A. & Vivo, P. Index distribution of gaussian random matrices. *Physical review letters* **103**, 220603 (2009).

[112] Zamponi, F. Mean field theory of spin glasses. *Arxiv preprint arXiv:1008.4844* (2010).

[113] Mézard, M., Parisi, G. & Virasoro, M. A. *Spin glass theory and beyond* (World Scientific, 1987).

[114] Georges, A. & Yedidia, J. How to expand around mean-field theory using high-temperature expansions. *Journal of Physics A: Mathematical and General* **24**, 2173 (1991).

[115] Plefka, T. Convergence condition of the tap equation for the infinite-ranged ising spin glass model. *Journal of Physics A: Mathematical and general* **15**, 1971 (1982).

[116] Georges, A., Mézard, M. & Yedidia, J. Low-temperature phase of the ising spin glass on a hypercubic lattice. *Physical review letters* **64**, 2937–2940 (1990).

[117] Yedidia, J. & Georges, A. The fully frustrated ising model in infinite dimensions. *Journal of Physics A: Mathematical and General* **23**, 2165 (1990).

[118] Yokota, T. Ordered phase for the infinite-range potts-glass model. *Physical Review B* **51**, 962 (1995).

[119] Plefka, T. Expansion of the gibbs potential for quantum many-body systems: General formalism with applications to the spin glass and the weakly nonideal bose gas. *Physical Review E* **73**, 016129 (2006).

[120] Ishii, H. & Yamamoto, T. Effect of a transverse field on the spin glass freezing in the sherrington-kirkpatrick model. *Journal of Physics C: Solid State Physics* **18**, 6225 (1985).

[121] De Cesare, L., Walasek, K. & Walasek, K. Cavity-field approach to quantum spin glasses: The ising spin glass in a transverse field. *Physical Review B* **45**, 8127 (1992).

[122] Biroli, G. & Cugliandolo, L. Quantum thouless-anderson-palmer equations for glassy systems. *Physical Review B* **64**, 014206 (2001).

[123] De Dominicis, C. & Giardina, I. *Random fields and spin glasses: a field theory approach* (Cambridge Univ Pr, 2006).

[124] Katz, R., Parlange, M. & Naveau, P. Statistics of extremes in hydrology. *Advances in water resources* **25**, 1287–1304 (2002).

[125] Lavenda, B. & Cipollone, E. Extreme value statistics and thermodynamics of earthquakes: aftershock sequences. *Annals of Geophysics* **43** (2000).

[126] Bouchaud, J. & Potters, M. *Theory of financial risk and derivative pricing: from statistical physics to risk management* (Cambridge Univ Pr, 2003).

[127] Gumbel, E. Statistics of extremes. 1958.

[128] Fréchet, M. Sur la loi de probabilité de l'écart maximum. *Ann. de la Soc. polonaise de Math* **6**, 93–116 (1927).

[129] Fisher, R. & Tippett, L. Limiting forms of the frequency distribution of the largest or smallest member of a sample. In *Mathematical Proceedings of the Cambridge Philosophical Society*, vol. 24, 180–190 (Cambridge Univ Press, 1928).

[130] von Mises, R. La distribution de la plus grande de n valeurs. *Rev. math. Union interbalcanique* **1** (1936).

[131] Gnedenko, B. Sur la distribution limite du terme maximum d'une serie aleatoire. *Annals of Mathematics* 423–453 (1943).

[132] Bouchaud, J. & Mézard, M. Universality classes for extreme-value statistics. *Journal of Physics A: Mathematical and General* **30**, 7997 (1997).

[133] Tracy, C. A. & Widom, H. Level-spacing distributions and the Airy kernel. *Phys. Lett. B* **305**, 115–118 (1993).

[134] Tracy, C. A. & Widom, H. Level-spacing distributions and the Airy kernel. *Communications in Mathematical Physics* **159**, 151–174 (1994).

[135] Tracy, C. A. & Widom, H. On orthogonal and symplectic matrix ensembles. *Communications in Mathematical Physics* **177**, 727–754 (1996).

[136] Tracy, C. A. & Widom, H. *Proc. International Congress of Mathematicians (Beijing, 2002)*, vol. 1 (2002).

[137] Edelman, A. & Persson, P. Numerical methods for eigenvalue distributions of random matrices. *Arxiv preprint math-ph/0501068* (2005).

[138] Soshnikov, A. Universality at the edge of the spectrum in wigner random matrices. *Communications in mathematical physics* **207**, 697–733 (1999).

[139] Sodin, S. The tracy–widom law for some sparse random matrices. *Journal of Statistical Physics* **136**, 834–841 (2009).

[140] Biroli, G., Bouchaud, J. & Potters, M. On the top eigenvalue of heavy-tailed random matrices. *EPL (Europhysics Letters)* **78**, 10001 (2007).

[141] Cizeau, P. & Bouchaud, J. Theory of lévy matrices. *Physical Review E* **50**, 1810 (1994).

[142] Majumdar, S. Random matrices, the ulam problem, directed polymers and growth models, and sequence matching, 2007. *Complex Systems (Les Houches Lecture Notes)* 179–216.

[143] Baik, J., Deift, P. & Johansson, K. On the distribution of the length of the longest increasing subsequence of random permutations. *JOURNAL-AMERICAN MATHEMATICAL SOCIETY* **12**, 1119–1178 (1999).

[144] Majumdar, S. & Nechaev, S. Exact asymptotic results for the bernoulli matching model of sequence alignment. *Physical Review E* **72**, 020901 (2005).

[145] Johansson, K. Shape fluctuations and random matrices. *Communications in mathematical physics* **209**, 437–476 (2000).

[146] Prähofer, M. & Spohn, H. Universal distributions for growth processes in 1+ 1 dimensions and random matrices. *Physical review letters* **84**, 4882–4885 (2000).

[147] Kardar, M., Parisi, G. & Zhang, Y. Dynamic scaling of growing interfaces. *Phys. Rev. Lett.* **56**, 889–892 (1986).

[148] Sasamoto, T. & Spohn, H. One-dimensional kardar-parisi-zhang equation: An exact solution and its universality. *Physical review letters* **104**, 230602 (2010).

[149] Calabrese P. et al. Exact solution for the kardar-parisi-zhang equation with flat initial conditions. *Phys. Rev. Lett.* **106**, 250603 (2011).

[150] Takeuchi, K. & Sano, M. Universal fluctuations of growing interfaces: evidence in turbulent liquid crystals. *Phys. Rev. Lett.* **104**, 230601 (2010).

[151] Takeuchi, K., Sano, M., Sasamoto, T. & Spohn, H. Growing interfaces uncover universal fluctuations behind scale invariance. *Scientific Reports* **1** (2011).

[152] Somoza, A., Ortuno, M. & Prior, J. Universal distribution functions in two-dimensional localized systems. *Phys. Rev. Lett.* **99**, 116602 (2007).

[153] Monthus, C. & Garel, T. Statistics of the two-point transmission at anderson localization transitions. *Physical Review B* **79**, 205120 (2009).

[154] Fridman, M., Pugatch, R., Nixon, M., Friesem, A. & Davidson, N. Measuring maximal eigenvalue distribution of wishart random matrices with coupled lasers. *Arxiv preprint arXiv:1012.1282* (2010).

[155] Yedidia, J. An idiosyncratic journey beyond mean field theory. *Advanced mean field methods: Theory and practice* 21–36 (2001).

[156] Stäring, J., Mehlig, B., Fyodorov, Y. & Luck, J. M. Random symmetric matrices with a constraint: The spectral density of random impedance networks. *Physical Review E* **67**, 047101 (2003).

[157] Shukla, P. Random matrices with correlated elements: A model for disorder with interactions. *Physical Review E* **71**, 026226 (2005).

[158] Bai, Z. & Zhou, W. Large sample covariance matrices without independence structures in columns. *Statistica Sinica* **18**, 425 (2008).

[159] Rambeau, J. & Schehr, G. To be published.

[160] Bray, A. & Moore, M. Evidence for massless modes in the'solvable model'of a spin glass. *Journal of Physics C: Solid State Physics* **12**, L441 (1979).

[161] Aspelmeier, T., Billoire, A., Marinari, E. & Moore, M. A. Finite-size corrections in the sherrington–kirkpatrick model. *Journal of Physics A: Mathematical and Theoretical* **41**, 324008 (2008).

[162] Cizeau, P. & Bouchaud, J. Mean field theory of dilute spin-glasses with power-law interactions. *Journal of Physics A: Mathematical and General* **26**, L187 (1993).

[163] Janzen, K., Hartmann, A. & Engel, A. Replica theory for levy spin glasses. *Journal of Statistical Mechanics: Theory and Experiment* **2008**, P04006 (2008).

[164] Janzen, K., Engel, A. & Mézard, M. Thermodynamics of the lévy spin glass. *Physical Review E* **82**, 021127 (2010).

[165] Andresen, J., Janzen, K. & Katzgraber, H. Critical behavior and universality in lévy spin glasses. *Physical Review B* **83**, 174427 (2011).

[166] Burda, Z., Jurkiewicz, J., Nowak, M., Papp, G. & Zahed, I. Random lévy matrices revisited. *Arxiv preprint cond-mat/0602087* (2006).

[167] Coluzzi, B., Marinari, E., Parisi, G. & Rieger, H. On the energy minima of the sherrington-kirkpatrick model. *Journal of Physics A: Mathematical and General* **33**, 3851 (2000).

[168] Leuzzi, L. Critical behaviour and ultrametricity of Ising spin-glass with long-range interactions. *J. Phys. A* **32**, 1417 (1999).

[169] Nakamura, T., ichi Endoh, S. & Yamamoto, T. Weak universality of spin-glass transitions in three-dimensional ±j models. *Journal of Physics A: Mathematical and General* **36**, 10895–10906 (2003). URL http://dx.doi.org/10.1088/0305-4470/36/43/015.

[170] Hukushima, K. & Nemoto, K. Exchange monte carlo method and application to spin glass simulations. *Journal of the Physical Society of Japan* **65**, 1604–1608 (1996). URL http://jpsj.ipap.jp/link?JPSJ/65/1604/.

[171] Marinari, E. Optimized Monte Carlo methods. In Kertész, J. & Kondor, I. (eds.) *Advances in Computer Simulation*, 50 (Springer-Verlag, Berlin, 1998).

[172] Swendsen, R. H. & Wang, J.-S. Replica monte carlo simulation of spin-glasses. *Phys. Rev. Lett.* **57**, 2607–2609 (1986).

[173] Earl, D. & Deem, M. Parallel tempering: Theory, applications, and new perspectives. *Physical Chemistry Chemical Physics* **7**, 3910–3916 (2005).

[174] Parisi, G., Ritort, F. & Slanina, F. Critical finite-size corrections for the sherrington-kirkpatrick spin glass. *J. Phys. A* **26**, 247–259 (1993).

[175] Billoire, A. *et al.* Finite-size scaling analysis of the distributions of pseudo-critical temperatures in spin glasses. *Journal of Statistical Mechanics: Theory and Experiment* **2011**, P10019 (2011).

[176] Vojta, T. Rare region effects at classical, quantum and nonequilibrium phase transitions. *Journal of Physics A: Mathematical and General* **39**, R143 (2006).

[177] Dean, D. & Majumdar, S. Large deviations of extreme eigenvalues of random matrices. *Physical review letters* **97**, 160201 (2006).

[178] Kotliar, G., Anderson, P. & Stein, D. One-dimensional spin-glass model with long-range random interactions. *Physical Review B* **27**, 602 (1983).

[179] K. Gunnarsson et al. Static scaling in a short-range Ising spin glass. *Phys. Rev. B* **43**, 8199–8203 (1991).

[180] Nair, S. & Nigam, A. K. Critical exponents and the correlation length in the manganite spin glass $Eu_{0.5}Ba_{0.5}MnO_3$. *Phys. Rev. B* **75**, 214415 (2007).

[181] Friedman, M. & Schwartz, A. *A monetary history of the United States, 1867-1960*, vol. 12 (Princeton Univ Pr, 1971).

[182] Schwarcz, S. Systemic risk. In *American Law & Economics Association Annual Meetings*, 20 (bepress, 2008).

[183] Upper, C. & for International Settlements, B. *Using counterfactual simulations to assess the danger of contagion in interbank markets* (BIS, 2007).

[184] Bullard, J., Neely, C. & Wheelock, D. Systemic risk and the financial crisis: a primer. *Federal Reserve Bank of St. Louis Review* **91**, 403–17 (2009).

[185] DiMartino, D. & Duca, J. The rise and fall of subprime mortgages. *FRBSF Economic Letter* (2007).

[186] Bernanke, B. Financial regulation and financial stability. In *Speech given at the Federal Deposit Insurance Corporations Forum on Mortgage Lending for Low and Moderate Income Households, Arlington, Virginia, July*, vol. 8 (2008).

[187] Lowenstein, R. *When genius failed: The rise and fall of Long-Term Capital Management* (Random House Trade Paperbacks, 2000).

[188] McDonough, W. Statement to congress, october 1, 1998,(federal reserve bank of new york's role in the recent private-sector recapitalization of long-term capital management). *Federal Reserve Bulletin* 1050–1054 (1998).

[189] Angelini, P., Maresca, G. & Russo, D. Systemic risk in the netting system. *Journal of Banking & Finance* **20**, 853–868 (1996).

[190] Boss, M., Elsinger, H., Summer, M. & Thurner, S. Network topology of the interbank market. *Quantitative Finance* **4**, 677–684 (2004).

[191] Iori, G., De Masi, G., Precup, O., Gabbi, G. & Caldarelli, G. A network analysis of the italian overnight money market. *Journal of Economic Dynamics and Control* **32**, 259–278 (2008).

[192] Furfine, C. Interbank exposures: Quantifying the risk of contagion. *Journal of Money, Credit and Banking* 111–128 (2003).

[193] James, C. The losses realized in bank failures. *Journal of Finance* 1223–1242 (1991).

[194] Kaufman, G. Bank contagion: A review of the theory and evidence. *Journal of Financial Services Research* **8**, 123–150 (1994).

[195] Eisenberg, L. & Noe, T. Systemic risk in financial systems. *Management Science* 236–249 (2001).

[196] Mistrulli, P. Assessing financial contagion in the interbank market: Maximum entropy versus observed interbank lending patterns. *Journal of Banking & Finance* **35**, 1114–1127 (2011).

[197] Sheldon, G. & Maurer, M. Interbank lending and systemic risk: An empirical analysis for switzerland. *REVUE SUISSE D ECONOMIE POLITIQUE ET DE STATISTIQUE* **134**, 685–704 (1998).

[198] Degryse, H. & Nguyen, G. Interbank exposure: An empirical examination of systemic risk in the belgian banking system. *CentER Discussion Paper No. 2004-04* (2004).

[199] Wells, S. Uk interbank exposures: systemic risk implications. *Financial Stability Review* 175–182 (2002).

[200] Upper, C. & Worms, A. Estimating bilateral exposures in the german interbank market: Is there a danger of contagion? *European Economic Review* **48**, 827–849 (2004).

[201] Allen, F. & Gale, D. Financial contagion. *Journal of political economy* 1–33 (2000).

[202] Iori, G., Jafarey, S. & Padilla, F. Systemic risk on the interbank market. *Journal of Economic Behavior & Organization* **61**, 525–542 (2006).

[203] Blien, U. & Graef, F. The application of the entrop procedure .

[204] Hartmann, A. & Weigt, M. *Phase transitions in combinatorial optimization problems* (Wiley Online Library, 2005).

[205] Hartmann, A. & Weigt, M. Statistical mechanics of the vertex-cover problem. *Journal of Physics A: Mathematical and General* **36**, 11069 (2003).

[206] Pretti, M. & Weigt, M. Sudden emergence of q-regular subgraphs in random graphs. *Europhysics Letters* **75**, 8 (2006). URL doi:10.1209/epl/i2006-10070-4.

[207] Körner, M., Katzgraber, H. & Hartmann, A. Probing tails of energy distributions using importance-sampling in the disorder with a guiding function. *Journal of Statistical Mechanics: Theory and Experiment* **2006**, P04005 (2006).

[208] Boss, M., Elsinger, H., Summer, M. & Thurner, S. An empirical analysis of the network structure of the austrian interbank market. *Oesterreichesche Nationalbank Financial stability Report* **7**, 77–87 (2004).